

# Polyfluorinated Peptides – Establishing A Novel Class Of Biopolymers

Inaugural-Dissertation  
to obtain the academic degree  
Doctor rerum naturalium (Dr. rer. nat.)

submitted to the Department of Biology, Chemistry, Pharmacy  
of Freie Universität Berlin

by  
**Thomas Hohmann, M. Sc.**

September 2023



---

The research presented in this doctoral thesis was performed under the supervision of Prof. Dr. Beate Koksch from February 2020 until August 2023 at the Institute of Chemistry and Biochemistry in the Department of Biology, Chemistry, Pharmacy of Freie Universität Berlin.

1<sup>st</sup> reviewer: Prof. Dr. Beate Koksch (Freie Universität Berlin)

2<sup>nd</sup> reviewer: Senior Lecturer Dr. Matthew Hopkinson (Newcastle University)

Date of defense: 04.12.2023





---

## **Declaration of Authorship**

I hereby confirm that I have prepared this dissertation entitled “Polyfluorinated Peptides – Establishing A Novel Class Of Biopolymers” solely by myself and independently. All external sources and resources have been specified and correctly cited or acknowledged. This thesis has not been submitted, accepted, rated as insufficient, or rejected in any other doctorate degree procedure.

Berlin, September 2023

Thomas Hohmann

---

## Publications

(1) S. Chowdhary, R. F. Schmidt, A. Kumar Sahoo, T. tom Dieck, T. Hohmann, B. Schade, K. Brademann-Jock, A. F. Thünemann, R. R. Netz, M. Gradzielski, B. Kokschi, *Nanoscale* **2022**, *14*, 10176–10189.

(DOI: 10.1039/D2NR01648F)

(2) J. Leppkes, N. Dimos, B. Loll, T. Hohmann, M. Dyrks, A. Wieseke, B. G. Keller, B. Kokschi, *RSC Chem. Biol.* **2022**, *3*, 773–782.

(DOI: 10.1039/D2CB00018K)

(3) T. Hohmann, M. Dyrks, S. Chowdhary, M. Weber, D. Nguyen, J. Moschner, B. Kokschi, *J. Org. Chem.* **2022**, *87*, 10592–10604.

(DOI: 10.1021/acs.joc.2c00522)

(4) T. Hohmann<sup>\*</sup>, S. Chowdhary<sup>\*</sup>, K. Ataka, J. Er, G. H. Dreyhsig, J. Heberle, B. Kokschi, *Chem. Eur. J.* **2023**, *29*, e202203860. (\*Authors contributed equally)

(DOI: 10.1002/chem.202203860)

(5) T. Hohmann, P. Dubatouka, K. Pfeifer, B. Kokschi, *Biomacromolecules* **2023**, *24*, 3357–3369.

(DOI: 10.1021/acs.biomac.3c00427)

(6) S. Chowdhary, T. Hohmann, A. Langhans, in *The Chemistry of Organofluorine Compounds* (Ed.: I. Marek, V. Gouverneur, M. Gandelman), Wiley-VCH, **2023**, accepted.

---

## Oral presentations

(1) *“Fluoropeptides: Systematic study of the impact of fluorination degree on peptide hydrophobicity and conformation”*, Symposium on foldamers, Bordeaux, France, **13.09.2021-15.09.2021**.

(2) *“Fluoropeptide: Systematische Studie zum Einfluss des Fluorierungsgrads auf die Hydrophobie und die Konformation von Peptiden“*, 19. Deutscher Fluortag, Schmitten im Taunus, Deutschland, **19.09.2022-21.09.2022**.

(3) *“Fluorine-containing amino acids as an orthogonal tool in coiled coil assembly”*, colloquium of the CRC 1349 “Fluorine-Specific Interactions: Fundamentals and Functions”, Berlin, Germany, **09.06.2023**.

(4) *“Fluorine-containing amino acids as an orthogonal tool in coiled coil assembly”*, 7<sup>th</sup> Fluorine Days, Poznań, Poland, **18.06.2023-22.06.2023**.

## Posters

(1) *“Fluoropeptides: Systematic study of the impact of fluorination degree on peptide hydrophobicity and conformation”*, colloquium of the CRC 1349 “Fluorine-Specific Interactions: Fundamentals and Functions”, Berlin, Germany, **27.08.2021**.

(2) *“Gram-scale asymmetric synthesis of fluorinated amino acids using a chiral Ni(II) complex”*, CGCh-Wissenschaftsforum Chemie, Online-Event, **29.08.2021-01.09.2021**.

(3) *“Fluoropeptides: Systematic study of the impact of fluorination degree on peptide hydrophobicity and conformation”*, 25<sup>th</sup> Winter Fluorine Conference, Clearwater, Florida, United States of America, **16.01.2022-21.01.2022**. (**Poster Prize**)

(4) *“Fluoropeptides: Systematic study of the impact of fluorination degree on peptide hydrophobicity and conformation”*; 20<sup>th</sup> European Symposium on Fluorine Chemistry, Berlin, Germany, **14.08.2022-19.08.2022**.

---

## Acknowledgments

First, I would like to thank Prof. Dr. Beate Koksch. Since I joined the research group in October 2018 as a research intern, I have received a lot of encouragement and support from Prof. Dr. Koksch. During my doctoral studies, I developed my ideas, explored them, attended conferences, and thus grew as a scientist. I am very grateful for that.

I also would like to thank Dr. Matthew Hopkinson for agreeing to be the second supervisor, as he did for my Master's thesis.

I want to thank all current and former members of the Koksch working group for the relaxed and productive working atmosphere. In particular, Dr. Jakob Leppkes introduced me to the working group, taught me a lot about the functioning of HPLC systems, has always supported me, and was a pivotal factor why I stayed with the working group. Additionally, I would like to thank Dr. Johann Moschner. He is a tremendous organic chemist from whom I could learn an incredible amount. I also thank Dr. Allison A. Berger for much support and many proofreading hours.

During my Ph. D., I was fortunate to supervise exceptionally talented students. I thank Michael Dyrks, Palina Dubatouka, Katharina Pfeifer, Jasmin Er, and Duy Nguyen for much help and support.

I would especially like to thank Suvrat Chowdhary. When I met him almost five years ago, I could not have imagined how strongly we would bond over this time. Suvrat is a great scientist and one of the warmest and loveliest people I have met in my life. Ultimately, this newfound friendship is the most important result of my Ph. D. years.

Additionally, I want to thank Prof. Dr. Joachim Heberle and Dr. Kenichi Ataka for a fruitful collaboration. Furthermore, I would like to acknowledge the assistance of the Core Facility BioSupraMol.

Furthermore, I would like to thank the CRC 1349 "Fluorine-Specific Interactions: Fundamentals and Functions" and the "Studienstiftung des deutschen Volkes" for financial support.

I thank my family, especially my mom and grandma, and my friends for a lot of support, love, and encouragement, without which none of this would be possible. Finally, I would like to thank Selina. She has been by my side throughout years of study and my Ph. D., making these the best years of my life.

---

## Abstract

Peptide and protein engineering are indispensable to obtaining biomolecules with specific properties. The element fluorine can be a valuable tool in this regard. In the last decades, the influence of fluorine on a wide range of different properties of peptides and proteins, such as secondary structure formation, protein-protein interactions, and proteolytic stability, was intensively studied. Various design principles for applying fluorinated amino acids to produce compounds with desired properties have been established. Nevertheless, peptides, which are predominantly composed of fluorinated building blocks, are still widely unexplored. Additionally, the application of highly fluorinated sequences in the rational design of peptide self-assembly processes is poorly understood, the outcome is still challenging to predict, and previous strategies exclusively relied on classic fluorous interactions.

In the first work of this doctoral thesis, the stereoselective gram-scale synthesis of different aliphatic fluorinated amino acids was developed. A chiral Ni(II) complex was used as a starting material to produce the desired Fmoc-protected fluorinated amino acids in a two-step synthesis. First, the respective complex was diastereoselectively alkylated with fluorinated alkyl iodides. Subsequently, acidic hydrolysis and Fmoc-protection yielded the desired product in great yields and with excellent enantiomeric purities. Additionally, a strategy to produce commercially unavailable fluorinated alkyl iodides from corresponding fluorinated alcohols was described. Finally, the obtained fluorinated amino acids were characterized concerning their hydrophobicity and  $\alpha$ -helix propensity. This work provided a crucial foundation for this doctoral thesis to allow subsequent investigation of new, highly fluorinated peptides.

The second project focused on synthesizing and characterizing *de novo* polyfluorinated peptides (fluoropeptides). A fluoropeptide library was synthesized with sequences of different lengths and degrees of fluorination. The structural properties of this new class of peptides were studied in the presence of micelles and liposomes. In general, for non-, mono-, and difluorinated side chains containing fluoropeptides,  $\beta$ -strand to  $\alpha$ -helix transition was observed in micelle and liposome environments. On the contrary, peptides consisting of trifluorinated residues displayed the formation of an extended polyproline type II helix. The corresponding structural properties were investigated *via* circular dichroism and a fluorescence-based leakage assay and confirmed by surface-enhanced infrared absorption spectroscopy. Additionally, log *P* values of the fluoropeptides were estimated and connected to observed trends. Finally, HPLC-based proteolytic resistance studies revealed that shorter fluoropeptides were degradable in the presence of two different serine proteases. This work demonstrated the intriguing potential of highly fluorinated peptides for developing polyfluorinated biomaterials.

---

Finally, fluorine-directed coiled coil assembly was investigated. In the context of this work, fluorinated derivatives of valine, isoleucine, and *allo*-isoleucine were incorporated at positions *a* of the parallel heterodimeric VPK/VPE model, resulting in a comprehensive combinatorial VPK/VPE peptide library. Using different diastereomers of trifluorovaline and trifluoroisoleucine residues allowed the study of the influence of fluorination and corresponding stereochemistry on structural and thermodynamic properties. Each coiled coil pair was investigated *via* circular dichroism, size exclusion chromatography, and Förster resonance energy transfer measurements. Thus, it was demonstrated that all fluorinated coiled coil pairs altered the oligomerization degree of the CC motif from dimeric to trimeric coiled coils. Furthermore, thermal denaturation studies revealed different trends in the respective stabilities between various combinations. These differences were exploited to design and predict fluorine-guided coiled coil assembly processes. Depending on the fluorinated amino acid used in this context, coiled coil formation was turned on or off, introducing a new tool for rationalizing and controlling peptide-peptide interactions.

---

## Kurzzusammenfassung

Das Peptid- und Protein-Engineering ist unerlässlich, um Biomoleküle mit spezifischen Eigenschaften zu erzeugen. Das Element Fluor kann in dieser Hinsicht ein wertvolles Werkzeug sein. In den letzten Jahrzehnten wurde der Einfluss von Fluor auf eine Vielzahl unterschiedlicher Eigenschaften von Peptiden und Proteinen, wie z. B. die Bildung von Sekundärstrukturen, Protein-Protein-Wechselwirkungen und proteolytische Stabilität, intensiv untersucht. Inzwischen sind verschiedene Designprinzipien für den Einsatz fluorierter Aminosäuren zur Herstellung von Verbindungen mit gewünschten Eigenschaften etabliert. Dennoch sind Peptide, die überwiegend aus fluorierten Aminosäuren bestehen, noch weitgehend unerforscht. Darüber hinaus ist die Anwendung hochfluorierter Sequenzen beim rationalen Design von Peptidselfassemblierungsprozessen nur unzureichend verstanden, das Ergebnis ist nach wie vor schwer vorherzusagen, und bisherige Strategien beruhen ausschließlich auf der Nutzung klassischer „fluoriger“ Wechselwirkungen.

In der ersten Arbeit dieser Dissertation wurde die stereoselektive Synthese von verschiedenen aliphatischen fluorierten Aminosäuren im Gramm-Maßstab entwickelt. Ein chiraler Ni(II)-Komplex wurde als Ausgangsmaterial verwendet, um die gewünschten Fmoc-geschützten fluorierten Aminosäuren in einer zweistufigen Synthese zu erhalten. Zunächst wurde der entsprechende Komplex diastereoselektiv mit fluorierten Alkyljodiden umgesetzt. Anschließend wurden nach saurer Hydrolyse und Fmoc-Schützung die gewünschten Produkte in guten Ausbeuten und mit ausgezeichneten enantiomeren Reinheiten isoliert. Darüber hinaus wurde eine Strategie zur Herstellung kommerziell nicht erhältlicher fluorierter Alkyljodide aus den entsprechenden fluorierten Alkoholen beschrieben. Schließlich wurden die erhaltenen fluorierten Aminosäuren im Hinblick auf ihre Hydrophobie und  $\alpha$ -Helix Propensität charakterisiert. Diese Arbeit lieferte eine entscheidende Grundlage für diese Doktorarbeit, um die anschließende Untersuchung von hochfluorierten Peptidmodellen zu ermöglichen.

Das zweite Projekt konzentrierte sich auf die Synthese und Charakterisierung von *de novo* polyfluorierten Peptiden (Fluorpeptiden). Es wurde eine Fluorpeptidbibliothek mit Sequenzen unterschiedlicher Länge und Fluorierungsgraden synthetisiert. Die strukturellen Eigenschaften dieser neuen Klasse von Peptiden wurden in Gegenwart von Mizellen und Liposomen untersucht. Im Allgemeinen wurde für nicht-, mono- und difluorierte Seitenketten enthaltende Fluorpeptide ein Übergang von einem  $\beta$ -Strang zu einer  $\alpha$ -Helix in der Umgebung von Mizellen und Liposomen beobachtet. Im Gegensatz dazu zeigten Peptide, die aus trifluorierten Bausteinen bestehen, die Bildung einer verlängerten Polyprolin Typ II Helix. Die entsprechenden strukturellen Eigenschaften wurden mittels Circular dichroismus und einem fluoreszenzbasierten „Leakage-Assay“ untersucht und durch „Surface enhanced infrared

---

absorption spectroscopy“ bestätigt. Zusätzlich wurden die  $\log P$  Werte der Fluoropeptide geschätzt und mit den beobachteten Trends in Verbindung gebracht. Abschließend zeigten HPLC-basierte proteolytische Resistenzstudien, dass kürzere Fluoropeptide in Gegenwart von zwei verschiedenen Serinproteasen abbaubar sind. Diese Arbeit verdeutlicht das faszinierende Potenzial hochfluorierter Sequenzen für die Entwicklung polyfluorierter Biomaterialien.

Schließlich wurde das fluorgesteuerte Assemblierungsverhalten von Coiled Coil Motiven untersucht. Im Rahmen dieser Arbeit wurden fluoriierte Derivate von Valin, Isoleucin und *allo*-Isoleucin an den Positionen *a* des parallelen heterodimeren VPK/VPE-Modells eingebaut, was in einer kombinatorischen Bibliothek bestehend aus VPK/VPE Peptiden resultierte. Die Verwendung verschiedener Diastereomere von Trifluorovalin- und Trifluorisoleucinresten ermöglichte die Untersuchung des Einflusses der Fluorierung und der entsprechenden Stereochemie auf die strukturellen und thermodynamischen Eigenschaften. Jede Kombination wurde mittels Circular dichroismus, Größenausschlusschromatographie und Förster-Resonanzenergietransfermessungen untersucht. Dabei zeigte sich, dass alle fluoriierten Paare den Oligomerisierungsgrad des CC-Motivs von dimeren zu trimeren Strukturen veränderten. Darüber hinaus ergaben thermische Denaturierungsstudien unterschiedliche Trends in Stabilitäten zwischen den jeweiligen Kombinationen. Diese Unterschiede wurden genutzt, um fluordirigierte Coiled Coil Assemblierungsprozesse rational zu steuern. Je nach der in diesem Zusammenhang verwendeten fluoriierten Aminosäure wurde die Bildung von Coiled Coil Strukturen ein- und ausgeschaltet, womit ein weiteres Werkzeug für das rationale Design und die Kontrolle von Peptid-Peptid-Wechselwirkungen eingeführt wurde.



---

## Table of Contents

<b>1</b>	<b>Introduction</b> .....	<b>1</b>
<b>2</b>	<b>Organofluorine Chemistry – The Nature of the C-F Bond</b> .....	<b>3</b>
	2.1 <i>Fundamental properties of fluorine</i> .....	3
	2.2 <i>The role of fluorine in non-covalent interactions</i> .....	14
	2.3 <i>Fluorine in medicinal and bioorganic chemistry</i> .....	21
<b>3</b>	<b>Synthetic Strategies to Obtain Fluorinated Amino Acids</b> .....	<b>28</b>
	3.1 <i>Stereoselective synthesis of fluorinated aliphatic amino acids</i> .....	29
	3.2 <i>Chiral nickel(II) complexes for the asymmetric synthesis of fluorinated amino acids</i> ...	35
<b>4</b>	<b>Highly Fluorinated Peptide Structures - Properties and Applications</b> .....	<b>44</b>
	4.1 <i>Peptide-based perfluorinated systems</i> .....	44
	4.2 <i>Perfluorinated coiled coil motifs</i> .....	53
<b>5</b>	<b>Aim of this doctoral thesis</b> .....	<b>63</b>
<b>6</b>	<b>Published work</b> .....	<b>65</b>
	6.1 <i>Gram-scale asymmetric synthesis of fluorinated amino acids using a chiral nickel(II) complex</i> .....	66
	6.2 <i>Introducing aliphatic fluoropeptides: perspectives on folding properties, membrane partition and proteolytic stability</i> .....	70
	6.3 <i>Establishing fluorine containing amino acids as an orthogonal tool in coiled coil assembly</i> .....	75
<b>7</b>	<b>Unpublished Results – All-Cis Pentafluorinated Cyclohexylalanine</b> .....	<b>81</b>
<b>8</b>	<b>Experimental Section</b> .....	<b>88</b>
	8.1 <i>General information</i> .....	88
	8.2 <i>Peptide synthesis and characterization</i> .....	91
<b>9</b>	<b>Summary and Outlook</b> .....	<b>95</b>
<b>10</b>	<b>Bibliography</b> .....	<b>102</b>

---

## List of abbreviations

X	electronegativity
6-FAM	6-carboxyfluorescein
(4 <i>R</i> )-Hyp	(4 <i>R</i> )-hydroxyproline
5-FU	5-Fluorouracil
3-NO <sub>2</sub> -Tyr	3-nitrotyrosine
aaRS	aminoacyl tRNA synthetases
Abu	2-aminobutyric acid
Aib	aminoisobutyric acid
AIBN	azobisisobutyronitril
ATP	adenosine triphosphate
AUC	analytical ultracentrifugation
BDE	bond-dissociation energy
Boc <sub>2</sub> O	<i>tert</i> -butoxycarbonyl anhydride
BPB	2-[ <i>N</i> -( <i>N</i> '-benzylpropyl)amino]-benzophenone
BPTI	bovine pancreatic trypsin inhibitor
CC	coiled coil
CD	circular dichroism
Cha	cyclohexylalanine
CH <sub>2</sub> FAH <sub>4</sub>	methylene tetrahydrofolic acid cofactor
CMBP	cyanomethylene tributylphosphorane
CPP	cell-penetrating peptide
DABCO	1,4-diazabicyclo[2.2.2]octane
DAST	diethylaminosulfur trifluoride
DEA	disulfide exchange assay
DFT	density functional theory
DIC	<i>N,N</i> ' diisopropylcarbodiimide
DIPEA	diisopropylethylamine
DMF	dimethylformamide
DNA	deoxyribonucleic acid
DSA	disulfide exchange assay
E <sub>ea</sub>	electron affinity
Fmoc	fluorenylmethoxycarbonyl
Fmoc-OSu	<i>N</i> -(fluorenyl-9-methoxycarbonyloxy)-succinimid

---

FRET	fluorescence resonance energy transfer
GABA	$\gamma$ -aminobutyric acid
HFA	hexafluoroacetone
HF <i>i</i> P	hexafluoroisopropanol
HPLC	high-performance liquid chromatography
HRMS	high-resolution mass spectrometry
IE	ionization energy
KHMDS	potassium hexamethyldisilazide
KIH	knobs-into-holes
LUV	large unilamellar vesicle
MRI	magnetic resonance imaging
NMP	<i>N</i> -methyl-2-pyrrolidone
NMR	nuclear magnetic resonance
NOESY	nuclear overhauser enhancement and exchange spectroscopy
<i>o</i> Abz	<i>ortho</i> -aminobenzoic acid
Oxyma	ethyl cyanohydroxyiminoacetate
PAAP	2-( <i>N</i> -( $\alpha$ -picolyl)amino)acetophenone
<i>p</i> Abz	<i>para</i> -aminobenzoic acid
PEG	polyethylene glycol
PFP	perfluoro- <i>n</i> -pentane
PNA	peptide nucleic acid
POPC	1-palmitoyl-2-oleoyl- <i>sn</i> -glycero-3-phosphocholine
POPG	1-palmitoyl-2-oleoyl- <i>sn</i> -glycero-3-(phosphor-rac-(1-glycerol))
PSE	periodic system of elements
PTFE	polytetrafluoroethylene
SDS	sodium dodecyl sulfate
SEC-MALS	size exclusion chromatography – multi-angle light scattering
SEIRAS	surface enhanced infrared absorption spectroscopy
SOAT	second order asymmetric transformation
SPPS	solid-phase peptide synthesis
TASF	tris(dimethylamino)sulfonium difluorotrimethylsilicate
TBAF( <i>t</i> BuOH) <sub>4</sub>	tetrabutylammonium tetra( <i>tert</i> -butanol) fluoride
TEMPO	(2,2,6,6-tetramethylpiperidin-1-yl)oxyl
TFA	trifluoroacetic acid
TFE	2,2,2-trifluoroethan-1-ol
TMGA	tetramethylguanidinium azide

---

---

tRNA	transfer ribonucleic acid
------	---------------------------

### Fluorinated amino acids

[2,3,4,5,6F]Phe	2,3,4,5,6-pentafluorophenylalanine
[2,3,5,6F][4I]Phe	2,3,5,6-tetrafluoro-4-iodophenylalanine
[3,5F]Phe	3,5-difluorophenylalanine
[4F]Phe	4-fluorophenylalanine
4-FPro	4-fluoroproline
DfeGly	difluoroethylglycine
DfpGly	difluoropropylglycine
F <sup>5</sup> -Cha	<i>all-cis</i> pentafluorinated cyclohexylalanine
F5-Phe	pentafluorophenylalanine
HfLeu	5,5,5',5',5'-hexafluoroleucine
HfVal	hexafluorovaline
MfeGly	monofluoroethylglycine
PfpGly	pentafluoropropylglycine
TfeGly	trifluoroethylglycine
TfIle	trifluoroisoleucine
TfLeu	trifluoroleucine
TfVal	trifluorovaline

The one- and three-letter code for the amino acids were used as recommended by the IUPAC-IUB Joint Commission in Biochemical Nomenclature (JCBN) [*Eur. J. Biochem.* **1984**, *138*, 9-37].

## 1 Introduction

„Man erhält diese wichtige Verbindung, wenn man ein Gemische von Fluorkalium und schwefelsaurem Methylen gelinde erwärmt, was in Glasgefäßen geschehen kann. Das neue Product ist ein Gas, welches man, um es von allen fremden Körpern zu befreien, über Wasser aufsammeln kann.“<sup>[1]</sup> (“This important compound is obtained by gently warming a mixture of potassium fluoride and sulfur acidic methylene, which can be accomplished in glass vessels. The new product is a gas which, in order to free it from all foreign bodies, can be collected over water.”) With these words, Dumas and Peligot described the first synthesis of an organofluorine compound, fluoromethane, half a century before the first isolation of elemental fluorine by Henri Moissan in 1886.<sup>[2,3]</sup> The achievements of the 19th century were the spark for the spectacular development of fluorine chemistry in the 20th century. In the 1930s, organofluorochemistry reached an industrial scale, which can be explained by the introduction of chlorofluorocarbons as refrigerants and by the start of the Manhattan Project and the associated development of highly resistant materials. Today, fluorine-containing compounds are essential in various fields, such as polymer and material sciences and the development of pharmaceuticals and agrochemicals.<sup>[4,5]</sup> Approximately 20% of drug molecules and 50% of agrochemicals developed in the last 30 years include fluorine.<sup>[3,6]</sup> The current trend indicates that these numbers will continue to rise over the next 10 to 15 years.<sup>[7]</sup>

This decisive role of fluorine in life sciences might be surprising at first glance since fluorine, despite its abundance in the earth's crust (13<sup>th</sup> most common element), scarcely occurs in the biosphere. The reasons for this are, firstly, the poor solubility of the main minerals, fluorspar ( $\text{CaF}_2$ ), fluorapatite ( $\text{Ca}_5(\text{PO}_4)_3\text{F}$ ), and cryolite ( $\text{Na}_3\text{AlF}_6$ ) and, secondly, the high oxidation potential of fluorine and the strong hydration of fluoride ions, which significantly lowers the corresponding nucleophilicity.<sup>[7]</sup> Nevertheless, some organisms have succeeded in producing fluorine-containing compounds. A well-known example is the poisonous *Dichapetalum cymosum*, from which the compound fluoroacetate **1** was isolated in 1943 (*Figure 1.1, a.*).<sup>[8]</sup> Additionally, several microorganisms, such as *Streptomyces cattleya*, also possess the ability to produce fluoroacetate. Fluoroacetate **1** is a highly toxic compound whose toxicity is caused by inhibiting the citrate cycle *via* corresponding metabolites.

Dong *et al.* elucidated the exact incorporation mechanism involving the fluorinase enzyme *via* crystallization studies (*Figure 1.1, b.*). Fluorinase increases the nucleophilicity of the fluoride ion by displacing water molecules and simultaneously forming a hydrogen bond network (*Figure 1.1, c.*).<sup>[9]</sup>

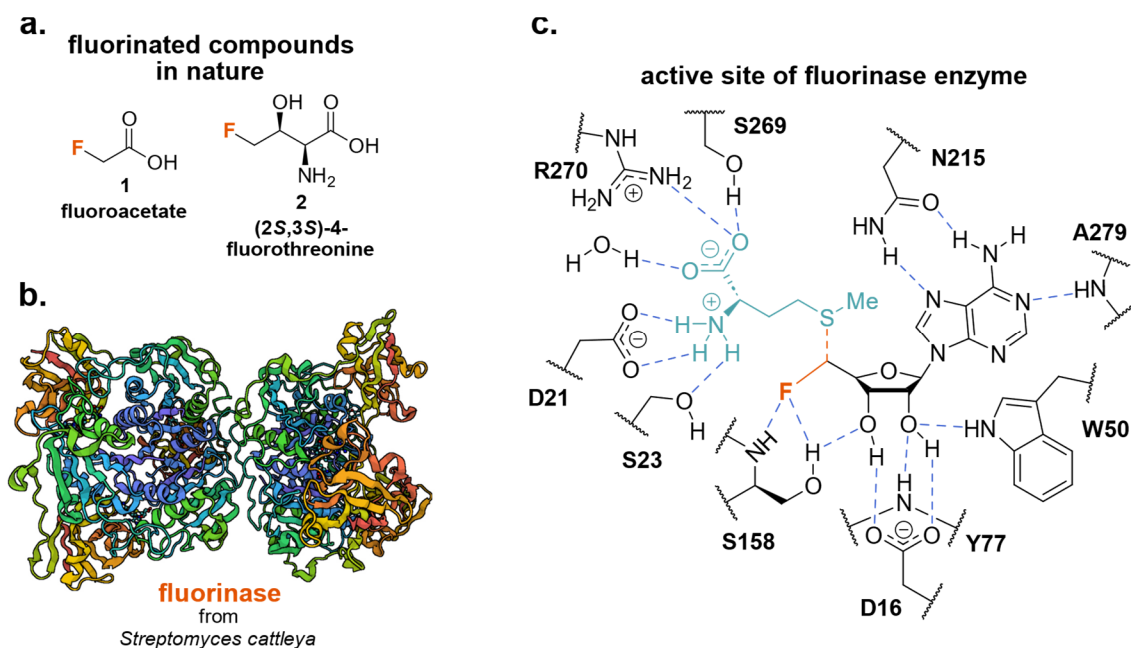


Figure 1.1: a. Structures of fluoroacetate and (2S,3S)-4-fluorothreonine. b. Crystal structure of fluorinase enzyme (PDB: 1RQP) (Created with BioRender®). c. Fluorination mechanism of fluorinase enzyme (active site shown).

An additional fluorinated compound produced in microorganisms *via* the fluorinase pathway is (2S,3S)-4-fluorothreonine **2**, the only fluorinated amino acid found in nature (Figure 1.1, a.).<sup>[7]</sup>

In the last years, general health concerns surrounding organofluorine compounds have emerged.<sup>[7,10]</sup> Deeper insights into the metabolism of fluorine-containing organic molecules hint at a potential health risk from the formation of toxic compounds, such as fluoroacetate. Furthermore, perfluorinated compounds, such as perfluoroalkyl acids, can cause environmental problems due to their chemical inertness and durability.<sup>[7]</sup>

In peptide and protein chemistry, fluorine has emerged as a precious tool affecting several different properties, such as thermal stability, proteolytic resistance, and secondary structure formation. In the last 30 years, some principles that allow rational design of fluorinated peptide and protein models with desired properties have been developed. However, usually incorporating fluorinated building blocks occurs in small numbers and at specific positions.<sup>[11–13]</sup> Peptides built exclusively by fluorinated amino acids are still widely unexplored. Nevertheless, studies of these systems could reveal intriguing properties that combine the advantages of perfluorinated organic molecules with the concomitant degradability of peptides, thus contributing to developing a new class of biopolymers.

## 2 Organofluorine Chemistry – The Nature of the C-F Bond

The multifaceted success story of organofluorine chemistry, lasting more than 150 years, can ultimately be attributed to one point of origin: the fascinating and fundamental properties of the element fluorine. In this chapter, the basic requirements for a rational design of fluorinated model systems in the field of bioorganic chemistry will be explained in detail. First, the atomic physical properties of fluorine will be discussed. Subsequently, it will be demonstrated how these can dominate the characteristics of the carbon-fluorine bond. From the nature of the C-F bond and its influence on different properties of organic molecules, the focus will be moved to perfluorinated compounds with a subsequent discussion of the respective physical and chemical properties. In the second part of this section, it will be shown that these properties can define the non-covalent interactions between molecules in many ways. Again, moving from partial introduction to polyfluorination, first, the influence of a single C-F bond, then of fluorinated groups, and finally of highly fluorinated molecules on the control of intermolecular interactions will be addressed. To conclude the chapter, the large footprint of the entity of the discussed atomic, molecular, and intermolecular properties of fluorine in medicinal and bioorganic chemistry will be highlighted.

### 2.1 Fundamental properties of fluorine

The look at the position of fluorine ( $1s^2 2s^2 2p^5$ ) in the periodic system of elements (PSE) rapidly illustrates the origin of its most fundamental properties (*Figure 2.1*).<sup>[14–17]</sup> The highest nuclear charge of all elements of the second period, besides the noble gas neon, leads to tight interactions with the electrons of the valence shell. This is evident by the small atomic radius of fluorine (64 pm).<sup>[15]</sup> For comparison, consideration of adjacent groups to the left of fluorine shows that the atomic radius increases as the charge of the nucleus declines. Needless to say, the main group elements of the third period feature a larger atomic radius due to an additional electron shell. Based on these considerations, further decisive properties of fluorine can be explained: ionization energy (IE), electron affinity ( $E_{ea}$ ), and bond-dissociation energy (BDE). Due to the tight holding of the electrons to the nucleus, a large amount of energy is needed to remove one electron from the respective valence shell, leading to the highest value of all main group elements (17.42 eV) besides the group 8 (noble gases) elements. Next to one of the highest IE values, fluorine also possesses the greatest electron affinity of the second period, following the expected trend from the left to the right side of the PSE.<sup>[15]</sup> The respective valence shell is fully occupied by accepting an additional electron, and the positive nucleus stabilizes the negative charge.

	<b>Li</b>	<b>Be</b>	<b>B</b>	<b>C</b>	<b>N</b>	<b>O</b>	<b>F</b>
	1.57 Å	1.11 Å	0.82 Å	0.77 Å	0.70 Å	0.66 Å	0.64 Å
IE [eV]	5.32	9.32	8.30	11.26	14.53	13.36	17.42
E <sub>ea</sub> [eV]	-0.62	+0.50	-0.28	-1.26	+0.07	-1.46	-3.40
X	0.98	1.57	2.04	2.55	3.04	3.44	3.98
X <sub>2</sub> BDE [kJ]	106.5	10	297	607	945.3	498.3	157.9
X <sub>2</sub> bond length [Å]	2.67	2.51	1.59	1.24	1.10	1.21	1.42

	<b>Na</b>	<b>Mg</b>	<b>Al</b>	<b>Si</b>	<b>P</b>	<b>S</b>	<b>Cl</b>
	1.91 Å	1.60 Å	1.43 Å	1.17 Å	1.10 Å	1.04 Å	0.99 Å
IE [eV]	5.14	7.64	5.98	8.15	10.49	10.36	12.97
E <sub>ea</sub> [eV]	-0.55	+0.40	-0.46	-1.39	-0.75	-2.08	-3.62
X	0.93	1.31	1.61	1.90	2.19	2.58	3.16
X <sub>2</sub> BDE [kJ]	77	8.6	186.2	326.8	489.5	425.0	242.6
X <sub>2</sub> bond length [Å]	/	/	/	/	/	/	1.98

Figure 2.1: Properties of the elements of the second and third period. The corresponding data were taken from references [14-17, 18].

Interestingly, chlorine has an even higher electron affinity value, although the nucleus is more distant from the valence shell. This can be explained by the destabilizing repulsive interactions of free electron pairs in the case of the fluorine atom.<sup>[5]</sup> Due to the larger size, this aspect plays a minor role in the chlorine atom. The repulsive interactions of the electron pairs also have significant importance for the low bond strength of the fluorine dimer. The BDE value for F<sub>2</sub> is significantly lower (157.9 kJ) than the respective values of the neighboring elements. The strong attraction of the positive cores towards the valence electrons ensures that the F-F bond is very short (1.42 Å), resulting in the proximity of the corresponding free electron pairs, thus strongly destabilizing the overall system.<sup>[4,5]</sup>

So, what effects can be expected when fluorine is introduced into organic molecules? To tackle this question, the immediate impact on the most fundamental building block of organofluorine chemistry, the carbon-fluorine bond, should be addressed first. Electronegativity ( $\chi$ ), introduced by Linus Pauling in 1932, describes the tendency of atoms in the context of chemical bonds to pull the corresponding bond electrons towards themselves. Suppose the strong attraction to electrons originating from the nucleus of the fluorine atom is considered. In that case, it is not surprising that the highest electron negativity value of the PSE was assigned to the element fluorine (3.98).<sup>[18]</sup> Also, according to the definition of electronegativity, in a bond between atom A and atom B (A-B), the difference in the electronegativity values of the two atoms ( $|\chi(A) - \chi(B)|$ ) describes the partial ionic character of the A-B bond.



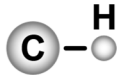
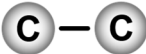
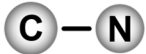
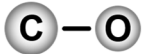
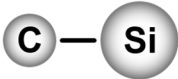
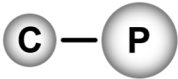
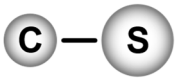
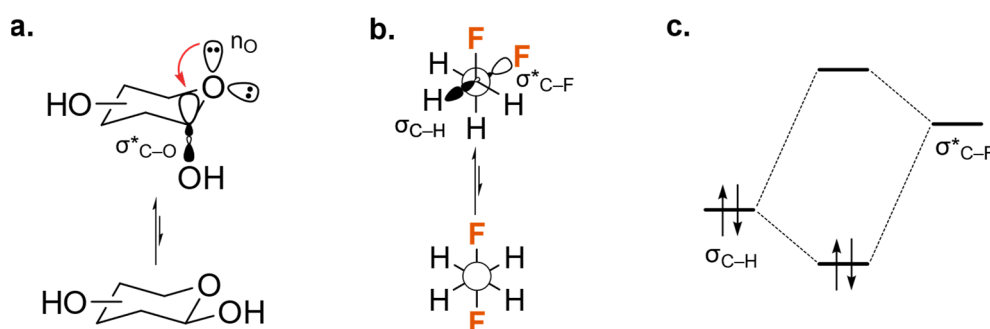
	<b>bond length [pm]</b>	109			
	<b>bond dissociation energy [kcal mol<sup>-1</sup>]</b>	98.8			
					
<b>bond length [pm]</b>	154	147	143	135	
<b>bond dissociation energy [kcal mol<sup>-1</sup>]</b>	83.1	69.7	84.0	105.4	
					
<b>bond length [pm]</b>	185	184	182	177	
<b>bond dissociation energy [kcal mol<sup>-1</sup>]</b>	73.1	63.1	69.0	83.1	

Figure 2.2: Properties of selected C-X bonds. The corresponding data were taken from references [14, 19].

In the case of the C-F bond, it means a difference in electronegativity values of 2.5, corresponding to a high ionic character of approximately 68%.<sup>[14]</sup> Therefore, the C-F bond can be better described as an ionic rather than a covalent bond. This consideration leads to two main properties of the carbon-fluorine bond: the short bond length (135 pm) and the highest bond dissociation energy in organic chemistry (105.4 kcal mol<sup>-1</sup>). Figure 2.2 compares the chemical bonds of carbon with other important elements.<sup>[14,19]</sup> It highlights the unique nature of the C-F bond in organic chemistry. Looking at the carbon bonds with other elements of the second and third periods shows that the C-F bond has the shortest length, except for the C-H bond, which has a length of 109 pm. These considerations and comparing atomic radii reveal another vital characteristic of organofluorine chemistry. The hydrogen atoms of organic compounds can be substituted by fluorine without introducing large steric perturbations into the molecule. At the same time, a hydrogen-fluorine exchange can fundamentally change the respective properties of the molecules, such as hydrophobicity and metabolic stability, which will be discussed in more detail later in this section. A more conservative approach is substituting a C-F bond for a C-O bond. This does not change the electronic properties of the molecule drastically as the respective C-H substitution but can significantly change the hydrogen bonding properties of the molecule.

So, as already noted, the introduction of fluorine causes a massive change in the **stereo-electronic properties** of organic molecules. Probably the most intuitive influence of fluorine on the steric of molecules are the **dipole-dipole interactions**. A look at the conformations of  $\alpha$ -fluorinated aldehyde<sup>[20]</sup>, ketone<sup>[21]</sup>, ester<sup>[22]</sup>, and amide<sup>[23]</sup> species demonstrates that the C-F bond has a strong preference to align itself *anti-periplanar* to the respective carbonyl group. This effect increases significantly with the strength of the dipole of the corresponding functional group next to the fluorine atom (amide>ester>ketone>aldehyde).

In the 70s, several studies focused on the structural properties of 1,2-difluoroethane, and a somewhat unusual conformational preference was observed. The sterically more hindered *gauche* conformation seemed more dominant over the sterically least demanding *anti*-conformation.<sup>[24]</sup> An explanation for this finding, described as the **fluorine *gauche* effect**, was hidden in a well-known phenomenon of carbohydrate chemistry: the anomeric effect (*Figure 2.3, a.*). It describes the preference of a heteroatomic group (e.g., C-O) to occupy the sterically more hindered axial position over the equatorial position when being in proximity to a heteroatom of a heterocyclic system.<sup>[24]</sup> The source of stabilization in this context is the hyperconjugation of a free electron pair of the heteroatom ( $n_o$ ) into the antibonding orbital of the C-O bond ( $\sigma^*_{C-O}$ ).



*Figure 2.3: a.* Anomeric effect in carbohydrate chemistry. *b.* Fluorine *gauche* effect in 1,2-difluoroethane. *c.* MO-scheme of the respective hyperconjugative interactions.

In 1990, Dunitz and co-workers achieved a milestone describing the anomeric effect in fluoromethylamine. High-level *ab initio* calculations revealed that the *anti*-conformation (free electron pair of nitrogen *anti-periplanar* to the C-F bond) is 7.5 kcal mol<sup>-1</sup> more stable than the respective *perpendicular* conformation. The corresponding hyperconjugation ( $n_N \rightarrow \sigma^*_{C-F}$ ) extends the length of the C-F bond and shortens the C-N bond.<sup>[25]</sup> Six years later, Christen *et al.* observed a similar effect investigating the conformational properties of (fluoromethyl)dimethylamine.<sup>[26]</sup> Two criteria must be met to ensure successful hyperconjugation: the correct orientation leading to a significant overlap of the respective orbitals and a small difference in orbital energies.<sup>[24]</sup> The strongest orbital overlap can be achieved when donor and acceptor groups adopt an *anti*-conformation (respective angle of 180°). Nevertheless, how can the seemingly favorable characteristics to participate in stabilizing hyperconjugation interactions of the anti-bonding molecule orbital of the C-F bond be explained? Again, the answer lies in the most fundamental properties of the fluorine atom. Due to the exceptionally high electronegativity of fluorine, the corresponding C-F bond has a low energy anti-bonding orbital ( $\sigma^*_{C-F}$ ) (*Figure 2.3, b., c.*).<sup>[19,24]</sup> This permits an accommodation of a free electron pair by the  $\sigma^*_{C-F}$  orbital. Now, the conformational preferences of 1,2-difluoroethane can be considered again. In this case, no free electron pair is available to stabilize the *gauche* conformation. However, a stabilizing hyperconjugation can occur between the binding  $\sigma_{C-H}$  orbital of the respective C-H bond and the

$\sigma^*_{\text{C-F}}$  orbital. Again, both bonds must adopt an *anti*-conformation.<sup>[19,24]</sup> In the instance of 1,2-difluoroethane, it quickly becomes evident that two simultaneous  $\sigma_{\text{C-H}} \rightarrow \sigma^*_{\text{C-F}}$  interactions stabilize the *gauche* conformation (refers to the two fluorine atoms) with a F-C-C-F dihedral angle of  $60^\circ$  (Figure 2.3, b.). Of course, when considering all the factors responsible for the classical fluorine *gauche* effect, it is evident that C-X can exchange the second C-F bond, with X being an electronegative substituent forming the F-C-C-X system. In the last two decades, fluorine *gauche* effect was observed with nitrogen<sup>[27]</sup>, oxygen<sup>[28]</sup>, and sulfur<sup>[29]</sup> atoms (Figure 2.4).

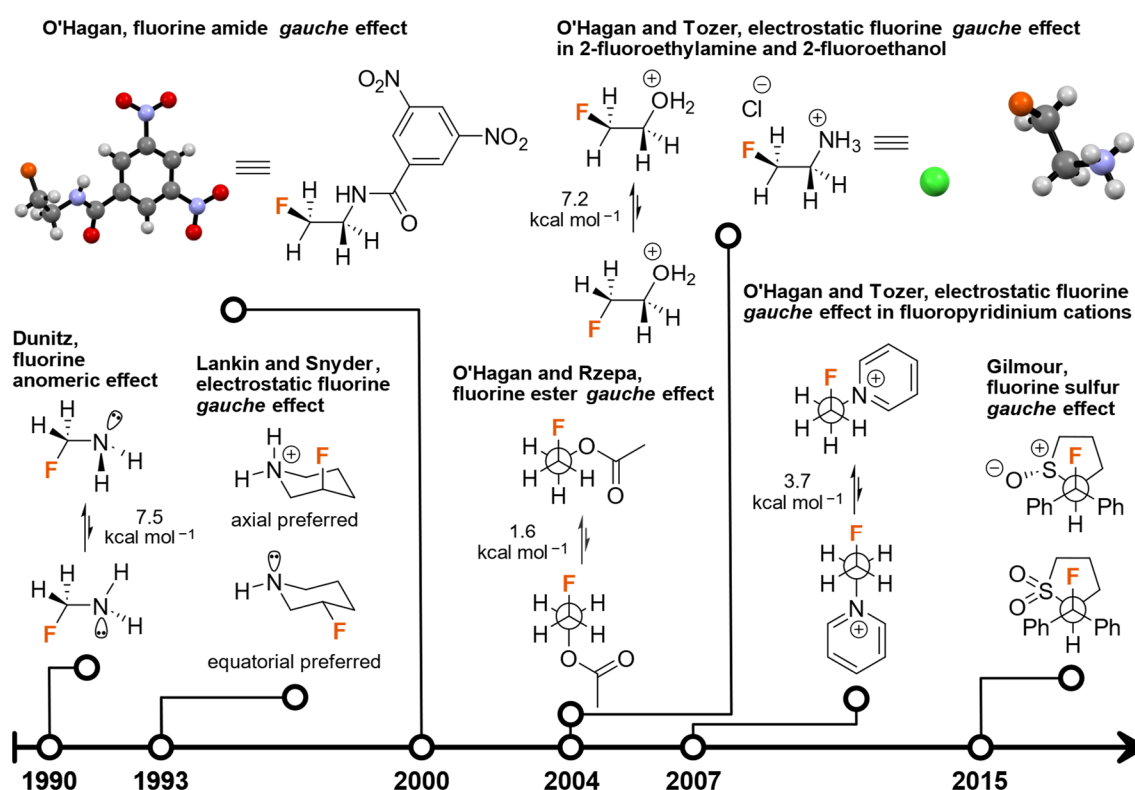
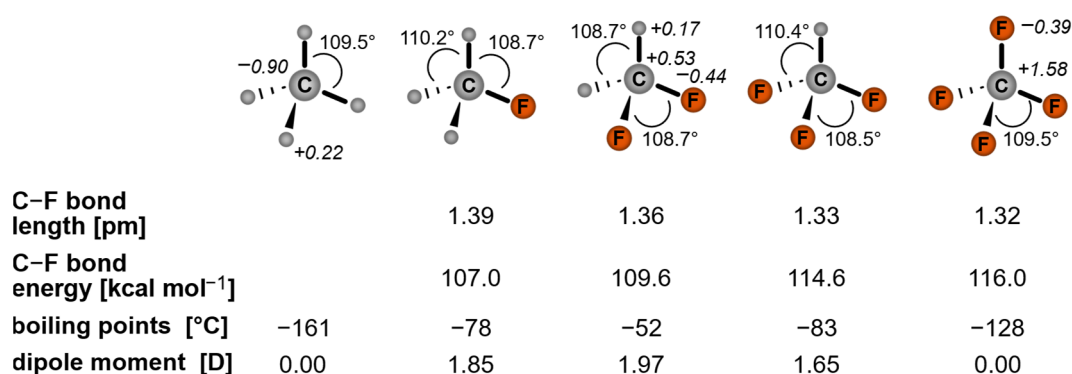


Figure 2.4: Development of the fluorine *gauche* effect over the last three decades (1-(*N*-(2-fluoroethyl)aminocarbonyl)-3,5-dinitrobenzene: CCDC number 143476; 2-fluoroethylammonium chloride: CCDC number 221927).

The fluorine *gauche* effect also has another dimension that can determine the conformational preference of the molecules. Snyder and Lankin were the first to describe the **electrostatic-driven fluorine *gauche* effect**. In 1993, protonated 3-fluoropiperidine compounds were investigated.<sup>[30]</sup> Solution nuclear magnetic resonance (NMR) studies<sup>[30]</sup> and, later, density functional theory (DFT) calculations<sup>[31]</sup> showed that the fluorine atom preferably occupies an axial position in protonated piperidine species (Figure 2.4). At the same time, the corresponding non-protonated structure accommodated the fluorine atom in the expected equatorial position. This strongly hints at favorable charge-dipole interactions, which direct the fluorine atom *syn-clinal* to the respective ammonium group. Later, the identical effect was described for dimethylammonium,<sup>[31]</sup> 4-membered and 8-membered heterocyclic structures<sup>[32]</sup>, quinoline

derivative<sup>[33]</sup>, protonated 2-fluorethylamine and 2-fluoroethanol systems<sup>[34]</sup>, and  $\beta$ -fluorinated pyridinium compounds.<sup>[35]</sup> The last example was studied to eliminate the possibility that intramolecular hydrogen bonds influence the conformational preferences of the described systems (*Figure 2.4*).

Up to this point, the influence of a single C-F bond on the steric properties of organic molecules was discussed. However, as already hinted by the consideration of 1,2-difluoroethane, introducing further C-F bonds leads to more complexity due to the resulting cooperative effects. A vivid illustration of this is the review of the **fluorinated derivatives of methane** (*Figure 2.5*).<sup>[4,19]</sup> Considering the series from fluoromethane to tetrafluoromethane, it quickly emerges that the bond length of the C-F bonds decreases while the respective bond dissociation energies increase. The strong ionic character of the C-F bond can explain these trends. With every additional fluorine atom attached to the carbon center, the positive charge density localized at the carbon atom increases. The negative charge density at the fluorine atoms remains nearly unaffected. This results in the formation of a  $C^{4\delta+}$  center in the case of the tetrafluoromethane, which exerts a stronger electrostatic attraction on the fluorine atoms compared to the  $C^{\delta+}$  carbon atom of the monofluorinated derivative. Next to the properties of the C-F bonds, adding other fluorine atoms influences the geometry of the individual molecules significantly. The H-C-H angle of fluoromethane is  $110.2^\circ$  and larger than the classical angle of a tetrahedral molecule of  $109.5^\circ$  but at the same time smaller than the corresponding angle of the difluorinated analog (*Figure 2.5*). The described trend can be explained by considering the orbital characteristics at the carbon center. Due to the low-lying  $\sigma^*$  orbital of the C-F bond, the  $sp^3$  hybridized carbon atom gains a stronger  $sp^2$  character, widening the corresponding H-C-H angle.<sup>[19]</sup>

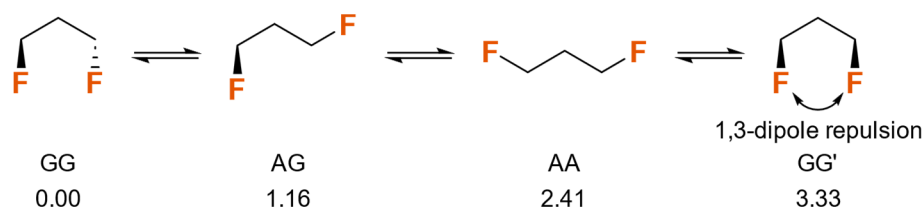


*Figure 2.5:* Properties of methane and its fluorinated analogs. Bond angles and partial charges are displayed within the structures. The corresponding data were taken from reference [4, 19].

Finally, by evaluating the dipole moments of the fluorinated methane series, the outcome of the fluorination grade on the polarity of the respective molecule is indicated. Partial fluorination leads to a more substantial overall dipole moment. Simultaneously, non-fluorinated

and tetrafluorinated molecules are nonpolar compounds. Similar considerations will reappear later when the influence of fluorination on the hydrophobicity of the molecules is discussed. Furthermore, the trend in polarity can be used to explain the respective boiling points of fluorinated methane derivatives. The non-polar  $\text{CH}_4$  and  $\text{CF}_4$  display the lowest boiling points, while the partially fluorinated species show significantly increased values (*Figure 2.5*).<sup>[4,19]</sup> The example of the fluorinated methane series powerfully demonstrates that the degree of fluorination must be considered when looking at fluorine's influence on the properties of organic molecules. Nevertheless, when the complexity arising from the synergy of several C-F bonds has a diverse outcome on the properties of one of the simplest organic molecules, methane, how will substituting multiple fluorine atoms into longer hydrocarbon chains affect their structural properties? To address this question, first, the influence of monofluorination at several positions and then the influence of total polyfluorination on the geometry of the hydrocarbons will be discussed.

The conformational preferences of 1,2-difluoroethane were already intensively discussed in the scope of this chapter. However, what would be the consequences of inserting a  $\text{CH}_2$  group between the two fluorinated carbon atoms on the corresponding conformational space? Will the *gauche* effect prevail as the most dominant factor, or should additional fluorine-induced interactions be considered? In the 1970s and 1980s, multiple studies were published focusing on the structural properties of 1,3-difluoropropane.<sup>[36–40]</sup> However, to this day, probably the most precise high-quality *ab initio* calculations were presented by Wu *et al.* in the late 1990s.<sup>[41]</sup> Respective energies of four possible conformations (GG: two  $\sigma_{\text{C-H}} \rightarrow \sigma^*_{\text{C-F}}$  interactions; AG: one  $\sigma_{\text{C-H}} \rightarrow \sigma^*_{\text{C-F}}$  interaction; AA: zero  $\sigma_{\text{C-H}} \rightarrow \sigma^*_{\text{C-F}}$  interactions; GG': two  $\sigma_{\text{C-H}} \rightarrow \sigma^*_{\text{C-F}}$  interactions) were calculated. The order of obtained conformational energies is as follows:  $\text{GG} < \text{AG} < \text{AA} < \text{GG}'$  (*Figure 2.6*). As expected, the conformational stability increases with increasing amount of stabilizing hyperconjugative interactions. Somewhat surprising in this context is the high energy of the GG' conformation despite the two stabilizing  $\sigma_{\text{C-H}} \rightarrow \sigma^*_{\text{C-F}}$  interactions.

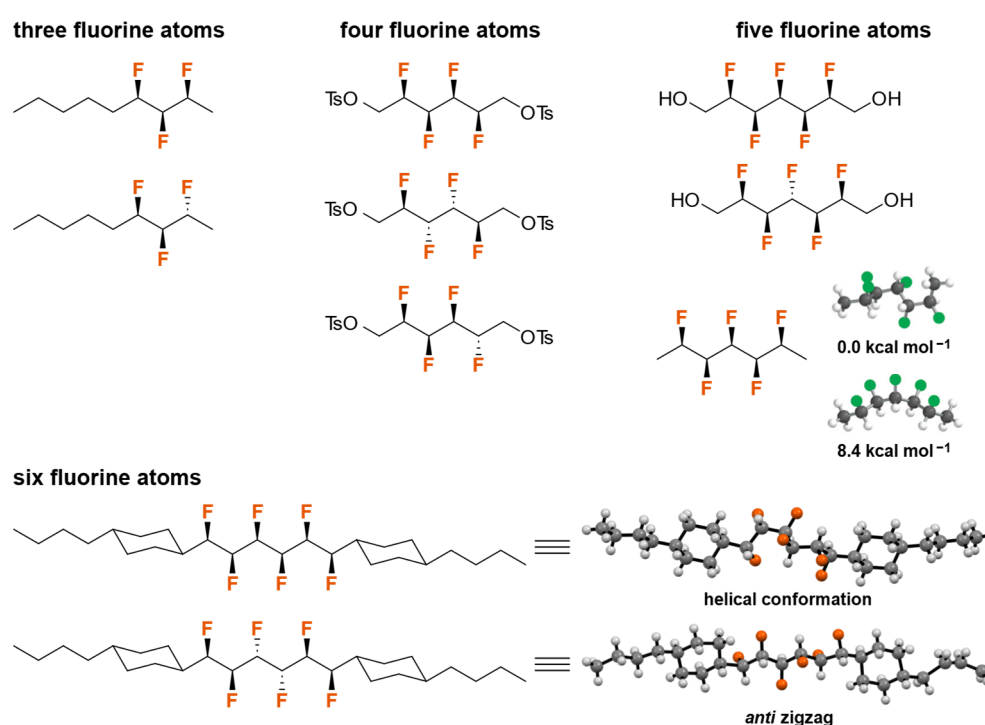


*Figure 2.6:* Four possible conformations of 1,3-difluoropropane.

This circumstance can be explained by the parallel orientation of the two C-F bonds and the resulting **1,3-dipole repulsion**. Furthermore, it is essential to emphasize that the destabilizing 1,3-interactions exhibit a stronger effect on the overall conformational stability than

the fluorine-induced *gauche* effect.<sup>[19,41]</sup> The interplay between the 1,2-*gauche* effect and the 1,3-dipole repulsion as directing forces behind the conformational properties of organofluorine compounds was further investigated by O'Hagan and co-workers by studying **partially fluorinated alkanes** with three, four, five, and six successive multivincinal fluoromethylene groups with fixed stereochemistries (*Figure 2.7*).<sup>[42–48]</sup>

Regardless of the number of fluoromethylene units, the conformational studies showed that the *all-syn* isomers preferentially adopted a helical arrangement, with the C-F bonds being rotated by 60° relative to the preceding one. The *anti*-isomers displayed a classical *anti* zigzag conformation. In both cases, the predominant force that directs the fluorinated molecule's conformational preference is avoidance of the 1,3-fluorine-fluorine dipole repulsion.<sup>[48]</sup>



*Figure 2.7:* Overview of multivincinal fluoromethylene compounds (1,1'-(1,2,3,4,5,6-hexafluorohexane-1,6-diyl)bis(4-*n*-butylcyclohexane): CCDC number 721047, 721048). DFT calculated (B3LYP/6-31G(d)) conformations of *all-syn* pentafluoroheptane were adapted from O'Hagan with permission (Copyright © 2012 American Chemical Society)<sup>[48]</sup>.

The O'Hagan working group continued to study multivincinal fluorinated systems, moving from acyclic to cyclic compounds. Introducing fluorine exclusively on one side of a cycloalkane molecule leads to the formation of a system with a fluorine face and a hydrogen face. To this consideration, this class of molecules owes its name **Janus face cycloalkanes**, named after the two-faced Roman god.<sup>[49]</sup> The first synthesis and structural analysis of such a molecule was described by Durie *et al.* in 2011.<sup>[50]</sup> The *all-syn*-1,2,3,4-tetrafluorocyclohexane **3** was synthesized in eight steps and analyzed using NMR spectroscopy and X-ray diffraction. In contrast to the multivincinal fluorinated acyclic models, stereoselectively fluorinated

cycloalkanes can force C-F bonds to engage in 1,3-dipole interactions since at least four substitutions lock two fluorine atoms into 1,3-diaxial arrangements. This interaction has the consequence of highly increasing the ground state energy of the system, which is the main reason for a broad range of specific properties of this class of fluorinated molecules that will be discussed later in this chapter.<sup>[50]</sup>

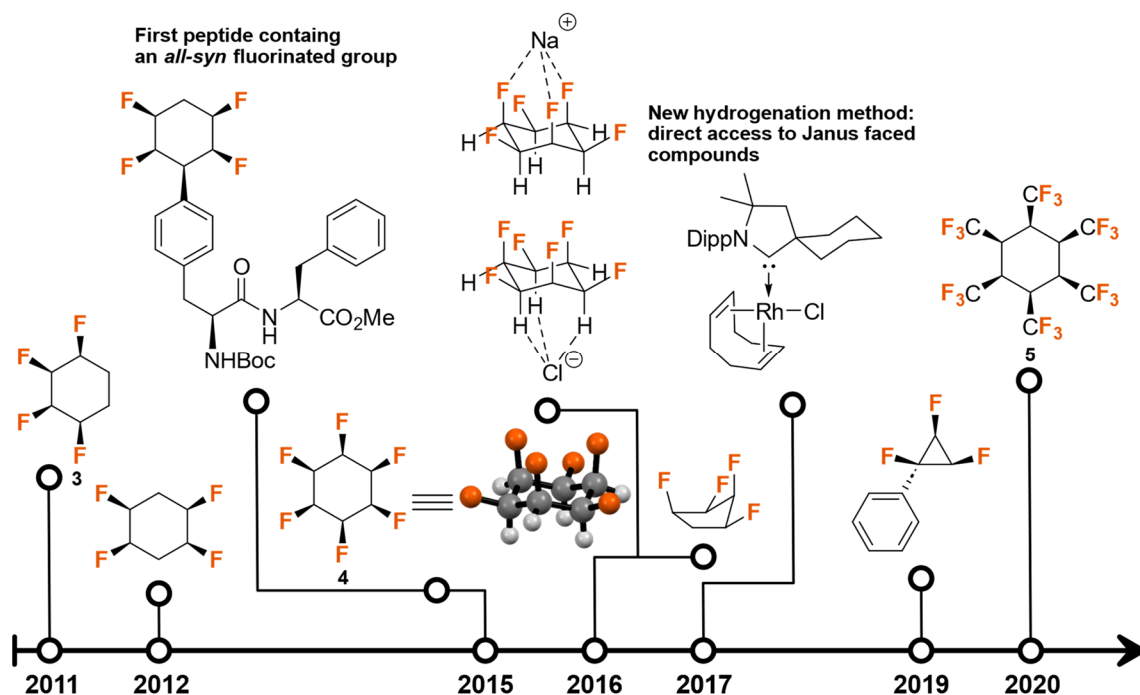
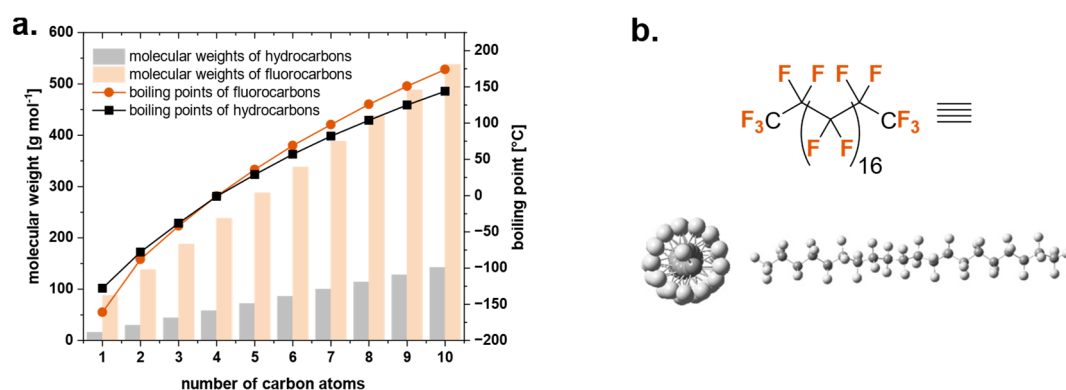


Figure 2.8: The fluorinated Janus face cycloalkanes developed over the last ten years (*all-cis*-1,2,3,4,5,6-hexafluorocyclohexane: CCDC number 1029724).

In general, over the past ten years, a series of different Janus face cycloalkanes was described: *all-syn* tetrafluorinated<sup>[50,51]</sup>, hexafluorinated<sup>[52]</sup>, and *all-syn* hexafluorinated cyclohexanes<sup>[53]</sup>; *all-syn* tetrafluorinated cyclopentane<sup>[54]</sup>; trifluorinated<sup>[55]</sup> and *all-syn* trifluorinated<sup>[56]</sup> cyclopropanes; and *all-syn* tetrafluorinated cyclohexane derivatives with different additional functionalities<sup>[57–61]</sup>. Some selected milestones are summarized in Figure 2.8. All these molecules accommodate 1,3-diaxial fluorine atoms, resulting in high molecular dipole moments. From the synthetical point of view, a significant breakthrough was achieved by the Glorius working group.<sup>[62–64]</sup> By describing the rhodium-catalyzed hydrogenation reaction, the important *all-syn*-1,2,3,4,5,6-hexafluorocyclohexane **4** could be obtained in one step<sup>[62]</sup> in contrast to the first-reported elaborate 12 steps synthesis.<sup>[53]</sup> Next to the cyclic systems containing fluoromethylene units, O'Hagan and co-workers introduced Janus face cyclohexanes with four and six CF<sub>3</sub>-groups placed on one side of the ring structure. Due to the highly demanding steric arrangement, *all-cis*-1,2,3,4,5,6-hexakis(trifluoromethyl)cyclohexane **5** has a ring inversion energy barrier of 27 kcal mol<sup>-1</sup>.<sup>[65]</sup>



Finally, the discussion of how the C-F bond can dominate the conformational composition of organic molecules can be moved to perfluorinated carbons. The first complete characterization of **polyfluorocarbons** with at least two carbon atoms was achieved by Simons and Block in 1937.<sup>[66]</sup> The comparison between the boiling points of hydrocarbons and their polyfluorinated analogs already demonstrates the fascinating nature of fluorocarbons. Despite the significantly larger molecular weights, the fluorocarbons have similar boiling points to the hydrocarbons with the same chain length (*Figure 2.9, a.*)<sup>[67]</sup> This observation can be explained by low intermolecular cohesion forces between the fluorocarbons. Other properties of fluorocarbons are their high compressibility, vapor pressure, and density.<sup>[4,5]</sup>



*Figure 2.9: a.* Differences in boiling points and molar weights between hydrocarbons and fluorocarbons. The corresponding data were taken from reference [67]. *b.* DFT calculated (B3LYP/6-31G\*\*) helical conformation of perfluoroicosane. Adapted from Cormanich *et al.* with permission (Copyright © 2017 Wiley-VCH.GmbH)<sup>[68]</sup>

Nevertheless, how does substituting all C-H bonds with C-F bonds change the conformational properties of the respective carbon chains? Bunn and Howells achieved the first milestone to address this question. In the respective study, the first crystal structure of polytetrafluoroethylene (PTFE) was discussed, showing that the polyfluoroalkane chain adopts a helical structure and not the *anti* zigzag structure known to be formed by hydrocarbons.<sup>[69]</sup> Over the next 50 years, the origin of this structural feature was discussed intensively in several studies.<sup>[4]</sup> The general assumption was that the C-F bonds at the 1,3-distance repel each other, causing the respective C-F bonds to twist by 60°, ultimately forming a helical structure.<sup>[70–73]</sup> However, in 2003, Jang *et al.* suggested that the main driving force behind the helical conformation of fluorocarbons is indeed simple electrostatic interactions.<sup>[74]</sup> The study of Fournier *et al.* showed an inconsistency in these two explanations. The work revealed that despite the presence of 1,3-dipole repulsion in the case of perfluoropropane, no helical structure formation could be observed, hinting that other factors might contribute to the helical preference of perfluoroalkanes.<sup>[75]</sup> Finally, Cormanich *et al.* could demonstrate by applying modern quantum mechanical tools that the origin of this conformational preference lies in the stabilizing hyperconjugation



between the  $\sigma_{\text{C-C}}$  and  $\sigma^*_{\text{C-F}}$  orbitals (*Figure 2.9, b.*). This effect becomes more pronounced the longer the corresponding perfluorinated alkane chains are.<sup>[68]</sup>

To sum up, this chapter demonstrated how the element fluorine can conduct the conformational properties of organic molecules. It is intriguing that despite the numerous diverse models characterized by different degrees of fluorination and arrangements of the corresponding C-F bonds, the actual source of the impact on the structural properties of the respective molecules can be traced back to the high electronegativity of fluorine, which is responsible for the polarity of the C-F bond and the presence of the low energy  $\sigma^*_{\text{C-F}}$  orbital. To conclude this section, the influence of fluorine on the hydrophobicity of organic molecules will be addressed.

Smart wrote an excellent review, discussing several properties of molecules that the introduction of fluorine can influence.<sup>[76]</sup> When it comes to the **hydrophobicity of fluorinated compounds**, Smart highlighted four trends that summarize the respective effects of fluorination:

- “1. Fluorination usually but not always increases lipophilicity.
2. Aromatic fluorination always increases lipophilicity.
3. Per/polyfluorination increases lipophilicity.
4. Fluorination adjacent to atoms with p-bonds increases lipophilicity, with exceptions for some fluorinated  $\alpha$ -carbonyl compounds.”<sup>[76]</sup>

The last three points are unambiguous statements that provide little room for interpretation. However, the first statement indicates that the outcome of fluorination on the hydrophobicity, especially of aliphatic molecules, should be examined in more detail. Partial monofluorination and difluorination of aliphatic hydrocarbons usually decrease the hydrophobicity (*Figure 2.10*).<sup>[77,78]</sup> The presence of a terminal  $\text{CF}_3$ -group in longer aliphatic chains decreases the lipophilicity, while in short aliphatic alkyls, the respective introduction can significantly increase the hydrophobicity of the system. These trends can be explained by the introduction of strongly polarized bonds in the case of partial fluorination, resulting in a polar character of the respective molecules.<sup>[77]</sup> In contrast, in the case of polyfluorination, the dipoles of the individual C-F bonds cancel each other out, increasing corresponding log *P* values. Finally, to conclude this section, the hydrophobicity of Janus face cycloalkanes will be briefly discussed. As previously mentioned, introducing fluorine exclusively at one face of the cycloalkane molecules results in an electronegative fluorine face and an electropositive hydrogen face. This arrangement creates a decisive dipole moment, increasing the polarity of the respective molecules. *All-syn* introduction of fluorine lowers the respective log *P* values relative to the non-fluorinated derivatives.<sup>[56,79]</sup>

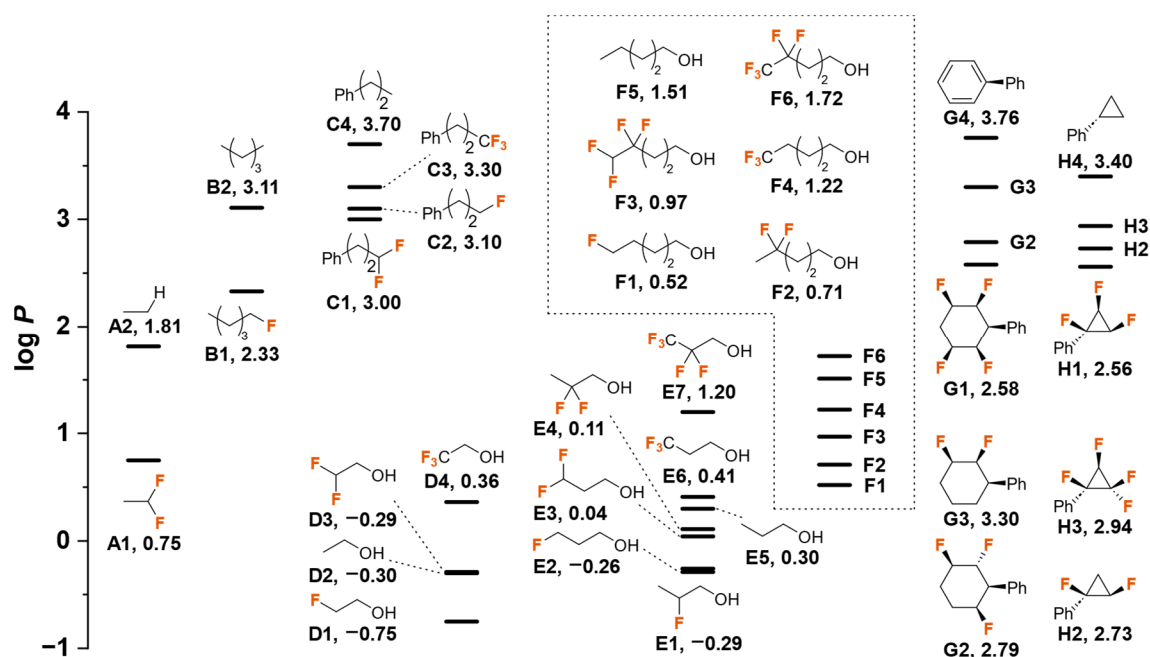


Figure 2.10: Trends in  $\log P$  values of fluorinated compounds. The corresponding data were taken from references [56, 77-79]

At this point, it is important to emphasize that the insertion of fluorine has a profound effect on other properties of molecules, such as  $\text{pK}_a$  values. Thus, the  $\text{pK}_a$  value of compounds decreases with the increasing degree of fluorination in the vicinity of the respective functionality (carboxylic acid, amine, alcohol), with the respective influence significantly diminishing with rising distance.<sup>[76,80-82]</sup>

## 2.2 The role of fluorine in non-covalent interactions

The preceding part of this thesis illustrated the diverse effects of fluorine substitution on the properties of organic molecules. Now, the outcome of fluorination on the non-covalent interactions between molecules will be discussed. Since fluorinated aromatic systems were not addressed in the scope of this work, this section will focus on interactions involving aliphatic systems. First, one of the probably most controversial topics will be addressed: fluorine's role in hydrogen bonding.

### Fluorine in hydrogen bonding interactions

“Organic fluorine hardly ever accepts hydrogen bonds” was the title of the highly cited work of Dunitz and Taylor from 1997.<sup>[83]</sup> In the scope of the respective study, the authors searched the Cambridge Structural Database and the Brookhaven Protein Data Bank for fluorine-involving hydrogen bonds. They combined this intensively deep data study with *ab initio* calculations. This work supported comparable publications and showed that fluorine is indeed a poor H-bond acceptor.<sup>[83]</sup> In this context, two examples will be briefly discussed. First, as

stated by Dunitz and Taylor, only two crystal structures containing definite O-H···F-C hydrogen bonds could be identified. One is the crystal structure of 2-fluoro-1,1,2-triphenylethane **6** (Figure 2.11, a.). The molecule formed a dimer connected by two symmetrical hydrogen bonds with respective bond lengths of 2.02 Å.<sup>[84]</sup> Additionally, the crystal structure of ammonium monofluoroacetate **7** indicated some involvement of fluorine in hydrogen bonding interactions with the N-H donor (Figure 2.11, b.). However, the distance to the oxygen atom (2.03 Å) is much shorter than the distance to the respective fluorine atom (2.29 Å).<sup>[85]</sup> The last example hints that fluorine can be a potential H-bond acceptor, but only when no better options exist. In their conclusion, Dunitz and Taylor also discussed the reasons for fluorine's poor H-bond acceptor capability. On the one hand, it is due to the energetically low-lying orbitals of the free electron pairs, which thus lie tightly to the core and are reluctant to be involved in intermolecular interactions. On the other hand, it is the low polarizability of fluorine and, therefore, the inability to change this situation.<sup>[83]</sup> Seven years after this work, Dunitz published a review that further underlined the statements made before.

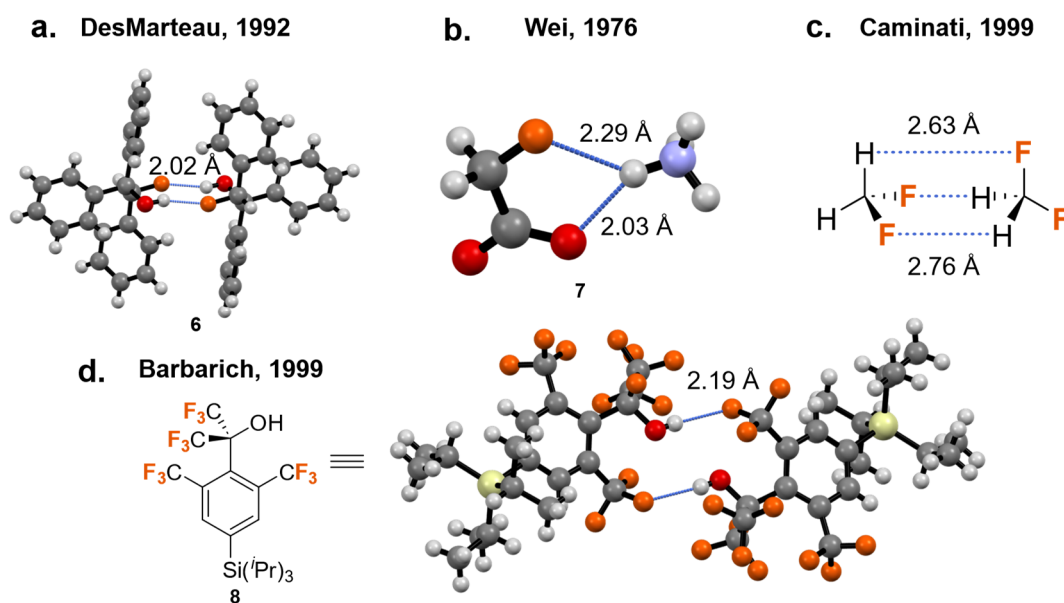


Figure 2.11: a. Crystal structure of 2-fluoro-1,1,2-triphenylethane (CCDC number 1199708). b. Crystal structure of ammonium monofluoroacetate (CCDC number 1102663). c. Difluoromethane dimer in the gas phase. d. Crystal structure of fluorinated alcohol **8** (CCDC number 1209705).

However, to finish the respective section Dunitz also highlighted that “*nowadays the occurrence of a genuine hydrogen bond involving organic fluorine seems to be regarded as sufficiently noteworthy*”.<sup>[86]</sup> Indeed, even though the potential of fluorine to form hydrogen bonds seems weak, some work in the late 1990s provided exciting examples of fluorine-containing hydrogen bonds. Using spectroscopic methods, Caminati *et al.* could demonstrate that difluoromethane forms dimers in the gas phase, which are stabilized by three C-H···F-C hydrogen bonds (Figure 2.11, c.).<sup>[87]</sup> Furthermore, Strauss and co-workers synthesized a

fluorinated alcohol **8**, and the respective crystal structure revealed the formation of a dimer with two intermolecular hydrogen bonds (*Figure 2.11, d.*). Additionally, the authors carried out NMR and IR experiments, which supported the presence of the hydrogen bonding network in the solid state and solution.<sup>[88]</sup> In the following years, the role of fluorine in hydrogen bond formation was still a highly discussed topic.

In 2012, Schneider published an critical review trying to tackle this ongoing problem.<sup>[89]</sup> Most importantly, he pointed out that the spectroscopic investigations in solution or the gas phase might be more suitable than the X-ray determination to detect and characterize such weak intermolecular interactions as fluorine-involved hydrogen bonds.<sup>[89]</sup> Three years later, Champagne *et al.* presented another review regarding this topic.<sup>[90]</sup> The authors focused solely on publications published between 2012 and 2015, not already mentioned by Schneider. Compared to Dunitz, the authors were much more confident about the role of fluorine as a H-bond acceptor, stating that “*since [the yearly 2000s] a greater deal of evidence supporting organic fluorine as a hydrogen-bond acceptor has been reported.*”<sup>[90]</sup> Nevertheless, at the same time, the authors mentioned that some examples discussed in the scope of their review could not be labeled as hydrogen bonds with absolute certainty since, in these cases, only crystal structures were available, and further investigations would be required. This slight inconsistency indicates that the questions surrounding the fluorine-involved hydrogen bonds remain. In recent years, more interesting publications were added to the discussion, focusing on theoretical calculations<sup>[91,92]</sup>, additional methods to determine the strength of the respective hydrogen bonds<sup>[93]</sup>, and further examples of novel intriguing intermolecular fluorine-containing hydrogen bonds.<sup>[94–96]</sup>

If the review of Champagne *et al.* is considered in more detail, then another vital aspect of fluorine-containing hydrogen bonds becomes quickly apparent. Of the 30 examples presented in this review, 87% of all cases involved **intramolecular hydrogen bonding**.<sup>[90]</sup> These are mainly sterically restricted molecules, forcing corresponding C-F bonds into spatial proximity to possible H-bond donors. Especially, Lectka and co-workers presented several examples of caged compounds with intramolecular H-bonds.<sup>[97,98]</sup>

As the final point of this section, the hydrogen bond capability of the CF<sub>2</sub>H group will now be outlined. Due to the two geminal fluorine atoms, the CF<sub>2</sub>H group is highly polarized, making the respective C-H bond a suitable hydrogen donor (*Figure 2.12, a.*)<sup>[99]</sup>

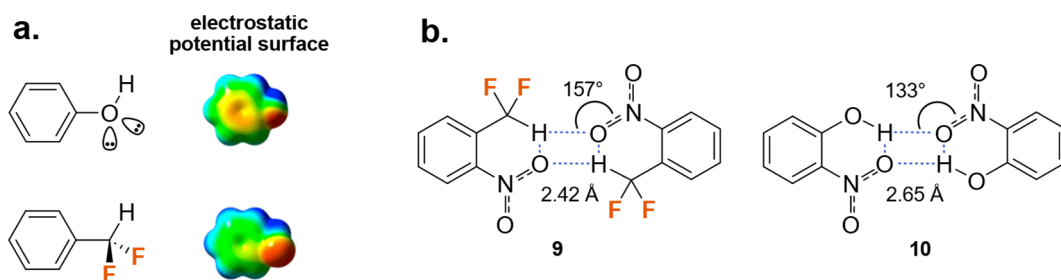


Figure 2.12: a. Comparison between the hydrogen bond donor abilities of the OH- and CF<sub>2</sub>H-groups. Electrostatic potential surfaces were adapted from Sessler *et al.* with permission (Copyright © 2017 American Chemical Society)<sup>[99]</sup> b. Hydrogen-bonded dimeric structures of *o*-nitro- $\alpha,\alpha$ -difluorotoluene **9** and *o*-nitrophenol **10**.

The hydrogen bond donor ability of the CF<sub>2</sub>H group has been known for over 20 years. For example, Erickson and McLoughlin carried out a structural investigation of a pyrazole carboxamide compound, combining IR and NMR spectroscopy with theoretical calculations. The presence of an intramolecular CF<sub>2</sub>H $\cdots$ O=C hydrogen bond could be revealed. Ab initio calculations revealed a binding energy of 1.0 kcal mol<sup>-1</sup> and a short H $\cdots$ O distance of 2.4 Å.<sup>[100]</sup> In recent years, several novel studies have been published investigating the potential of the CF<sub>2</sub>H group as a hydrogen bond donor. Sessler *et al.* examined the hydrogen donor properties of *o*-nitro- $\alpha,\alpha$ -difluorotoluene **9** and compared them with *o*-nitrophenol **10**. Both molecules formed dimers in the solid state connected *via* two hydrogen bonds (Figure 2.12, b.).

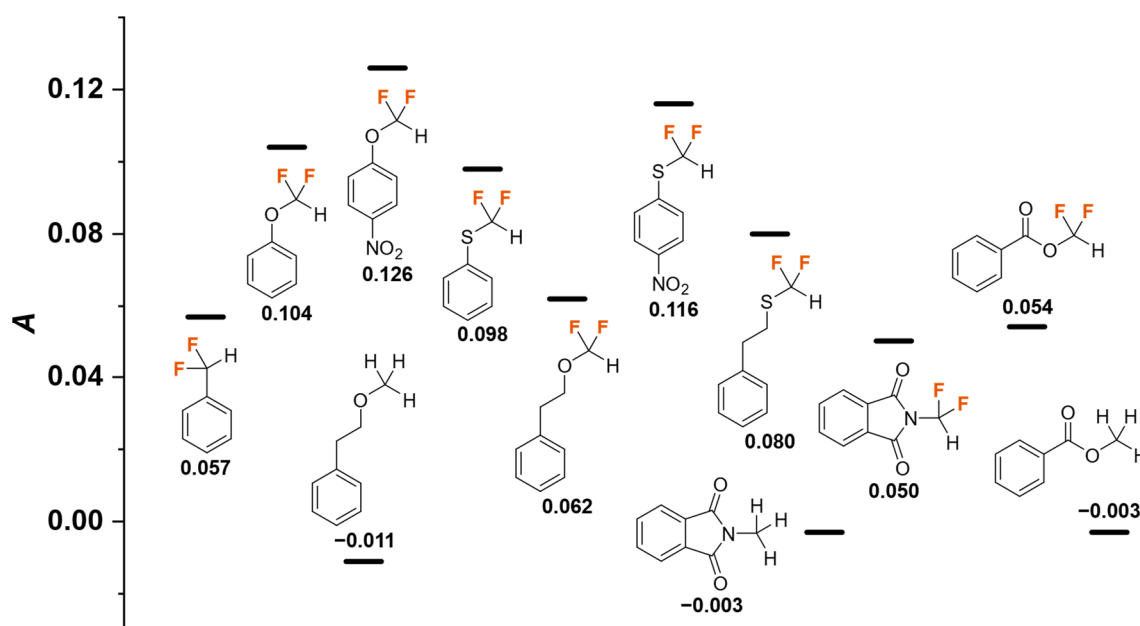


Figure 2.13: Hydrogen bond donor strength of different XCF<sub>2</sub>H groups. A-values describe the hydrogen bond acidity of molecules and can be obtained from <sup>1</sup>H NMR measurements (reference: A(phenol) = 0.62).<sup>[101]</sup>

The presence of the respective intermolecular interactions was supported by additional spectroscopic and theoretical methods, highlighting the bioisosterism between CF<sub>2</sub>H and OH functionalities.<sup>[99]</sup> Zafrani *et al.* conducted two studies on the hydrogen bond donor strength of

XCF<sub>2</sub>H groups with X = O or S attached to different functionalities, such as aryl, alkyl, ether, or electron-withdrawing groups. The respective studies demonstrated that the CF<sub>2</sub>H group is a relatively weak hydrogen bond donor. Additionally, the hydrogen bond donor ability highly depends on the electronic properties of the rest connected to the CF<sub>2</sub>H group (Figure 2.13).<sup>[101,102]</sup> Finally, Shanahan *et al.* demonstrated the design of a metal-ligand with a CF<sub>2</sub>H functionality. Attached to palladium, CF<sub>2</sub>H group can form hydrogen bonds with substrates that coordinate to the Pd center. Experimental and theoretical methods displayed a binding energy of 3 kcal mol<sup>-1</sup>.<sup>[103]</sup>

### Intermolecular interactions between polyfluorinated compounds

In Section 1.1, the unique properties of fluorocarbons were illustrated. Especially the differences in the respective hydrocarbon analogs were highlighted. Since the mid-twentieth century, another property of hydrocarbons and fluorocarbons has been known to have had an essential influence on the development of organofluorine chemistry: the immiscibility of these two classes of molecules.<sup>[104–108]</sup> A mixture of water, hydrocarbons, and fluorocarbons forms a third **fluorous phase**, immiscible both with the aqueous and organic phases.<sup>[109]</sup> Nevertheless, it is important to emphasize that the driving forces behind forming a fluorous phase are not attractive interactions between fluorinated species. On the contrary, the intermolecular dispersion forces between hydrocarbons are greater than between hydrocarbons and fluorocarbons. In other words, the hydrocarbons exclude the fluorocarbons from the organic phase.<sup>[106,110]</sup> This phenomenon has been called the “**fluorous effect**” in recent literature.<sup>[109]</sup> In 1949, Hildebrand *et al.* also demonstrated that the miscibility of perfluorinated alkanes and hydrocarbons is temperature-dependent.<sup>[104]</sup> In contrast to the observation that fluorocarbons are usually insoluble in water and hydrocarbons, the term “fluorous” originates from recent literature. In 1994, Horváth and Rábai introduced the concept of “**fluorous biphasic catalysis**”.<sup>[111]</sup> In their highly recognized manuscript, the authors could show that the fluorocarbon phase combined with a classical organic solvent and a highly fluorinated reagent or catalyst can drastically simplify the purification process after the performed chemical reaction.

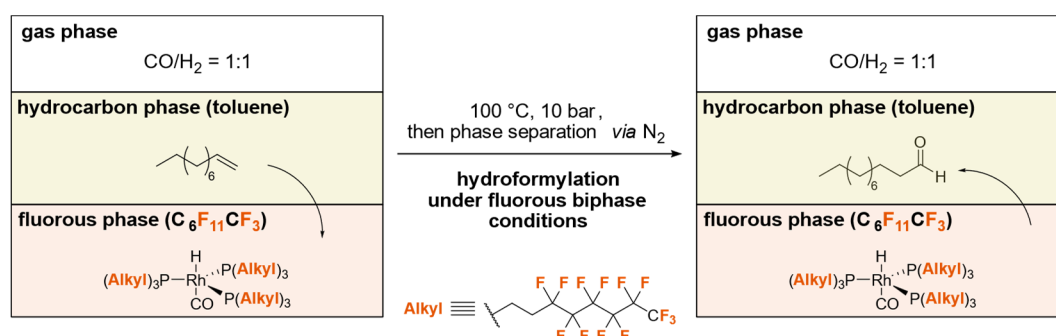
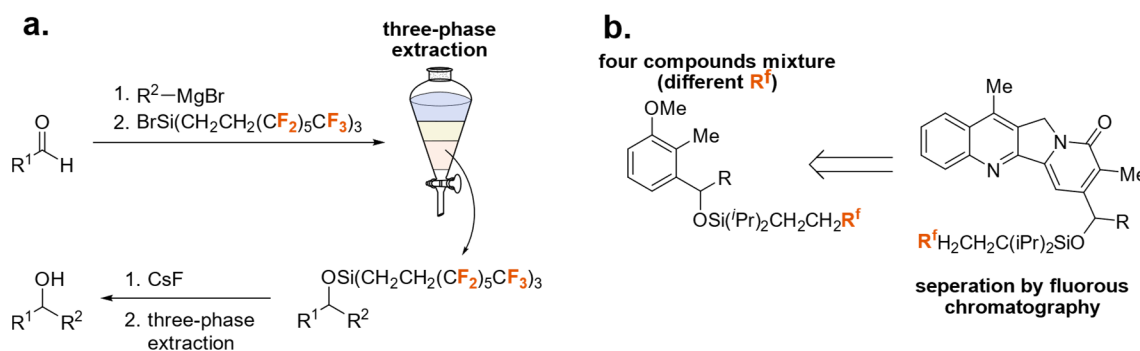


Figure 2.14: Concept of “fluorous biphasic catalysis”: hydroformylation of dec-1-ene.

This concept was demonstrated for the hydroformylation of alkenes (*Figure 2.14*). As already mentioned, the authors introduced the term “fluorous” for the first time. It was used similarly to the term “aqueous” to highlight the preferred solubility of the catalyst in the perfluorinated solvent.<sup>[108,111]</sup>

In the following years, Curran and co-workers further expanded the field of fluorous chemistry, introducing this concept to classic organic synthesis.<sup>[112,113]</sup> Organic molecules can be tagged with highly fluorinated functionalities. After performing chemical reactions, a three-phase liquid extraction (water, organic solvent, fluorocarbon) can be used to isolate the desired tagged products (*Figure 2.15, a.*). The respective organic and inorganic impurities end up in the aqueous and organic phases, and the fluorine-tagged product can be obtained from the fluorous phase without additional purification methods.<sup>[112]</sup>



*Figure 2.15:* a. Application of fluorous chemistry in organic synthesis. b. Concept of fluorous mixture synthesis.

Furthermore, Curran and co-workers extended this concept to mixture synthesis. Different organic compounds were labeled with fluorous tags of different lengths. The mixture of all tagged compounds was submitted to a multi-step synthesis. The final products could be separated *via* fluorous chromatography (*Figure 2.15, b.*)<sup>[113]</sup> Next to the fields of catalysis and separation methods, fluorous chemistry has had a significant effect on several scientific areas, such as supramolecular chemistry<sup>[110,114]</sup> and biomedical applications.<sup>[109]</sup>

Up to this point, no **attractive fluorine-fluorine interactions** were discussed. On the contrary, the weak dispersion forces between fluorocarbons were highlighted in the scope of this section. Still, attractive  $F\cdots F$  interactions are a topic that has been mentioned in the literature to a certain extent. Ramasubbu *et al.* described two types of possible halogen-halogen interactions.<sup>[115]</sup> Type I interactions are forced by the respective packing geometry and do not contribute to the overall stabilization. Type II interactions (halogen bond interactions) are caused by polarization and are described as energetically favorable interactions (*Figure 2.16, a.*)<sup>[115,116]</sup> Reichenbächer *et al.* analyzed the Cambridge Structural Database and found 788 compounds with promising  $F\cdots F$  interactions. However, only 13 compounds could be assigned



to type II.<sup>[117]</sup> This hints that fluorine-fluorine interactions are probably less significant than other fluorine-involved intermolecular interactions. Still, during the last decade, the role of fluorine-fluorine interaction was further investigated.

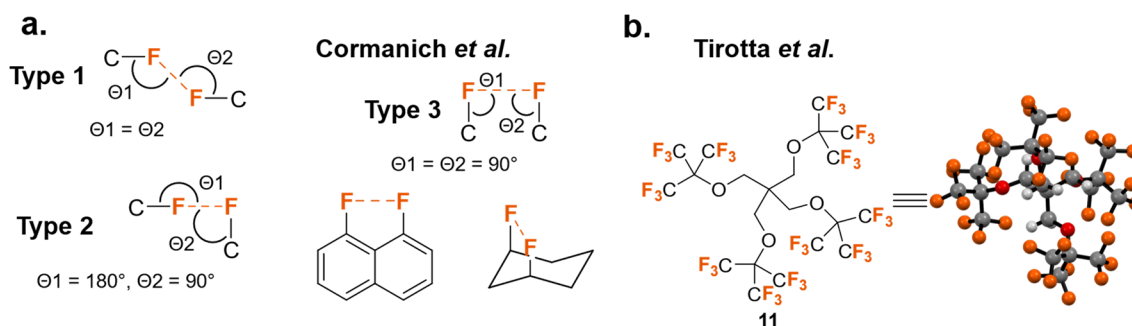


Figure 2.16: a. Different types of fluorine-fluorine interactions. b. PERFECTA molecule **11** displays slightly stabilizing fluorine-fluorine contacts (PERFECTA **11**: CCDC number 993466).

In 2011, Osuna *et al.* presented a theoretical study analyzing intermolecular interaction between fluorinated dimers. The authors could demonstrate that the respective dimers are stabilized by several fluorine-fluorine interactions with respective bond energies of 0.21-0.41 kcal mol<sup>-1</sup>. Furthermore, the calculation showed that F...F interactions are driven by dispersion or by electrostatics, depending on the corresponding geometry.<sup>[118]</sup> In 2014, Cormanich *et al.* used a novel calculation method to study the nature of fluorine-fluorine interactions in a series of different fluorinated compounds, such as *all-syn* Janos cyclohexanes and fluorinated naphthalene analogs (Figure 2.16, a).<sup>[119]</sup> The calculations revealed that all close F...F contacts were described as attractive interactions. However, by applying the respective method, the interactions between two fluorine atoms can be characterized as repulsive only in the case of a strong repulsion. Therefore, the authors emphasized that “these [attractive fluorine-fluorine interactions] can be weak and may not govern actual isomer stabilities or conformational preferences”.<sup>[119]</sup> One year later, Omorodion *et al.* investigated the solid state of a polyfluorinated carboxylic acid by X-ray diffraction.<sup>[120]</sup> In combination with additional DFT calculations, it was shown that the respective structure is stabilized by several F...F interactions. Although each fluorine-fluorine contact made a rather small energetic contribution to the stabilization, the sum of all interactions provided an energy value of 13 kcal mol<sup>-1</sup>. Additionally, Metrangolo and Resnati working groups developed a perfluorinated <sup>19</sup>F MRI agent called PERFECTA **11**.<sup>[121]</sup> This highly fluorinated compound crystallized from hexafluoroisopropanol, revealing a series of close fluorine-fluorine contacts in the solid state.

In conclusion, fluorous interactions significantly influenced a diverse range of scientific areas. Still, in most cases, the driving force of these interactions is not attractive F...F contacts. Stabilizing fluorine-fluorine interactions might be present in specific cases but seem to occupy a minor role compared to other fluorine-specific interactions.



## 2.3 Fluorine in medicinal and bioorganic chemistry

Sections 1.1 and 1.2 illustrated in detail the many faces of the element fluorine to shape the properties of organic molecules and control intermolecular interactions. In this chapter, the diverse influence of fluorine on the field of medicinal and bioorganic chemistry will be demonstrated. For each previously discussed fundamental properties of fluorine, several examples will be presented, starting with the great strength of the C-F bond. It is important to mention that there are many other examples for each characteristic feature of fluorine, and the ones discussed here only illustrate the great diversity of fluorine in both fields. Several detailed reviews have been published in recent years, highlighting fluorine's role in medicinal chemistry.<sup>[122–128]</sup>

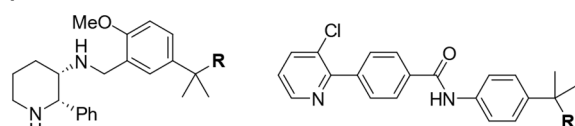
Considering the enormous **strength of the C-F bond**, the positive influence of fluorine on the **metabolic stability** of compounds does not seem surprising. Indeed, the exchange of labile C-H with C-F bonds and fluorination of electron-rich aryl groups can significantly enhance metabolic stability. *Figure 2.17, a.* displays a series of examples.<sup>[123]</sup> Furthermore, the remarkable stability of C-F can play a central role in the function of mechanism-based inhibitors.<sup>[124]</sup> 5-Fluorouracil **12** (5-FU) is used in cancer treatment and acts as an inhibitor of thymidylate synthase. *Figure 2.17, a.* illustrates the key intermediate of the respective mechanism. 5-FU **12** is covalently bound to the methylene tetrahydrofolic acid cofactor (CH<sub>2</sub>FAH<sub>4</sub>). In the case of the natural uracil, the hydrogen atom at position 5 would be abstracted by a base. However, the fluorinated analog cannot undergo the respective elimination reaction, blocking the enzyme and preventing deoxyribonucleic acid (DNA) replication.<sup>[124]</sup>

**The proteolytic stability of fluorinated peptides** is an intriguing example to discuss the **steric consequences of fluorine substitution**. In 2018, Huhmann and Kokschi provided an excellent overview of this topic.<sup>[129]</sup> The authors emphasized that the outcome of fluorination on the proteolytic stability of peptides is challenging to predict and depends on the position and the respective nature of fluorinated amino acids. Highly fluorinated and sterically demanding amino acids can improve the proteolytic stability of peptides. Gottler *et al.* introduced 5,5,5,5',5',5'-hexafluoroleucine **30** (HfLeu) into the sequence of the antimicrobial MSI-78 peptides.<sup>[130]</sup> MSI-78 and the fluorinated version form a random structure in solution and adopt an  $\alpha$ -helical structure in the presence of liposomes. Interestingly, the unstructured peptides were both degraded rather rapidly. With liposomes, the fluorinated version displayed significantly higher proteolytic stability than the nonfluorinated MSI-78 (*Figure 2.17, b.*)<sup>[130]</sup> These results highlight that besides the possible effects of fluorination, different factors might be crucial for the proteolytic stability of peptides.

O'Hagan and co-workers synthesized 2,3-difluorosuccinamides **13a,b** and studied the respective conformational properties *via* X-ray diffraction.

**a. C-F bond stability**

improved metabolic stabilities

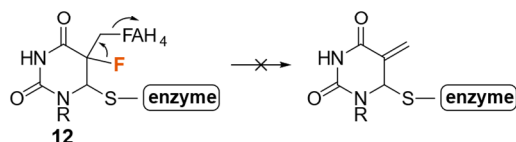

 HLM  $Cl_{int}$  [ $\mu\text{L}/\text{min}/\text{mg}$ ]:

 $R = \text{CH}_3$ : 87.9  
 $= \text{CF}_3$ : 44.7

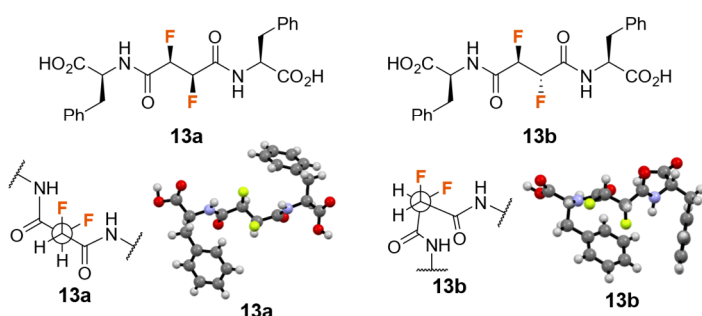
 HLM  $Cl_{int}$  [ $\mu\text{L}/\text{min}/\text{mg}$ ]:

 $R = \text{CH}_3$ : 87.9  
 $= \text{CF}_3$ : 44.7

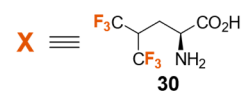
inhibition of thymidylate synthase by 5-fluorouracil


**c. dipole-dipole interactions**

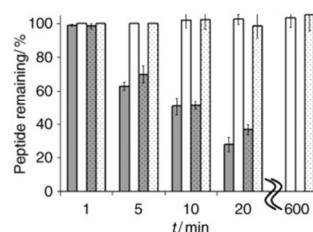
influence on peptide conformation


**b. steric effects of fluorine**

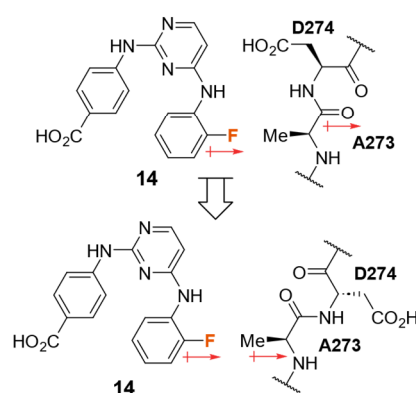
fluorinated MSI-78:

 GXGKF $\text{X}$ KKAKKFGKAFVK $\text{XX}$ KK


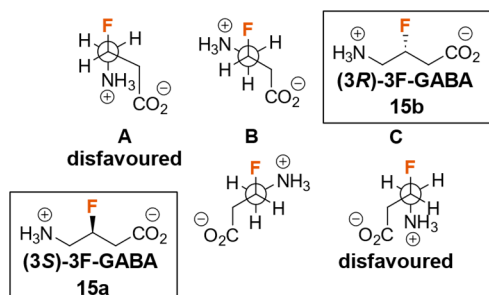
increased proteolytic stability:



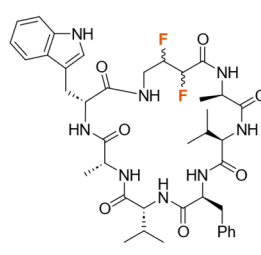
dipole-induced inhibition of Aurora A kinase


**d. fluorine gauche effect**

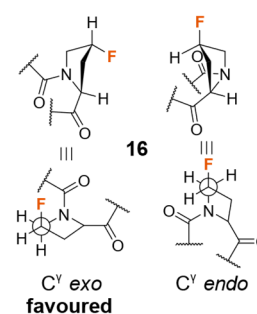
electrostatic fluorine gauche effect



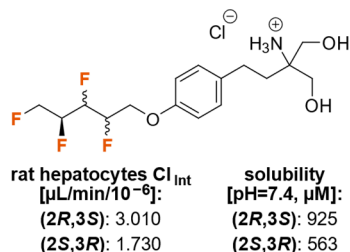
Unguisin A



(4R)-fluoroproline conformation


**e. multivincinal fluoroalkane motifs**

multiple sclerosis drug, Gilenya



antiviral candidates with all-syn fluorocyclohexyl group

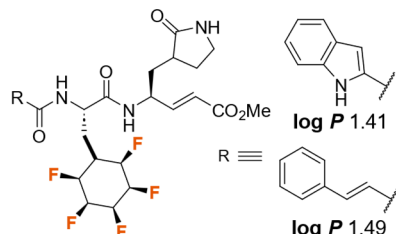
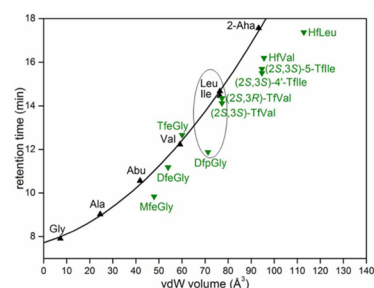

**f. hydrophobicity**


Figure 2.17: Fluorine in bioorganic and medicinal chemistry: a. C-F bond strength. b. Steric effect of fluorine substitution. Proteolytic digestion data were adapted from Gottler *et al.* with permission (Copyright © 2008 American Chemical Society)<sup>[130]</sup> c. Dipole-dipole interactions (2,3-difluorosuccinamides: CCDC numbers 271257, 271258). d. Fluorine gauche effect. e. Multivincinal fluoroalkane motifs. f. Fluorine-induced hydrophobicity. Hydrophobicity plot was adapted from Berger *et al.* with permission (Copyright © 2017 American Chemical Society).<sup>[131]</sup>

Depending on the stereocenter, different conformations were observed. The C-F bonds align *anti-periplanar* to the C=O bonds of the amide functionalities, which can be explained by the favorable **dipole-dipole interactions**.<sup>[132]</sup> Another impressive example of the role of dipole-dipole interaction is provided by the fluorinated version of the Aurora A kinase inhibitor **14**. Introducing a fluorine atom to the aryl group of the inhibitor imposed a conformational change within the enzyme, moving Asp274 away from the adenosine triphosphate (ATP) binding site and leading to improved inhibition (*Figure 2.17, c.*).<sup>[133]</sup>

The significance of the electrostatic **fluorine *gauche* effect** was demonstrated by O'Hagan and co-workers, studying the fluorinated analogs of the  $\gamma$ -aminobutyric acid **15** (GABA) neurotransmitter. Both fluorinated isomers displayed similar interactions with the GABA<sub>A</sub> receptors while showing different binding affinities to the GABA transaminase enzyme. This indicated different binding conformations for both cases. GABA seems to interact with the receptors *via* conformation B (accessible by both isomers) and with the enzyme *via* conformation A (accessible only by (*S*)-isomer **15a**) since (*S*)-isomer displayed a higher binding affinity for the transaminase (*Figure 2.17, d.*).<sup>[134]</sup> A similar principle was used to direct the conformational preferences of the cyclic heptapeptide unguisin A. Within the GABA residue, a vicinal difluoro motif was introduced. Different secondary structures could be determined, depending on the respective stereochemistry and based on favorable fluorine *gauche* interactions (*Figure 2.17, d.*).<sup>[135]</sup> Additionally, the fluorine *gauche* effect is crucial to understanding the conformational behavior of 4-fluoroproline (4-FPro). (*4R*)-FPro **16** adopts the C $\gamma$ -*exo* ring pucker, stabilizing the *trans*-backbone conformation. In contrast, (*4S*)-FPro favors the C $\gamma$ -*endo* ring pucker and, consequently, the *cis*-backbone conformation (*Figure 2.17, d.*).<sup>[131]</sup>

The **multivincinal fluoroalkane motif** was investigated by Gilmour and co-workers in the context of the multiple sclerosis drug Gilenya. Multiple favorable  $\sigma_{\text{C-H}} \rightarrow \sigma^*_{\text{C-F}}$  interactions controlled the conformational properties. Furthermore, fluorine stereochemistry of Gilenya derivatives resulted in different physicochemical properties (*Figure 2.17, e.*).<sup>[136]</sup> Clark *et al.* approached possible applications of *all-syn* fluorinated Janus cyclohexanes in medicinal chemistry. For this purpose, *all-syn*-2,3,4,5,6-pentafluorocyclohexylalanine amino acid was synthesized. Several antiviral candidates were prepared based on this building block (*Figure 2.17, e.*).<sup>[61]</sup>

The hydrophobicity of fluorinated amino acids is crucial for the rational design of fluorinated peptides and proteins. Kokschi and co-workers developed a high-performance liquid chromatography- (HPLC-) based assay to estimate the hydrophobicity of a series of fluorinated amino acids, relating van der Waals volumes of the fluorinated side chains to respective retention times (*Figure 2.17, f.*).

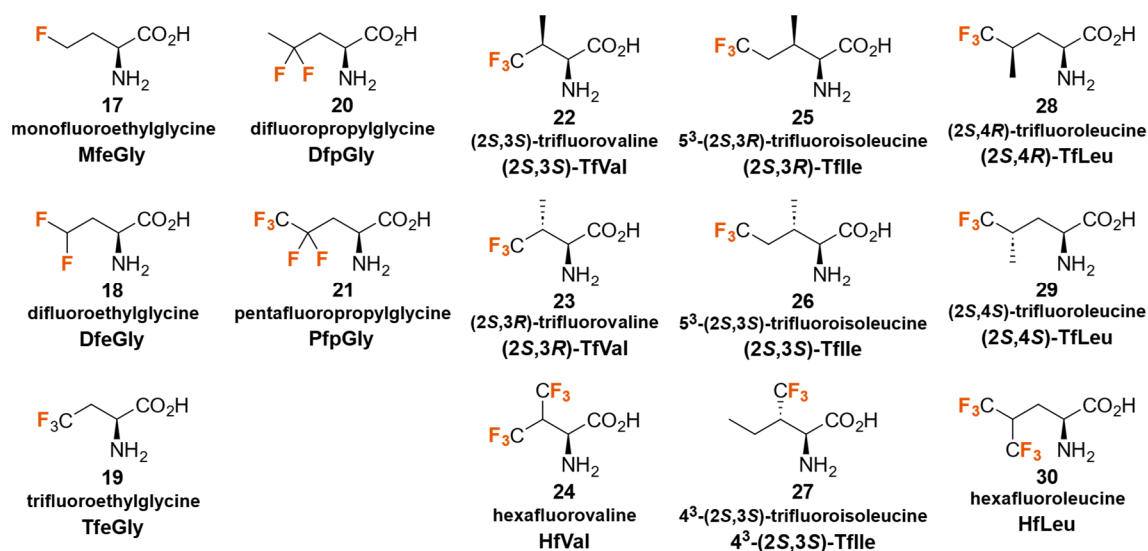


Figure 2.18: Summary of selected fluorinated amino acids.

The introduction of  $\text{CF}_3$ -groups significantly raises the hydrophobicity (HfLeu **30**; hexafluorovaline **24**, HfVal), while partial fluorination results in increased polarity (monofluoroethylglycine **17**, MfeGly; difluoroethylglycine **18**, DfeGly; difluoropropylglycine **20**, DfpGly). Figure 2.18 presents an overview of selected fluorinated amino acids. Another crucial intrinsic property of fluorinated amino acids is the secondary structure propensity. The  $\alpha$ -helix propensity of fluorinated amino acids relates to the hydrophobicity trends and the steric branching at the  $\beta$ -position (Table 2.1).<sup>[131]</sup>

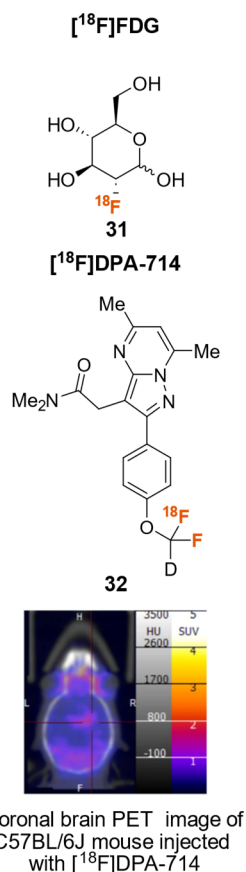
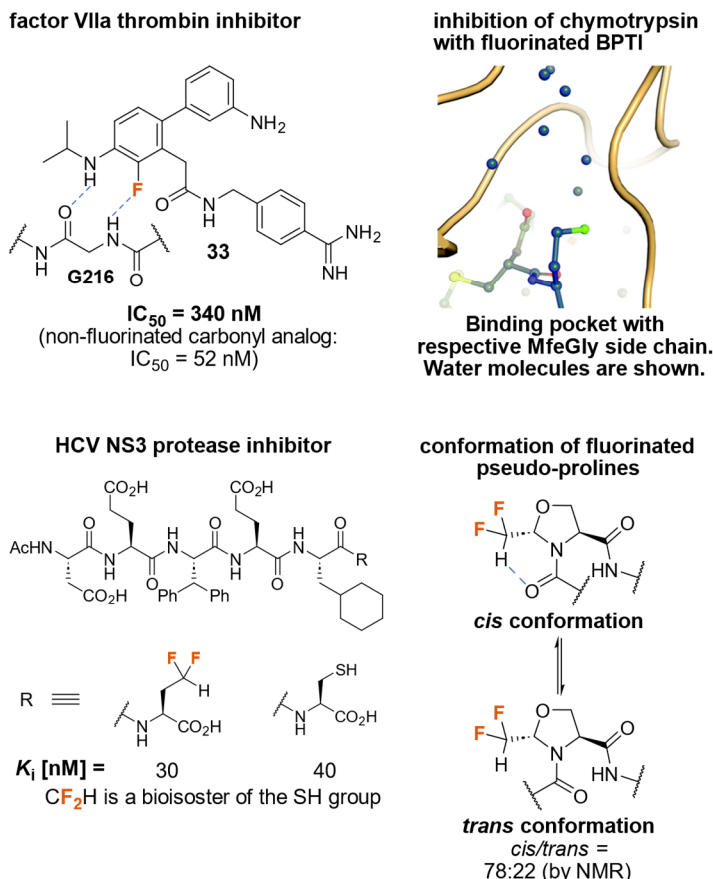
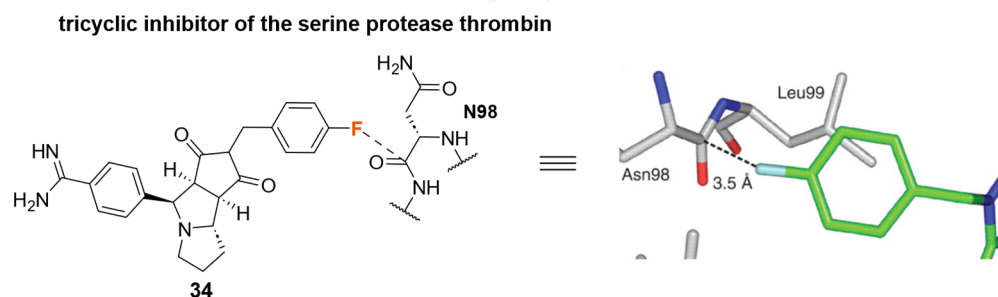
Table 2.1:  $\alpha$ -Helix propensities of several non-fluorinated and fluorinated amino acids. The corresponding data were taken from reference [11].

amino acid	$\alpha$ -helix propensity
Ala	1.46±0.01
Abu	1.22±0.14
Leu	0.99±0.09
MfeGly <b>17</b>	0.87±0.07
DfeGly <b>18</b>	0.50±0.06
Val	0.41±0.04
5 <sup>3</sup> -(2S,3S)-TfIle <b>26</b>	0.26±0.03
HfLeu <b>30</b>	0.13±0.02
TfeGly <b>19</b>	0.06±0.02
(2S,3S)-TfVal <b>22</b>	0
4 <sup>3</sup> -(2S,3S)-TfIle <b>27</b>	0

The [ $^{18}\text{F}$ ] isotope has yet to be discussed in the context of this thesis. However, due to its longer half-life ( $t_{1/2} = 110$  min), [ $^{18}\text{F}$ ] tracers are essential in nuclear medicine. Different

radionuclides have been used, especially in positron emission tomography (PET), providing significant metabolic information. In this context, 2-deoxy-2- $^{18}\text{F}$ fluoro-D-glucose **31** ( $^{18}\text{F}$ FDG) is one of the most frequently used radiopharmaceuticals (*Figure 2.18, a.*). Due to the stronger glucose uptake of cancer cells and the inability to undergo glycolysis,  $^{18}\text{F}$ FDG plays a central role in oncology.<sup>[124]</sup> In general, the Gouverneur working group developed many different  $^{18}\text{F}$  labeling methods, increasing the scope of accessible  $^{18}\text{F}$  containing pharmaceuticals. In a recent example,  $^{18}\text{F}$ difluorocarbene chemistry was introduced to the field of radiochemistry for the first time. In the scope of the respective work, the authors could demonstrate the labeling of DPA-714 analog **32** with an  $^{2\text{H}^{18}\text{F}}$ OCF<sub>2</sub>H radiotracer, allowing subsequent *in vivo* studies (*Figure 2.18, a.*).<sup>[137]</sup>

As already intensively discussed in *Section 1.2*, C-F hydrogen bond acceptor ability is a highly debatable topic. Of course, bioorganic and medicinal chemistry is no exception. As stated by Meanwell in his extensive review, a distinction between fluorine-involved hydrogen bonding and multipolar interactions is complicated.<sup>[123]</sup> Still, introducing fluorine can be a powerful strategy to modify protein-ligand interaction. For example, the C-F group can be used as a substitute for carbonyl functionalities in aromatic structures. The introduction of fluorine to the factor VIIa thrombin inhibitor **33** retained its activity. The respective crystal structure revealed a close contact (3.4 Å) between C-F and the amide group of the enzyme.<sup>[123]</sup> In the context of peptide and protein chemistry, Kokschi and co-workers presented a fascinating study investigating the activity of the bovine pancreatic trypsin inhibitor (BPTI). The authors demonstrated that the inhibitor activity could be restored by introducing fluorine to the hydrophobic chain of 2-aminobutyric acid (Abu). Furthermore, X-ray diffraction studies revealed meaningful non-covalent interactions between the fluorinated side chains and water molecules, which were crucial for the dramatically improved inhibitor activity compared to the non-fluorinated analog (*Figure 2.18, a.*).<sup>[138]</sup> More recently, Leppkes *et al.* studied the inhibitor activity of BPTI towards  $\alpha$ -chymotrypsin. Especially fluorinated amino acids containing the CF<sub>2</sub>X groups (X = H or CH<sub>3</sub>) improved the respective inhibition, again indicating the vital role of fluorine-induced polarity.<sup>[139]</sup> However, a theoretical study published by Wehrhan *et al.* suggested that the water network within the binding pocket of BPTI and trypsin is not responsible for the enhanced inhibitor activity of fluorinated analogs.<sup>[140]</sup> In contrast to the controversial role of C-F groups in hydrogen bonding interactions, the importance of the CF<sub>2</sub>H group is not a matter of debate. The ability of the CF<sub>2</sub>H group to act as a hydrogen bond donor was demonstrated by studying the inhibitor of HCV NS3 protease. Here, DfeGly **18** was used as a bioisoster for a cysteine residue.

**a. [<sup>18</sup>F] isotope**

**b. fluorine in hydrogen bonding**

**c. interactions between C-F and C=O groups**


**Figure 2.18:** Fluorine in bioorganic and medicinal chemistry: *a.* Applications of the [<sup>18</sup>F] isotope. The coronal brain PET image was adapted from Sap *et al.* with permission (Copyright © 2022 Springer Nature)<sup>[137]</sup> *b.* Fluorine in hydrogen bonding. Crystal structure of BPTI(MfeGly)-α chymotrypsin binding pocket was adapted from Leppkes *et al.* with permission (Copyright © 2022 Royal Society of Chemistry)<sup>[139]</sup> *c.* Interactions between C-F and C=O functionalities. The crystal structure was adapted from Müller *et al.* with permission (Copyright © 2007 American Association for the Advancement of Science).<sup>[125]</sup>

Contrary to the non-fluorinated Abu-containing analog, the inhibitor activity could significantly be improved, indicating the importance of the hydrogen bond donor ability at the corresponding position (Figure 2.18, *b.*)<sup>[141]</sup> In peptide chemistry, Malquin *et al.* showed that the CF<sub>2</sub>H moiety can be used to direct secondary structure formation. The authors studied the conformational preferences of CF<sub>2</sub>H-containing pseudo-proline residues. The results revealed

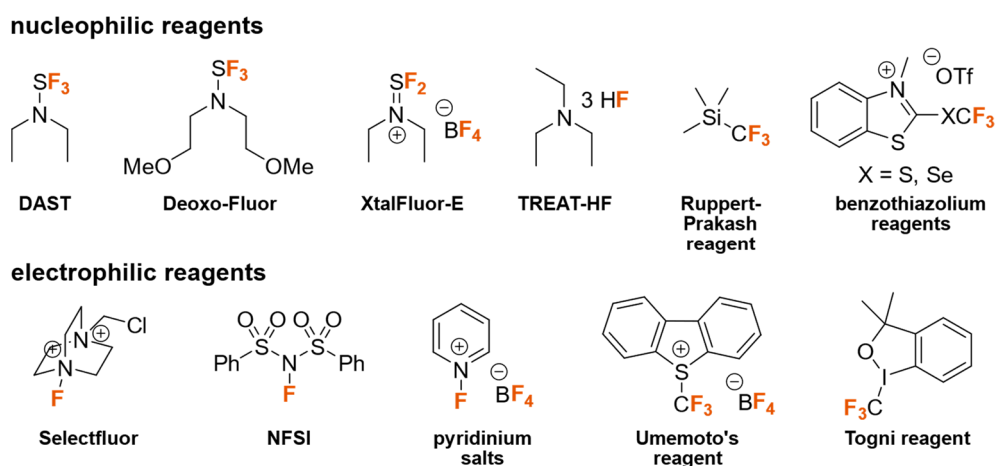
that the *cis* conformer was strongly preferred, stabilized by a hydrogen bond between CF<sub>2</sub>H and C=O groups (*Figure 2.18, b.*).<sup>[142]</sup>

Finally, the analysis of crystal structures in the CSD and the PDB revealed that the interactions between C-F and C=O of an amide group are common.<sup>[123]</sup> A well-known example is the interaction between the tricyclic inhibitor **34** and thrombin. X-ray diffraction showed a favorable C-F $\cdots$ C=O interaction (*Figure 2.18, c.*). Additionally, compared to the non-fluorinated version, the binding affinity of the fluorinated thrombin inhibitor was increased by a factor of 6.<sup>[125,143]</sup>

The role of fluorine interactions in peptide and protein chemistry will be discussed in *Section 4.1* of this thesis.

### 3 Synthetic Strategies to Obtain Fluorinated Amino Acids

As demonstrated in *Section 1*, the element fluorine can dominate a broad spectrum of molecular properties. Therefore, it is unsurprising that the development of different fluorination methods has accelerated considerably in the last decades. In general, fluorination reagents can be classified into two categories: nucleophilic and electrophilic reagents. Additionally, different methods have been developed, transforming different chemical groups, such as C-H, C-OH, C=O, and others, into diverse fluorine-containing moieties. *Figure 3.1* presents a selection of fluorinating reagents that can be applied in the organic synthesis of fluorinated compounds. Of course, this overview illustrates only a small portion of existing reagents. Several detailed reviews were published in the last ten years, summarizing different fluorination approaches and respective reagents.<sup>[3,144–146]</sup>



*Figure 3.1:* Overview of selected fluorinating reagents.<sup>[3,144–147]</sup>

Fluorinated  $\alpha$ -amino acids represent a new class of amino acids with fascinating and tunable properties. Furthermore, they are fundamental building blocks for synthesizing fluorine-containing peptides and proteins. So, many synthetic protocols were developed over the years to facilitate access to this intriguing class of biomolecules. In 2019, Moschner *et al.* presented an in-depth literature review of synthetic strategies for obtaining fluorinated  $\alpha$ -amino acids.<sup>[148]</sup>

In *Section 3.1*, the current state of the art for the synthesis of several fluorinated amino acids relevant to this thesis will be discussed. This work focused on the fluorinated variants of aliphatic canonical and non-canonical L-amino acids: MfeGly **17**, DfeGly **18**, DfpGly **20**, pentafluoropropylglycine (PfpGly) **21**, both diastereomers of trifluorovaline (TfVal) **22** and **23**, and both diastereomers of trifluoroisoleucine (TfIle) **25** and **26**. Furthermore, it is important to mention that only stereoselective strategies will be presented.



### 3.1 Stereoselective synthesis of fluorinated aliphatic amino acids

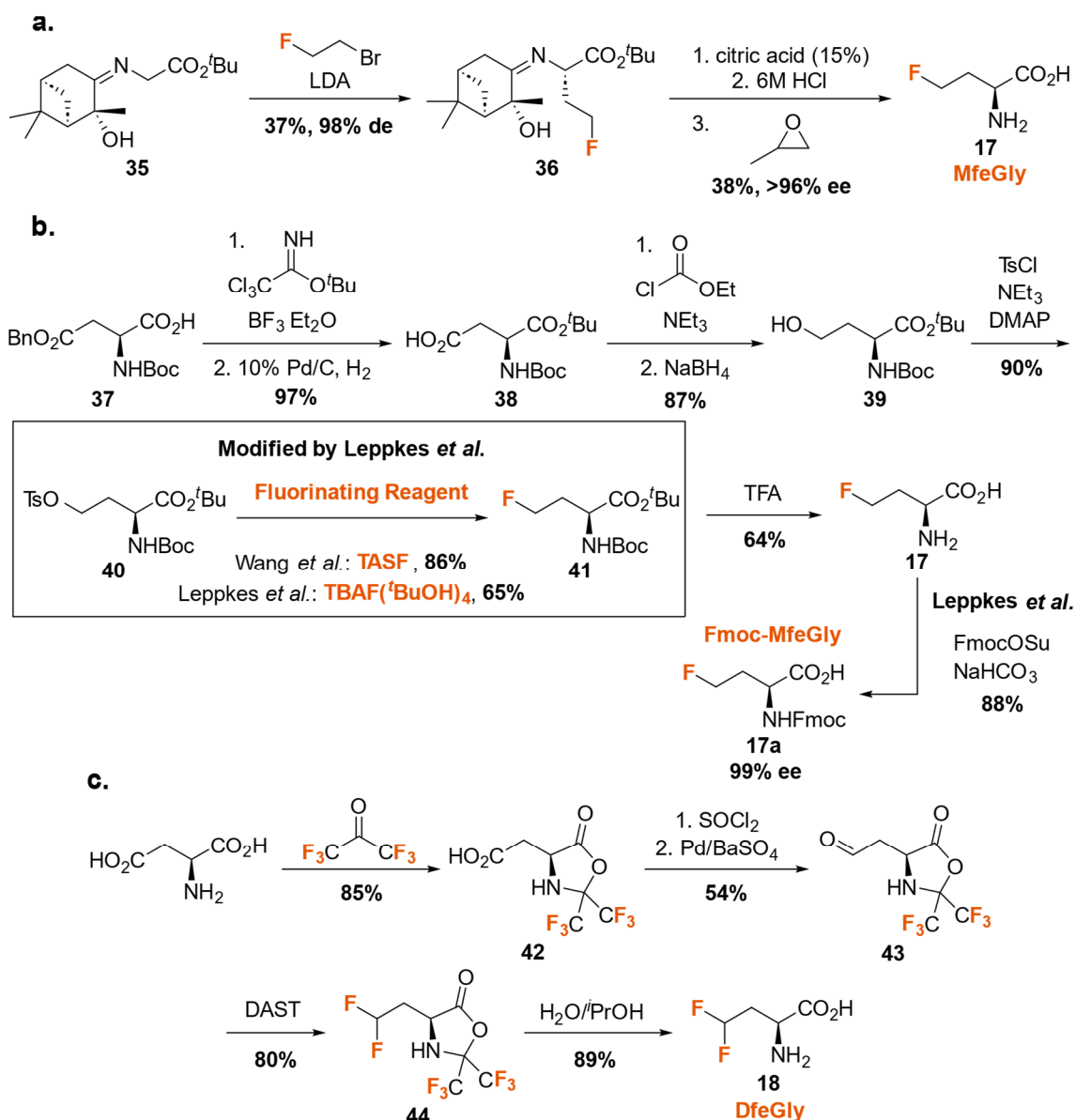
#### Fluorinated Analogs of 2-Aminobutyric Acid (Abu)

The fluorinated derivatives of Abu are widely used building blocks in the design of fluorine-containing peptides and proteins. The access to the respective amino acids with different degrees of fluorination allows a systematic approach for studying the influence of fluorination on the properties of these biopolymers.<sup>[11]</sup>

Two different strategies for the stereoselective synthesis of MfeGly **17** have been described in the literature. Laue *et al.* applied a strategy using a chiral auxiliary, specifically a chiral Schiff base of a (-)- $\alpha$ -pinene derivative **35**. In the first step, the Schiff base **35** was stereoselectively alkylated with 1-bromo-2-fluoroethane. The corresponding product **36** was obtained in excellent diastereomeric purity of 98% de but only in a moderate yield of 37%. Finally, after the two-step deprotection, (2*S*)-MfeGly **17** was isolated with great enantiomeric purity (>96% ee) and an overall yield of 14% (*Scheme 3.1, a.*)<sup>[149]</sup>

The second approach was described by Wang *et al.* and later improved by Kocsch and co-workers (*Scheme 3.1, b.*)<sup>[150,151]</sup> Protected aspartic acid ester **37** was used as the starting material for the respective strategy. After protecting the carboxylic acid group, the benzyl group of the side chain was removed *via* hydrogenation. Two-step reduction led to the formation of a homoserine derivative **39**. The introduction of fluorine was achieved by, first, converting the alcohol function to a tosylate **40**, which was subsequently fluorinated by nucleophilic substitution with tris(dimethylamino)sulfonium difluorotrimethylsilicate (TASF). In the final step, treatment with trifluoroacetic acid (TFA) gave the desired product **17** in an overall yield of 42%.<sup>[150]</sup> Leppkes *et al.* modified this synthetic procedure in two important points. First, the key fluorination step was improved by exchanging the costly TASF reagent with the less expensive tetrabutylammonium tetra(*tert*-butanol) fluoride (TBAF(*t*BuOH)<sub>4</sub>). Additionally, for the first time, the synthesis of the fluorenylmethoxycarbonyl- (Fmoc-) protected (2*S*)-MfeGly **17a** was described, providing a building block suitable for solid-phase peptide synthesis (SPPS). (2*S*)-Fmoc-MfeGly **17a** was obtained in an overall yield of up to 50% and an excellent enantiomeric purity of 99% ee.<sup>[151]</sup>

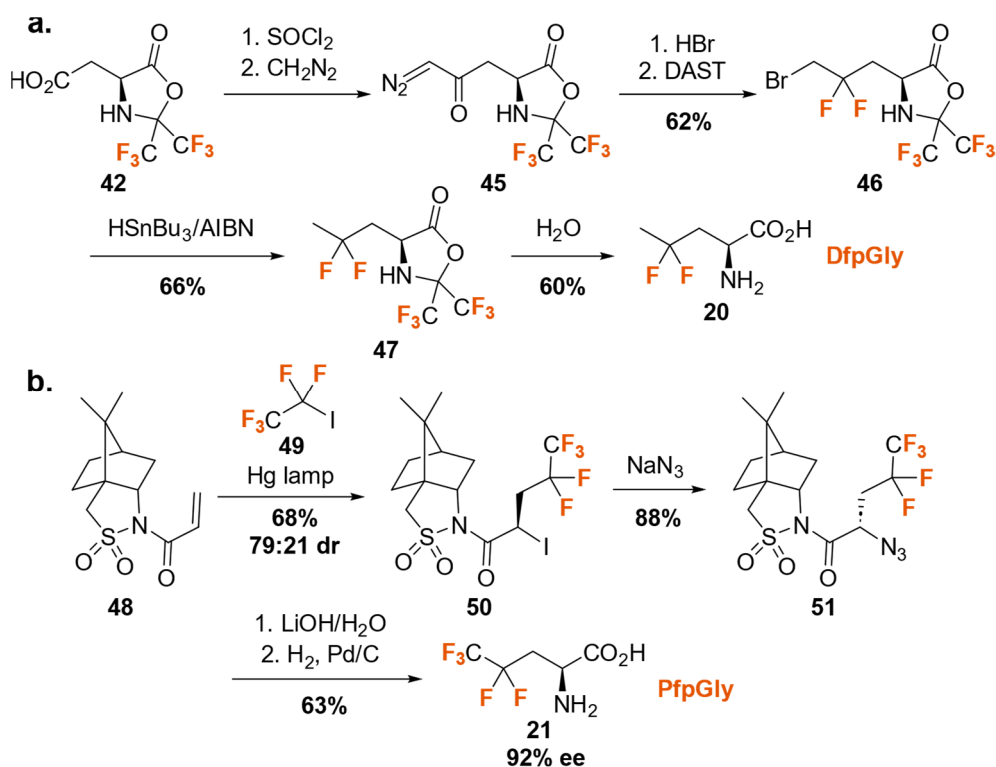
The synthesis of the difluorinated derivative, DfeGly **18**, was described by Winkler *et al.* First, aspartic acid was reacted with hexafluoroacetone (HFA) to give the oxazolidinone **42**. The free carboxylic acid functionality of the side chain was converted to the respective acyl chloride using thionyl chloride, and subsequent hydrogenation with the Pd/BaSO<sub>4</sub> catalyst provided the corresponding aldehyde **43**. The transformation of the aldehyde moiety to the CF<sub>2</sub>H group was achieved by deoxygenative fluorination with diethylaminosulfur trifluoride (DAST). The final product, (2*S*)-DfeGly **18**, was isolated after hydrolysis with H<sub>2</sub>O/PrOH in an overall yield of 33%. (*Scheme 3.1, c.*)<sup>[152]</sup>



Scheme 3.1: a. Synthesis of MfeGly **17** described by Laue *et al.* b. Synthesis of MfeGly **17** described by Wang *et al.* and Leppkes *et al.* c. Synthesis of DfeGly **18** described Winkler *et al.*

### Fluorinated Versions of Norvaline

The synthesis of DfpGly **20** was achieved by Osipov *et al.*, using similar chemistry as already described for the synthesis of DfeGly **18**. In the first step, the side chain of the oxazolidine **42** was extended using thionyl chloride and diazomethane to give the respective diazo compound **45**. The conversion of **45** with HBr and DAST gave the bromo-difluoro-oxazolidinone **46**. Debromination was achieved using tributyltin hydride and azobisisobutyronitril (AIBN), yielding the difluoropropylglycine derivative **47**. Finally, the desired product was isolated after hydrolysis with an overall yield of 25%, starting from **45** (Scheme 3.2, a).<sup>[153]</sup>



Scheme 3.2: a. Synthesis of DfpGly **20** described by Osipov *et al.* b. Synthesis of PfpGly **21** described by Yajima and Nagano.

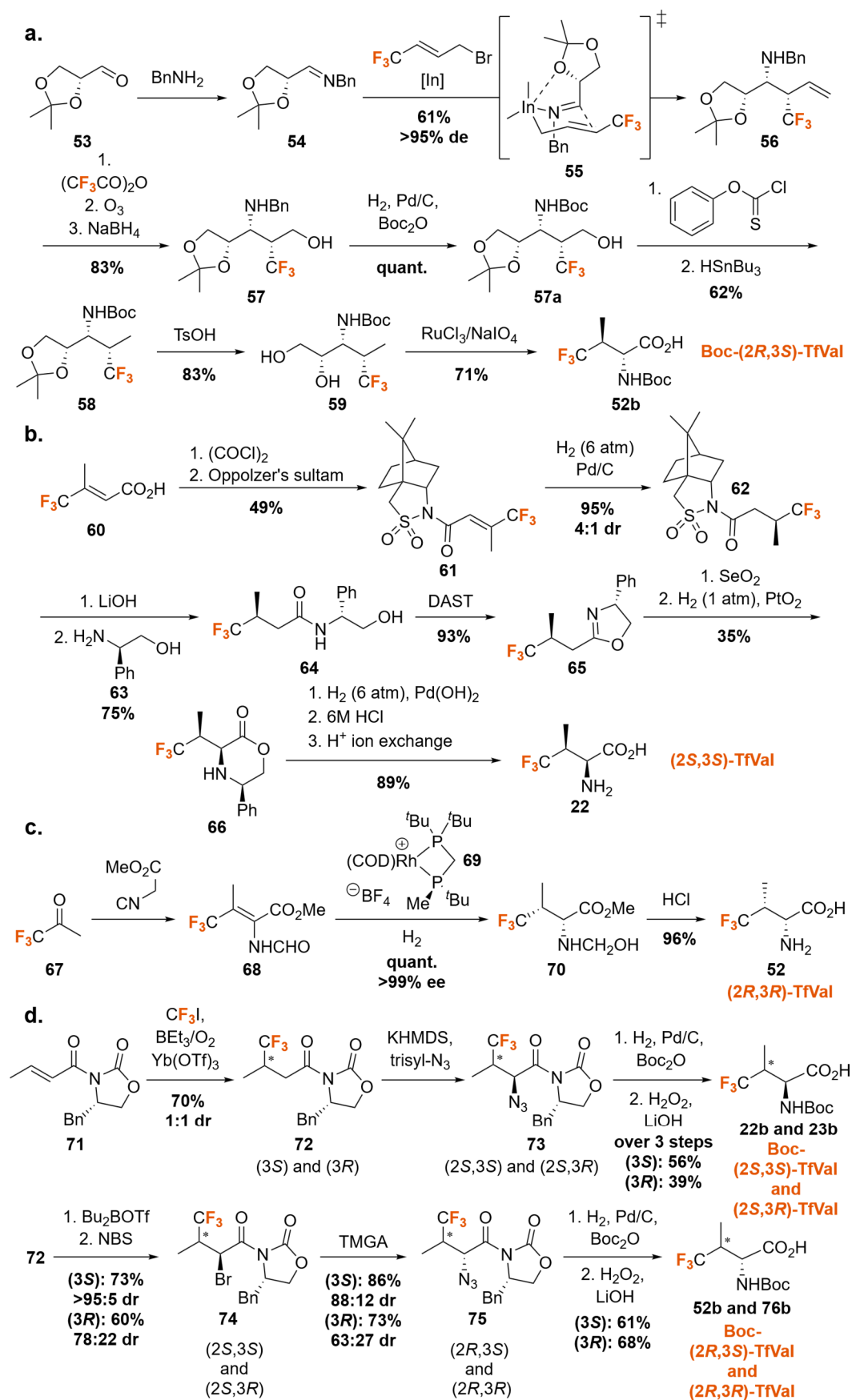
To synthesize the pentafluorinated version of norvaline, PfpGly **21**, Yajima and Nagano used Oppolzer's sultam auxiliary **48** as the starting material (Scheme 3.2, b.).<sup>[154]</sup> In the key step of the protocol, sultam **48** was alkylated with 1,1,1,2,2-pentafluoro-2-iodoethane **49** in the presence of Na<sub>2</sub>S<sub>2</sub>O<sub>3</sub> under photoirradiation. The respective iodoperfluoroethyl product **50** was obtained in good yield and diastereoselectivity of 79:21. The nucleophilic substitution with sodium azide of the major diastereomer was carried out under inversion of stereochemistry. The obtained azide **51** was first hydrolyzed to remove Oppolzer's auxiliary and subsequently hydrogenated to give the desired PfpGly **21** in an overall yield of 38% and with enantiomeric excess of 92% ee.<sup>[155]</sup>

The first synthetic strategy to obtain both molecules was described by Larsson *et al.*<sup>[156]</sup> Corresponding fluorinated carboxylic acids were used as precursors, and the amine functionality was introduced using a chiral Evans auxiliary.

### Trifluorinated Valine

Four different strategies for the synthesis of trifluorinated analogs of valine have been published. Chen *et al.* reported the first stereoselective procedure to obtain (2*R*,3*S*)-4,4,4-trifluorovaline **52** ((2*R*,3*S*)-TfVal). First, chiral aldehyde **53** was converted to the respective imine **54**. Indium-mediated allylation was imagined as the key step, introducing both relevant stereocenters to the structure.

## Synthetic Strategies to Obtain Fluorinated Amino Acids



Scheme 3.3: Synthesis of four isomers of TfVal: a. Method described by Chen *et al.* b. Method described by Pigza *et al.* c. Method described by Benhaim *et al.* d. Method described by Erdbrink *et al.*

The reaction proceeded with excellent diastereoselectivity (>95% de) to give the desired amine **56**. The transition state **55**, crucial for stereoselectivity, is shown in *Scheme 3.3, a*. The amine **56** was treated with trifluoroacetic anhydride, subjected to ozonolysis, and reduced with NaBH<sub>4</sub> to give the alcohol **57**. The benzyl group was removed under standard hydrogenation conditions, and the respective amine was protected with *tert*-butoxycarbonyl anhydride (Boc<sub>2</sub>O). Two-step Barton-McCombie deoxygenation gave the desired product **58**. Subsequently, the ketal group was removed, and the respective diol **59** was oxidized with RuCl<sub>3</sub>/NaIO<sub>4</sub> to give the Boc-protected (2*R*,3*S*)-TfVal **52b**. The desired amino acid was synthesized over ten steps with an overall yield of 18%.<sup>[157]</sup>

Three years later, Pigza *et al.* described a strategy to obtain (2*S*,3*S*)-TfVal **22**. Similar to the synthesis of PfpGly **21**, Oppolzer's sultam was used to establish the desired stereochemistry. The respective chiral auxiliary was attached to (*E*)-4,4,4-trifluoro-3-methylbut-2-enoic acid **60** in two steps. Stereoselective hydrogenation of sultam **61** provided product **62** with sufficient diastereomeric purity (4:1 dr). Hydrolysis of **62** and subsequent coupling with amine **63** afforded the amide **64**. Oxazoline **65** was obtained by treating **64** with the DAST reagent. Subsequently, oxidative rearrangement of **65** with SeO<sub>2</sub> provided the respective oxazinone, which was further subjected to hydrogenation with PtO<sub>2</sub> to give **66** as a mixture of diastereomers. The major isomer could be separated from the minor product by flash chromatography. Finally, hydrogenation over Pd(OH)<sub>2</sub> and subsequent treatment with 6M HCl provided (2*S*,3*S*)-TfVal **22** in an overall yield of 4% (*Scheme 3.3, b*).<sup>[158]</sup>

Benhaim *et al.* described a less time-consuming strategy to obtain (2*R*,3*R*)-TfVal **52** (*Scheme 3.3, c*). First, alkene **68** was obtained from 1,1,1-trifluoroacetone **67**, applying Schollkopf's procedure. In the key stereoselective hydrogenation step with [((*R*)-trichickenfootphos)Rh(COD)]BF<sub>4</sub> catalyst **69**, the desired TfVal derivative **70** was obtained with excellent enantiomeric purity (>99% ee). Treatment of **70** with conc. HCl in acetone gave (2*R*,3*R*)-TfVal **52** in an overall yield of 96%, starting from alkene **68**.<sup>[159]</sup>

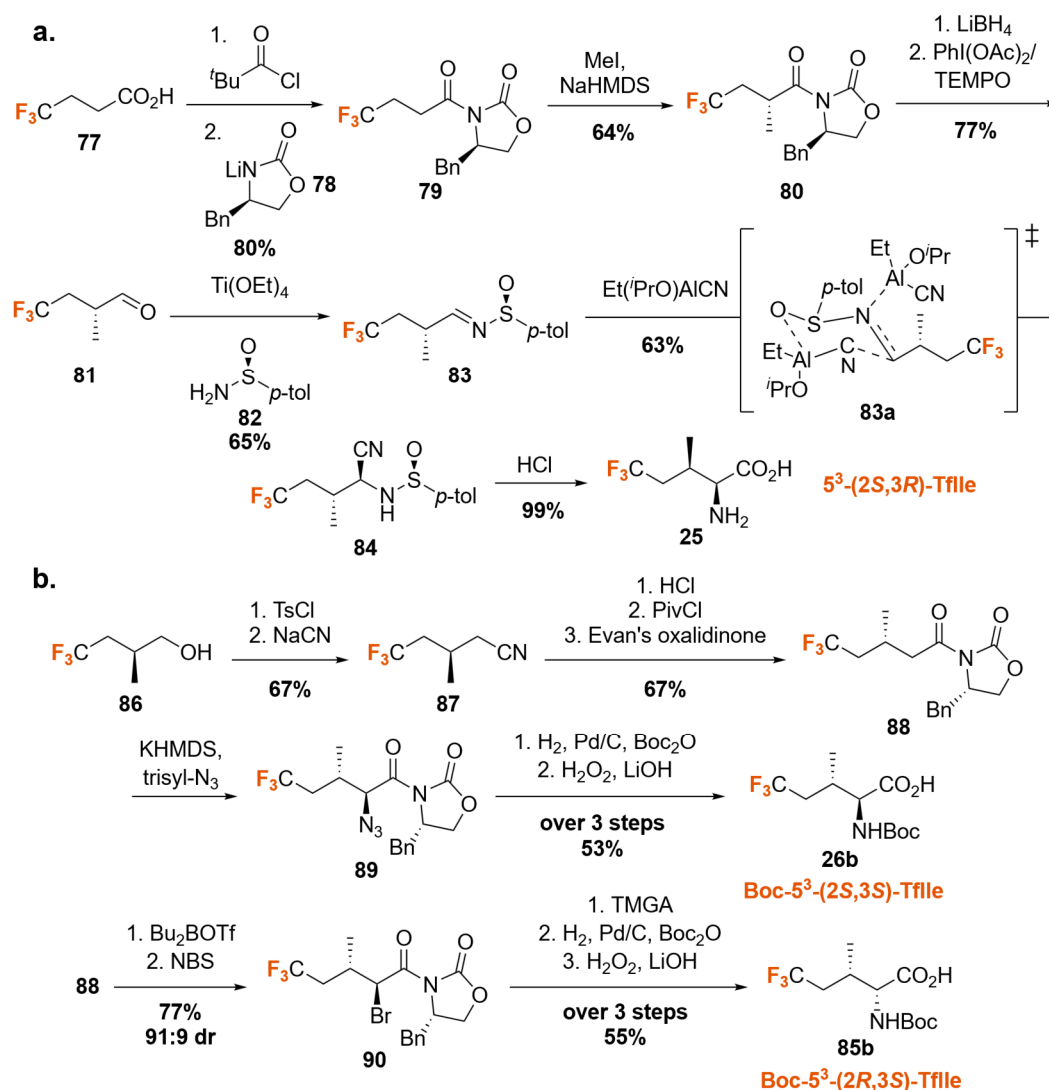
The only work that describes the synthesis of all four diastereomers of TfVal was reported by Erdbrink *et al.* (*Scheme 3.3, d*). Evans oxazolidinone **71** was used as the starting material. In the first step, the respective Michael system **71** was trifluoromethylated using CF<sub>3</sub>I, BEt<sub>3</sub>/O<sub>2</sub>, and ytterbium triflate hydrate. The reaction proceeded with excellent β-regioselectivity but without diastereoselectivity. The respective diastereomers could be separated by flash chromatography. From (3*S*)- and (3*R*)-oxazolidinone **72**, both diastereomers of (2*S*)-TfVal could be synthesized in three steps. The α-amine functionality was introduced by treatment of **72** with KHMDS and trisyl azide and subsequent hydrogenation and Boc protection. Removal of the Evans auxiliary with H<sub>2</sub>O<sub>2</sub> and LiOH gave Boc-(2*S*,3*S*)- **22b** or Boc-(2*S*,3*R*)-TfVal **23b** in an overall yield of 20% (2*S*,3*S*) and 11% (2*S*,3*R*). To generate the corresponding (2*R*)-TfVal

diastereomers, first,  $\alpha$ -bromination of (3*S*)- or (3*R*)-oxazolidinone **72** gave the desired products **74**. Nucleophilic substitution of **74** with tetramethylguanidinium azide (TMGA) proceeded with inversion of stereochemistry to give azide **75**. As already described for the conversion of **73** to **22b** and **23b**, Boc-(2*R*,3*S*)- **52b** or Boc-(2*R*,3*R*)-TfVal **76b** was obtained in an overall yield of 12% (2*R*,3*S*) and 5% (2*R*,3*R*).<sup>[160]</sup>

Additionally, Kumar and co-workers presented a method for enantiomeric resolution of all four diastereomers of TfVal.<sup>[161]</sup>

### Trifluorinated Isoleucine

In 2008, Wang and Resnick described an asymmetric strategy to obtain 5<sup>3</sup>-(2*S*,3*R*)-TfIle **25**.<sup>[162]</sup>



The stereochemistry of the side chain was established *via* Evans auxiliary chemistry. First, 4,4,4-trifluorobutyric acid **77** was activated using a mixed anhydride approach and subsequently reacted with the chiral oxazolidinone **78**. The obtained amide **79** was stereoselectively methylated in the  $\alpha$ -position, giving the desired product **80** as a single diastereomer. Reduction of **80** with  $\text{LiBH}_4$  and subsequent oxidation with  $\text{PhI}(\text{OAc})_2/\text{TEMPO}$  gave the chiral aldehyde **81**. The asymmetric Strecker reaction described by Davis and co-workers was applied to introduce the amine moiety. In the first step, the reaction of aldehyde **81** with (*S*)-(+)-toluenesulfinamide **82** in the presence of  $\text{Ti}(\text{OEt})_4$  gave sulfinimine **83**. Treatment of **83** with  $\text{Et}^i(\text{PrO})\text{AlCN}$  led to the formation of amino nitrile **84**. The transition state **83a**, which establishes the respective stereochemistry, is illustrated in *Scheme 3.4, a*.<sup>[163]</sup> After recrystallization, the product was obtained with a diastereomeric ratio of >99:1. Hydrolysis of **84** provided 5<sup>3</sup>-(2*S*,3*R*)-TfIle **25** in an overall yield of 16% (*Scheme 3.4, a*).

Erdbrink *et al.* described the stereoselective synthesis of Boc-5<sup>3</sup>-(2*S*,3*S*)-TfIle **26b** and Boc-5<sup>3</sup>-(2*R*,3*S*)-TfIle **85b**. Chiral alcohol **86**, whose synthesis has already been discussed in the context of the protocol of Wang and Resnick, was selected as the starting material. However, compared to the approach of Wang and Resnick, another strategy was envisioned for the asymmetric introduction of the amino group. Chiral alcohol **86** was converted to the respective tosylate and treated with sodium cyanide to give nitrile **87**. Hydrolysis of **87** gave chiral carboxylic acid, which was further coupled with oxazolidinone. From the corresponding amide **88**, both diastereomers of 5<sup>3</sup>-TfIle were obtained. The same chemistry was used, as already discussed, for the synthesis of TfVal diastereomers by Erdbrink *et al.* Boc-5<sup>3</sup>-(2*S*,3*S*)-TfIle **26b** was obtained with an overall yield of 22%, and the respective Boc-(2*R*,3*S*)-isomer **85b** was synthesized with an overall yield of 17%.<sup>[164]</sup>

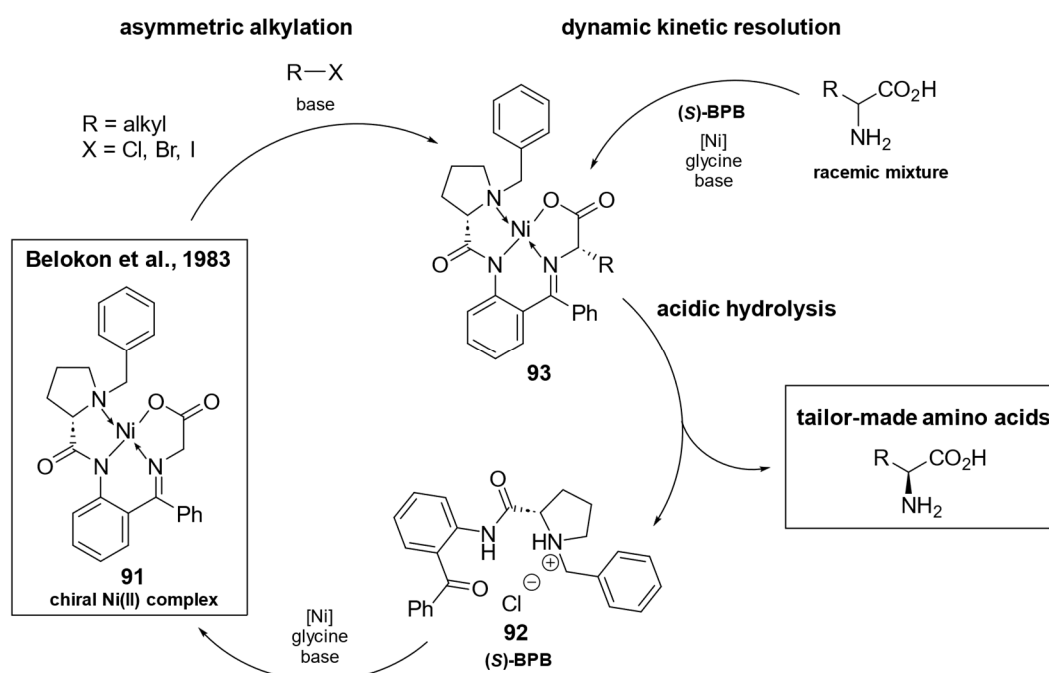
Furthermore, Biava and Budisa described a chiral resolution method using acylase I from *Aspergillus melleus* to obtain enantiomerically pure 5<sup>3</sup>-(2*S*,3*S*)-TfIle **26** and 5<sup>3</sup>-(2*S*,3*R*)-TfIle **25**.<sup>[165]</sup>

Moschner *et al.* addressed an entire chapter of their review to a particular method for synthesizing fluorinated amino acids: application of chiral nickel complexes.<sup>[148]</sup> In the following section, advantages and existing limitations will be outlined.

### 3.2 Chiral nickel(II) complexes for the asymmetric synthesis of fluorinated amino acids

Schiff bases of glycine analogs can be powerful tools in synthesizing non-canonical amino acids.<sup>[166–168]</sup> In 1983, Belokon *et al.* described copper(II) complexes, which could be used for asymmetric synthesis and chiral resolution of  $\alpha$ -amino acids.<sup>[169]</sup> Two years later, Belokon *et al.* presented a modified version of the same approach, introducing respective chiral

nickel(II) complexes.<sup>[170]</sup> Compared to the previously reported Cu(II) complex, the Ni(II) derivatives showed improved reactivity and stability.<sup>[166]</sup> The classic **Belokon complex 91** consists of the chiral (*S*)-2-[*N*-(*N'*-benzyl)prolyl]amino]-benzophenone ((*S*)-BPB) ligand **92** and a glycine residue (*Scheme 3.5*). The synthesis of **91** from proline is straightforward, can be carried out on a gram-scale, and has been further improved over the years.<sup>[171]</sup> The chemistry of this methodology can be categorized into two different approaches. First, (*S*)-BPB **92** can be directly used for dynamic kinetic resolution of racemic mixtures of  $\alpha$ - and  $\beta$ -amino acids. Secondly, the chiral Ni(II) complex **91** can undergo further transformations at the glycine moiety to give tailor-made non-canonical amino acids.<sup>[172]</sup>



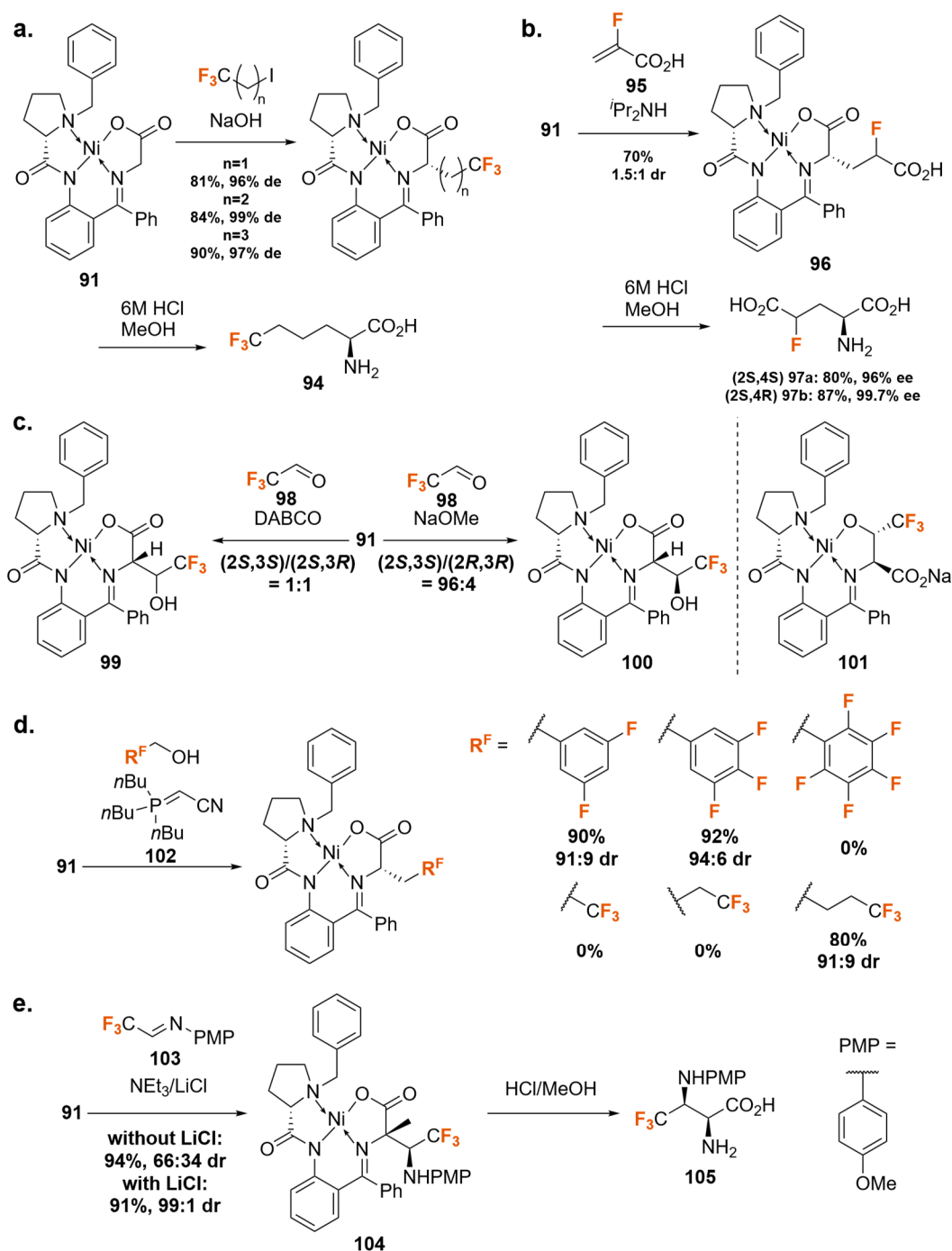
*Scheme 3.5:* Asymmetric synthesis of tailor-made amino acids using Belokon complex **91**.

A prominent example is the asymmetric alkylation of **91** in the presence of a base, providing the alkylated Ni(II) complex **93**. Subsequent hydrolysis gives the desired amino acid. Additionally, (*S*)-BPB ligand **92** can be recovered and recycled for further use. The stereoselectivity of the respective alkylation reaction can be explained by the stereochemical nature of (*S*)-BPB ligand **92**. The nitrogen atom of the proline residue, which coordinates to Ni(II), is chiral. The stereocenter of proline's  $\alpha$ -carbon solely controls the respective stereochemistry. This feature ensures that the aryl group blocks the top face of the molecule, thereby imposing stereoselectivity on further transformations.<sup>[166,172,173]</sup>

Next to alkyl halide alkylations, other reaction types, such as Michael addition, Aldol reaction, Mitsunobu-Tsunoda alkylation, and Mannich-type reaction, have been applied in the context of the synthesis of fluorinated amino acids (*Scheme 3.6*). Wang *et al.* presented the



synthesis of linear trifluorinated amino acids with varying side chain lengths. Fluorinated alkyl iodides were used as electrophiles, and the respective alkylations were carried out in the presence of sodium hydroxide. All transformations proceeded with excellent diastereoselectivities (>96% de). Hydrolysis gave the trifluorinated analog of norleucine **94** (Scheme 3.6, a).<sup>[174]</sup> Belokon *et al.* investigated the Michael addition of **91** to methyl 2-fluoroacrylate **95** in the presence of diisopropylamine.



Scheme 3.6: Different methods for synthesizing fluorinated amino acids using Belokon complex **91**: a. Asymmetric alkylation. b. Michael addition. c. Aldol reaction. d. Mitsunobu-Tsunoda reaction. e. Mannich-type reaction.

The reaction proceeded under excellent stereocontrol at the  $\alpha$ -carbon. However, diastereoselectivity at  $\gamma$ -carbon could not be achieved, and a mixture of both (*S*)-diastereomers **96** was obtained with a ratio of 1.5:1. Separation on a Toyopearl HW-55F column and subsequent hydrolysis gave (2*S*,4*S*)- **97a** and (2*S*,4*R*)-4-fluoroglutamic acids **97b** (Scheme 3.6, b.).<sup>[175]</sup>

Soloshonok *et al.* elaborated on the aldol reaction of the Ni(II) complex with a series of fluorinated aliphatic aldehydes. The authors could demonstrate that the respective diastereoselectivity was highly dependent on the base used. The reaction of **91** and fluorinated aldehyde **98** with 1,4-diazabicyclo[2.2.2]octane (DABCO) in chloroform gave a mixture of two diastereomers **99**. As expected, the stereoselectivity at the  $\alpha$ -carbon could be controlled, while at the  $\beta$ -carbon, no stereochemical preference could be observed. In contrast, the aldol reaction with the same starting materials but the presence of NaOMe in methanol provided the Ni(II) complex of (2*S*,3*S*)-trifluorothreonine **100** as the major product and Ni(II) complex of (2*R*,3*R*)-trifluorothreonine as the minor product (96:4 dr). The formation of an additional intermediate **101** explained the differences in respective reactivities. Deprotonation of the side chain hydroxyl group leads to a rearrangement, discoordinating the carboxylic acid group from the metal center and coordinating the respective alkoxide. Perfluoroalkyl functionality interacts with the metal center and adopts a conformation opposite the *N*-benzyl substituent.<sup>[166]</sup> After hydrolysis in the presence of methanol and 2M HCl, both fluorinated  $\beta$ -hydroxyamino acids were obtained (Scheme 3.6, c.).<sup>[176]</sup>

Drouet *et al.* adopted the Mitsunobu-Tsunoda method to alkylate **91** with fluorinated aromatic and aliphatic alcohols in the presence of cyanomethylene-tributylphosphorane **102** (CMBP). Most fluorinated benzyl alcohols could be alkylated in high yield and with great diastereomeric purities. Perfluorobenzyl alcohol was an exception, failing to undergo the respective transformation. Fluorinated aliphatic alcohols were alkylated with lower yield compared to aromatic analogs. 2,2,2-Trifluoroethanol and 3,3,3-trifluoropropan-1-ol could not successfully be employed in the scope of this method, indicating that the trifluorinated group should have a greater distance to the hydroxyl functionality (Scheme 3.6, d.).<sup>[177]</sup>

Soloshonok *et al.* described a Mannich-type reaction of the Ni(II) complex **91** and protected fluoroimine **103** in the presence of triethylamine and lithium chloride. The respective addition of LiCl significantly improved the diastereomeric ratio of this transformation (from 66:34 to 99:1). Hydrolysis gave 4,4,4-trifluoro-2,3-diaminobutanoic acid **105** (Scheme 3.6, e.).<sup>[178]</sup>

The selection of transformations discussed here illustrates the versatility and limitations of the chiral Ni(II) complex **91** in synthesizing fluorinated amino acids. Of course, other examples exist for each reaction type, which has been discussed in several reviews.<sup>[166,172]</sup> After

Belokon and co-workers first described the Ni(II) complex chemistry, other chiral ligands have been developed.<sup>[179]</sup> Figure 3.2 summarizes the respective development.<sup>[179–186]</sup>

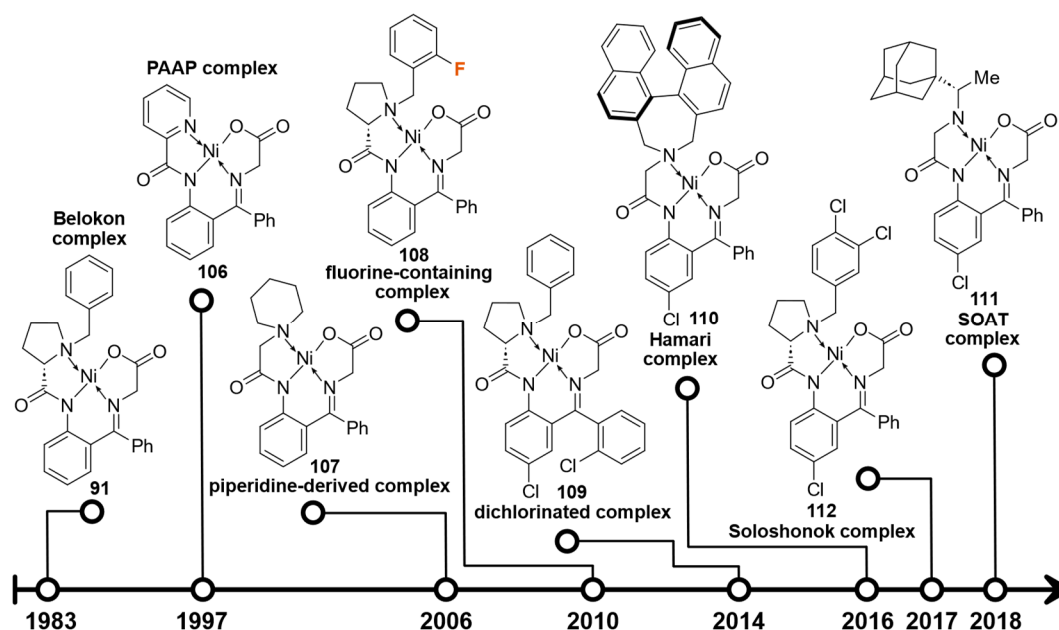


Figure 3.2: Selected milestones in the development of chiral Ni(II) complexes.

Recently, Soloshonok and co-workers introduced the Ni(II) complex **112** with two chlorine atoms at the benzyl group and an additional chlorine atom at the aminobenzophenone moiety. Soloshonok complex **112** displayed significantly improved reactivity and control over stereochemistry, especially in reactions with electrophiles.<sup>[172,179]</sup> The role of the **Soloshonok complex 112** in synthesizing fluorinated amino acids will be discussed in the next part of this section.

### Soloshonok Complex

The crystal structures of methylated and non-methylated versions of both Ni(II) complexes were studied to explain the improved stereocontrol of the Soloshonok complex **112** compared to Belokon's original version **91** (Figure 3.3).<sup>[187]</sup> Surprisingly, the crystal structure of the Belokon complex **91** did not reveal any aromatic-aromatic interactions. The distance between the benzyl ring and the *ortho*-hydrogen of the aminobenzophenone phenyl ring was 4.30 Å, hence too long for attractive interactions. The crystal structure of the Soloshonok complex **112** displayed a different picture. The benzyl ring adopted a conformation close to the aminobenzophenone moiety. The respective interactions can be described as a mixture of edge-face and offset-stacked aromatic-aromatic interactions. Additional stabilization was attributed to electrostatic interactions between the benzyl group's chlorine atoms and the aminobenzophenone ring's hydrogen atoms. Both crystal structures of methylated Ni(II)

complexes provided a deeper understanding of the origin of respective abilities to control the stereochemistry. In contrast to the non-methylated Belokon complex **91**, the methylated version **113** revealed distinct aromatic-aromatic interactions between the benzyl ring and the aminobenzophenone group. Methylated Soloshonok complex **114** showed even stronger aromatic interactions with both phenyl rings in nearly perfect parallel alignment. The differences in the respective aromatic group's conformational arrangement shape the chelate ring's geometry. This results in different dihedral angles between the respective methyl groups and the chelate ring, leading to different spatial proximities of the methyl group to the phenyl group of the aminobenzophenone moiety. Consequently, it means that in the methylated Belokon complex **113**, steric repulsion between the methyl group and the aminobenzophenone phenyl ring is much more pronounced than in the case of the methylated Soloshonok complex **114**.

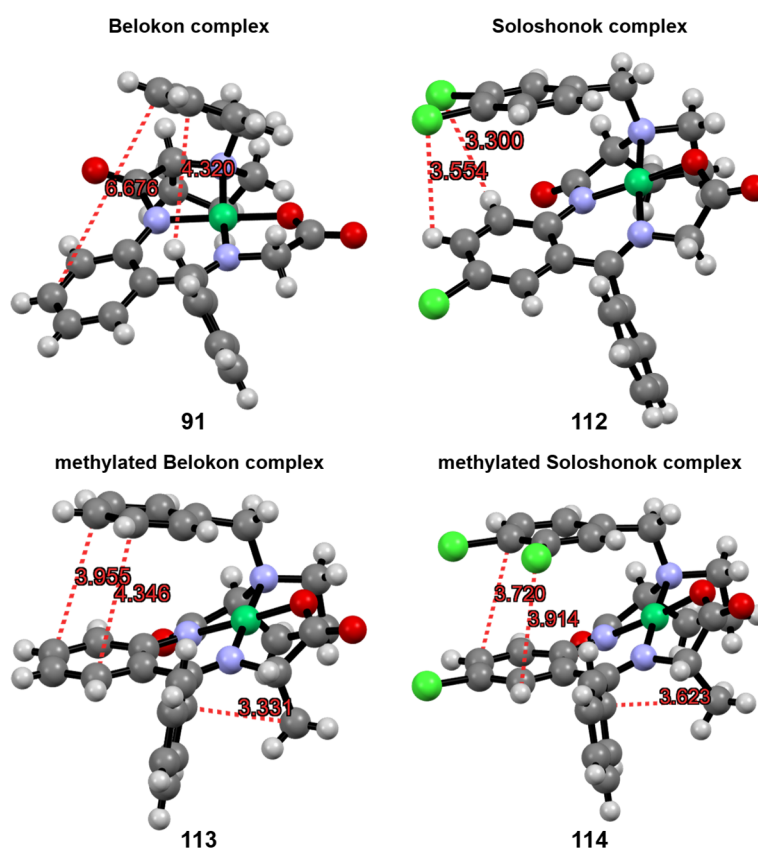
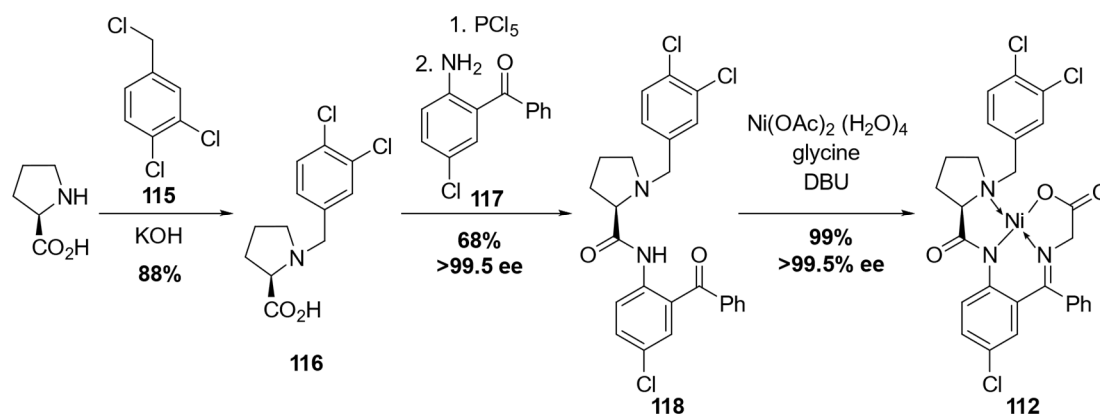


Figure 3.3: Crystal structures of non-methylated and methylated versions of Belokon complex and Soloshonok complex (Belokon complex **91**: CCDC number 1520061, Soloshonok complex **112**: CCDC number 1520062, methylated Belokon complex **113**: CCDC number 1520063, methylated Soloshonok complex **114**: CCDC number 1026566).

At the same time, this explains the different thermodynamic stabilities of complexes **113** and **114**, revealing the origin of the observed differences in respective diastereoselectivities.<sup>[187]</sup> Furthermore, Levitskiy *et al.* conducted theoretical calculations to study further the non-covalent interactions in both Ni(II) complexes. The results supported the conclusions

drawn from the study of corresponding crystal structures.  $\pi$ - $\pi$ -Stacking interactions in Belokon complex **91** are weaker compared to the Soloshonok complex **112**. Furthermore, in the case of the unfavorable (*R*)-configuration of **114**, the steric repulsion is much more destabilizing than in the (*R*)-substituted Belokon complex **113**. In other words, Belokon complex **91** is more likely to tolerate the unfavorable conformation, which explains the poorer stereochemical control of this compound.<sup>[188]</sup>

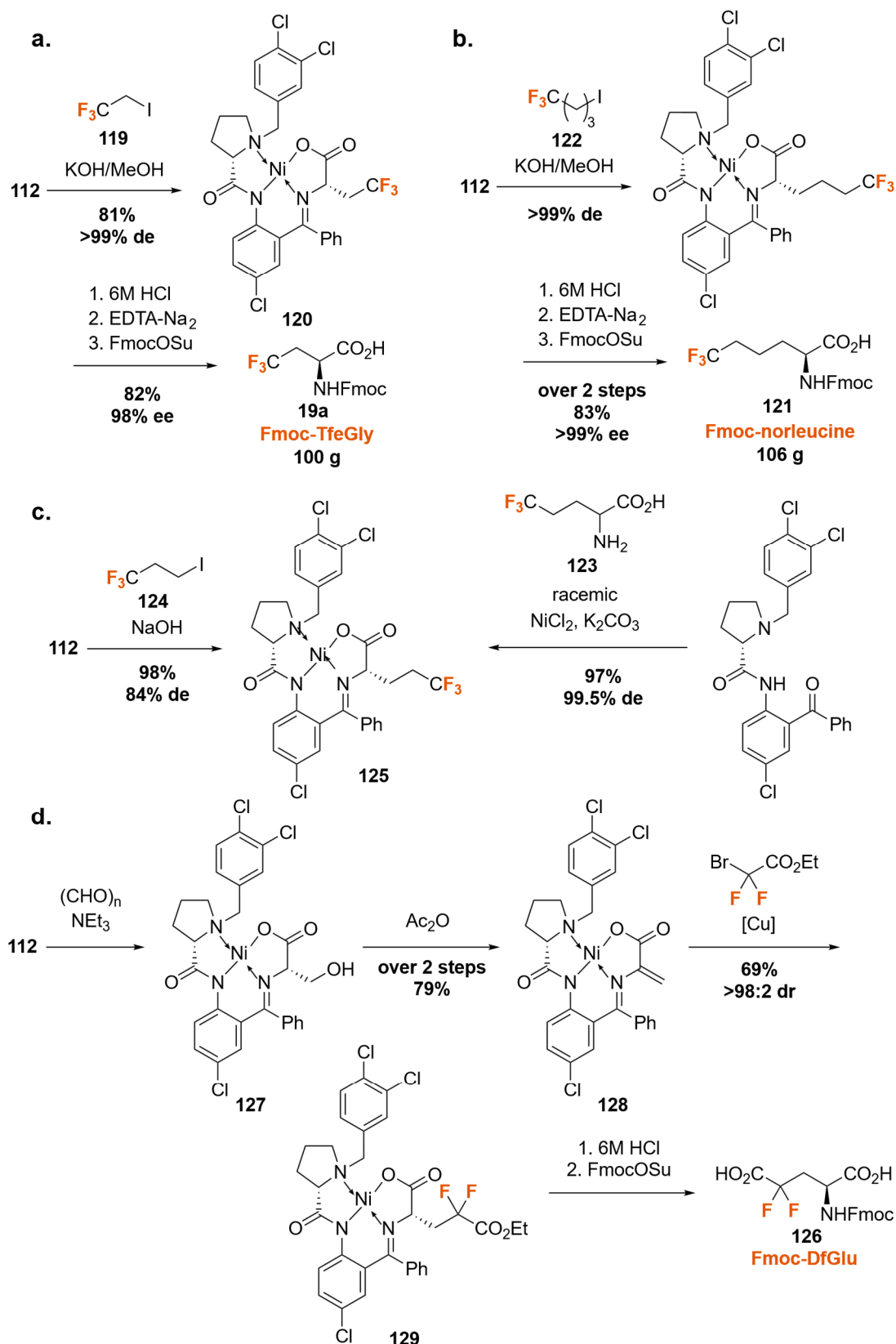
A highly intriguing goal within the field of fluorinated amino acids is the ability to synthesize respective compounds on a large scale. It is crucial to synthesize the respective complexes on a gram-scale to achieve this objective by applying the chemistry of chiral Ni(II) complexes. Regarding the synthesis of chiral Ni(II) complex **112**, a remarkable breakthrough was achieved by Soloshonok and co-workers. In 2017, Romoff *et al.* described a modified approach to synthesize the chlorinated version of the BPB ligand **118**. In the first step, the amine group of proline was protected with 3,4-dichlorobenzyl chloride **115** in the presence of potassium hydroxide to give (3,4-dichlorobenzyl)-D-proline **116**. Coupling of **116** with 2-amino-5-chlorobenzophenone **117** after pre-activation with  $\text{PCl}_5$  provided the chlorinated BPB ligand **118**.<sup>[189]</sup> In 2020, Romoff *et al.* finalized this modified strategy. The reaction of chlorinated BPB **118**, glycine,  $\text{Ni}(\text{OAc})_2 \cdot 4\text{H}_2\text{O}$ , and DBU in MeOH yielded the respective Ni(II) complex **112** in 71% overall yield.



Scheme 3.7: Multigram-scale synthesis of the Soloshonok complex **112**.

Soloshonok complex **112** could be synthesized on a kilogram-scale and with an excellent enantiomeric purity (>99.5% ee).<sup>[190]</sup>

In the context of synthesizing fluorinated amino acids, Soloshonok complex **112** could already hint at its potential. In 2019, Han *et al.* described a new method for synthesizing TfeGly **19**. Asymmetric alkylation of the Soloshonok complex **112** with 2,2,2-trifluoro-1-iodoethane **119** using potassium hydroxide in methanol as a base gave the respective alkylated Ni(II) complex **120** with an excellent diastereomeric purity (>99% de).



*Scheme 3.8:* Synthesis of fluorinated amino acids using Soloshonok complex **112**. **a.** Gram-scale synthesis of Fmoc-TfeGly **19a**. **b.** Gram-scale synthesis of Fmoc-trifluoronorleucine **121**. **c.** Synthesis of trifluoronorvaline **123**. **d.** Synthesis of Fmoc-DfGlu **126**.

Acidic hydrolysis of **120** and subsequent Fmoc-protection using *N*-(fluorenyl-9-methoxycarbonyloxy)-succinimid (Fmoc-OSu) were carried out in a one-pot fashion. Both reaction steps were performed on a multi-gram scale and did not require time-consuming purification techniques. Fmoc-TfeGly **19a** was synthesized on a 100 g scale, and the desired product was obtained in an overall yield of 66% and enantiomeric purity of 98% ee (*Scheme 3.8, a.*).<sup>[191]</sup>

As described by Yin *et al.*, similar conditions could be used to synthesize Fmoc-(2*S*)-6,6,6-trifluoronorleucine **121**. Stereoselective alkylation of **112** with the corresponding fluorinated alkyl iodide **122**, acidic hydrolysis, and Fmoc-protection yielded the desired fluorinated amino acid **121** in 84% overall yield and with an excellent enantiomeric excess of >99% ee.<sup>[192,193]</sup>

Additionally, Mei *et al.* studied the synthesis of 5,5,5-trifluoronorvaline **123** using Soloshonok complex **112** as the starting material. However, direct alkylation of **112** with 3,3,3-trifluoro-1-iodopropane **124** led to unsatisfying results. The respective alkylated Ni(II) complex **125** was isolated with a diastereomeric purity of 84% de. The authors demonstrated that dynamic kinetic resolution was the more suitable alternative to produce the respective fluorinated amino acid.<sup>[194]</sup>

Finally, Tokairin *et al.* described the preparation of 4,4-difluoroglutamic acid **126** (DfGlu). In this case, a dehydroalanine version of the Soloshonok complex was used, which can be described as Umpolung of the respective reactivity. Dehydroalanine Soloshonok complex **128** is a Michael system that can react with nucleophiles. Classic Soloshonok complex **112** was transformed in two steps to give the dehydroalanine version **128**. Treatment of **112** with formaldehyde provided the corresponding serine complex **127**. Acetylation and subsequent elimination under reflux conditions yielded the dehydroalanine Ni(II) complex **128**. Michael addition of BrCF<sub>2</sub>CO<sub>2</sub>Et/Cu system to **128** gave the Ni(II) complex of DfGlu **129** with an excellent diastereomeric purity. Hydrolysis and Fmoc-protection provided Fmoc-DfGlu **126**.<sup>[195]</sup>

The goal of this chapter was to show, on the one hand, the many different, time-consuming methods necessary to produce stereoselectively fluorinated amino acids. On the other hand, chiral Ni(II) complexes represent a class of compounds that, due to their strong stereocontrol, can play an essential part in synthesizing fluorinated amino acids. In particular, gram-scale synthesis is feasible with Ni(II) complexes and, if properly used, could be an important factor in preparing highly fluorinated peptides and proteins.

## 4 Highly Fluorinated Peptide Structures - Properties and Applications

In the preceding chapters, first, fluorine's unique role in peptide and protein sciences was illustrated in some examples, and second, the synthesis of fluorinated amino acids, the central building blocks of these biomolecules, was elucidated. In this section, the highly fluorinated peptide systems will be discussed. The incorporation of fluorine into peptides and proteins can be achieved in multiple ways. First, fluorinated amino acids can be incorporated into peptide and protein sequences *via* standard SPPS. Furthermore, biosynthetic machinery can be exploited by introducing fluorinated amino acids to endogenous aminoacyl tRNA synthetases (aaRS), resulting in a covalent binding to the respective transfer ribonucleic acid (tRNA). The fluorinated amino acid-tRNA complex relocates to the ribosome, and the respective unnatural building block is inserted at the desired position. Finally, synthesized peptides and proteins can be fluorinated with conventional fluorinating reagents. This allows the implementation of fluorine over the entire sequence. The last two methods play an important role mainly in producing fluorinated proteins.<sup>[13]</sup> Although this chapter will focus on the peptide models, it is important to note that highly fluorinated proteins have also been studied. The introduction of numerous fluorinated residues or groups can provide important structural information.<sup>[196]</sup> In 2020, perfluorination of proteins was reviewed by Miller and Sletten in more detail.<sup>[197]</sup> Regarding highly fluorinated peptide systems, a distinction can be made between peptides and peptidomimetics with attached polyfluorinated alkyl tags and peptides containing multiple fluorinated residues.

### 4.1 Peptide-based perfluorinated systems

#### Peptides and peptidomimetics with polyfluorinated alkyl tags

To limit the scope of this section, only the peptide models whose perfluorinated groups contain more than three fluorine atoms are presented here. Preslar *et al.* designed peptide amphiphiles with a hydrophilic region consisting of lysine or glutamic acid residues at the C-terminus, a hydrophobic region consisting of valine and alanine residues, and a polyfluoroalkyl chain located at the N-terminus. The peptide amphiphiles exhibited pH-dependent self-assembly to supramolecular structures. Interestingly, cylindrical nanostructures formed at lower pH showed a strong magnetic resonance signal, while ribbon-type structures formed at higher pH had a significantly reduced signal (*Figure 4.1, a.*)<sup>[198]</sup> Later, a  $\text{Ca}^{2+}$  concentration-dependent shift in  $^{19}\text{F}$  NMR intensity was observed for ribbon-type nanostructures, providing a tool to image  $\text{Ca}^{2+}$  concentrations in a biological context.<sup>[199]</sup>



Another approach to developing polyfluorinated self-assembling peptides for  $^{19}\text{F}$  magnetic resonance imaging (MRI) was reported by Yuan *et al.* The respective peptide contained a ( $t$ BuS)-protected cysteine residue and a lysine residue with an additional 3,5-bis(trifluoromethyl)benzoic acid moiety. Peptide self-assembly was mediated by glutathione reduction, and formed nanostructures could subsequently be disassembled using legumain protease or caspase 3/7, allowing on-off switching of the  $^{19}\text{F}$ -NMR/MRI signal.<sup>[200,201]</sup>

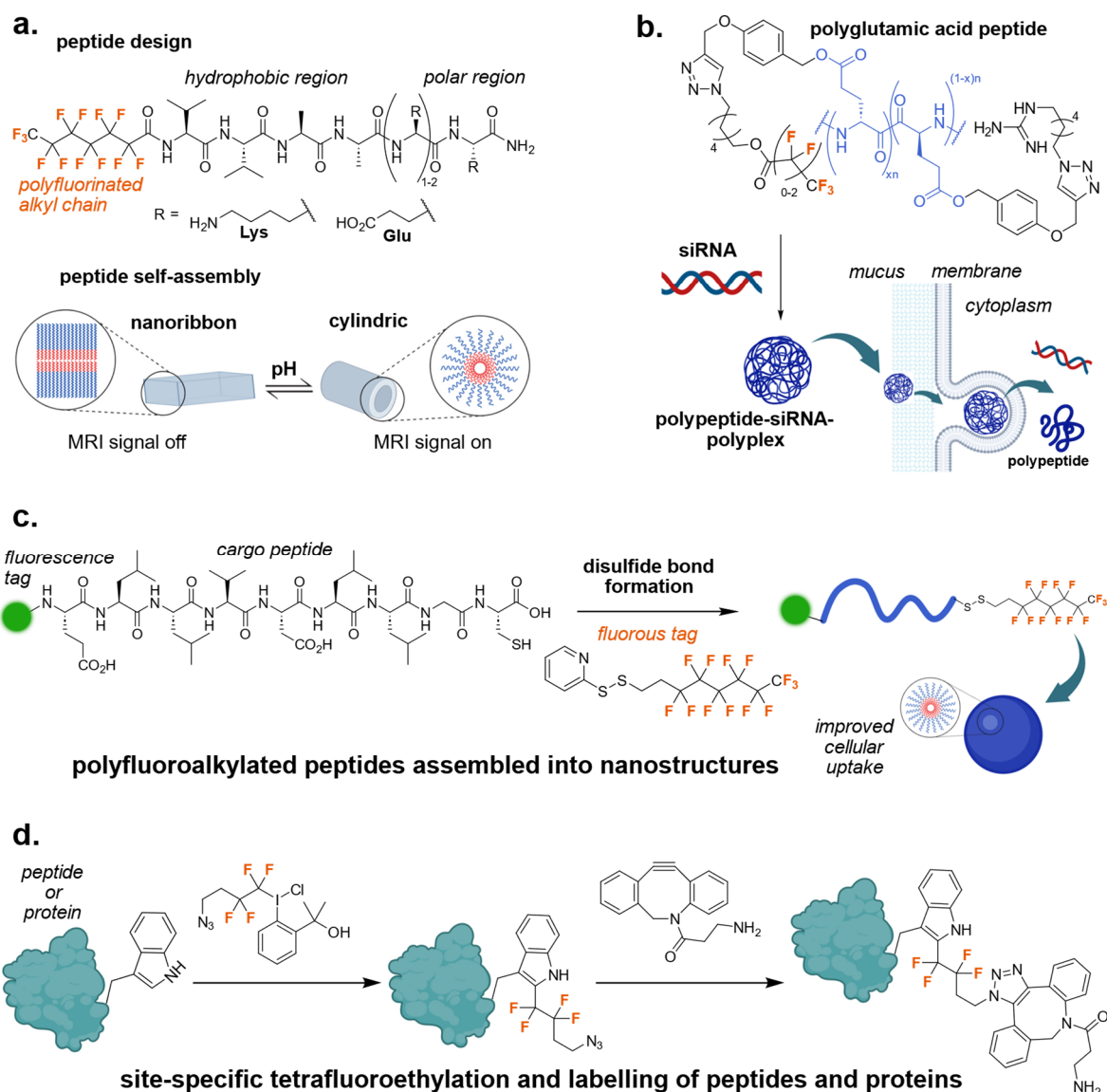
Yin and co-workers introduced  $\alpha$ -helical polyglutamic acid peptides. The respective carboxylic acid moieties were replaced by benzyl ester groups, which were further covalently attached to perfluorinated and guanidinated functionalities *via* click chemistry. The polypeptides formed polyplexes in the presence of siRNA, enabling siRNA transmembrane delivery. Furthermore, polyfluorination enormously facilitated the mucus permeation by approximately 240 folds (*Figure 4.1, b.*).<sup>[202]</sup>

Yang and co-workers investigated Ala-Ala dipeptides attached to a polyfluorinated alkyl chain. The respective peptides self-assembled into nanofibers and nanoribbons, where the handedness of the formed supramolecular structures was controlled by the chirality of the alanine residue at the N-terminus. Additionally, the helicity of the perfluoroalkyl chain (M or P) was determined by the handedness of the self-assembled structures.<sup>[203,204]</sup>

In 2020, Rong *et al.* demonstrated that introducing the fluorous tag at the N-terminus of several cargo peptides enhanced the peptide delivery into cells *via* endocytic pathways (*Figure 4.1, c.*). Furthermore, perfluoroalkylated peptides showed improved proteolytic stability and polyfluorinated proapoptotic peptides displayed anticancer activity both *in vitro* and *in vivo*.<sup>[205]</sup>

However, perfluorocarbons do not necessarily have to be covalently linked to the peptides to enhance the corresponding cell permeability. Perfluorinated compounds can be used as activators for this purpose. Thus, perfluorinated fatty acids can significantly improve the delivery of cell-penetrating peptides (CPPs) into cells. Chuard *et al.* demonstrated that perfluorinated fatty acids could self-assemble in the membrane environment and attract the arginine-rich CPPs because of their respective weak basicity, enhancing delivery into HeLa cells.<sup>[206]</sup>

Perfluorinated groups can also be employed to label peptides or proteins. In this context, several hypervalent iodine reagents were described, providing a tool to introduce different tetrafluoroethyl groups to peptides and proteins (*Figure 4.1, d.*). Furthermore, high selectivity for either cysteine or tryptophan residues was observed depending on the hypervalent iodine reagent used.<sup>[207,208]</sup>



**Figure 4.1:** a. pH-dependent self-assembly of polyfluorinated peptide amphiphiles. b. Fluorinated polyglutamic acid peptide-siRNA complex with improved mucus permeability. c. Design of a fluorous tagged cargo peptide for improved cellular delivery. d. Site-specific tetrafluoroethylation of peptides and proteins. Created with BioRender®.

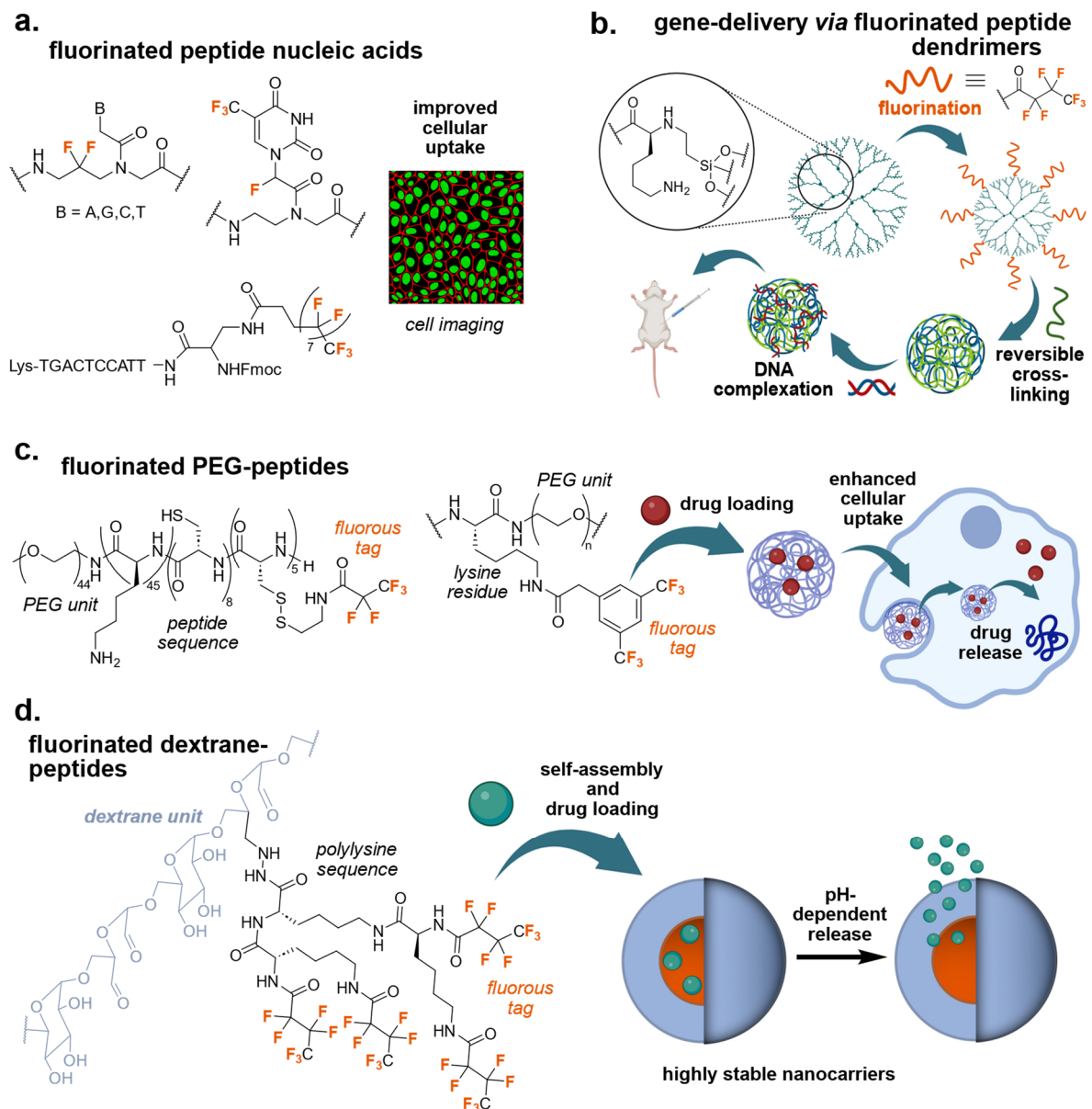
In addition to <sup>19</sup>F-NMR applications, enhancement of cell permeability, and peptide labeling, perfluorinated groups can also be used for fluorous separation of peptides. Inspired by the works of Horváth, Rábai, and Curran (*Section 1.2*), Brittain *et al.* introduced the concept of “fluorous proteomics”.

After protein digestion, a specific class of peptides can be selectively tagged with a fluorous group, subsequently isolated *via* fluorous solid-phase extraction, and analyzed by mass spectrometry (MS).<sup>[209]</sup>

Polyfluorinated groups can be introduced not only *via* fluorous alkyl chains but also by incorporating highly fluorinated amino acids. Interestingly, although some syntheses of highly fluorinated amino acids have been described, they have yet to be utilized in peptide and protein

chemistry.<sup>[197]</sup> Perfluoro-*tert*-butyl-group provides a common motif for the structure of highly fluorinated amino acids. Numerous perfluoro-*tert*-butyl-containing derivatives of amino acids, such as homoserine, tyrosine, and 4-hydroxyproline, have been described. In all cases, the respective perfluorinated amino acids served as excellent  $^{19}\text{F}$  NMR probes, providing great sensitivity and enabling detection at nM concentrations.<sup>[210–214]</sup>

Up to this point, only perfluorinated peptide models have been discussed. However, peptide analogs consisting of additional structures were also studied in the context of fluororous chemistry.



**Figure 4.2:** a. Design and application of fluorinated peptide nucleic acids. b. Fluorinated peptide dendrimers with improved gene delivery. c. Structure and mechanism of action of fluorinated PEG-peptides. d. Design and self-assembly properties of fluorinated dextrane-peptides. Created with BioRender®.

A fascinating example is the class of peptide nucleic acids (PNAs). Fluorinated PNAs usually exhibited higher thermal stabilities and improved delivery into cells (*Figure 4.2, a.*). Although, the respective effects depended on the respective fluorination's type and position.<sup>[215–217]</sup>

Gu and co-workers developed highly fluorinated peptide dendrimers based on a polylysine network. These fluorinated peptide dendrimers displayed several intriguing features, such as improved cell delivery and excellent resistance to protein interactions, facilitating DNA transport to the nucleus, and improving small interfering RNA delivery (*Figure 4.2, b.*).<sup>[218,219]</sup>

Additionally, fluorinated polyethylene glycol (PEG) peptide conjugates were described as valuable self-assembling structures for delivering small drug and DNA molecules (*Figure 4.2, c.*). In this context, different polypeptides were utilized and conjugated to perfluorinated functionalities, enhancing cellular uptake and enabling image-traceability.<sup>[220–222]</sup>

Finally, He and Gu research groups presented dextrane-based polylysine networks conjugated to perfluorinated alkane chains that self-assembled into well-defined spherical nanostructures. The respective fluorinated dendrons displayed excellent cell viability, pH-controlled drug release ability, and enhanced tumor penetration capacity combined with the iRGD peptide (*Figure 4.2, d.*).<sup>[223–225]</sup>

In this literature survey concerning the properties of perfluoroalkylated peptides, one feature prevailed, like a common thread through the entire section: the enhanced cytosolic delivery of respective structures. This demonstrates the outstanding disposition of polyfluorinated alkyl groups to take a pivotal role in transporting bioactive molecules into cells.

### **Peptides built-up by multiple fluorinated amino acids**

Now, literature-known peptide models whose sequences contain at least three fluorinated amino acids will be presented. It rapidly transpires that this amounts to a relatively limited number of examples.

Godbout *et al.* described a 21-residue peptide, LX2, consisting of 15 leucine and six TfeGly **19** residues (*Figure 4.3, a.*). The respective fluorinated building blocks were placed in *i*, *i+3* or *i+4* distance to each other, resulting in the formation of a fluorinated surface in the case of an  $\alpha$ -helical conformation. This enormously hydrophobic structure was investigated utilizing circular dichroism in hexafluoroisopropanol (HFIP) and in the presence of 1-palmitoyl-2-oleoyl-sn-glycero-3-phosphocholine (POPC)/cholesterol liposomes. The respective conformational studies revealed that LX2 adopts predominantly an  $\alpha$ -helix structure. Additional fluorescence assays displayed the ability of LX2 to serve as an artificial ion channel, facilitating the transport of numerous cations. Furthermore, *in silico* calculations confirmed the formation of a tetrameric structure in the presence of liposomes.<sup>[226]</sup> Later, Auger *et al.* studied the

properties of LX2 and the respective acetylated analog, Ac-LX2, in the presence of eukaryotic membrane models, displaying membrane insertion and slightly different locations in the membrane environment.<sup>[227]</sup>

Medina *et al.* designed a novel peptide  $F_F F_F F_F GGGCCGGKGRGD-NH_2$ , with  $F_F = 2,3,4,5,6$ -pentafluorophenylalanine ([2,3,4,5,6F]Phe). This peptide demonstrated the ability to form nanoparticles at the perfluoro-*n*-pentane (PFP) droplet surface. The respective self-assembly process is enabled by three [2,3,4,5,6F]Phe residues placed at the N-terminus of the peptide sequence.

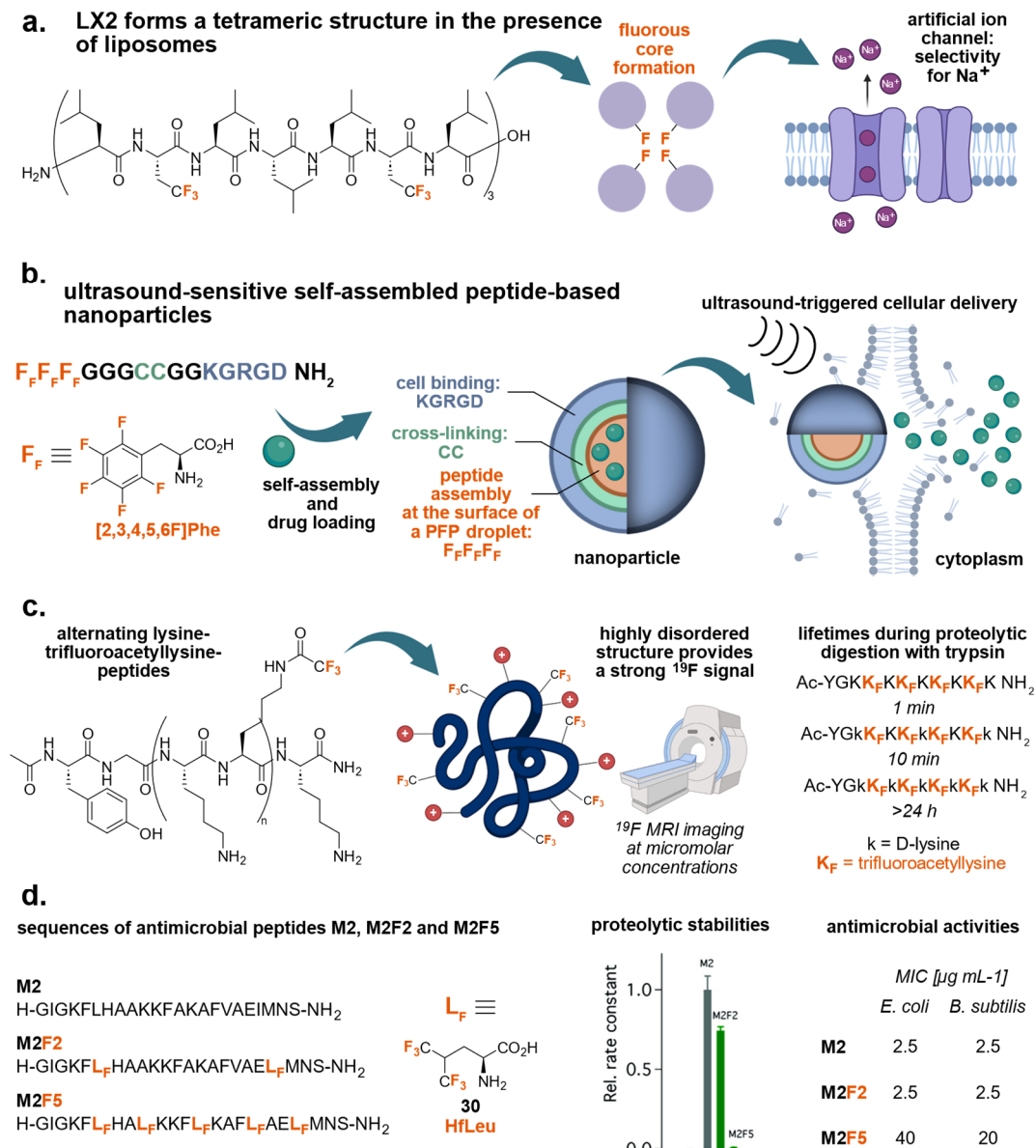


Figure 4.3: a. Design and application of the LX2 peptide. b. Structure and design of ultrasound-sensitive self-assembled peptide-based nanoparticles. c. Fluorinated lysine-rich peptides for  $^{19}F$  MRI. d. Sequences and proteolytic stabilities of fluorinated M2 peptides. Created with BioRender. Proteolytic degradation data were adapted from Meng and Kumar with permission (Copyright © 2007 American Chemical Society).<sup>[228]</sup>

Cysteine residues were introduced to provide additional stabilization for the supramolecular structure *via* disulfide cross-linking. The bioactive RDG-based hydrophilic region at the C-terminus facilitated cell-surface localization. The formed peptide-based nanoparticles could be used as a carrier system to transport biomolecular cargo into cells. The cytosolic delivery was triggered by ultrasound vaporization (*Figure 4.3, b.*).<sup>[229]</sup>

Pomerantz and co-workers introduced peptides with alternating lysine and trifluoroacetyllysine residues as a new class of high-signal agents for <sup>19</sup>F MRI imaging (*Figure 4.3, c.*). Furthermore, the proteolytic stability of the fluorinated peptides was investigated *via* trypsin assay. In *Section 1.3*, the multi-dimensional role of fluorine in the context of the proteolytic resistance of peptides was discussed. In this case, the authors observed a complete digestion of L-lysine-peptide after one minute. However, by substituting native L-lysine residues with D-derivatives, the peptide lifetime could be extended to over 24 hours. This is an intriguing example, indicating that the effect of D-amino acids on the proteolytic stability of peptides is much more explicit than in the case of fluorinated amino acids.<sup>[230]</sup>

Likewise, Meng and Kumar explored the resistance to hydrolysis by trypsin of different fluorinated peptides. The proteolytic stabilities of the peptide M2, a derivative of the antimicrobial peptide magainin, di- (M2F2) and pentafluorinated (M2F5) versions were investigated by an reversed-phase HPLC-based assay. M2F5 showed a remarkable increase in stability to proteolysis compared to M2 and M2F2. While M2 was fully degraded after 40 minutes, 78% of the M2F5 peptide remained in the solution after three hours, indicating the importance of steric bulk for proteolytic stability. At the same time, M2F5 displayed decreased antimicrobial activity relative to M2 and M2F2 peptides due to the formation of helical bundles in solution, demonstrating the diverse effects of fluorination on the different biological properties of peptides (*Figure 4.3, d.*).<sup>[228]</sup>

Fibrous collagen is the most abundant animal protein, consisting of three polypeptides, which self-assemble into a triple helix. The respective polypeptide chains have the repeating sequence Xaa-Yaa-Gly. Pro commonly occupies the Xaa position, while (4*R*)-hydroxyproline ((4*R*)-Hyp) is typically located in position Yaa. To explain the high stability of the collagen helix, first, an intramolecular hydrogen bond network between (4*R*)-Hyp residues, supported by water molecules, was proposed. However, the Raines research group could demonstrate in their significant study that the inductive effect, exerted by the hydroxyl functionality of (4*R*)-Hyp, is the source of the respective collagen stability.<sup>[231]</sup> The authors used (4*R*)-FPro **16** as a substitute for the (4*R*)-Hyp residue. The fluorine *gauche* effect was expected to exhibit a stronger influence on the respective ring structure's conformational properties than the inductive effect of the hydroxyl group. Furthermore, due to its poor hydrogen bond acceptor ability, fluorine should not participate in the water-mediated hydrogen bond network (*Sections 1.1 and 1.2*).

(Pro-Pro-Gly)<sub>10</sub>, (Pro-(4*R*)-Hyp-Gly)<sub>10</sub>, and (Pro-(4*R*)-FPro-Gly)<sub>10</sub> were synthesized and characterized *via* circular dichroism (CD) measurements, showing that (Pro-(4*R*)-FPro-Gly)<sub>10</sub> displayed higher thermal stability than the (4*R*)-Hyp-containing peptide. As discussed in *Section 1.3*, fluorine *gauche* effect forces (4*R*)-FPro **16** to adopt the C<sup>γ</sup>-exo conformation. In the case of the collagen triple helix, this results in a favorable organization of dipole-dipole interactions, leading to improved thermal stability.<sup>[231,232]</sup> Additionally, Raines and co-workers explored the positional dependence of monofluorinated proline derivatives on the stability of the collagen triple helix. They could show that (4*R*)-FPro **16** exhibits a stabilizing effect in position Yaa and a destabilizing effect in position Xaa.

*Table 4.1:* Melting points of selected collagen peptides. The corresponding data were taken from references [231,233].

Xaa-Yaa-Gly	T <sub>M</sub> [°C]
(Pro-Pro-Gly) <sub>10</sub>	41
(Pro-(4 <i>R</i> )-Hyp-Gly) <sub>10</sub>	69
(Pro-(4 <i>R</i> )-FPro-Gly) <sub>10</sub>	91
(Pro-(4 <i>R</i> )-FPro-Gly) <sub>7</sub>	45
((4 <i>R</i> )-FPro-Pro-Gly) <sub>7</sub>	no helix
(Pro-(4 <i>S</i> )-FPro-Gly) <sub>7</sub>	no helix
((4 <i>S</i> )-FPro-Pro-Gly) <sub>7</sub>	33

In contrast, (4*S*)-FPro in position Xaa has a stabilizing effect on thermal stability but a destabilizing effect in position Yaa.<sup>[233,234]</sup> Finally, Dones *et al.* investigated the ((4*S*)-FPro-(4*R*)-Hyp-Gly)<sub>7</sub> peptide, which showed the ability to form a stable triple helix with (Pro-Pro-Gly)<sub>7</sub> but not with itself. Therefore, this study hinted at the potential of ((4*S*)-FPro-(4*R*)-Hyp-Gly)<sub>7</sub> in the detection of damaged collagenous tissue for clinical applications.<sup>[235]</sup>

Niemz and Tirrell studied the consequences arising from fluorination of melittin, a component of bee venom. In this context, the authors synthesized mono- and tetrafluorinated versions, incorporating 5,5,5-trifluoroleucine (TfLeu) at various leucine positions. The fluorinated derivatives displayed a more vital ability to self-assemble into the tetrameric structure in aqueous solution and showed enhanced affinity to insert into lipid bilayers.<sup>[236]</sup>

Probably one of the most impressive studies in the field of highly fluorinated peptides, published to date, was described by Chowdhary *et al.* in 2022. A series of fluorinated peptides with alternating lysine and fluorinated building block sequences were synthesized and characterized. To study the influence of the fluorination degree in a systematic fashion, non-fluorinated Abu and three fluorinated amino acids were used: MfeGly **17**, DfeGly **18**, and TfeGly **19**, resulting in a total number of four 16-residues long peptides AbuK16, MfeGlyK16, DfeGlyK16,



and TfeGlyK16 (Figure 4.4, a.). Hydrophobicity studies *via* the RP-HPLC-based assay revealed the expected trends, showing increasing hydrophobicity with the number of fluorine atoms within the side chain (Figure 4.4, b.). However, MfeGlyK16 displayed lower hydrophobicity than the non-fluorinated derivative, which can be explained by the polarity of the mono-fluorinated side chain (Sections 1.1 and 1.3).

Conformational studies illustrated different structural compositions for each peptide. TfeGlyK16 formed  $\beta$ -sheet structures at all studied concentrations, which can be easily explained by its hydrophobic nature. AbuK16 and DfeGly16 formed a PPII helix at low concentrations and shifted to a  $\beta$ -sheet structure at higher concentrations.

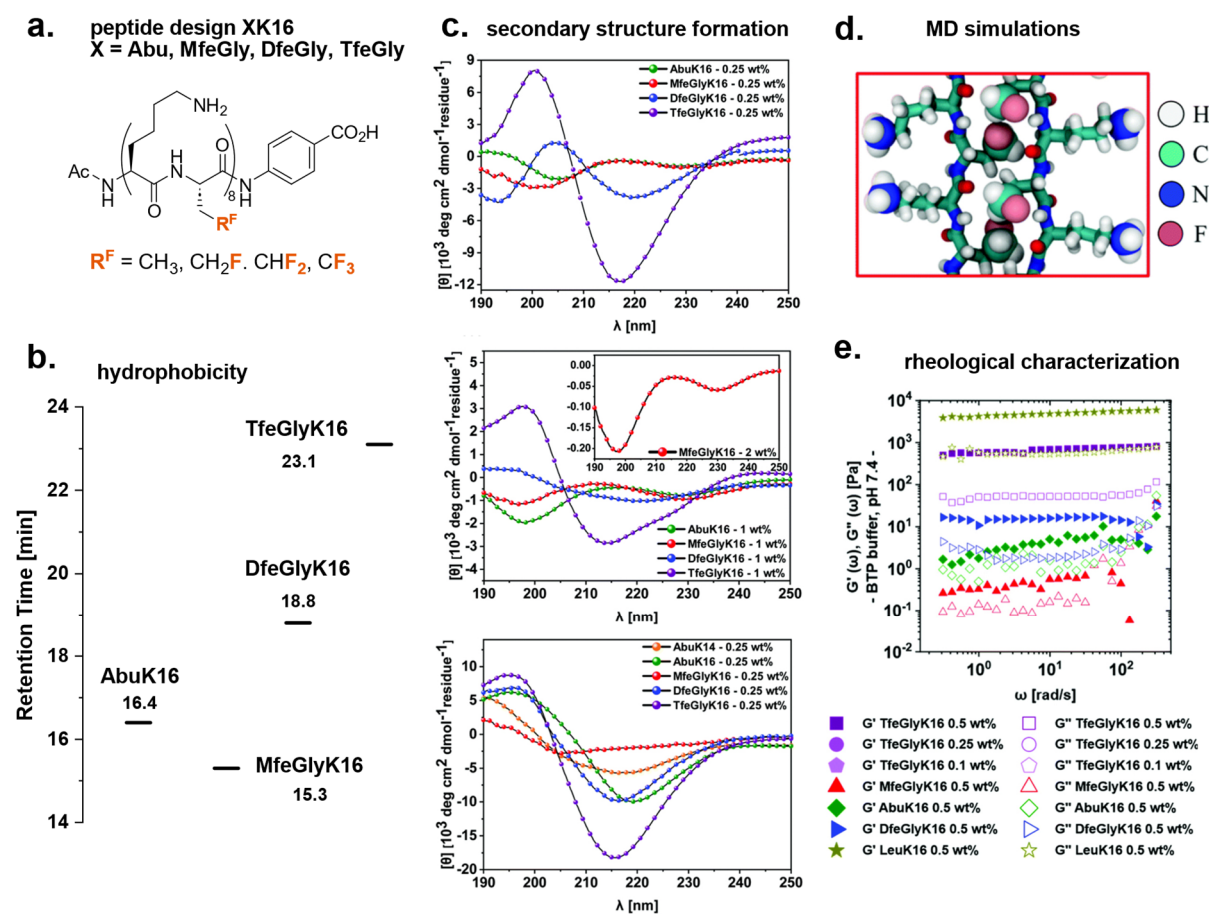


Figure 4.4: a. Peptide design of XK16 peptides (X = Abu, MfeGly 17, DfeGly 18, TfeGly 19). b. Hydrophobicity of fluorinated XK16 peptides. c. Structural properties of XK16 peptides. d. MD simulations of MfeGlyK16 demonstrating intrastrand bonding between monofluorinated side chain and amide backbone. e. Rheological characterization of XK16 peptides. Adapted from Chowdhary *et al.* with permission (Copyright © 2022 Royal Society of Chemistry).<sup>[237]</sup>

Finally, MfeGlyK16 did not show the tendency to form a  $\beta$ -sheet structure at any concentration and pH value (Figure 4.4, c.). Molecular dynamics (MD) simulations revealed that the polarized side chains of MfeGly form an intrastrand contact with backbone hydrogen atoms, preventing peptide self-assembly (Figure 4.4, d.). Additionally, hydrogel properties of the



respective peptides were investigated *via* rheology measurements, revealing a correlation between the greater degree of fluorination and improved viscoelastic stability of the corresponding hydrogels (*Figure 4.4, e.*).<sup>[237]</sup>

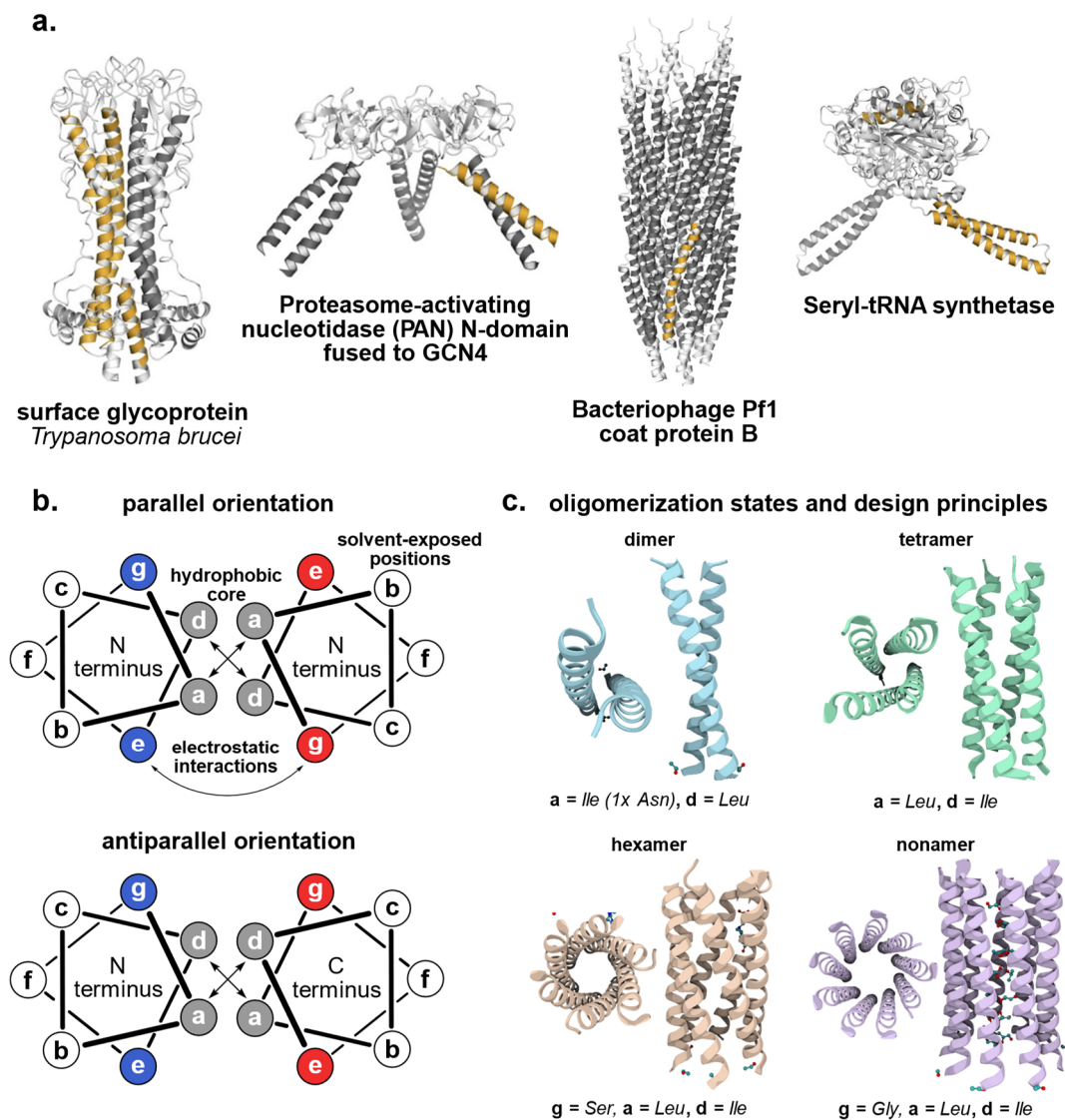
This section illustrated the immense potential of highly fluorinated peptide systems in biological applications, especially in the context of membrane permeability and cytosolic delivery of different cargo molecules. At the same time, sequences containing high amounts of fluorinated amino acids are still underexplored, providing a chance to shift the focus from polyfluorinated alkanes to more biocompatible systems. Up to this point, one class of peptides, arguably the most intensively studied concerning the effects of multiple fluorinations, still needs to be discussed. The last section will review the consequences of perfluorination on the properties of coiled coil peptides.

## 4.2 Perfluorinated coiled coil motifs

Francis Crick and Linus Pauling described the structures of keratin and myosin as twisted helices, introducing a novel protein motif to the scientific community: the **coiled coil (CC)**. The CC motif has been extensively studied in the last seven decades, revealing its essential role in various biological processes such as intracellular transport, transmembrane signaling, membrane fusion, and signal transduction.<sup>[238,239]</sup> Today, the CC structure is one of the most researched protein motifs with well-understood structural principles, allowing the rational design of *de novo* CC-forming peptides (*Figure 4.5, a.*).<sup>[240,241]</sup>

Crick had already described the interactions between the respective helical peptides as knobs-into-holes (KIH) interactions, with the side chain of one helix (the knob) pointing into the diamond-shaped cavity (the hole) of the other helix. The CC motif usually comprises several repeating KIH interactions.<sup>[241]</sup> In this context, the repetitive sequence of seven amino acids (*abcdefg*), called heptad repeat, represents the foundation of the respective motif. The positions *a* and *d* are occupied by hydrophobic residues (*hpphppp*; *h* = hydrophobic residue, *p* = polar residue), such as valine, leucine, and isoleucine. These amphiphilic sequences can assemble into left-handed suprahelical structures with varying degrees of oligomerization. The CC motif is stabilized by hydrophobic interactions between the residues *a* and *d*, forming the hydrophobic core of the respective tertiary structure, and by electrostatic interactions between positions *e* and *g*. The solvent-exposed positions *b*, *c*, and *f* do not participate in the intermolecular bonding interactions (*Figure 4.5, b.*).<sup>[240]</sup> Essentially, both homomeric and heteromeric arrangements can be formed. In the case of a homomeric CC peptide, the respective monomer self-assembles into the respective CC motif. A heteromeric system comprises two or more peptides that can assemble into the suprahelical structure. A common design principle is the utilization of strictly acidic (all positions *e* and *g* occupied by glutamic acid) and strictly basic

(all positions *e* and *g* occupied by lysine) peptides. This promotes the formation of heteromeric structures while suppressing the respective homomeric assembly.<sup>[240]</sup> Additionally, the peptide strands can adopt a parallel or an antiparallel arrangement. In a parallel CC the hydrophobic core comprises layers with *a-a'* and *d-d'* interactions. The respective salt bridges are formed between *g(n)* and *e'(n+1)* residues.



**Figure 4.5:** a. Diversity of the CC motif in the protein world. Adapted from Lupas and Bassler with permission (Copyright © 2017 Elsevier Ltd.). b. Helical wheel representation of a CC dimer. c. Different oligomerization states and design principles of CC peptides (Dimer: PDB 4DZM; tetramer: PDB 3R4A; hexamer: PDB 4PN9; nonamer: PDB 7BIM) (Created with BioRender®).

In contrast, the hydrophobic packing of an antiparallel arrangement is composed of *a-d'* and *d-a'* layers. Electrostatic interactions emerge between positions *e-e'* and *g-g'* (Figure 4.5, b.). The distinctly different packing situations of the two CC orientations allow design rules to prioritize a specific arrangement.<sup>[240]</sup> If the hydrophobic positions are considered in more detail, further subtleties of the motif become apparent. In the CC dimer, the  $\alpha$ - $\beta$  bond vector of the

side chain in position  $d$  shows directly into the hydrophobic interior. On the contrary, the  $\alpha$ - $\beta$  bond vectors of the residues at positions  $a$  point away from each other. The differences between the hydrophobic positions are crucial for the oligomerization state of the CC motif. The placement of  $\beta$ -branched amino acids in position  $a$  (Val, Ile) and leucine in position  $d$  favors the dimeric oligomerization state. The combination  $a = d = \text{Ile}$  facilitates the trimer formation, while  $a = \text{Leu}$  and  $d = \text{Ile}$  promotes the tetrameric structure.<sup>[240,241]</sup> But not only hydrophobic amino acids can play a crucial role in the determination of the CC oligomerization state. The leucine-zipper peptide GCN4-p1 contains one asparagine residue at position  $a16$ . This design principle can be exploited to promote dimer formation. For example, substituting one Val residue in position  $a$  with Asn reduces the system's overall stability while significantly increasing the specificity for forming the dimeric oligomerization state.<sup>[240]</sup> Additionally, Woolfson and co-workers developed other design principles to obtain higher CC oligomerization states (*Figure 4.5, c.*).

In general, a higher degree of oligomerization can be accessed by expanding the hydrophobic core of the CC motif. Utilizing Ile, Ala, and Gly residues in positions  $e$  and  $g$  can lead to the formation of  $\alpha$ -helical barrels with oligomerization states ranging from a pentamer to a nonamer.<sup>[242,243]</sup> Simultaneously, stabilizing electrostatic interactions shift to previously solvent-exposed positions  $b$  and  $c$ . This overview demonstrates that the CC motif, which, at first glance, might appear rather straightforward, is a susceptible system. Every substitution can significantly influence the CC motif's stability, orientation, or oligomerization state. Additionally, it illustrates the importance of understanding the fundamental forces behind tertiary structure formation. As stated by Woolfson in his excellent review, "*the sequence-to-structure rules can be rationalized in terms of the underlying noncovalent forces.*"<sup>[240]</sup>

The detailed understanding of non-covalent CC interactions allowed chemists to develop different strategies to guide peptide self-assembly and to obtain supramolecular structures. In this context, the formation of fibers<sup>[244,245]</sup>, hydrogels<sup>[246]</sup>, or supramolecular cages<sup>[247]</sup> was achieved. Additionally, the design of self-sorting CC peptide systems was described, enabling orthogonal peptide recognition and assembly. For example, Diss and Kennan introduced different polar functionalities into the hydrophobic core of a CC model. The authors exploited differences in the stabilities of Asn-Asp, Asn-Glu, and guanidine-acid pairs to create an orthogonal CC recognition platform.<sup>[248]</sup> Woolfson and co-workers developed an algorithm to design heterodimeric CC pairs containing peptides with high specificity for each other. Based on the respective algorithm, six peptides were synthesized and equilibrated in a redox buffer. After 48 hours, only the formation of three different pairs was observed.<sup>[249]</sup> Furthermore, Aronsson et al. described the design of four CC peptides, which displayed self-sorting properties. Only the most stable and the least stable pair was formed from four possible dimers. The

authors used the different hydrophobic combinations, Val-Leu and Ile-Leu, to ensure significant differences between the stabilities of the respective CC pairs, enabling orthogonal peptide assembly.<sup>[250]</sup>

Over the last two decades, the influence of fluorine on the properties of the CC motif was intensively investigated. The studies were mainly performed by Tirrell, Kumar, Marsh, and Kokscho working groups and will be summarized in the following section.

### Fluorinated Coiled Coils

In the scope of this section, highly fluorinated CC structures will be reviewed. Still, first, the work of the Kokscho working group should be mentioned in this context. Even though mainly the influence of single substitutions of fluorinated amino acids on CC motif properties was investigated, the corresponding results revealed the position-dependent differences and the role of the microenvironment on the stability of CC structures.<sup>[251–255]</sup>

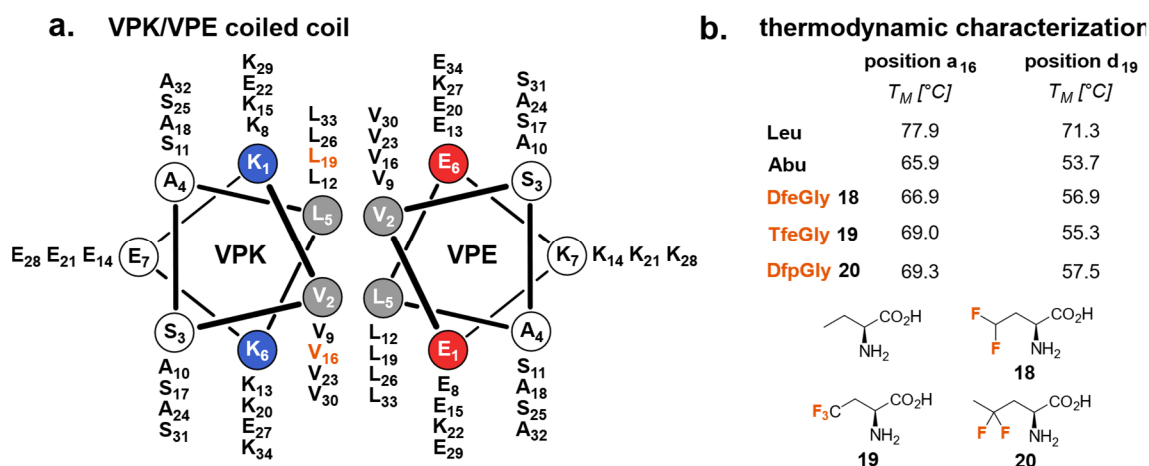


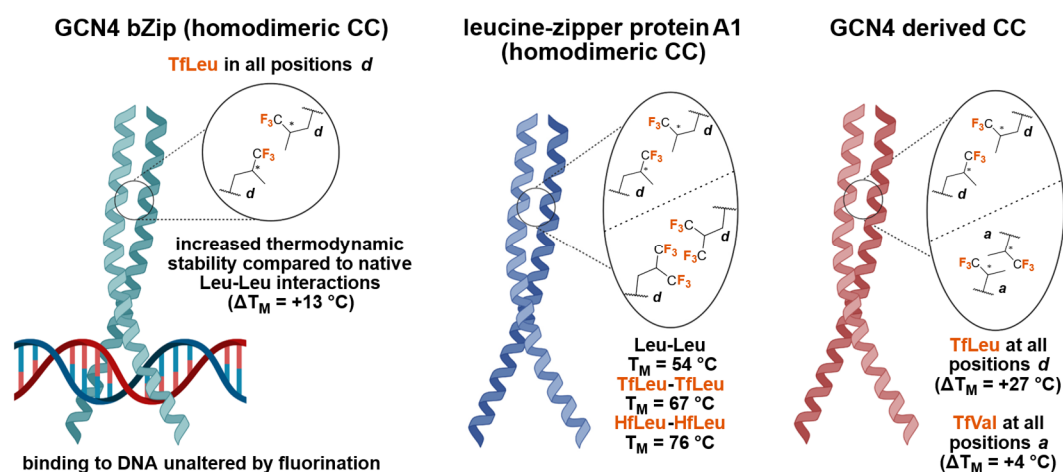
Figure 4.6: a. Helical wheel representation of the parallel VPK/VPE dimer. b. Thermodynamic characterization of fluorinated analogs of VPK/VPE peptides.<sup>[255]</sup>

For example, the thermal stability of the heterodimeric, parallel VPE/VPK system ( $a = \text{Val}$ ,  $d = \text{Leu}$ ) was studied *via* the introduction of various fluorinated amino acids (DfeGly **18**, TfeGly **19** and DfpGly **20**) at positions  $a_{16}$  and  $d_{19}$  of the VPK peptide (Figure 4.6). VPE peptide retained nonfluorinated, allowing the investigation of non-covalent interactions between different fluorinated and non-fluorinated canonical residues. In all cases, the CC stability was decreased compared to the parental system. Additionally, thermal denaturation experiments revealed that the destabilization of the CC structure by introducing the fluorinated residues was much more pronounced in position  $d_{19}$ . DfpGly **20** displayed the least destabilizing character within the VPK/VPE model, compared to DfeGly **18** and TfeGly **19** residues. This was surprising since contrary results were obtained in previous studies investigating an antiparallel CC motif. The packing properties of both antiparallel and parallel CC structures differ

in the directions of the respective  $\alpha$ - $\beta$  vectors, explaining the differences in the thermal stabilities of the corresponding CC motifs.<sup>[256]</sup>

In 2001, Tirrell and DeGrado working groups investigated the introduction of trifluoroleucine (TfLeu) at position *d* of GCN4-p1d. GCN4-bZip is a 56 residue-long DNA binding region of the eukaryotic transcription factor GCN4. The N-terminus of the bZip sequence binds to the DNA, and the GCN4-p1d-containing C-terminus promotes the formation of the dimeric CC structure. Incorporation of TfLeu at all four positions *d* increased the corresponding thermal and chemical stabilities of GCN4-p1d and GCN4-bZip without affecting the DNA-binding affinity of the protein (*Figure 4.7*).<sup>[257]</sup>

The fluorinated leucine-zipper protein A1 properties were studied in a comparable work (*Figure 4.7*). In this context, TfLeu was introduced at 92% of all Leu positions (six residues in the heptad repeats and two at C and N-terminus), using LeuRS (FA1-92). CD measurements did not show any structural perturbations compared to the non-fluorinated version and the melting point of the fluorinated protein was increased by 13 °C.<sup>[258]</sup>

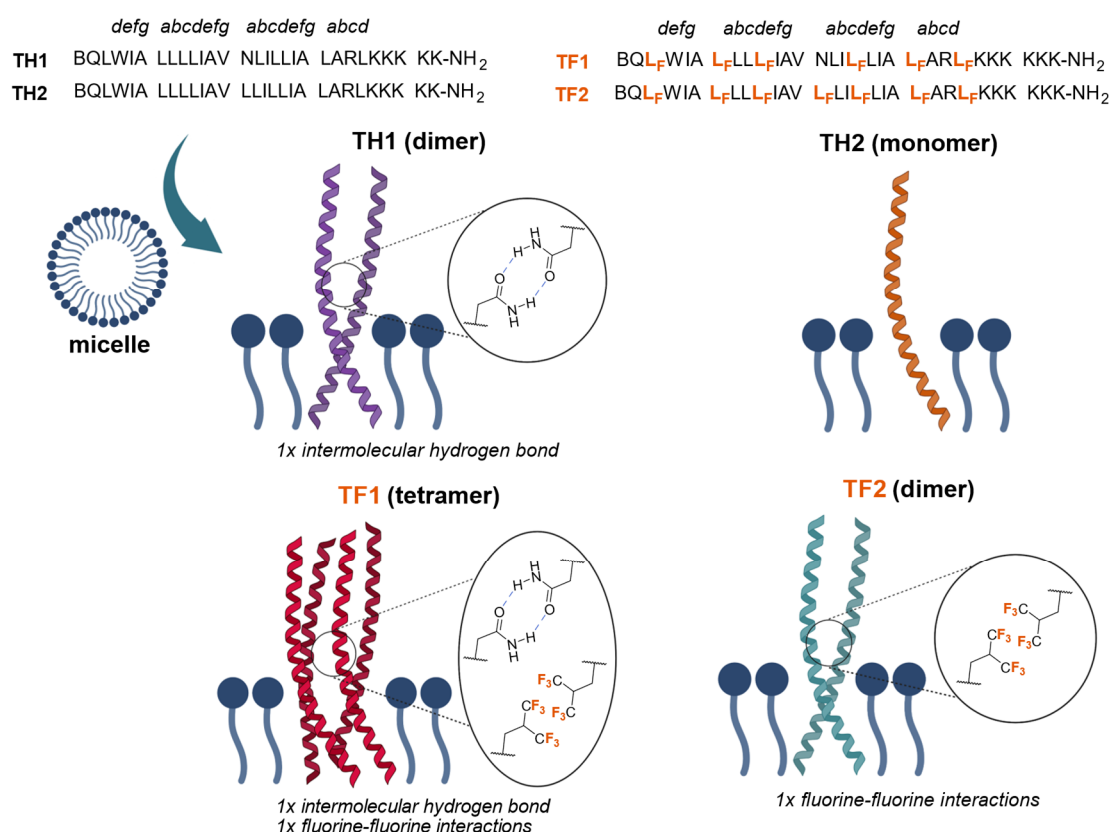


*Figure 4.7:* Impact of fluorination of the hydrophobic core on the thermal stability of CC dimers (Created with BioRender®).

Later, Tang *et al.* demonstrated that HfLeu **30** can be incorporated into the leucine-zipper A1 protein (HA1) using LeuRS with elevated activity. In this case, the denaturation temperature was increased by 22 °C.<sup>[259]</sup> Furthermore, the position-dependent influence of fluorination was studied in the context of GCN4-derived CC models, introducing TfIle at position *d* or TfVal at position *a*. Significant differences in the stabilization of both peptides were observed (*Figure 4.7*). TfIle-peptide displayed an increase in thermal stability of  $\Delta 27$  °C, while TfVal-peptide only showed a moderate elevation of  $\Delta 4$  °C. To explain the respective difference, the authors highlighted that the steric interactions between the  $CF_3$ -group and the amide backbone are entropically unfavorable.<sup>[260]</sup>

Like the Tirrell working group, Kumar and co-workers studied the consequences of introducing fluorinated amino acids into the hydrophobic core of the GCN4-p1d peptide. Four TfLeu residues were incorporated in position *d*, and three TfVal residues were introduced at position *a* while retaining Asn16 at one position *a* to promote dimer formation. This work provided the first example of a CC motif with a fully fluorinated hydrophobic core. The respective fluorinated CC displayed an elevated thermal stability ( $\Delta 15\text{ }^{\circ}\text{C}$ ) compared to the non-fluorinated parental system and, interestingly, was less susceptible to an increase in helicity promoted by 2,2,2-trifluoroethan-1-ol (TFE).<sup>[261]</sup>

In 2004, Bilgiçer *et al.* studied the influence of fluorination on membrane-active peptides.<sup>[262]</sup> Two highly hydrophobic sequences, TH1 (1x Asn at *a*; 6x Leu at *a* and *d*) and TH2 (7x Leu at *a* and *d*) were designed based on a CC motif with additional solubility tag at the C-terminus of the peptide, consisting of five Lys residues. The Asn residue in TH1 was introduced to promote interhelical interactions. Fluorinated derivatives, TF1 (1x Asn at *a*; 6x HfLeu at *a* and *d*) and TF2 (7x HfLeu at *a* and *d*) were synthesized, and the respective structural properties were compared to the non-fluorinated peptides in the presence of micelles (*Figure 4.8*).



*Figure 4.8:* Oligomerization state of TH1, TH2, TF1, and TF2 peptides in the presence of micelles (Created with BioRender®). [261]

Analytical ultracentrifugation (AUC) and fluorescence resonance energy transfer (FRET) experiments displayed the formation of higher oligomerization states in the

hydrophobic environment: TH1 (dimer), TF2 (dimer), and TF1 (tetramer). TH2 remained as a monomer in the presence of micelles. The authors explained the obtained trends by considering two non-covalent interactions. The intermolecular hydrogen bond formation stabilized the TH1 dimer. In the case of TF2, fluorine-fluorine interactions were proposed as the driving force behind the dimer formation. Consequently, both interactions were considered responsible for forming the tetrameric structure in the case of TF1.<sup>[262]</sup> The properties of TH1, TH2, and TF1 peptides were further studied by Kumar and Steinem research groups. The peptides were investigated in the presence of large unilamellar vesicles (LUVs). The fluorescence of the tryptophane residue was used to localize the peptides in the liposome environment, indicating the insertion into the liposome membrane for all three peptides. TH2 retained a monomeric structure, while TF1 and TH1 displayed a more sophisticated oligomerization behavior, described as a monomer-trimer equilibrium.<sup>[263]</sup>

In 2009, Kumar and Tirrell working groups investigated the effect of the stereochemistry of two TfLeu isomers ((2S,4S)-**28** and (2S,4R)-**29**) on the efficiency of the CC biosynthesis. Incorporating (2S,4S)-TfLeu **28** was improved compared to the corresponding (2S,4R)-isomer **29**. Interestingly, thermal denaturation experiments revealed that the CC motif, comprised of both isomers, was more stable than the CC structures, which accommodated only one isomer of TfLeu.<sup>[264]</sup>

In contrast to Kumar and Tirrell working groups, Marsh laboratory tried to illuminate the driving force behind the increased stabilization of fluorinated CC structures. In this context, a *de novo* antiparallel tetrameric CC peptide ( $\alpha$ 4-H) was designed, consisting of three heptad repeats with Leu at positions *a* and *d* (*Figure 4.9*).<sup>[265]</sup> First, the effect of fluorination on the hydrophobicity of Leu was investigated *via* partition experiments between H<sub>2</sub>O/heptanol and H<sub>2</sub>O/perfluoroheptanol ( $\Delta G(\text{Leu}) = -2.1 \text{ kcal mol}^{-1}$ ;  $\Delta G(\text{HfLeu } \mathbf{30}) = -2.5 \text{ kcal mol}^{-1}$ ), indicating that the expected increase in stabilization due to hydrophobic interactions should be approximately  $0.4 \text{ kcal mol}^{-1}$  per HfLeu **30** residue. Additionally,  $\alpha$ 4-F2(13,17) peptide was synthesized, incorporating two HfLeu **30** residues in the second heptad of the peptide sequence. Both peptides displayed a helical structure and formed tetramers in solution. <sup>19</sup>F NMR and hydrophobic dye-binding experiments illustrated that the respective hydrophobic cores were well-packed in both CC structures. The guanidine hydrochloride (Gnd-HCl) unfolding graph was fitted to a two-state equilibrium, and the corresponding  $\Delta G$  values were determined. The fluorinated peptide was stabilized by  $0.3 \text{ kcal mol}^{-1} \text{ residue}^{-1}$ , which is in good agreement with the expected increase in stability due to increased hydrophobicity.<sup>[265]</sup>

Later,  $\alpha$ 4-F2(13,17),  $\alpha$ 4-F4 (4x HfLeu **30** in 2 heptads), and  $\alpha$ 4-F6 (6x HfLeu **30**) were synthesized, and the respective thermodynamic properties were studied (*Figure 4.9*). All peptides formed tetrameric CCs at high concentrations. The calculated  $\Delta G$  values, derived from



the chemical denaturation experiments, demonstrated that the fluorine-caused enhancement in stability decreased with increasing amount of fluorine atoms ( $\alpha 4\text{-H} \rightarrow \alpha 4\text{-F2}$ :  $0,3 \text{ kcal mol}^{-1} \text{ residue}^{-1}$ ;  $\alpha 4\text{-F2} \rightarrow \alpha 4\text{-F4}$ :  $0,12 \text{ kcal mol}^{-1} \text{ residue}^{-1}$ ;  $\alpha 4\text{-F4} \rightarrow \alpha 4\text{-F6}$ :  $0,12 \text{ kcal mol}^{-1} \text{ residue}^{-1}$ ). Additional  $^{19}\text{F}$ -NMR experiments showed that the structure of the  $\alpha 4\text{-F6}$  peptide was more structured with less detectable end-fraying effects.<sup>[266]</sup>

In 2008, the proteolytic stability of  $\alpha 4\text{-H}$  and  $\alpha 4\text{-F6}$  was investigated.  $\alpha 4\text{-F6}$  peptide displayed a significantly increased enzymatic stability than the non-fluorinated analog. Furthermore, the stability towards solvent denaturation was investigated using various hydrocarbon solvents (MeOH, EtOH, and  $i$ PrOH). MeOH did not affect the CC structure of  $\alpha 4\text{-H}$  while adding EtOH and  $i$ PrOH resulted in an unfolding of the CC motif. In contrast, the hydrocarbon solvents did not influence the stability of  $\alpha 4\text{-F6}$ , which agrees with the low solubility of highly fluorinated structures in hydrocarbon solvents. As expected, TFE increased the helicity of the  $\alpha 4\text{-H}$  peptide. Interestingly, TFE also has not affected the stability of the fluorinated peptide despite the increased solubility of fluorinated side chains in this solvent. AUC experiments in TFE displayed that both peptides were present as monomers in the solution.<sup>[267]</sup> Buer *et al.* synthesized other model peptides:  $\alpha 4\text{-F2(6,24)}$ ,  $\alpha 4\text{-F2(10,20)}$ ,  $\alpha 4\text{-F2(13,17)}$ ,  $\alpha 4\text{-F3a}$  (3x HfLeu **30** at three positions *a*) and  $\alpha 4\text{-F3d}$  (3x HfLeu **30** at three positions *d*) (Figure 4.9).

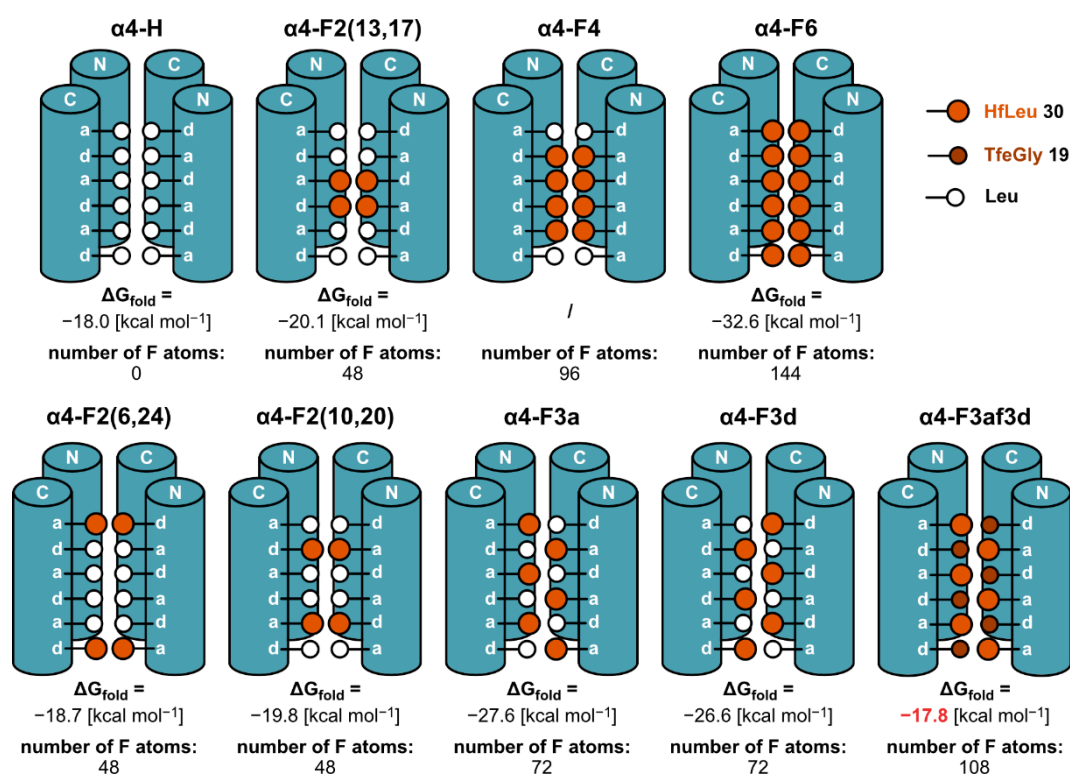
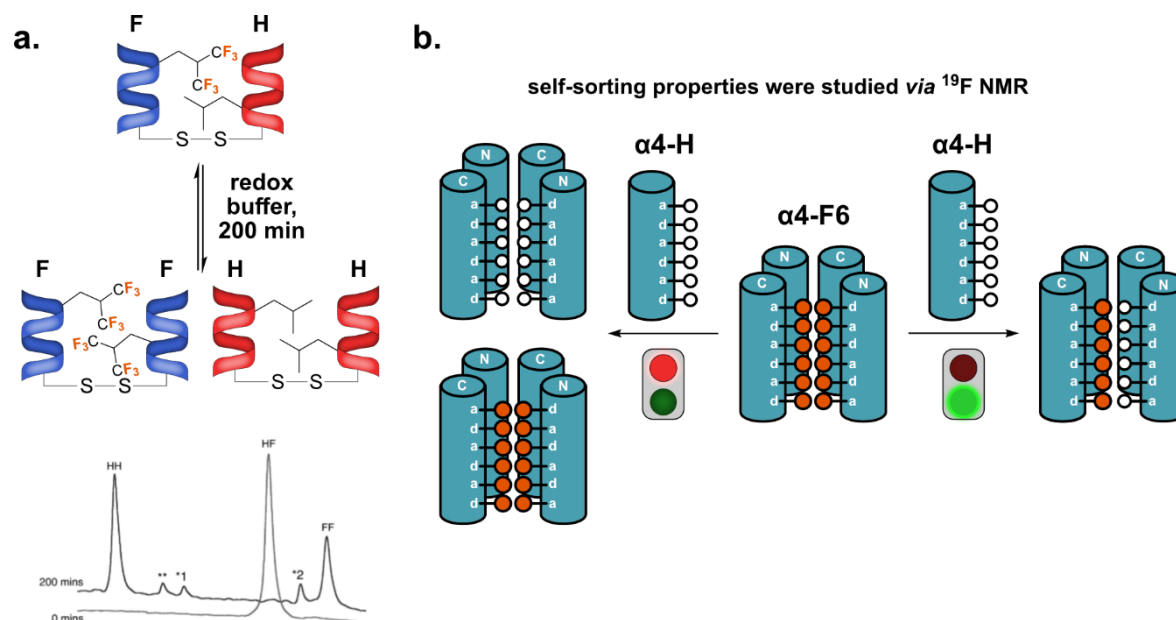


Figure 4.9: Summary of the fluorinated  $\alpha 4\text{-H}$  library. Free energy of folding ( $\Delta G_{\text{fold}}$ ) reflects respective thermodynamic stabilities.



$^{19}\text{F}$  NMR spectra and calculated  $\Delta\text{G}$  values of the five model peptides were compared, revealing that the packing properties exert a stronger impact on the stability of the CC motif than fluorine-fluorine interactions. For example,  $\alpha\text{4-F3a}$  and  $\alpha\text{4-F3d}$  displayed improved stability compared to the peptides with direct fluorine-fluorine contacts.<sup>[268]</sup> Furthermore,  $\alpha\text{4-H}$  and  $\alpha\text{4-F3a}$  tetramers were crystallized, and there was no evidence of conformations that maximize fluorine-fluorine contacts or reduce fluorine-hydrocarbon interactions. Furthermore,  $\alpha\text{4-F3af3d}$  peptide (3x HfLeu **30** at *a*; 3x TfeGly **19** at *d*) was synthesized and characterized. Sterically less demanding TfeGly **19** residue was introduced to compensate for the increased volume of the HfLeu **30** residue compared to the native Leu side chain. Gnd-HCl denaturation yielded a  $\Delta\text{G}$  value for  $\alpha\text{4-F3af3d}$  of  $-17.8 \text{ kcal mol}^{-1}$  ( $\alpha\text{4-H}$ :  $-18.0 \text{ kcal mol}^{-1}$ ), indicating that steric effects are responsible for the increased stabilization of the CC motif and not respective fluorine-fluorine interactions.<sup>[269]</sup> Finally, Van't Hoff analysis was carried out with  $\alpha\text{4-H}$ ,  $\alpha\text{4-F3a}$ ,  $\alpha\text{4-F3af3d}$ , and  $\alpha\text{4-F6}$  peptides, revealing that the enhanced stability of the fluorinated CC structures derives from the classic hydrophobic effect and not from unusual fluorine-fluorine interactions.<sup>[270]</sup>

In this section's introduction, design principles were discussed to allow orthogonal recognition between different CC peptides. Surprisingly, fluorine-driven orthogonal coiled coil assembly has hardly been studied so far.



**Figure 4.10:** a. Disulfide exchange experiment showed the formation of the fully fluorinated dimer (FF). HPLC chromatograms were adapted from Bilgiçer *et al.* with permission (Copyright © 2001 American Chemical Society).<sup>[271]</sup> b. The formation of mixed bundles was observed after the addition of  $\alpha\text{4-H}$  peptide to the fluorinated  $\alpha\text{4-F6}$  peptide.

In this context, Kumar and co-workers designed the CC-forming peptides H (non-fluorinated) and F (fluorinated, 1x Asn at *a*; 7x HfLeu **30** at *a* and *d*) with an additional GGC 61

sequence at the N-termini, allowing the formation of disulfide-bonded pairs. The respective HF dimer was incubated in a redox buffer, and after 200 min, only HH and FF dimers could be detected in the solution (*Figure 4.10, a.*). Furthermore, the melting point of the FF dimer was drastically increased compared to HH and HF dimers. However, AUC experiments hinted that peptide F assembled into a tetrameric structure.<sup>[271,272]</sup> The Marsh research group investigated the self-segregating properties of  $\alpha$ 4-H and  $\alpha$ 4-F6 peptides. Unexpectedly, NMR spectra revealed that the  $\alpha$ 4-F6 peptide formed bundles with the non-fluorinated peptide, contradicting the results of Kumar and co-workers (*Figure 4.10, b.*).<sup>[267]</sup> These two efforts show that the assembly behavior of fluorinated CC peptides is not easy to predict, and further studies are required that focus on the assembly properties between differently fluorinated CC peptides.

## 5 Aim of this doctoral thesis

This doctoral thesis aims to investigate two different peptide systems consisting of unusually high amounts of fluorinated amino acids. First, a new synthetic platform will be developed to accomplish this objective, permitting the rapid preparation of various fluorinated amino acids on a gram-scale. In this context, the chiral Ni(II) complex will be used to synthesize a broad range of aliphatic fluorinated amino acids, including fluorinated building blocks with additional stereogenic centers within the respective side chains (Figure 5.1, a).

Subsequently, polyfluorinated peptides, built almost exclusively by fluorinated amino acids, will be synthesized using microwave-assisted SPPS. The obtained fluorinated peptides will be characterized regarding their structural properties, focusing on hydrophobic environments. The respective properties will be investigated *via* CD spectroscopy, HPLC-based assays, and fluorescence spectroscopy in the presence of micelles and liposomes.

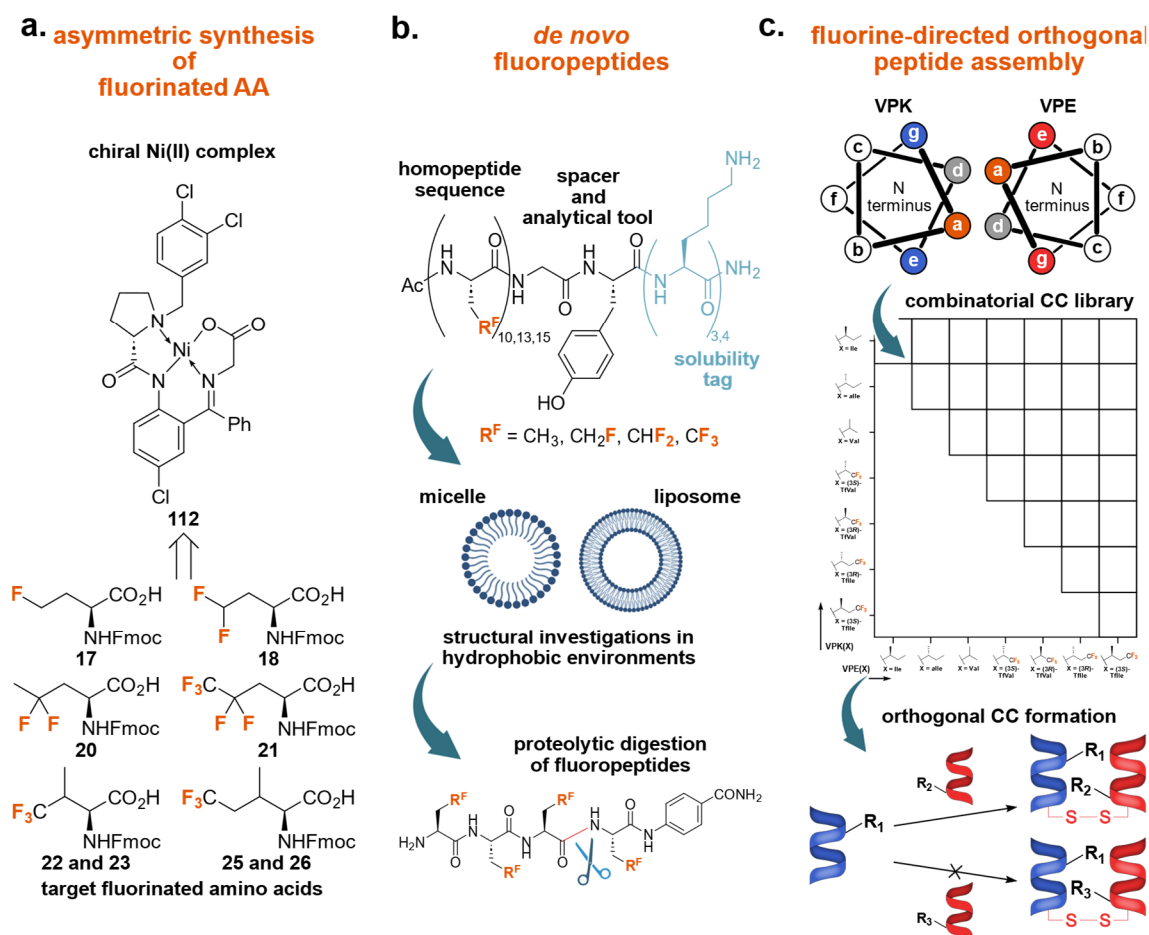


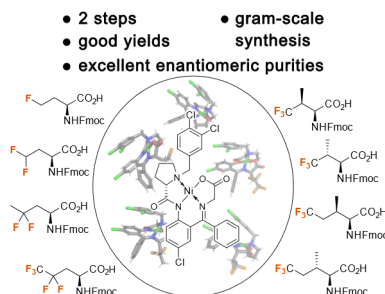
Figure 5.1: Aim of the doctoral thesis. a. Asymmetric synthesis of fluorinated amino acids. b. Synthesis and characterization of *de novo* fluoropeptides (Created with BioRender®). c. Fluorine-directed orthogonal assembly of CC peptides. Adapted from Hohmann *et al.* with permission (Copyright © 2023 American Chemical Society)<sup>[273]</sup>

Additionally, the proteolytic stability of these highly fluorinated peptide models will be investigated for the first time (*Figure 5.1, b.*).

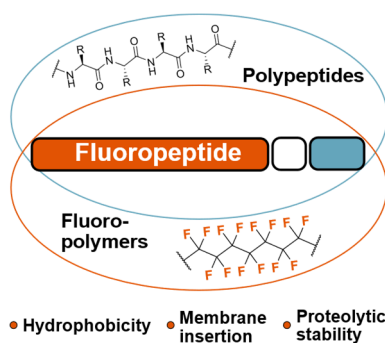
Finally, the potential of fluorine to direct the assembly properties of CC peptides will be studied (*Figure 5.1, c.*). A combinatorial library of VPK/VPE CC peptides will be synthesized, accommodating fluorinated derivatives of valine and isoleucine at all positions *a* of the CC motif. The peptide library will be investigated regarding CC structure, stability, orientation, and oligomerization *via* CD spectroscopy, size exclusion chromatography – multi-angle light scattering (SEC-MALS), and FRET measurements. In the second part, fluorine-guided CC assembly will be studied using a disulfide exchange assay.

## 6 Published work

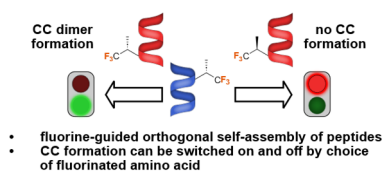
Summary of peer-reviewed publications presented in this section:



T. Hohmann, M. Dyrks, S. Chowdhary, M. Weber, D. Nguyen, J. Moschner, B. Kocsch, *J. Org. Chem.* **2022**, *87*, 10592–10604.



T. Hohmann\*, S. Chowdhary\*, K. Ataka, J. Er, G. H. Dreyhsig, J. Heberle, B. Kocsch, *Chem. Eur. J.* **2023**, e202203860. (\* = Authors contributed equally)



T. Hohmann, P. Dubatouka, K. Pfeifer, B. Kocsch, *Biomacromolecules* **2023**, *24*, 3357–3369.

## 6.1 Gram-scale asymmetric synthesis of fluorinated amino acids using a chiral nickel(II) complex

T. Hohmann, M. Dyrks, S. Chowdhary, M. Weber, D. Nguyen, J. Moschner, B. Kokschi, *J. Org. Chem.* **2022**, *87*, 10592–10604.

*Submitted: 7 March 2022; Publication date: 4 August 2022*

Published by American Chemical Society

The published work is available online: <https://doi.org/10.1021/acs.joc.2c00522>

### Individual contributions of the authors

I (Freie Universität Berlin) developed the overall project, carried out the synthesis of fluorinated amino acids, performed optimization screenings, set up crystallization experiments, carried out the HPLC-based hydrophobicity assay for the fluorinated amino acids, synthesized and characterized peptides for the determination of  $\alpha$ -helix propensity, performed CD measurements, and wrote the manuscript. Beate Kokschi (Freie Universität Berlin) guided project planning. M. Dyrks (Freie Universität Berlin) assisted me in the implementation of the optimization screenings. Suvrat Chowdhary (Freie Universität Berlin) assisted in synthesizing the chiral Ni(II) complex. Manuela Weber (Freie Universität Berlin) performed the X-ray diffraction measurements and solved the respective structures. Duy Nguyen (Freie Universität Berlin) assisted me in the synthesis of Fmoc-DfeGly, peptide synthesis, and CD measurements. Johann Moschner provided additional expertise and feedback.

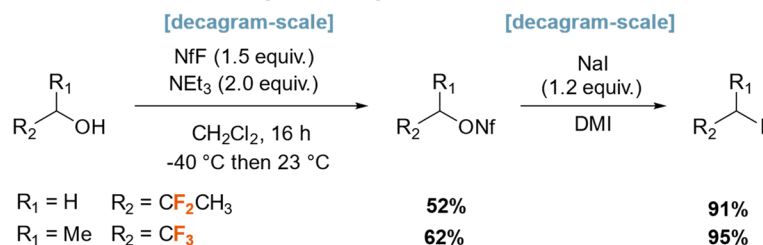
### Rationale and summary of the project

Fluorinated amino acids can be utilized as powerful tools to fine-tune the properties of peptides and proteins, such as secondary structure propensity, thermal stability, and proteolytic resistance. Consequently, numerous synthetic strategies were developed in the last decades to obtain these essential building blocks. In most cases, the respective approaches were time-consuming multi-step syntheses, and the desired fluorinated products were prepared on a milligram-scale.

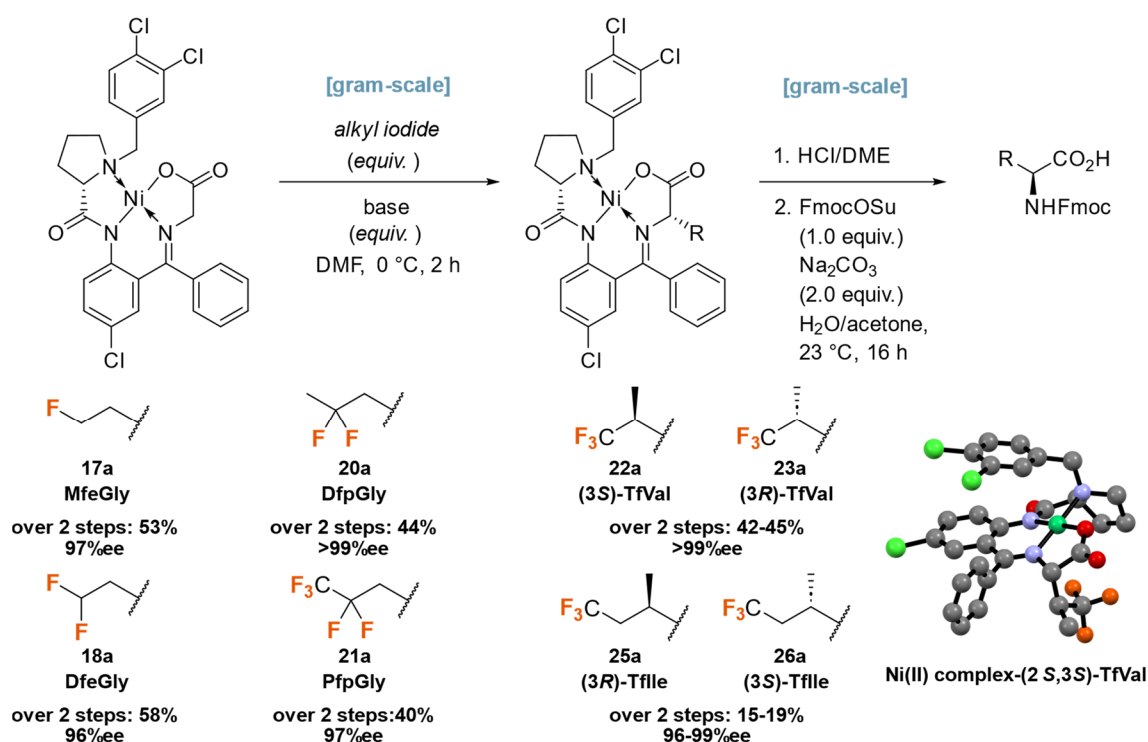
In this work, the chiral Ni(II) complex **112**, previously introduced by Soloshonok and co-workers, was used as the starting material for synthesizing various aliphatic fluorinated amino acids. In this context, Fmoc-MfeGly **17a**, Fmoc-DfeGly **18a**, Fmoc-DfpGly **20a**, Fmoc-PfpGly **21a**, Fmoc-(2*S*,3*S*)-TfVal **22a**, Fmoc-(2*S*,3*R*)-TfVal **23a**, Fmoc-5<sup>3</sup>-(2*S*,3*R*)-TfIle **25a**, and Fmoc-5<sup>3</sup>-(2*S*,3*S*)-TfIle **26a** were selected as target molecules.

First, the synthesis of commercially unavailable fluorinated alkyl iodides from respective fluorinated alcohols was established. The fluorinated alcohols were transformed into the respective nonaflates in the first step.

### a. synthesis of fluorinated alkyl iodide precursors



### b. gram-scale synthesis of target fluorinated amino acids



### c. intrinsic properties of fluorinated amino acids

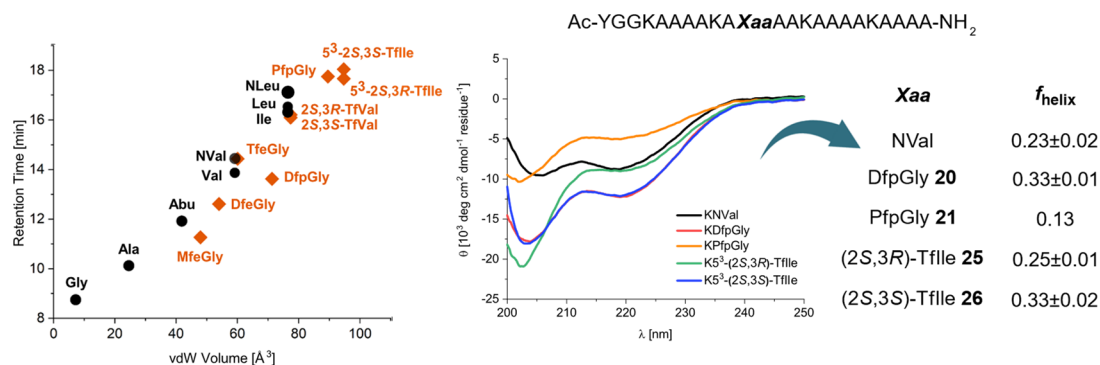


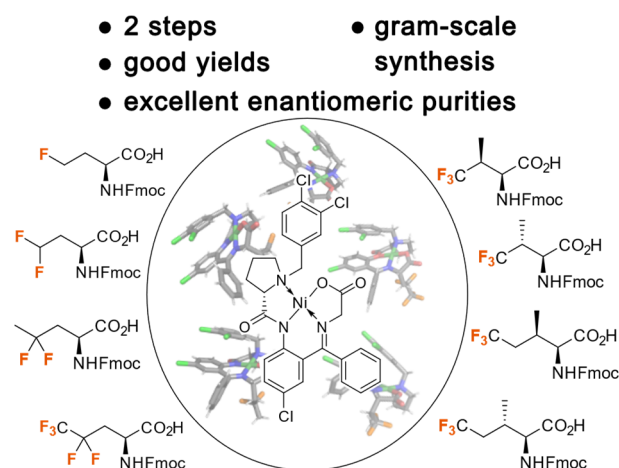
Figure 6.1: a. Gram-scale synthesis of fluorinated alkyl iodides. b. Asymmetric synthesis of fluorinated amino acids using Soloshonok complex **112** (Ni(II) complex of (2S,3S)-TfVal: CCDC number 2152776). c. Characterization of obtained fluorinated amino acids. Adapted from Hohmann *et al.* with permission (Copyright © 2022 American Chemical Society)<sup>[274]</sup>

Subsequent iodination provided the desired alkyl iodides in a good yield and on a decagram-scale (*Figure 6.1, a.*). To synthesize tailor-made amino acids, the Ni(II) complex **112** was first reacted with a suitable alkyl halide. Subsequent hydrolysis of the alkylated complex and Fmoc protection yielded the desired compounds (*Figure 6.1, b.*). To establish the optimal conditions for every fluorinated amino acid studied in this work, up to 50 conditions were screened for the alkylation reactions of the chiral Ni(II) complex **112**. Afterward, the corresponding alkylation reactions were performed on a decagram-scale, and the desired products were isolated in good yields and with great diastereomeric purities. In the case of  $\beta$ -branched amino acids, the alkylation step provided two diastereomers, which could be separated by flash column chromatography. The stereochemistry of the alkylated Ni(II) complexes was confirmed *via* X-ray diffraction and 1D nuclear overhauser enhancement and exchange spectroscopy (NOESY) experiments. After acidic hydrolysis and Fmoc-protection, the fluorinated amino acids were obtained in good overall yields and with excellent enantiomeric purities.

Finally, the synthesized fluorinated amino acids were characterized regarding hydrophobicity and  $\alpha$ -helix propensity (*Figure 6.1, c.*). To estimate the hydrophobicity of fluorinated amino acids, an HPLC-based assay was used, demonstrating that partial fluorination of the norvaline residue results in a decrease in hydrophobicity. At the same time, perfluorination significantly increases the hydrophobicity of the side chain. Additionally, the crucial importance of stereochemistry for the hydrophobicity of fluorinated amino acids was highlighted by the two Tflle diastereomers. Despite the identical van der Waals volume and comparable steric properties, the diastereomers displayed a noticeable difference in retention times. Finally,  $\alpha$ -helical peptides with the sequence Ac-YGGKAAAAKAXaaAAKAAAAK-NH<sub>2</sub> (Xaa = norvaline, DfpGly **20**, PfpGly **21**, 5<sup>3</sup>-(2S,3R)-Tflle **25**, and 5<sup>3</sup>-(2S,3S)-Tflle **26**) were synthesized and characterized *via* CD measurements. The respective  $\alpha$ -helical peptide values were calculated from obtained molar ellipticity values at 222 nm. Partial fluorination increased  $\alpha$ -helix propensity. Consequently, PfpGly displayed no observable propensity to form helical structures, demonstrating the negative effect of perfluorination on this property. Furthermore, Tflle diastereomers showed significant differences in their ability to stabilize the  $\alpha$ -helical structure, illustrating the importance of CF<sub>3</sub>-group orientation for the properties of peptides.



## Publication and supporting information



### Gram-Scale Asymmetric Synthesis of Fluorinated Amino Acids Using a Chiral Nickel(II) Complex

T. Hohmann, M. Dyrks, S. Chowdhary, M. Weber, D. Nguyen, J. Moschner, B. Kocsch, *J. Org. Chem.* **2022**, *87*, 10592–10604.

DOI: 10.1021/acs.joc.2c00522

For copyright reasons, the article is not included in the online version of this thesis. An electronic version of the article is available (<https://doi.org/10.1021/acs.joc.2c00522>).

## 6.2 Introducing aliphatic fluoropeptides: perspectives on folding properties, membrane partition and proteolytic stability

T. Hohmann\*, S. Chowdhary\*, K. Ataka, J. Er, G. H. Dreyhsig, J. Heberle, B. Kokschi, *Chem. Eur. J.* **2023**, e202203860.

\*Authors contributed equally

Submitted: 9 December 2022; Publication date: 1 February 2023

Published by Wiley-VCH GmbH

The published work is available online: <https://doi.org/10.1002/chem.202203860>

### Individual contributions of the authors

Suvrat Chowdhary and I (both Freie Universität Berlin) conceived the overall project and wrote the manuscript. I synthesized and isolated Abu<sub>10</sub>GY(K)<sub>3</sub>, MfeGly<sub>10</sub>GY(K)<sub>3</sub>, DfeGly<sub>10</sub>GY(K)<sub>3</sub>, Abu<sub>13</sub>GY(K)<sub>4</sub>, MfeGly<sub>13</sub>GY(K)<sub>4</sub>, DfeGly<sub>13</sub>GY(K)<sub>4</sub>, Abu<sub>15</sub>GY(K)<sub>4</sub>, MfeGly<sub>15</sub>GY(K)<sub>3</sub>, and DfeGly<sub>15</sub>GY(K)<sub>4</sub> peptides, carried out CD studies, and performed the HPLC-based assay to estimate the respective hydrophobicity of the fluoropeptides. Suvrat Chowdhary synthesized and purified the peptides TfeGly<sub>10</sub>GY(K)<sub>3</sub>, TfeGly<sub>13</sub>GY(K)<sub>4</sub>, Abu<sub>4</sub>[4]Abz, MfeGly<sub>4</sub>[4]Abz, DfeGly<sub>4</sub>[4]Abz, and TfeGly<sub>4</sub>[4]Abz, performed CD studies, membrane leaking assays (6-FAM), and proteolytic degradation assays. Beate Kokschi (Freie Universität Berlin) provided guidance on data analysis, interpretation, and manuscript writing. Kenichi Ataka (Freie Universität Berlin) conducted SEIRAS studies and wrote the manuscript. Jasmin Er (Freie Universität Berlin) assisted me in estimating log *P* values. Gesa Heather Dreyhsig (Freie Universität Berlin) assisted Suvrat Chowdhary in SPPS and proteolytic digestion assays. Joachim Heberle (Freie Universität Berlin) provided additional expertise.

### Rationale and summary of the project

Highly fluorinated peptide-based systems represent an exciting class of biopolymers with multiple applications in cytosolic delivery and <sup>19</sup>F NMR/MRI. To date, a high amount of fluorine has been introduced by incorporating perfluorinated functional groups or polyfluorinated alkyl chains. Peptides composed almost exclusively of fluorinated amino acids have yet to be described.

In this work, the first generation of fluoropeptides is presented. The respective fluorinated biopolymers consist of a fluorinated homopeptide sequence, a lysine-based solubility tag at the C-terminus, a tryptophane residue for concentration determination, and a glycine

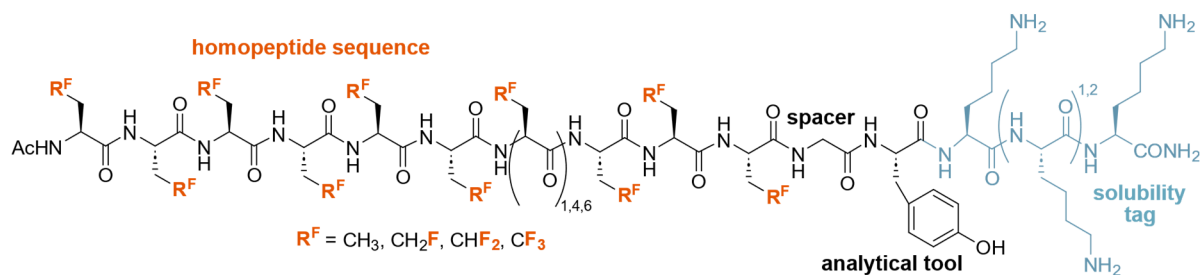
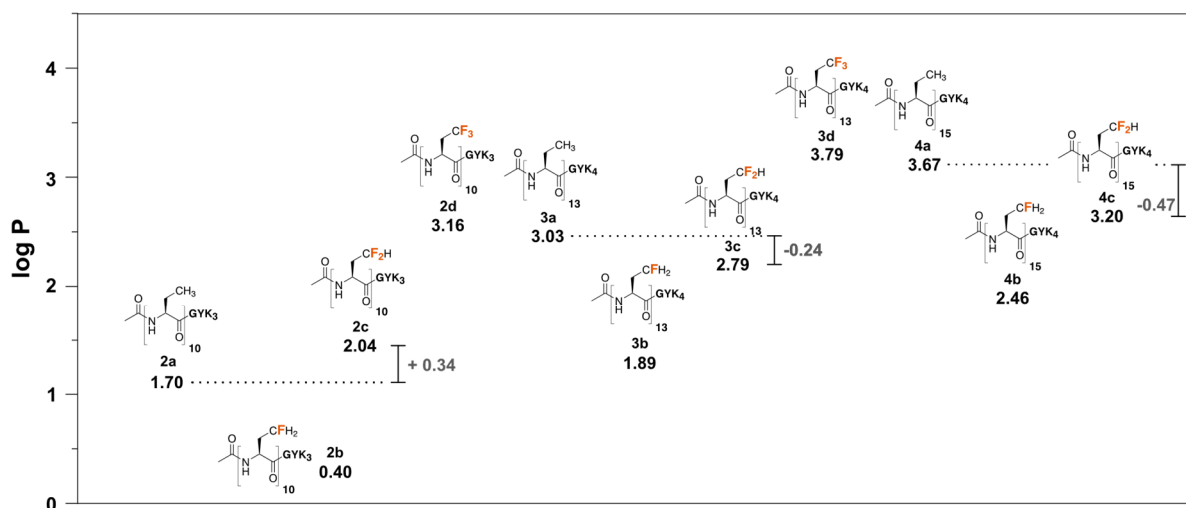
spacer. Two different dimensions were studied regarding the properties of *de novo* fluoropeptides: the length and the fluorination degree of the homopeptide sequence (*Figure 6.2, a.*). Consequently,  $X_{10}GY(K)_3$ ,  $X_{13}GY(K)_4$ , and  $X_{15}GY(K)_4$  ( $X = Abu$ , MfeGly **17**, DfeGly **18**, or TfeGly **19**) peptides were synthesized. TfeGly<sub>15</sub>GY(K)<sub>4</sub> was only obtained in traces and could not be isolated.

First, the hydrophobicity of fluoropeptides was investigated, adapting an HPLC-based approach to estimate respective  $\log P$  values (*Figure 6.2, b.*). In this context, a library of short tri-, tetra-, and pentapeptides with known  $\log P$  values was synthesized, and respective retention times were measured *via* reversed-phase HPLC. Subsequently, the obtained correlation between retention times and  $\log P$  values was used to calculate the unknown  $\log P$  values of fluoropeptides. In the case of  $X_{10}GY(K)_3$ , the expected trends were observed: monofluorination drastically lowered the  $\log P$  value compared to the non-fluorinated analog ( $\log P(Abu_{10}GY(K)_3) = 0.40$ ;  $\log P(MfeGly_{10}GY(K)_3) = 1.70$ ), while di- and trifluorination increased the hydrophobicity. Interestingly, this trend changes in the case of longer sequences. Both DfeGly<sub>13</sub>GY(K)<sub>4</sub> ( $\log P = 2.79$ ) and DfeGly<sub>15</sub>GY(K)<sub>4</sub> ( $\log P = 3.20$ ) are less hydrophobic than the non-fluorinated analogs with the same length ( $\log P(Abu_{13}GY(K)_4) = 3.03$ ;  $\log P(Abu_{15}GY(K)_4) = 3.67$ ), indicating a cooperative effect for the difluorinated biopolymers.

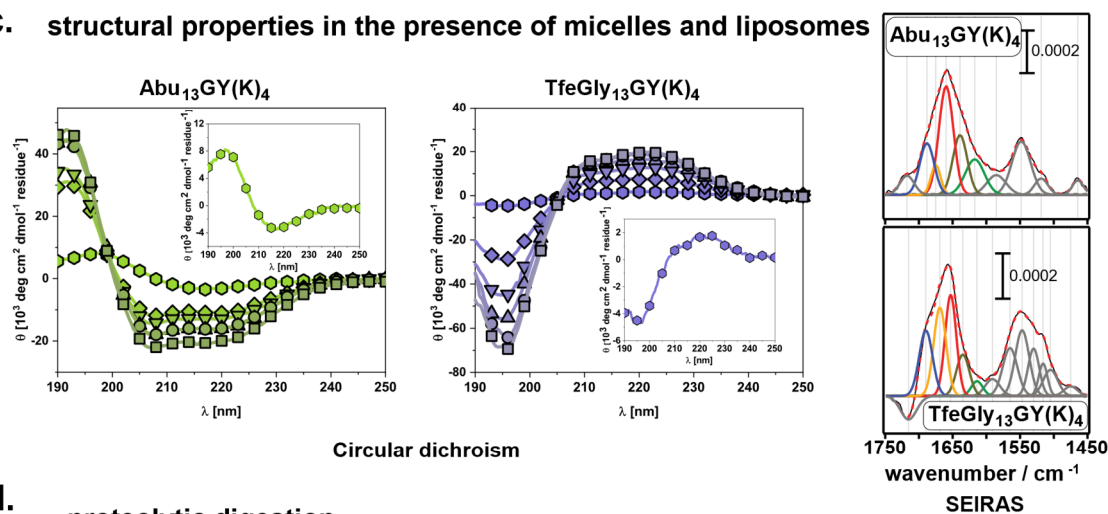
CD measurements were carried out in the presence of sodium dodecyl sulfate (SDS) micelles to collect structural information on fluoropeptides in hydrophobic environments (*Figure 6.2, c.*). A general trend was observed for Abu-, MfeGly-, and DfeGly-containing peptides: the fluoropeptides formed  $\beta$ -strands in aqueous solution and  $\alpha$ -helices in the presence of SDS. The two-state transition was most pronounced for the Abu peptides, while mono- and difluorination disrupted the respective  $\alpha$ -helix formation in the SDS environment. As expected, longer sequences showed a more pronounced tendency to form  $\alpha$ -helical structures. Intriguing, TfeGly peptides displayed a radically different picture. TfeGly<sub>13</sub>GY(K)<sub>4</sub> formed a PPII helix in an aqueous buffer and in the presence of SDS, revealed by CD measurements (minimum at 196 nm; maximum at 220 nm). TfeGly<sub>10</sub>GY(K)<sub>3</sub> showed a more complex conformational composition, consisting of  $\beta$ -strand and PPII-type helical structures. A prominent example of a polypeptide that also forms a PPII helix is poly-L-lysine. In this context, electrostatic repulsion of charged amine groups, placed at a distance of  $i, i+4$ , was used to explain this structural preference. The analogous rationale can be applied in the case of TfeGly peptides, where CF<sub>3</sub>-groups reject spatial proximity to each other, thus forming an extended PPII helix.

Similar trends were revealed performing CD measurements in the presence of unilamellar vesicles.

## a. peptide design

b. estimation of log *P* values

## c. structural properties in the presence of micelles and liposomes



## d. proteolytic digestion

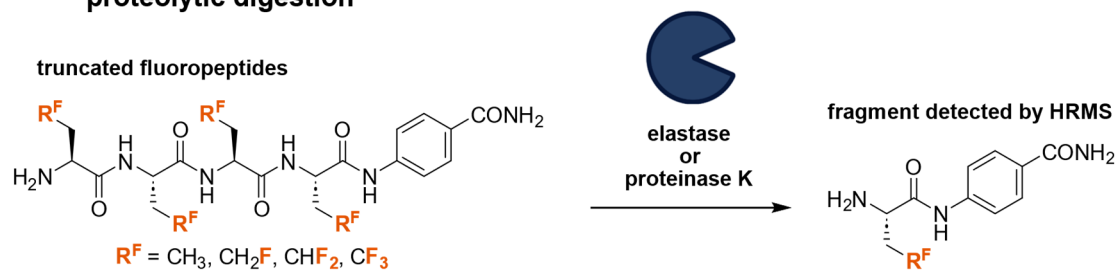
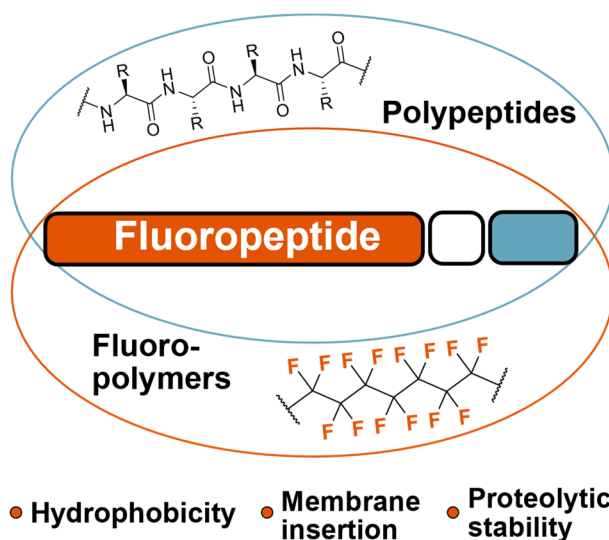


Figure 6.2: a. Sequence and design of *de novo* fluoropeptides. b. Estimated log *P* values of fluoropeptides studied in the scope of this work. c. Circular dichroism and SEIRAS spectra of Abu<sub>13</sub>GY(K)<sub>4</sub> and TfeGly<sub>13</sub>GY(K)<sub>4</sub> peptides. d. Proteolytic digestion of truncated fluoropeptides. Create with BioRender®. Adapted from Hohmann, Chowdhary *et al.* with permission (Copyright © 2023 Wiley-VCHGmbH)<sup>[275]</sup>

POPC and 1-palmitoyl-2-oleoyl-sn-glycero-3-(phosphor-rac-(1-glycerol)) (POPG) lipids (1:1 ratio) were used to form the respective liposomes. Most pronounced  $\alpha$ -helix formation was observed for Abu<sub>13</sub>GY(K)<sub>4</sub>, Abu<sub>15</sub>GY(K)<sub>4</sub>, and DfeGly<sub>15</sub>GY(K)<sub>4</sub>. TfeGly-containing peptides displayed a maximum in the 220 nm region, indicating the presence of a PPII-type helix. Shorter MfeGly- and DfeGly-containing sequences showed the lowest tendency to form an  $\alpha$ -helical structure. A fluorescence-based leakage assay was performed utilizing 6-carboxyfluorescein (6-FAM) as a fluorescence dye to confirm that the fluoropeptides insert into the membrane of the liposomes. For all fluoropeptides an increase in fluorescence was observed, indicating disruptive peptide-membrane interactions. Additionally, the respective measurements displayed that the insertion of fluoropeptides into the liposome membrane is slow, taking up to ten hours. Furthermore, surface-enhanced infrared absorption spectroscopy (SEIRAS) measurements were performed with the X<sub>13</sub>GY(K)<sub>4</sub> series, confirming the extended duration of the respective fluoropeptide-membrane interactions, reaching saturation after 200 to 600 minutes. Helical conformation was preferred in the case of Abu- and TfeGly-containing peptides. In contrast, MfeGly<sub>13</sub>GY(K)<sub>4</sub> and DfeGly<sub>13</sub>GY(K)<sub>4</sub> displayed a significant decrease in the helical content, presenting a complex conformational composition and confirming preceding CD studies.

Finally, the proteolytic stability of fluoropeptides was investigated. To ensure the solubility of the system, the fluoropeptide sequence had to be truncated. Uncapped fluorinated tetrapeptides, X<sub>4</sub>pAbz (X = Abu, MfeGly **17**, DfeGly **18**, or TfeGly **19**; pAbz = *para*-aminobenzoic acid) were synthesized. For concentration determination, pAbz was placed at the C-terminus of the sequence. In the scope of this work, proteolytic resistance was probed towards elastase and proteinase k (*Figure 6.2, d.*). The respective study was performed *via* an HPLC-based assay. Intriguingly, all four peptides were degraded by both enzymes. After 6 hours of incubation in the presence of elastase, the following amounts of fluoropeptides were detected: Abu<sub>4</sub>pAbz (4.3±0.1%), MfeGly<sub>4</sub>pAbz (6.6±1.1%), DfeGly<sub>4</sub>pAbz (10.9±3.8%), and TfeGly<sub>4</sub>pAbz (19.3±4.0%). This data showed that increasing fluorination degree can improve proteolytic stability. Nevertheless, the fact that sequences consisting exclusively of fluorinated amino acids are proteolytically degradable biopolymers is of crucial importance, and the corresponding sequences could potentially provide an exciting alternative for resistant polyfluoroalkyl chains.

**Publication and supporting information**



Introducing Aliphatic Fluoropeptides: Perspectives on Folding Properties, Membrane Partition and Proteolytic Stability

T. Hohmann\*, S. Chowdhary\*, K. Ataka, J. Er, G. H. Dreyhsig, J. Heberle, B. Kocsch, *Chem. Eur. J.* **2023**, e202203860. (\* = Authors contributed equally)

DOI: 10.1002/chem.202203860

The original paper with supporting information is available at:

<https://doi.org/10.1002/chem.202203860>

This paper is an open access article and reproduced under the terms of the Creative Commons Attribution License (<https://creativecommons.org/licenses/by-nc-nd/4.0/>).

# Introducing Aliphatic Fluoropeptides: Perspectives on Folding Properties, Membrane Partition and Proteolytic Stability

Thomas Hohmann<sup>+, [a]</sup> Suvrat Chowdhary<sup>+, [a]</sup> Kenichi Ataka,<sup>[b]</sup> Jasmin Er,<sup>[a]</sup> Gesa Heather Dreyhsig,<sup>[a]</sup> Joachim Heberle,<sup>[b]</sup> and Beate Kokschr<sup>\*[a]</sup>

**Abstract:** A de novo designed class of peptide-based fluoropolymers composed of fluorinated aliphatic amino acids as main components is reported. Structural characterization provided insights into fluorine-induced alterations on  $\beta$ -strand to  $\alpha$ -helix transition upon an increase in SDS content and revealed the unique formation of PPII structures for trifluorinated fluoropeptides. A combination of circular dichroism, fluorescence-based leaking assays and surface enhanced infrared absorption spectroscopy served to examine the insertion and folding processes into unilamellar

vesicles. While partitioning into lipid bilayers, the degree of fluorination conducts a decrease in  $\alpha$ -helical content. Furthermore, this study comprises a report on the proteolytic stability of peptides exclusively built up by fluorinated amino acids and proved all sequences to be enzymatically degradable despite the degree of fluorination. Herein presented fluoropeptides as well as the distinctive properties of these artificial and polyfluorinated foldamers with enzyme-degradable features will play a crucial role in the future development of fluorinated peptide-based biomaterials.

## Introduction

The introduction of fluorine into bioactive compounds as well as the utilization of fluorocarbon-based polymers attract growing interest in biochemical and pharmaceutical research.<sup>[1]</sup> Several reports have shown that selective fluorination often can enhance hydrophobic properties and biological activity.<sup>[2]</sup> It is not surprising that, presently, about 20–25% of commercially available pharmaceuticals do contain fluorinated residues, and perfluorocarbons (PFCs) are widely studied as fluorous tags in the context of gene, protein, and peptide delivery in vitro and in vivo.<sup>[3]</sup> In general, PFCs are both hydrophobic and lipophobic which ensures superior membrane permeability as well as a promising potential for mediating drug delivery and cell internalization for pharmaceutical applications.<sup>[4]</sup> For example, conjugation or co-assembly of fluoroalkanes with cargo

peptides and proteins was reported to significantly enhance intracellular uptake.<sup>[5]</sup> A notable drawback of perfluorinated compounds, however, comprises their biological inertness prohibiting biodegradation by digestive enzymes, microbes, and metabolic processes. As a result, PFCs have shown to be very persistent in the environment and can undergo bioaccumulation and biomagnification.<sup>[6]</sup> Consequently, the development of biodegradable fluoropolymers is of paramount importance to design next-generation biomaterials.<sup>[3b]</sup>

Incorporation of fluorinated amino acids into peptide & proteins has gained significant relevance in biosciences as it imparts unique biophysical features, like an enhancement in thermal and chemical stability or modulation of folding properties.<sup>[7]</sup> Depending on the degree of fluorination and side chain pattern, these synthetic building blocks can be used to fine-tune peptide secondary structure formation and bioactivity.<sup>[8]</sup> Replacing a hydrophobic amino acid with its fluorinated counterpart was reported to facilitate peptide self-assembly in membrane environments, mimicking the properties of fluoroalkyl tags discussed before. For example, Godbout et al. reported a fluorinated 21-residue peptide and showed that fluorous interactions, derived from six residues of (2S)-4,4,4-trifluoroethylglycine (TfeGly), drive the assembly into helical superstructures. These biomaterials functioned for the generation of artificial ion channels in lipid bilayers.<sup>[9]</sup> Furthermore, Naarmann et al. and Bilgiçer et al. described the incorporation of hexafluoroisoleucine (up to seven residues) into a coiled-coil motif to efficiently drive the formation of defined helical bundles in lipid bilayers and SDS micelles.<sup>[10]</sup> Finally, fluorine can be a powerful tool to study the interaction of membrane-active peptides with lipids using <sup>19</sup>F NMR and has an essential significance for in vivo <sup>19</sup>F magnetic resonance imaging.<sup>[11]</sup>

[a] T. Hohmann,<sup>+</sup> S. Chowdhary,<sup>+</sup> J. Er, G. H. Dreyhsig, Prof. Dr. B. Kokschr  
 Institute of Chemistry and Biochemistry  
 Freie Universität Berlin  
 Arnimallee 20, 14195 Berlin (Germany)  
 E-mail: beate.kokschr@fu-berlin.de

[b] Dr. K. Ataka, Prof. Dr. J. Heberle  
 Department of Physics  
 Freie Universität Berlin  
 Arnimallee 14, 14195 Berlin (Germany)

[\*] Authors contributed equally.

Supporting information for this article is available on the WWW under <https://doi.org/10.1002/chem.202203860>

© 2023 The Authors. Chemistry - A European Journal published by Wiley-VCH GmbH. This is an open access article under the terms of the Creative Commons Attribution Non-Commercial NoDerivs License, which permits use and distribution in any medium, provided the original work is properly cited, the use is non-commercial and no modifications or adaptations are made.

The Kocsch laboratory has recently established the access to a variety of aliphatic fluorinated amino acids in gram scale, enabling the fabrication of synthetic peptides consisting of multiple of these building blocks.<sup>[12]</sup> One of our recent works demonstrated the impact of fluorine-specific interactions to be controlled by the degree of side chain fluorination as well as the overall proportion of fluorinated building blocks.<sup>[13]</sup> Our ultimate goal, therefore, is the systematic de novo design of peptide-based fluoropolymers with distinct fluorine-driven folding & assembly properties while the peptide scaffold is predestined to maintain biodegradability and biocompatibility.

In this study, we introduce the first generation of fluorine-rich peptide oligomers with diverse chain lengths and degrees of side chain fluorination by the consecutive coupling of either 2-aminobutyric acid **1a** or its fluorinated analogs (2S)-4-monofluoroethylglycine (MfeGly) **1b**, (2S)-4,4-difluoroethylglycine (DfeGly) **1c** or (2S)-4,4,4-trifluoroethylglycine (TfeGly) **1d**. These fluoropeptides were studied with respect to a wide range of biophysical parameters such as hydrophobicity, secondary structure formation, but also the allocation and conformation within interfacial layers of artificial membranes using a combination of CD spectroscopy, 6-FAM leaking assays and surface enhanced infrared absorption spectroscopy (SEIRAS)<sup>[14]</sup>. Furthermore, we present investigations on the proteolytic stability of these fluoropeptides with an exceptional fluorine content (up to 28.5%). To our own surprise, obtained experimental data revealed these fluoropeptides to be enzymatically degradable, regardless of the degree of side chain fluorination. Hence, this data set provides insights into an unexplored class of foldamers constituted at the multidisciplinary interface of peptide science and fluorine chemistry.

## Results and Discussion

### Peptide design & synthesis

With the aim of systematically studying the impact of fluorination degree of the single building blocks on the overall hydrophobicity, folding and proteolytic stability, the corresponding sequences were constructed from amino acids with different amounts of fluorine. For this purpose, we used 2-aminobutyric acid **1a** and its fluorinated analogs MfeGly **1b**, DfeGly **1c**, and TfeGly **1d** (Figure 1a).

A solubility tag consisting of three or four lysine residues was introduced at the C-terminus of each peptide to facilitate solubility in physiological conditions. The concentration determinations by UV absorbance were achieved by the incorporation of a tyrosine residue. Finally, we included a glycine residue to separate the fluoropeptide sequence from the solubility tag. The N-terminus of the peptides was acetylated. In addition to the degree of fluorination, we examined the influence of the length of the fluoropeptide fragment on above-discussed properties of the respective peptides. Three different lengths, 10, 13, and 15, were selected for this purpose, with three lysine residues (as solubility tag) added to the decamers and four lysines attached to the longer sequences 13

and 15. Hence, a total of twelve peptides was to be synthesized:  $X_{10}GY(K)_3$  ( $X=A$ , Abu **2a**; M, MfeGly **2b**; D, DfeGly **2c**; T, TfeGly **2d**),  $X_{13}KY(K)_4$  ( $X=A$ , Abu **3a**; M, MfeGly **3b**; D, DfeGly **3c**; T, TfeGly **3d**), and  $X_{15}GY(K)_4$  ( $X=A$ , Abu **4a**; M, MfeGly **4b**; D, DfeGly **4c**; T, TfeGly **4d**) (Figure 1a). All peptides studied in this work were synthesized using microwave-assisted solid-phase peptide synthesis (SPPS). By using optimized coupling conditions recently published by Leppkes et al.,<sup>[15]</sup> all fluorinated amino acids could be incorporated with using only 1.5 equivalents of fluorinated species. *N,N'*-Diisopropylcarbodiimide (DIC) and ethyl cyanohydroxyiminoacetate (oxyma) were used as the coupling reagents (Figure 1b). After full cleavage from the resin, the peptides were purified by RP-HPLC (Figure 1c).

Looking at the yields of the peptides, it quickly emerges that the trifluorinated sequences are by far the most difficult to synthesize (Figure 1d). The yields of TfeGly<sub>10</sub>GY(K)<sub>3</sub> **2d** and TfeGly<sub>13</sub>GY(K)<sub>4</sub> **3d** are among the lowest in the series. TfeGly<sub>15</sub>GY(K)<sub>4</sub> **4d** was only synthesized in traces and could not be isolated. The highest yield was achieved with the non-fluorinated decamer Abu<sub>10</sub>GY(K)<sub>3</sub> **2a**. In general, longer homooligopeptide sequences are, as expected, more difficult to generate, which can be explained by the increased tendency to aggregate.<sup>[16]</sup> Therefore, structural investigations were carried out with eleven isolated peptides.

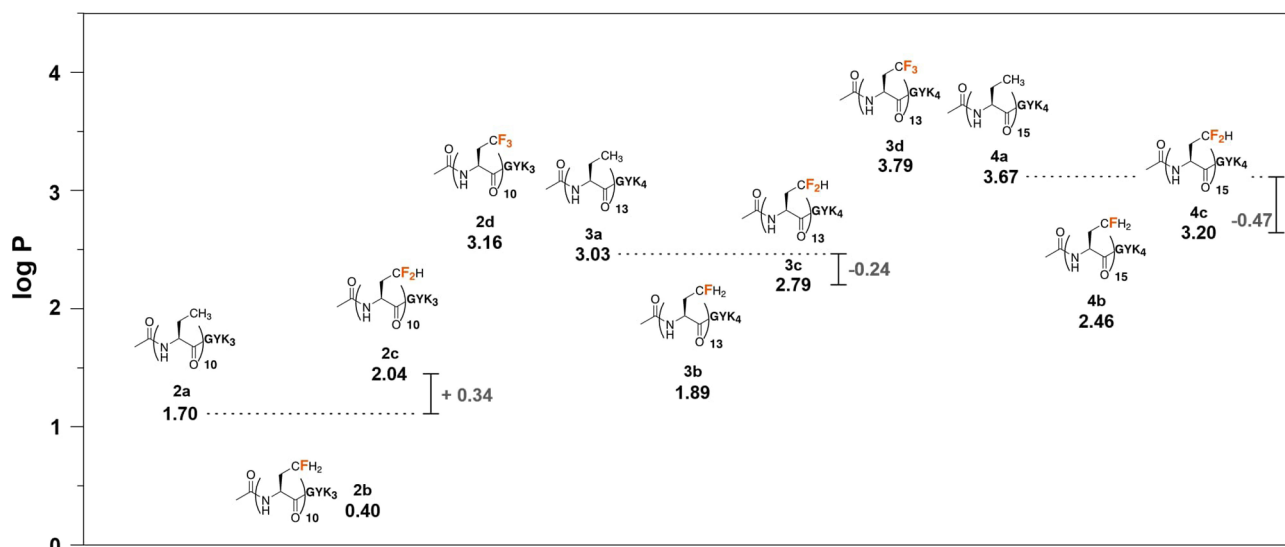
### Hydrophobicity of fluoropeptides

Since PFCs can be used as efficient tools to facilitate the uptake by cell membranes, we were especially eager to study the properties of fluoropeptides not only in aqueous but also in lipophilic environments. We assumed that hydrophobicity of the corresponding peptide sequences should be a driving force behind the interactions with membrane models. To quantify the corresponding individual lipophilicity values for each peptide studied in this work, we adapted an HPLC-based assay that was used to estimate the log *P* values of small organic molecules. A library of tri-, tetra- and pentameric peptides with known log *P* values was used to determine the unknown log *P* values for the peptides of interest using their retention times on a reversed-phase C18 column (Supporting Information). In Figure 2, the corresponding data are presented. The comparison to the hydrophobicity of the Fmoc-protected amino acids (Supporting Information, Figure S33), which were previously determined and published in our group, shows that the log *P* values of  $X_{10}GY(K)_3$  peptides ( $X=$  Abu **2a**, MfeGly **2b**, DfeGly **2c**, TfeGly **2d**) have the same tendencies.

Monofluorination lowers the hydrophobicity compared to the non-fluorinated variant while the di-, and trifluorination increase the log *P* values. The elevation of polarity by monofluorination was expected and has already been discussed extensively in the literature.<sup>[8]</sup> This finding can be readily explained by the fluorine-induced dipole moment within the aliphatic side chain. Furthermore, it is characteristic how considerably the trifluorination increases the hydrophobicity of the peptide: the log *P* of the five residues shorter TfeGly<sub>10</sub>GY(K)<sub>3</sub> **2d** peptide (3.16) is nearly the same as the value of the







**Figure 2.** Determined log P values of the fluorinated peptides. The relative increase in polarity of the difluorinated peptides with respect to the nonfluorinated analogues was highlighted.

the  $\alpha$ -helix in the case of Abu<sub>15</sub>GY(K)<sub>4</sub> **4 a**, an SDS concentration of 2.5 mM was already sufficient. Similar transition was observed for the mono- and difluorinated peptides. An important distinction, compared to the non-fluorinated compounds, is both the stronger influence of the length of the corresponding fluoropeptide sequence, and the minimal amount of SDS required for the stabilization of the  $\alpha$ -helix. This trend can be described very well in the case of DfeGly peptides. DfeGly<sub>10</sub>GY(K)<sub>3</sub> **2 c** peptide forms a  $\beta$ -strand structure in water. With increasing amount of SDS, the signal diminishes significantly indicating an unordered structure and peptide precipitation at high SDS concentrations.

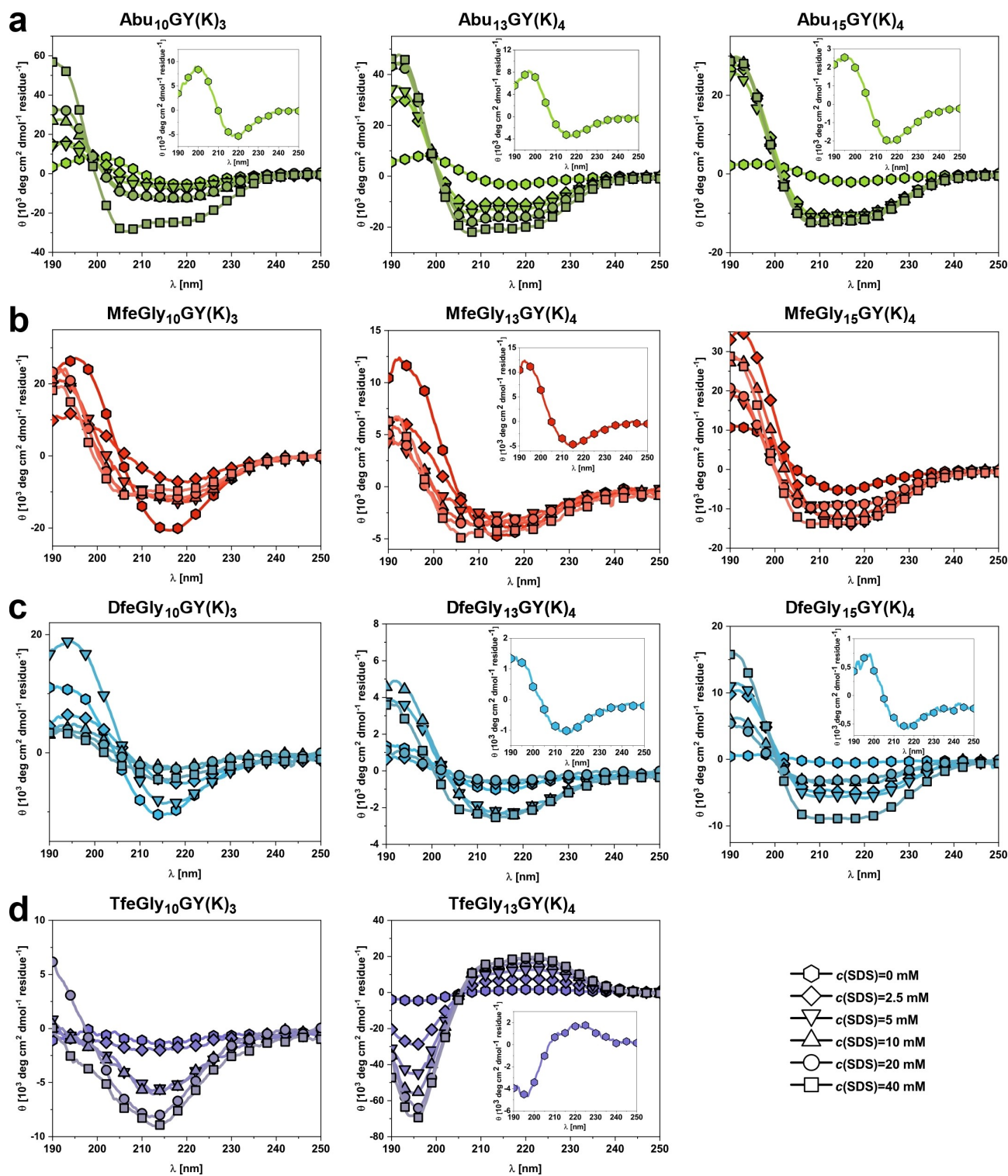
In the case of DfeGly<sub>13</sub>GY(K)<sub>4</sub> **3 c** and DfeGly<sub>15</sub>GY(K)<sub>4</sub> **4 c**, a  $\beta$ -strand to  $\alpha$ -helix transition was observed as well. Nevertheless, especially for DfeGly<sub>13</sub>GY(K)<sub>4</sub> **3 c**, a concentration of 40 mM was required to see a distinct band in the 208 nm region. Analogous conclusions can be drawn for the monofluorinated peptides. A longer sequence or higher SDS amount is needed for the stabilization of the  $\alpha$ -helical conformation in a SDS environment. For DfeGly<sub>15</sub>GY(K)<sub>4</sub> **4 c** and apart from one exception for DfeGly<sub>13</sub>GY(K)<sub>4</sub> **3 c**, an isodichroic point near 200 nm could be detected indicating a two-state transition. Dual wavelength parametric test supports a two-state model, with larger deviations in the slope of the  $\theta_{208}$  vs.  $\theta_{222}$  correlation seen in the case of DfeGly<sub>13</sub>GY(K)<sub>4</sub> **3 c** (Supporting Information, Figures S38, 39). This was not observed in the case of MfeGly peptides, suggesting a more complex composition of multiple conformations, besides  $\alpha$ -helix and  $\beta$ -strand structures.

At this point, it should be mentioned that despite the Lys-tag, the solubility of the peptides in the aqueous medium was severely limited. Therefore, the CD studies described in this work were performed at concentrations between 25 and 50  $\mu$ M. Apart from DfeGly<sub>10</sub>GY(K)<sub>3</sub> **2 c**, no peptide precipitation was observed upon increasing the SDS concentration.

Subsequently, we wanted to use the obtained log P values to explain the tendency to form  $\alpha$ -helical structure in the presence of SDS micelles for Abu, MfeGly and DfeGly peptides. The Figure S34 shows the normalized molar ellipticity at 208 nm of the corresponding peptides at different SDS concentrations, which is characteristic for the transition from a  $\beta$ -strand structure to an  $\alpha$ -helix. The presented trends show that four of the peptides with the highest log P values also exhibit the strongest  $\alpha$ -helical structure formation. An exception is Abu<sub>10</sub>GY(K)<sub>3</sub> **2 a**, which, despite its comparatively low hydrophobicity, displays a strong tendency to  $\alpha$ -helix formation in the presence of SDS. In addition to hydrophobicity, the length of the peptides seems to be a crucial factor for the stabilization of the  $\alpha$ -helical structure in a membrane environment. The X<sub>10</sub>GY(K)<sub>3</sub> **2 a-d** and X<sub>13</sub>GY(K)<sub>4</sub> **3 a-d** peptides of mono and difluorinated amino acids exhibit the lowest helical content in the vicinity of micelles. In conclusion, mono- and difluorination tend to disrupt the  $\alpha$ -helix formation in a hydrophobic environment, which is somewhat consistent with the increase in polarity relative to the non-fluorinated sequences.

Quite unexpectedly, the trifluorinated peptides revealed a completely different picture. Neither an  $\alpha$ -helix nor a  $\beta$ -strand conformation could be identified. For TfeGly<sub>10</sub>GYK<sub>3</sub> **2 d**, a minimum at 214 nm was observed, which is significantly blue shifted from a minimum at 218 nm that corresponds to a  $\beta$ -strand structure. Additionally, a band at 198 nm was not observed making a  $\beta$ -strand conformation highly unlikely. The CD spectrum of TfeGly<sub>13</sub>GY(K)<sub>4</sub> **3 d** shows a minimum at 196 nm and a broad positive band in the 220 nm region. Since the later CD spectrum is somewhat more distinct, we will start our discussion with the structural properties of TfeGly<sub>13</sub>GY(K)<sub>4</sub> **3 d**.

Both bands are signatures of a polyproline type II (PPII) helix.<sup>[18]</sup> Poly(L-prolines), their derivatives, poly(L-lysine) and comparable peptides are known to adapt a PPII conformation<sup>[19]</sup>, an extended left-handed helix (3.1 Å per



**Figure 3.** CD spectra of (fluorinated) peptides (25  $\mu\text{M}$ ) in aqueous solution (phosphate buffer, 10 mM, pH = 7.4) and in the presence of SDS (2.5, 5, 10, 20, 40 mM); a. CD spectra of Abu oligomers; b. CD spectra of MfeGly oligomers; c. CD spectra of DfeGly oligomers; d. CD spectra of TfeGly oligomers. The insets show the zoomed-in spectra at a SDS concentration of 0 mM.

residue) and defined by backbone dihedral angles  $\phi$ ,  $\psi$  of  $-75^\circ$  and  $+145^\circ$  (CD spectrum: minimum at 206 nm; maximum at 225 nm).

In the case of TfeGly<sub>13</sub>GY(K)<sub>4</sub> **3d**, the intensity of both bands increases drastically with the amount of SDS indicating a stabilization of a PPII helix in a hydrophobic environment (additional discussion corresponding the PPII structure is placed

in the Supporting Information). This was rather surprising, since the hydrogen bond network between backbone and water molecules is generally considered to be the greatest stabilizing factor for the PPII conformation.<sup>[18a,d,20]</sup> Nevertheless, the Budisa research group could already demonstrate based on their work on octahydroindole-2-carboxylic acid oligomers that a PPII conformation can also be formed in a transmembrane environment.<sup>[21]</sup> In this context, it should be mentioned that these are highly rigid structures which are locked in a PPII conformation. Flexible peptides, analogous to TfeGly oligomers, that can form a PPII helix in a membrane environment are, to the best of our knowledge, unknown. In addition to the backbone solvation, other factors, such as side chain-side chain interactions or side chain conformational entropy, were discussed as possible ways to stabilize a PPII conformation.<sup>[18a,22]</sup> Particularly in the case of poly(L-lysine) peptides, the repulsion between positive charges of the corresponding side chains was discussed as an important factor for the formation of a PPII structure forcing the peptide chain into an extended conformation.<sup>[22–23]</sup> Similar considerations could also apply to TfeGly oligomers. Recently, we reported a structural study discussing an alternating peptide structure consisting of TfeGly and lysine residues. Molecular dynamics simulations showed that the most stable structural state of CF<sub>3</sub> groups decline spatial proximity to each other.<sup>[13]</sup> Here we observe something comparable: In contrast to Abu, MfeGly, and DfeGly oligomers, an  $\alpha$ -helical structure is not formed in the presence of SDS. In case of TfeGly-derived fluoropeptides, the CF<sub>3</sub> residues with *i, i + 4* spacing turn out to be unfavorable and, thus adopt an extended PPII conformation. Furthermore, an isodichroic point near 206 nm was detected. Additionally, an excellent correlation with a constant slope was observed for the wavelengths at 196 and 221 nm (Supporting Information, Figure S40). Both factors highly support a two-state transition model for the TfeGly<sub>13</sub>GY(K)<sub>4</sub> **3 d** peptide in the presence of SDS. It should be mentioned that in the case of TfeGly<sub>13</sub>GY(K)<sub>4</sub> **3 d**, the band at 220 nm appears very broad compared to poly(L-lysine). This might be due to the influence of tyrosine on the one hand, but on the other hand it could also involve secondary solvent effects. Kubyskin et al. showed in their work that especially the positive band of the PPII conformation can be very strongly influenced by the environment.<sup>[24]</sup>

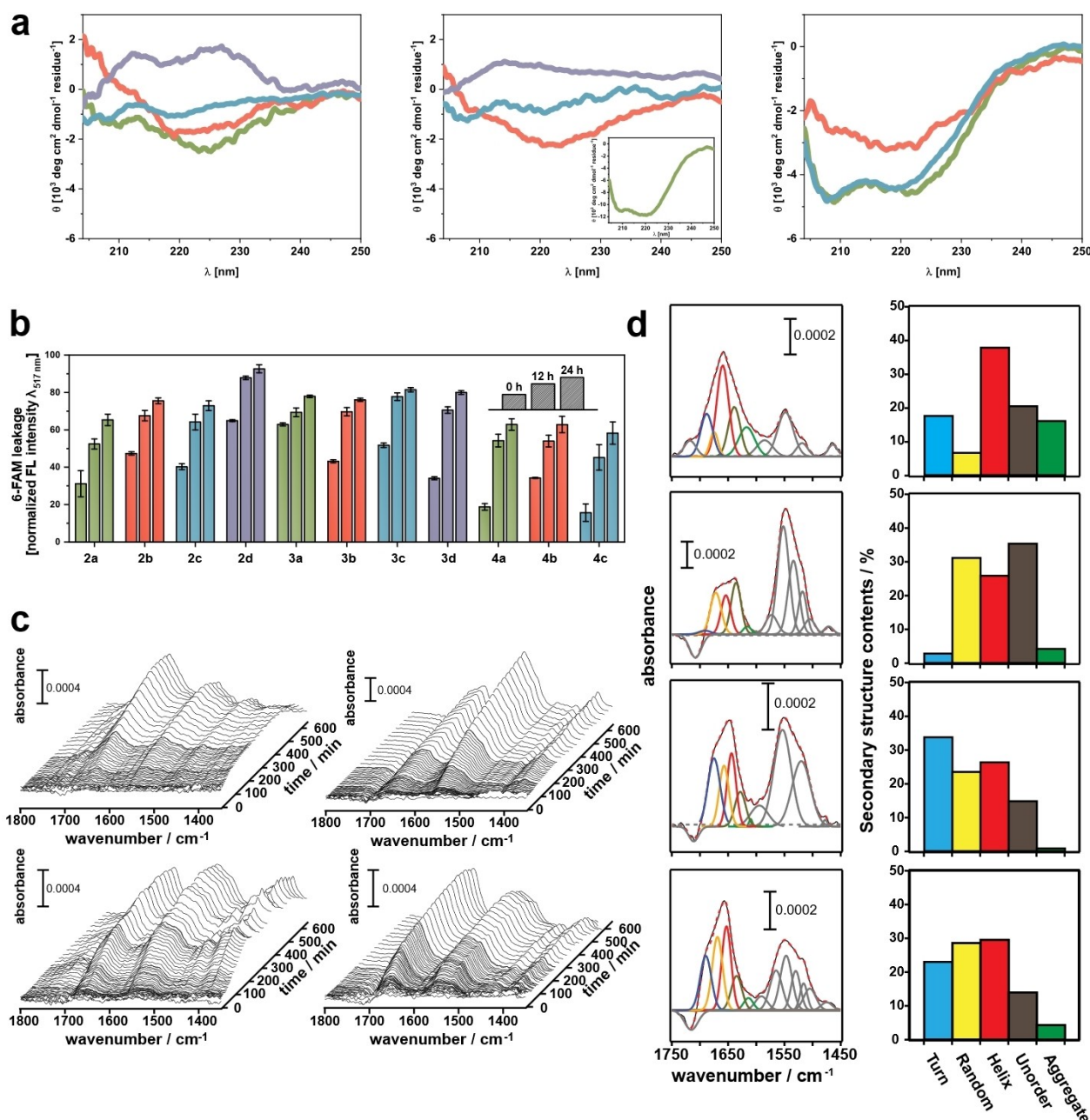
To get a better insight into the structural properties of TfeGly<sub>10</sub>GY(K)<sub>3</sub> **2 d**, we explored the influence of multiple solvents with varying polarity on its structure (Supporting Information, Figure S41). Octan-1-ol simulates an strong hydrophobic environment. Consistent with the results of TfeGly<sub>13</sub>GY(K)<sub>4</sub> **3 d**, TfeGly<sub>10</sub>GY(K)<sub>3</sub> **2 d** adopts a PPII conformation as well. Moreover, it seems that the TfeGly<sub>10</sub>GY(K)<sub>3</sub> **2 d** peptide adopts a PPII conformation in membrane-like environment while in a more polar environment at least one further conformation may be present. In hexafluoroisopropanol (HFIP), representing a fluorous-polar solvent, the CD spectrum showed a minimum below 200 nm, but a positive band at a wavelength above 210 nm was absent. This finding could be indicative of a higher random coil fraction.<sup>[25]</sup> Consequently, experimental data confirms the PPII structure in the case of TfeGly oligomers more

likely to be supported by a hydrophobic environment. Subsequently, the structure of TfeGly<sub>10</sub>GY(K)<sub>3</sub> **2 d** in phosphate buffer was examined more closely (Supporting Information, Figure S42). At a 25 mM concentration, the spectrum is reminiscent of a random coil structure. The spectrum at 50 mM showed a minimum at 214 nm, as mentioned earlier. The inset in Supporting Information shows divergence in the CD spectra of TfeGly<sub>10</sub>GY(K)<sub>3</sub> **2 d** at 25  $\mu$ M and at 50  $\mu$ M in phosphate buffer. The corresponding spectrum resembles a  $\beta$ -strand type CD spectra.<sup>[20a,26]</sup> In general, PPII helix is mostly in a multi-conformational equilibrium with  $\beta$ -strand,  $\beta$ -turn and unordered structures, which can be explained by the great similarities in the corresponding backbone dihedral angles.<sup>[18d]</sup> Therefore, it seems only consistent and completes the picture that TfeGly<sub>10</sub>GY(K)<sub>3</sub> **2 d** forms multiple conformations, like  $\beta$ -strand, besides the PPII helix. Furthermore, the comparison between TfeGly<sub>10</sub>GY(K)<sub>3</sub> **2 d** and TfeGly<sub>13</sub>GY(K)<sub>4</sub> **3 d** shows that the longer peptide seems to be better accommodated in a more hydrophobic environment. If TfeGly<sub>10</sub>GY(K)<sub>3</sub> **2 d** shows a PPII helix in a strictly hydrophobic medium, as a consequence, it intercalates less strongly with the micelles in the presence of SDS, resulting in a CD spectrum with a higher  $\beta$ -strand fraction.

### Structural studies in presence of POPC/POPG

To further deepen our insights into the structural properties of fluoropeptides, especially focusing on their interactions with biomembrane models, CD measurements were carried out in the presence of unilamellar vesicles. The corresponding liposomes were composed of 1-palmitoyl-2-oleoyl-glycero-3-phosphocholine (POPC) and 1-palmitoyl-2-oleoyl-sn-glycero-3-(phosphor-rac-(1-glycerol)) (POPG) lipids (1:1 ratio). Negatively charged POPG was used to facilitate the peptide-liposome interactions. Figure 4a summarizes the CD spectra of all eleven peptides in the presence of POPC/POPG. It must be noted that the measurements were made at a much smaller liposome/peptide ratio of 150:1 compared to the studies with SDS (SDS/peptide = 1600:1, for 40 mM SDS concentration). CD measurements at higher liposome concentrations and at wavelengths below 200 nm were not possible due to the absorbance properties of the liposome suspension. Overall, it can be stated that almost identical trends, compared to the SDS studies, were observed. Again, the most pronounced  $\alpha$ -helical structures were formed by Abu<sub>13</sub>GY(K)<sub>4</sub> **3 a**, Abu<sub>15</sub>GY(K)<sub>4</sub> **4 a** and DfeGly<sub>15</sub>GY(K)<sub>4</sub> **4 c**. For other difluorinated peptides and especially for the monofluorinated analogs, CD spectra with higher  $\beta$ -strand content were detected. In synergy to prior data, the length of the peptides and their hydrophobicity are the two decisive factors for the formation of a helical structure in a hydrophobic environment, with monofluorination reducing the stability of that conformation. Both TfeGly peptides adopt a different structure under these conditions. A maxima at wavelengths above 210 nm could be observed indicating the formation of PPII structures. Interestingly, in the case of liposomes, TfeGly<sub>10</sub>GY(K)<sub>3</sub> **2 d** adopts this conformation as well. In a time-dependent manner, comparable to the SDS CD





**Figure 4.** a. Circular dichroism spectra of fluorinated peptides (25  $\mu$ M) in the presence of POPC:POPG = 1 : 1 (liposome:peptide = 150 : 1) in phosphate buffer (10 mM, pH = 7.4) [left: X<sub>10</sub>GY(K)<sub>3</sub> / center: X<sub>13</sub>GY(K)<sub>4</sub> / right: X<sub>15</sub>GY(K)<sub>4</sub>]; b. Monitored leakage of the 6-FAM dye (ratio: 1 : 100 peptide:lipid); c. In-situ SEIRA spectra of the adsorption process of X<sub>13</sub>GY(K)<sub>4</sub> 3 a–d peptides on the POPG/POPC lipid bilayer; d. Peak fittings of the amide band of the fluorinated peptides adsorbed on the lipid (left) and contents of the secondary structure components (right) of Abu<sub>13</sub>GY(K)<sub>4</sub> 3 a (first row), MfeGly<sub>13</sub>GY(K)<sub>4</sub> 3 b (second row), DfeGly<sub>13</sub>GY(K)<sub>4</sub> 3 c (third row), and TfeGly<sub>13</sub>GY(K)<sub>4</sub> (fourth row).

spectra, a minimum at 214 nm is formed and the maximum disappears (Supporting Information, Figure S44). This contradicts the hypothesis that a PPII conformation occurs almost exclusively in a hydrophobic environment as TfeGly<sub>10</sub>GY(K)<sub>3</sub> 2 d seems rather to exhibit several conformations (PPII,  $\beta$ -strand) in the presence of micelles as well as in the presence of liposomes. For TfeGly<sub>13</sub>GY(K)<sub>4</sub> 3 d peptide, no time-dependent structural changes were observed.

The disruptive interactions of fluoropeptides with liposome vesicles was studied by a fluorescence-based leakage assay using 6-carboxyfluorescein (6-FAM) as a fluorescence dye. For all eleven peptides an increase in fluorescence could be observed due to an intrusion of peptides into the membrane bilayer (Figure 4b). What was already indicated by CD data was also demonstrated by the leakage assay: the penetration of fluoropeptides into the liposomes is a slow process, with fluorescence saturation occurring after approximately 10 h. To

study the structure formation in the course of peptide-membrane interactions, we subsequently carried out infrared spectroscopy experiments.

### Surface enhanced infrared absorption spectroscopy (SEIRAS)

Since conventional FTIR spectroscopy is not sufficiently sensitive to detect the peptide oligomers at the given concentration, we employed Surface-Enhanced Absorption Spectroscopy (SEIRAS).<sup>[27]</sup> For this purpose, large unilamellar vesicles (LUV) of POPC/POPG (1:1) were casted over the SEIRA active gold film surface to form a solid-supported lipid bilayer. The lipid-modified SEIRA chip was submitted to a PBS buffer and the peptides were subsequently added. The sample SEIRA spectra were simultaneously measured to observe adsorption/folding process of the polypeptides on the solid-supported lipid bilayer.<sup>[27]</sup> For these studies, the X13 K peptides were selected, since here, both all degrees of fluorination were present and the structural diversity within the series was the most pronounced.

Figure 4c shows SEIRA spectra of each peptide. Three-dimensional presentation of these spectra provides overviews on the adsorption process of the peptides. As the peptides were added, two marker bands appeared at around  $\sim 1650$  and  $\sim 1550$   $\text{cm}^{-1}$  and increased with time. These bands are assigned to amide I and II vibrational modes of the peptide backbone. Increase of these bands indicates a greater partitioning of peptides on the supported lipid bilayer with time. What was already indicated by CD measurements and fluorescence leakage assay was confirmed by SEIRA measurements: the increasing rate of the amide bands for each peptide is relatively slow, with saturation intensity being reached after 200 to 600 minutes depending on the degree of fluorination. SEIRA spectra at the saturation coverage of each adsorbed peptide illustrated that the spectral features of each peptide are very different to each other (Figure 4d). In the non-fluorinated peptide, Abu<sub>13</sub>GY(K)<sub>4</sub> **3a**, amide I and II appear as broad and symmetrical features peaking at 1659 and 1549  $\text{cm}^{-1}$ , respectively. These peak positions are typical of  $\alpha$ -helical structure of long-chain peptides or proteins, suggesting that the lipid adsorbed Abu<sub>13</sub>GY(K)<sub>4</sub> **3a** is present as an  $\alpha$ -helix. On the other hand, amide bands of the fluorinated peptides **3b-d** show characteristic asymmetrical features different from those of Abu<sub>13</sub>GY(K)<sub>4</sub> **3a**. This is consistent with the obtained CD data (see above), which showed different conformational compositions depending on the degree of fluorination.

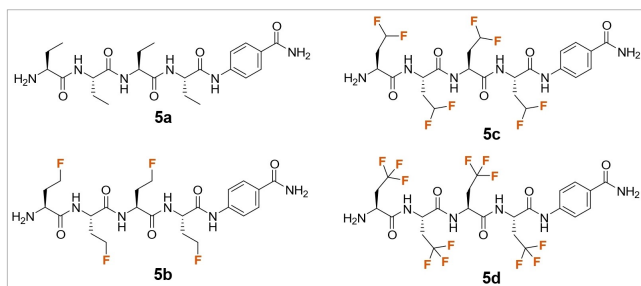
Peak fitting of the amide I band was carried out and the integrated peak areas were used to quantify the individual secondary structure components. Details of the peak fittings are described in the Supporting Information, section 3.6. We limited the analysis to five representative structures, namely 'Turn/Bend', 'Random', 'Helix', 'Unordered', and ' $\beta$ -aggregate/sheet'. Since distinction between  $\beta$ -sheet and  $\beta$ -aggregate is difficult due to overlap of absorption region, the contribution from  $\beta$ -sheet structure is included in ' $\beta$ -aggregate' structures. The component bands appear in the range of 1675–1695  $\text{cm}^{-1}$

(Turn), 1660–1675  $\text{cm}^{-1}$  (Random), 1660–1645  $\text{cm}^{-1}$  (helix), 1630–1645  $\text{cm}^{-1}$  (Unordered), 1610–1630  $\text{cm}^{-1}$  (Aggregate), respectively (Figure 4d). For non-fluorinated Abu<sub>13</sub>GY(K)<sub>4</sub> **3a** peptide, the predominant component is a helical structure, which occupies about 40% of the conformational space. This is in agreement with our CD measurements, which showed that Abu oligomers have the highest tendency of all investigated peptides to form  $\alpha$ -helical structures. In the case of both MfeGly<sub>13</sub>GY(K)<sub>4</sub> **3b** and DfeGly<sub>13</sub>GY(K)<sub>4</sub> **3c**, the helical fraction decreases significantly (26% for MfeGly<sub>13</sub>GY(K)<sub>4</sub> **3b** and DfeGly<sub>13</sub>GY(K)<sub>4</sub> **3c**). Something similar was also shown by the CD spectra, which indicated a more complex conformational composition with a lower  $\alpha$ -helical content in a hydrophobic environment. If the TfeGly<sub>13</sub>GY(K)<sub>4</sub> **3d** is compared with DfeGly<sub>13</sub>GY(K)<sub>4</sub> **3c**, it can be observed that the proportion of bend/turn structures decreases (from 34 to 23%) and slightly increases in the case of the helical structure (26 to 30%). As discussed in detail in the previous sections, no alpha helix was observed during CD experiments with trifluorinated peptides. Unfortunately, the discrimination of different helical structures by IR spectroscopy is difficult. Therefore, we interpret the observed higher content of helical structure, compared to the monofluorinated and difluorinated peptides, as presence of an extended helical conformation.

### Truncated fluoro-peptides: folding, membrane partition and proteolysis

As discussed before, PFCs hardly degrade under environmental conditions and are often characterized as persistent. Therefore, we raised the question about the proteolytic stability of the fluoro-peptides. Preliminary studies showed that fluoro-peptides with solely fluorinated residues about  $n \geq 6$  are insoluble in aqueous conditions. To accomplish efficient proteolysis studies, a sufficient solubility of starting material is required. The GYK<sub>3/4</sub> tag in above-discussed library would immediately be degraded by the protease and, thus, cannot serve for elucidation of the fluoro-peptides' degradability. We, therefore, established a small new library of truncated fluoro-peptides (X<sub>4</sub>[4]Abz; with X = Abu (Abu<sub>4</sub>[4]Abz) **5a**, MfeGly (MfeGly<sub>4</sub>[4]Abz) **5b**, DfeGly (DfeGly<sub>4</sub>[4]Abz) **5c** & TfeGly (TfeGly<sub>4</sub>[4]Abz) **5d**) which are soluble in given conditions of the peptide digestion assay. On the C-terminus, *para*-aminobenzoic acid [4]Abz was attached for determination of peptide stock concentrations.<sup>[28]</sup> Acetylation of the N-terminus was omitted to provide a somewhat net charge on this hydrophobic scaffold (Figure 5).

At first, we aimed to explore whether previously described observations on fluorine-directed peptide folding in lipid environments can be also complied to truncated derivatives. CD experiments were done in physiological conditions at 100  $\mu\text{M}$  peptide concentration and varying amounts of SDS (10 mM, 20 mM, 40 mM) as discussed before (Figure 6a). We observed for the labeled tetrapeptides Abu<sub>4</sub>[4]Abz **5a** and DfeGly<sub>4</sub>[4]Abz **5c** a global minimum at 198–200 nm and a shallow minimum at 218 nm. This CD pattern can be interpreted as a mixture of disordered peptide ( $\lambda_{\text{min}} = 198$  nm) and



**Figure 5.** Chemical structures of labeled fluoropeptides ( $X_4[4]Abz$  series).

minor amounts of  $\beta$ -strand-like conformations ( $\lambda_{\min} = 218$  nm). This evaluation is in accordance with prior work by Schweitzer-Stenner and co-workers.<sup>[29]</sup> The latter minimum was not observed for the MfeGly-derived tetrapeptide, indicating a major presence of random coils. The general absence of  $\beta$ -sheet to  $\alpha$ -helix transitions as described for the  $X_{10}GY(K)_3$ ,  $X_{13}GY(K)_4$  and  $X_{15}GY(K)_4$  series can be explained by the short sequence length of the  $[X]_4[4]Abz$  series and, consequently, a lack of the typical backbone  $i \rightarrow i-4$  hydrogen bonding pattern as indispensable criterion for  $\alpha$ -helical structures.

For TfeGly<sub>4</sub>[4]Abz **5d**, however, we determined the typical course of adsorption for  $\beta$ -strands due to the negative band between 218–220 nm and positive band between 195–200 nm. Upon addition of SDS (10 mM–20 mM) the  $\beta$ -strand content increases significantly as observed in the wavelength shift for the negative band to around 215 nm and increased ellipticity at 195 nm. These results are in good agreement with prior reports by Barnham and co-workers about SDS-generated stabilization of A $\beta$ -derived  $\beta$ -sheet conformers.<sup>[30]</sup> It is most noteworthy that higher amounts of SDS (40 mM) lead to a further shift of the global minimum to about 210 nm, indicating a coexistence of different folding patterns. As discussed before for TfeGly<sub>10</sub>GY(K)<sub>3</sub> **3d** and TfeGly<sub>13</sub>GY(K)<sub>4</sub> **4d**, this data set would corroborate our considerations about a multiconformational equilibrium in membrane-like environments. Consequently, the observed blue-shift in the CD spectra can be assigned to a growing content of extended PPII-like conformations caused by side chain – side chain interactions. As reported by Rausch et al., a rising degree of structured peptides through SDS addition can correspond to  $\beta$ -strand driven intercalation into lipid bilayers.<sup>[31]</sup> In a similar manner, 6-FAM leaking assays with POPC:POPG liposomes revealed all  $X_4[4]Abz$  peptides to disrupt artificial lipid bilayers but with superior potency for TfeGly<sub>4</sub>[4]Abz **5d** after 24 h (about 67%) in comparison to **5a–c** (about 35%) (Figure 6b).

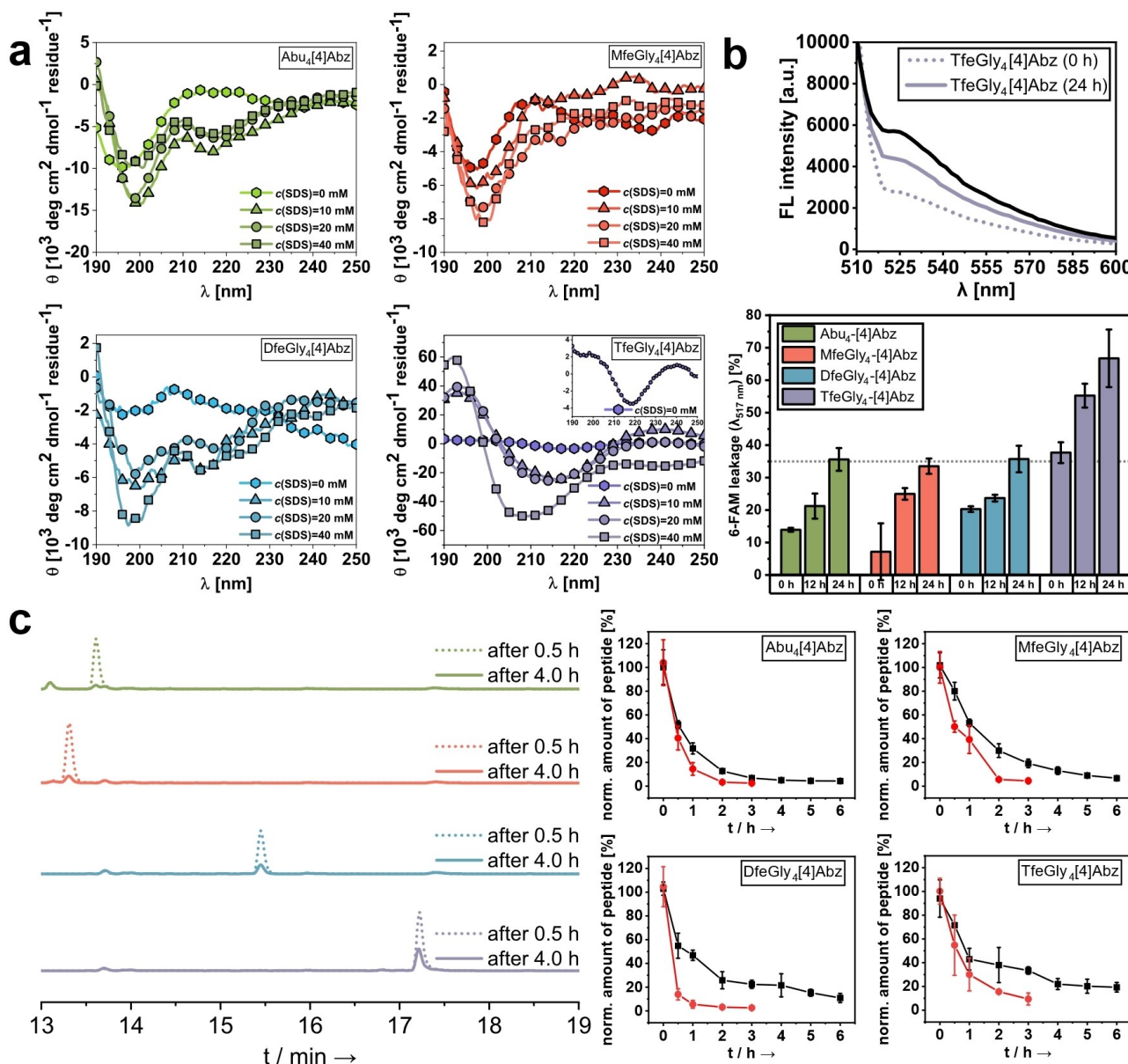
Finally, we studied whether these fluoropeptides can be degraded through digestive enzymes. The incorporation of non-natural amino acids in high proportion is a well-known strategy to alter or even eliminate peptide proteolysis.<sup>[32]</sup> In the context of side chain fluorinated amino acids, a wide range of studies exist with diverse outcomes of such modifications. Moreover, the enzymatic degradation of peptides consisting mainly of fluorinated amino acids has not been studied yet.<sup>[33]</sup>

In this work, we probed the stability of these fluoropeptides towards peptide digestion by the serine proteases elastase and proteinase k. Both endoproteases possess a particular specificity to cleave the amide bonds of aliphatic amino acids at the P1 position.<sup>[34]</sup> All  $X_4[4]Abz$  peptides were dissolved in physiological buffer supplemented with 25% DMSO and, after addition of enzyme, the amount of degradation was determined via HPLC analysis. Quite unexpectedly, we observed peptide degradation for all fluoropeptides upon incubation with both enzymes (see Figure 6c (left) and Supporting Information, Figure S49). After 6 h incubation after addition of elastase (Figure 6c (right), black line), we found major proportions of all labeled tetrapeptides to be digested. Remaining amounts of Abu<sub>4</sub>[4]Abz **5a** ( $4.3 \pm 0.1\%$ ), MfeGly<sub>4</sub>[4]Abz **5b** ( $6.6 \pm 1.1\%$ ), DfeGly<sub>4</sub>[4]Abz **5c** ( $10.9 \pm 3.8\%$ ) and TfeGly<sub>4</sub>[4]Abz ( $19.3 \pm 4.0\%$ ) **5d** appoint a synergy between the growing degree of fluorination and enhanced proteolytic stability with up to 4.4-fold improved rates upon CH<sub>3</sub> (Abu) to CF<sub>3</sub> (TfeGly) substitution. Nevertheless, these astonishing results display an overall accommodation of the fluoropeptides within the enzymes active site. Real-time monitoring of peptide digestion by proteinase k (Figure 6c (right), red line) validated the enzymatic degradability properties of all fluoropeptides. After 3 h of incubation, TfeGly<sub>4</sub>[4]Abz **5d** was mainly degraded by the enzyme but remained in about 3.7-fold increased amounts ( $9.3 \pm 5.0\%$ ) than the Abu-derived tetrapeptide ( $2.5 \pm 0.1\%$ ). Further comparison with leftovers detected for MfeGly<sub>4</sub>[4]Abz **5b** ( $4.4 \pm 2.2\%$ ) and DfeGly<sub>4</sub>[4]Abz **5c** ( $2.6 \pm 0.3\%$ ) after 3 h highlights the scope of substrate acceptance of both enzymes regardless to the fluorinated side chain pattern. Furthermore, we were engaged to determine predominant cleaving sites via HPLC/MS-assisted analysis (experimental data and discussion are provided in the Supporting Information, Figure S51–S54). It is most noteworthy that the [4]Abz-labeled amino acids Abu, MfeGly, DfeGly or TfeGly were found as remaining digestion fragments for both serine proteases. This confirms a main P1-P1' scissile bond in which the fluorinated amino acids act as both P1 and P1' residues, thereby proving susceptibility towards enzymatic degradation in terms of elastase or proteinase K.<sup>[35]</sup>

Prior studies from our laboratory<sup>[33a]</sup>, but also the research groups of Jakubke<sup>[36]</sup>, Kumar<sup>[37]</sup> and Marsh<sup>[38]</sup> came to somewhat contradictory outcomes about the proteolytic stability of peptides when incorporating one or a few fluorinated amino acids. In this study, we investigated the enzymatic degradability of fluoropeptides containing exclusively fluorinated aliphatic amino acids. Experimental evidence obtained in this work let us conclude that these fluoropeptides can be rather considered as biodegradable fluoropolymers than synthetic & persistent PFC-mimicries.

## Conclusion

In this work, we present the first series of artificial fluoropeptides ever reported. Depending on the sequence-length and degree of side chain fluorination, we found notable differences in peptide secondary structure formation under membrane-



**Figure 6.** a. CD spectra of truncated fluoropeptides (100 μM) in aqueous solution (phosphate buffer, 10 mM, pH = 7.4) and in the presence of SDS (10, 20, 40 mM). b. Monitored increase in FL intensity resulting from dye-release in case of TfeGly<sub>4</sub>[4]Abz 5d (100 μM) during incubation [at the start of experiment (dashed line) and after 24 h incubation (solid line)] in POPC:POPG liposome solution (liposome:peptide = 50:1). The FL intensity derived from the positive control [5% (v/v) Triton X-100 in buffer] is illustrated as black line (top). Also, calculated percentages of 6-FAM dye leakage (X<sub>4</sub>[4]Abz series, liposome:peptide = 50:1) reveal superior membrane-disrupting properties upon CH<sub>3</sub> to CF<sub>3</sub> substitution (5d). Lower degrees of dye leaking resembled by average FL values of about 35% were found similarly for 5a, 5b and 5c and are marked as grey-colored dotted line (bottom). c. Real-time monitoring of peptide proteolysis for 5a–5d by the serine protease elastase depicted after 0.5 h (dashed line) and 4 h (solid line) incubation (colors are the same as presented in a. and b.) via HPLC analysis (Supporting Information, Table S20) (left). Normalized amounts of remaining tetrapeptides (230 μM) determined during enzymatic degradation by elastase (0.91 μM, black line) and proteinase k (0.0091 μM, red line) (right).

mimicking environments. A wide range of experimental techniques ranging from CD spectroscopy to SEIRAS, and FL-based leaking assays served to elucidate the intercalation of these fluoropeptides into lipid bilayers and resulting folding patterns. In general, a β-sheet to α-helix transition was observed in most cases series. For the TfeGly-containing fluoropeptides, however, experimental data indicates a unique fluorine-driven formation of PPII structures. Monitoring the partition into POPC:POPG lipid bilayers exposed alterations in

structural compositions, like a decrease in α-helical content in response to the total degree of fluorination. Moreover, proteolysis studies of truncated fluoropeptides exclusively built up from fluorinated amino acids revealed an overall degradability. This study lays the foundation for the development of de novo designed foldamers with fluorine-directed folding and membrane-disrupting properties by maintaining biodegradability. We consider this class of peptide-based fluorooligomers to serve as initial templates in the future design of fluorinated



biomaterials as, for example, fluorous tags for biomolecule or drug delivery. Ongoing work focusses on the biocompatibility of these fluoropeptides and will provide further insights into potential biomedical applications.

## Experimental Section

**General methods:** HRMS were determined on an Agilent 6220 ESI-TOF MS instrument (Agilent Technologies, Santa Clara, CA, USA). For analysis, the MassHunter Workstation Software Version B.02.00 (Agilent Technologies, Santa Clara, CA, USA) was used. All chemicals were purchased from commercial sources (Merck, Sigma-Aldrich, VWR, Fluorochem) and used without further purification. The fluorinated amino acids MfeGly, DfeGly and TfeGly were synthesised according to literature.<sup>[12b]</sup>

**Synthesis and purification of peptides:** All fluoropeptides ( $X_{10}GY(K)_3$ ,  $X_{13}GY(K)_4$  and  $X_{15}GY(K)_4$  series) were synthesized with a microwave-equipped Liberty Blue™ peptide synthesizer (CEM, Matthews, NC, USA). A Rink Amide ProTide™ resin (CEM, Matthews, NC, USA) was utilized and the synthesis was performed either in 0.05 mmol or 0.1 mmol scale using Oxyma/DIC as activating reagents. Detailed coupling protocols are listed in the Supporting Information. Acetylation was done manually in three batches using acetic anhydride (10% v/v) and DIPEA (10% v/v) in DMF (6 mL). The labeled tetrapeptides  $X_4[4]Abz$  were synthesized through standard manual SPPS.

All peptides were cleaved from the resin by treatment with TFA/TIPS/H<sub>2</sub>O (90/5/5) [1 mL cleavage cocktail per 50 mg resin] for three hours using sonication at room temperature. Then the resins were washed with TFA and DCM, and excess of solvents were removed by evaporation. Peptides were dried by lyophilization before purification with preparative reversed phase HPLC. Purification of synthesized peptides was performed on a Knauer low-pressure HPLC system (Knauer GmbH, Berlin, Germany) sold by VWR (Darmstadt, Germany), comprising a LaPrep Sigma preparative pump (LP1200), a ternary low-pressure gradient, a dynamic mixing chamber, a 6-port-3-channel injection valve with an automated preparative 10 mL sample loop, a LaPrep Sigma standard 1-channel-UV-detector (LP3101), a flow cell with 0.5 mm thickness and a 16-port LaPrep Sigma fractionation valve (LP2016). A Kinetex RPC18 endcapped (5 μM, 100 Å, 250 × 21.2 mm, Phenomenex®, USA) HPLC-column was used. A Security Guard™ PREP Cartridge Holder Kit (21.20 mm, ID, Phenomenex®, USA) served as pre-column. As eluents water and ACN, both containing 0.1% (v/v) TFA were applied. HPLC runs were performed with a flow rate of 15.0 mL/min, UV-detection occurred at 220 nm for respective peptides. Data analysis occurred with an EZChrom Elite-Software (Version 3.3.2 SP2, Agilent). After separation, the purity of the collected fractions was determined by analytical HPLC. Analytical HPLC was carried out on a Chromaster 600 bar DAD-System with CSM software or a Hitachi Primaide™ UV-HPLC system (both from VWR/Hitachi, Darmstadt, Germany). A Kinetex® RP-C18 (5 μM, 100 Å, 250 × 4.6 mm, Phenomenex®, USA) column and a SecurityGuard™ Cartridge Kit equipped with a C18 cartridge (4 × 3.0 mm, Phenomenex®, USA) as pre-column was used. Otherwise, a Luna® RP-C8 (5 μM, 100 Å, 150 × 3 mm, Phenomenex®, USA) column was used. As eluents water and ACN, both containing 0.1% (v/v) TFA were applied. A flow rate of 1 mL/min was used and UV-detection occurred at 220 nm or 280 nm for respective peptides. Data analysis was done with EZ Chrom ELITE software (version 3.3.2, Agilent). The resulting pure peptides (> 95%) were obtained after lyophilization of the collected fractions. All essential data for the quantification of

purified peptides (HPLC chromatograms, HRMS spectra) can be found in the Supporting Information.

**CD spectroscopy:** Circular dichroism experiments were performed using a Jasco J-810 spectropolarimeter fitted with a recirculating chiller. Data were recorded using 0.1 mm or 0.2 mm Quartz Suprasil® cuvettes (Hellma) equipped with a stopper. Spectra were recorded at 37 °C from 190 to 250 nm at 0.2 nm intervals, 1 nm bandwidth, 4 s response time and a scan speed of 100 nm min<sup>-1</sup>. Baselines were recorded and were subtracted from the data. Each reported CD value represents the average of minimum three measurements.

**Lyophilization:** To lyophilize the synthesized peptides a laboratory freeze dryer ALPHA 1–2 LD (Christ Gefriertrocknungsanlagen GmbH, Osterode am Harz, Germany) was used.

**Preparation of large unilamellar vesicles (LUV):** POPC and POPG were each dissolved in chloroform (1 mL). From these stock solutions, POPC and POPG (1:1) were suspended in phosphate buffer (10 mM, pH=7.4) at a concentration of 3.75 mM. The suspension was submitted to ten freeze and thaw cycles. Subsequently, large unilamellar vesicles (LUVs) were prepared by extrusion across a polycarbonate Nuclepore™ track-etched membrane (0.1 μm pore size, Whatman International Ltd., Kent, United Kingdom) using an Avanti extruder (Avanti Polar Lipids, Birmingham, AL, USA).

**6-Carboxyfluorescein [6-FAM] leakage assay:** At first, stocks of 1-palmitoyl-2-oleoyl-sn-glycero-3-phosphocholine (POPC) and 1-palmitoyl-2-oleoyl-sn-glycero-3-[phospho-rac-(1-glycerol)] (POPG) were prepared by dissolving the compounds in CHCl<sub>3</sub> in a concentration of 10 mg/mL. Aliquots were taken from both stocks and CHCl<sub>3</sub> was evaporated. The amount of aliquots corresponded to a liposome solution of POPC/POPG (1:1, each 5 mM [1 mL]). The lipid film was dried *in vacuo* overnight and then dissolved in 50 mM 6-carboxyfluorescein (6-FAM) in 10 mM phosphate buffer, pH 7.4. The pH of this solution was adjusted to pH 7.4 with a 1 N NaOH solution before addition to the lipid film. The suspension was submitted to ten freeze–thaw cycles and then rest for 1 h at rt for equilibration. Untrapped dye was removed by gel filtration on PD-10 desalting columns containing Sephadex G-25. To prepare peptide/lipids sample, aliquots were taken from respective peptide stocks in HFIP and dried under a gentle stream of nitrogen. Then, dried peptide films were dissolved in 25 μL buffer and mixed for 5–10 seconds to obtain a homogeneous mixture. Subsequently, 25 μL of liposome solution were added and the solution was gently mixed for 5 seconds. The final concentrations were: 50 μM ( $X_{10}GY(K)_3$  -  $X_{13}GY(K)_4$  -  $X_{15}GY(K)_4$  series) or 100 μM peptide ( $X_4[4]Abz$ ) + 5 mM POPG:POPG (1:1, each 2.5 mM). The leakage of 6-FAM was detected by measuring the fluorescence intensity at 37 °C and an excitation wavelength of 493 nm; fluorescence emission was recorded at 517 nm. 100% dye release was achieved from the liposomes with the addition of 5% (v/v) Triton X-100 in buffer. A negative control was constituted by measuring FL emission of the liposome solution only containing buffer. All samples were transferred on BRAND® microplates (size: 96 wells, color: black; Sigma-Aldrich), sealed to prevent evaporation and placed in an Infinite M Nano+ plate reader (Tecan Deutschland GmbH, Crailsheim, Germany). Fluorescence intensity was followed over 24 h after sample preparation and a fluorescence scan was measured every 30 min.

**Estimation of log P values:** The estimation of log P values was carried out according a HPLC-based protocol adapted from the O'Hagan working group. A library of short peptides with known log P values was synthesized and analyzed by HPLC. The corresponding retention times were measured using a reversed-phase C18 column. Subsequently, the correlation between known log P values and

retention times was fitted. The obtained linear function was used to estimate the log P values of fluoropeptides from the corresponding measured retention times. A detailed description of the protocol can be found in the Supporting Information.

**Peptide digestion assay:** For all enzymes, following buffer mixture was used: 50 mM bis-tris propane + 20 mM CaCl<sub>2</sub>, pH 8 [75%] + DMSO [25%]. All samples were dissolved in buffer (400 μL) and then were gently mixed to obtain a homogeneous solution. Afterwards, 40 μL of an enzyme-solution in buffer (elastase: 10 μM / proteinase k: 0.1 μM) were added and the samples were again gently mixed for 5 seconds. The concentration of each enzyme was adjusted before to obtain well-detectable digestion kinetics. The final concentrations were: 230 μM X<sub>4</sub>[4]Abz peptide + 0.91 μM elastase or 0.0091 μM proteinase k. All samples were incubated at 30 °C over a period of 3–6 h. Aliquots of 15 μL were taken at fixed time points and quenched with 90 μL of a solution of 30% AcOH in water containing 130 μM Ac-[4]Abz-Gly-OH as reference. Afterwards, peptide degradation was monitored by HPLC analysis. In all cases, the peaks corresponding to each peptide sample (full-length peptides) and the reference sample were integrated and used to determine the amount of substrate still present in solution. The content of starting material after 5 min was termed as absolute amount for simplicity. For the detection of peptide fragments derived from proteolysis, all samples were prepared accordingly and incubated at 30 °C over a period of 24 h. Afterwards, aliquots of the reaction mixture were monitored by HPLC analysis. To identify the cleaving site of each peptide, each HPLC signal from a digestion fragment cleaved from the full-length peptide was isolated and analyzed by ESI-ToF mass analysis on an Agilent 6220 ESI-ToF-MS spectrometer (Agilent Technologies, Santa Clara, CA, USA).

**Surface enhanced infrared absorption spectroscopy (SEIRAS):** The required amount of a 1:1 volume ratio of 1-palmitoyl-2-oleoyl-glycero-3-phosphocholine (POPC) and 1-palmitoyl-2-oleoyl-sn-glycero-3-phospho-1'-rac-glycerol (POPG) (Avanti Polar Lipids, Alabama, USA) dissolved in chloroform was placed in a septum capped glass tube and dried under a gentle flow of argon. The dried lipid was resuspended in 10 mM phosphate buffer (pH 6.0). The suspension was freeze-thawed at least 5 times, followed by extrusion with a 100 nm filter to form Large Unilamellar Vesicles (LUV) of POPC/POPG. Then, ~1.2 mg/ml of lipid LUV was casted over the surface of Au film substrate to form a solid-supported lipid layer by spontaneous vesicle fusion. After incubation in the lipid containing solution for overnight (> 12 h), the Au film surface was thoroughly rinsed with Milli-Q water and the buffer solution to remove excess amount of the lipid accumulated over the solid supported lipid bilayer. SEIRAS experiments were conducted as described before.<sup>[39]</sup> Briefly, Attenuated Total Reflection (ATR) optical configuration was employed with a micro-grooved silicon chip crystal as internal reflection element (IRE, from IRUBIS GmbH, München, Germany). A SEIRA active gold film was formed on reflection surface of IRE by chemical deposition. A background spectrum was taken on the gold surface with presence of the solid supported POPC/POPG bilayer in 200 μL of 10 mM phosphate buffer solution with pH = 7.4 prior to the sample measurement. Then, 200 μL of the peptide samples dissolved in same buffer was added to the solution and sample IR spectra were subsequently measured to monitor the adsorption process on the lipid surface. Final concentration of each peptide during the adsorption measurement was kept ~25 μg/ml. Baseline of the obtained spectra were corrected at the position of 1800 cm<sup>-1</sup>, where no absorption from the band relate to the samples occur, to become zero.

## Author contributions

T.H. and S.C. developed the overall project, provided fluorinated amino acids, synthesized & purified all fluoropeptides and wrote the manuscript. B.K. provided guidance on data analysis and interpretation. T.H. performed CD studies, structural studies with POPC/POPG liposomes and determination of hydrophobicity. S.C. performed CD studies, leaking & peptide digestion assays. K.A. performed SEIRAS studies and wrote the manuscript. J.E. assisted T.H. in synthesis and analysis. G.H.D. assisted S.C. in synthesis and digestion assays. J.H. provided expertise and feedback.

## Acknowledgements

The authors gratefully acknowledge financial support by the Deutsche Forschungsgemeinschaft (DFG) through the collaborative research center CRC-1349 "Fluorine-Specific Interactions" project no. 387284271. T.H. thanks the Studienstiftung des deutschen Volkes for financial support. We thank Dr. Stephan Block, Dr. Katharina G. Hugentobler and Dr. Stephanie Wedepohl for scientific discussions and expertise. We thank Balu and Honey for continuous encouragement and support. We would like to acknowledge the assistance of the Core Facility *BioSupraMol* supported by the DFG. Open Access funding enabled and organized by Projekt DEAL.

## Conflicts of interest

There are no conflicts to declare.

## Data Availability Statement

The data that support the findings of this study are available in the supplementary material of this article.

**Keywords:** fluorinated biomaterials · fluoropeptides · fluorour amino acids · foldamers · membrane disruption

- [1] a) I. Ojima, *J. Org. Chem.* **2013**, *78*, 6358–6383; b) J. M. Wolfe, C. M. Fadzen, R. L. Holden, M. Yao, G. J. Hanson, B. L. Pentelute, *Angew. Chem. Int. Ed.* **2018**, *57*, 4756–4759; c) E. N. G. Marsh, B. C. Buer, A. Ramamoorthy, *Mol. BioSyst.* **2009**, *5*, 1143–1147.
- [2] a) M. P. Krafft, *Adv. Drug Delivery Rev.* **2001**, *47*, 209–228; b) H.-J. Böhm, D. Banner, S. Bendels, M. Kansy, B. Kuhn, K. Müller, U. Obst-Sander, M. Stahl, *ChemBioChem* **2004**, *5*, 637–643.
- [3] a) J. Han, A. M. Remete, L. S. Dobson, L. Kiss, K. Izawa, H. Moriwaki, V. A. Soloshonok, D. O'Hagan, *J. Fluorine Chem.* **2020**, *239*, 109639; b) J. Lv, Y. Cheng, *Chem. Soc. Rev.* **2021**, *50*, 5435–5467.
- [4] T. Song, Y. Gao, M. Song, J. Qian, H. Zhang, J. Zhou, Y. Ding, *Med. Drug Discovery* **2022**, *14*, 100123.
- [5] a) Z. Zhang, W. Shen, J. Ling, Y. Yan, J. Hu, Y. Cheng, *Nat. Commun.* **2018**, *9*, 1377; b) G. Rong, C. Wang, L. Chen, Y. Yan, Y. Cheng, *Sci. Adv.* **2020**, *6*, eaaz1774.
- [6] a) T. Stahl, D. Mattern, H. Brunn, *Environ. Sci. Europe* **2011**, *23*, 38; b) V. Ochoa-Herrera, J. A. Field, A. Luna-Velasco, R. Sierra-Alvarez, *Environ. Sci. Process. Impacts* **2016**, *18*, 1236–1246.

- [7] C. Jäckel, M. Salwiczek, B. Koksich, *Angew. Chem. Int. Ed.* **2006**, *45*, 4198–4203.
- [8] A. A. Berger, J.-S. Völler, N. Budisa, B. Koksich, *Acc. Chem. Res.* **2017**, *50*, 2093–2103.
- [9] a) R. Godbout, S. Légaré, M. Auger, C. Carpentier, F. Otis, M. Auger, P. Lagüe, N. Voyer, *PLoS One* **2016**, *11*, e0166587–e0166587; b) M. Auger, T. Lefèvre, F. Otis, N. Voyer, M. Auger, *Pept. Sci.* **2019**, *111*, e24051.
- [10] a) B. Bilgiçer, K. Kumar, *Proc. Natl. Acad. Sci. USA* **2004**, *101*, 15324–15329; b) N. Naarmann, B. Bilgiçer, H. Meng, K. Kumar, C. Steinem, *Angew. Chem. Int. Ed.* **2006**, *45*, 2588–2591.
- [11] a) B. Meng, S. L. Grage, O. Babii, M. Takamiya, N. MacKinnon, T. Schober, I. Hutsikalov, O. Nassar, S. Afonin, S. Koniev, I. V. Komarov, J. G. Korvink, U. Strähle, A. S. Ulrich, *Small* **2022**, e2107308; b) S. E. Kirberger, S. D. Maltseva, J. C. Manulik, S. A. Einstein, B. P. Weegman, M. Garwood, W. C. K. Pomerantz, *Angew. Chem. Int. Ed. Engl.* **2017**, *56*, 6440–6444; c) P. Wadhvani, P. Tremouilhac, E. Strandberg, S. Afonin, S. Grage, M. Ieronimo, M. Berditsch, A. S. Ulrich, in *Current Fluoroorganic Chemistry*, Vol. 949, American Chemical Society, **2007**, pp. 431–446.
- [12] a) J. Leppkes, T. Hohmann, B. Koksich, *J. Fluorine Chem.* **2020**, *232*, 109453; b) T. Hohmann, M. Dyrks, S. Chowdhary, M. Weber, D. Nguyen, J. Moschner, B. Koksich, *J. Org. Chem.* **2022**, *87*, 10592–10604.
- [13] S. Chowdhary, R. F. Schmidt, A. K. Sahoo, T. tom Dieck, T. Hohmann, B. Schade, K. Brademann-Jock, A. F. Thünemann, R. R. Netz, M. Gradzielski, B. Koksich, *Nanoscale* **2022**, *14*, 10176–10189.
- [14] K. Ataka, T. Kottke, J. Heberle, *Angew. Chem. Int. Ed.* **2010**, *49*, 5416–5424.
- [15] J. Leppkes, N. Dimos, B. Loll, T. Hohmann, M. Dyrks, A. Wieseke, B. G. Keller, B. Koksich, *RSC Chem. Biol.* **2022**, *3*, 773–782.
- [16] M. Paradis-Bas, J. Tulla-Puche, F. Albericio, *Chem. Soc. Rev.* **2016**, *45*, 631–654.
- [17] P. Wallimann, R. J. Kennedy, J. S. Miller, W. Shalongo, D. S. Kemp, *J. Am. Chem. Soc.* **2003**, *125*, 1203–1220.
- [18] a) A. A. Adzhubei, M. J. E. Sternberg, A. A. Makarov, *J. Mol. Biol.* **2013**, *425*, 2100–2132; b) Z. Shi, K. Chen, Z. Liu, N. R. Kallenbach, *Chem. Rev.* **2006**, *106*, 1877–1897; c) Z. Shi, R. W. Woody, N. R. Kallenbach, in *Advances in Protein Chemistry*, Vol. 62, Academic Press, **2002**, pp. 163–240; d) B. Bochicchio, A. M. Tamburro, *Chirality* **2002**, *14*, 782–792.
- [19] P. M. Cowan, S. McGavin, *Nature* **1955**, *176*, 501–503.
- [20] a) F. Eker, K. Griebenow, R. Schweitzer-Stenner, *J. Am. Chem. Soc.* **2003**, *125*, 8178–8185; b) Z. Liu, K. Chen, A. Ng, Z. Shi, R. W. Woody, N. R. Kallenbach, *J. Am. Chem. Soc.* **2004**, *126*, 15141–15150.
- [21] V. Kubyshkin, S. L. Grage, J. Bürck, A. S. Ulrich, N. Budisa, *J. Phys. Chem. Lett.* **2018**, *9*, 2170–2174.
- [22] A. L. Rucker, T. P. Creamer, *Protein Sci.* **2002**, *11*, 980–985.
- [23] A. I. Arunkumar, T. K. S. Kumar, C. Yu, *Biochim. Biophys. Acta (BBA) – Protein Structure and Molecular Enzymology* **1997**, *1338*, 69–76.
- [24] V. Kubyshkin, J. Bürck, O. Babii, N. Budisa, A. S. Ulrich, *Phys. Chem. Chem. Phys.* **2021**, *23*, 26931–26939.
- [25] J. L. S. Lopes, A. J. Miles, L. Whitmore, B. A. Wallace, *Protein Sci.* **2014**, *23*, 1765–1772.
- [26] Z. Shi, C. A. Olson, D. Rose George, L. Baldwin Robert, R. Kallenbach Neville, *Proc. Nat. Acad. Sci.* **2002**, *99*, 9190–9195.
- [27] K. Ataka, J. Drauschke, V. Stulberg, B. Koksich, J. Heberle, *Biochim. Biophys. Acta Biomembr.* **2022**, *1864*, 183873.
- [28] K. Pagel, K. Seeger, B. Seiwert, A. Villa, A. E. Mark, S. Berger, B. Koksich, *Org. Biomol. Chem.* **2005**, *3*, 1189–1194.
- [29] a) T. J. Measey, R. Schweitzer-Stenner, *J. Am. Chem. Soc.* **2006**, *128*, 13324–13325; b) R. Schweitzer-Stenner, T. Measey, A. Hagarman, F. Eker, K. Griebenow, *Biochemistry* **2006**, *45*, 2810–2819.
- [30] D. J. Tew, S. P. Bottomley, D. P. Smith, G. D. Ciccotosto, J. Babon, M. G. Hinds, C. L. Masters, R. Cappai, K. J. Barnham, *Biophys. J.* **2008**, *94*, 2752–2766.
- [31] J. M. Rausch, J. R. Marks, R. Rathinakumar, W. C. Wimley, *Biochemistry* **2007**, *46*, 12124–12139.
- [32] Z. Lai, X. Yuan, H. Chen, Y. Zhu, N. Dong, A. Shan, *Biotechnol. Adv.* **2022**, *59*, 107962.
- [33] a) S. Huhmann, B. Koksich, *Eur. J. Org. Chem.* **2018**, *2018*, 3667–3679; b) R. Smits, B. Koksich, *Curr. Top. Med. Chem.* **2006**, *6*, 1483–1498.
- [34] L. Hedstrom, *Chem. Rev.* **2002**, *102*, 4501–4524.
- [35] a) I. Schechter, A. Berger, *Biochem. Biophys. Res. Commun.* **1967**, *27*, 157–162; b) I. Schechter, A. Berger, *Biochem. Biophys. Res. Commun.* **1968**, *32*, 898–902.
- [36] B. Koksich, N. Sewald, H.-J. Hofmann, K. Burger, H.-D. Jakubke, *J. Peptide Sci.* **1997**, *3*, 157–167.
- [37] H. Meng, K. Kumar, *J. Am. Chem. Soc.* **2007**, *129*, 15615–15622.
- [38] L. M. Gottler, R. de la Salud Bea, C. E. Shelburne, A. Ramamoorthy, E. N. G. Marsh, *Biochemistry* **2008**, *47*, 9243–9250.
- [39] a) N. J. Harris, E. Reading, K. Ataka, L. Grzegorzewski, K. Charalambous, X. Liu, R. Schlesinger, J. Heberle, P. J. Booth, *Sci. Rep.* **2017**, *7*, 8021; b) A. Baumann, S. Kerruth, J. Fitter, G. Büldt, J. Heberle, R. Schlesinger, K. Ataka, *PLoS One* **2016**, *11*, e0151051; c) K. Ataka, S. T. Stripp, J. Heberle, *Biochim. Biophys. Acta Biomembr.* **2013**, *1828*, 2283–2293.

Manuscript received: December 9, 2022  
Accepted manuscript online: February 1, 2023  
Version of record online: March 15, 2023

# Chemistry–A European Journal

Supporting Information

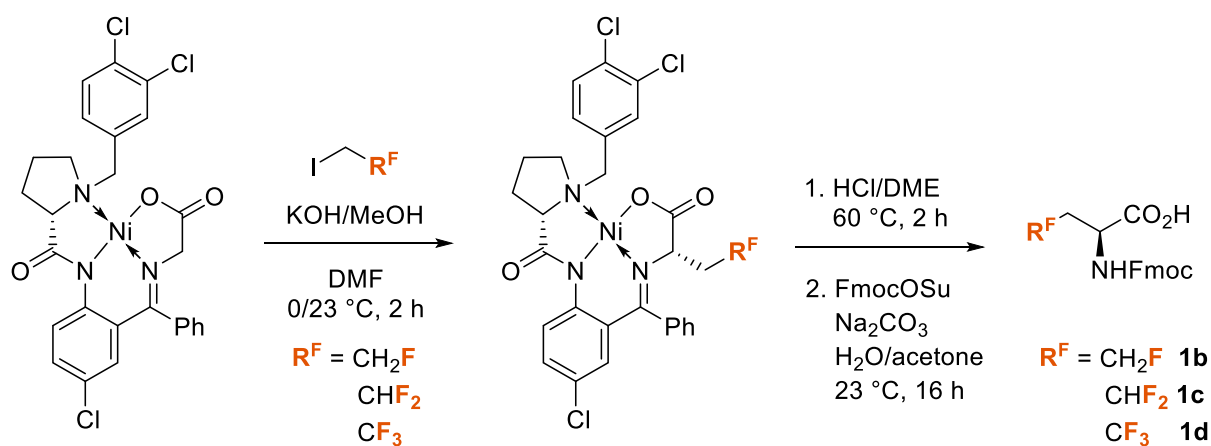
## **Introducing Aliphatic Fluoropeptides: Perspectives on Folding Properties, Membrane Partition and Proteolytic Stability**

Thomas Hohmann, Suvrat Chowdhary, Kenichi Ataka, Jasmin Er, Gesa Heather Dreyhsig,  
Joachim Heberle, and Beate Kocsch\*

# Content

1. Synthesis of fluorinated amino acids.....	1
2. Solid-phase peptide synthesis (SPPS) – synthesis and purification .....	2
2.1 Microwave-assisted solid-phase peptide synthesis.....	2
2.2 Manual solid-phase peptide synthesis .....	4
2.3 Preparative & analytical HPLC .....	6
2.4 Peptide synthesis: HPLC chromatograms and HRMS spectra .....	8
2.4.1 Abu <sub>10</sub> GY(K) <sub>3</sub> 2a .....	9
2.4.2 MfeGly <sub>10</sub> GY(K) <sub>3</sub> 2b .....	10
2.4.3 DfeGly <sub>10</sub> GY(K) <sub>3</sub> 2c.....	11
2.4.4 TfeGly <sub>10</sub> GY(K) <sub>3</sub> 2d.....	12
2.4.5 Abu <sub>13</sub> GY(K) <sub>4</sub> 3a .....	13
2.4.6 MfeGly <sub>13</sub> GY(K) <sub>4</sub> 3b .....	14
2.4.7. DfeGly <sub>13</sub> GY(K) <sub>4</sub> 3c.....	15
2.4.8 TfeGly <sub>13</sub> GY(K) <sub>4</sub> 3d.....	16
2.4.9 Abu <sub>15</sub> GY(K) <sub>4</sub> 4a .....	17
2.4.10 MfeGly <sub>15</sub> GY(K) <sub>4</sub> 4b .....	18
2.4.11 DfeGly <sub>15</sub> GY(K) <sub>4</sub> 4c.....	19
2.4.12 Abu <sub>4</sub> [4]Abz 5a .....	20
2.4.13 MfeGly <sub>4</sub> [4]Abz 5b.....	21
2.4.14 DfeGly <sub>4</sub> [4]Abz 5c.....	22
2.4.15 TfeGly <sub>4</sub> [4]Abz 5d .....	23
3. Circular Dichroism and SEIRAS Infrared Spectroscopy – further data .....	24
3.1 Fundamentals: Hydrophobicity Studies.....	24
3.2 Parametric dual wavelength two-state test .....	25
3.1.1 Abu <sub>10</sub> GY(K) <sub>3</sub> 2a .....	25
3.1.2 Abu <sub>13</sub> GY(K) <sub>4</sub> 3a .....	25
3.1.3 Abu <sub>15</sub> GY(K) <sub>4</sub> 4a .....	26
3.1.4 DfeGly <sub>13</sub> GY(K) <sub>4</sub> 3c.....	26
3.1.5 DfeGly <sub>15</sub> GY(K) <sub>4</sub> 4c.....	27
3.1.6 TfeGly <sub>13</sub> GY(K) <sub>4</sub> 3d.....	27
3.3 TfeGly <sub>10</sub> GY(K) <sub>3</sub> 2d.....	28
3.4 Poly(L-lysine).....	28
3.5 Time-dependent measurements in the presence of POPC/POPG .....	30
3.6 Additional SEIRAS Spectra .....	31
4. Estimation of log P values by HPLC.....	34
5. 6-FAM leaking assay – further data .....	38
6. Peptide digestion assay .....	39
7. References.....	44

## 1. Synthesis of fluorinated amino acids



**Figure S1:** Synthesis of Fmoc-protected fluorinated amino acids (Fmoc-MfeGly **1b**, Fmoc-DfeGly **1c**, Fmoc-TfeGly **1d**) using a chiral Ni(II) complex.

The compounds **1b-d** were synthesized according to the procedures described by Hohmann *et al.*<sup>[1]</sup> and Han *et al.*<sup>[2]</sup>

## 2. Solid-phase peptide synthesis (SPPS) – synthesis and purification

### 2.1 Microwave-assisted solid-phase peptide synthesis

Peptide synthesis ( $X_{10}GY(K)_3$ ,  $X_{13}GY(K)_4$  and  $X_{15}GY(K)_4$  series) was performed with a Liberty Blue automated microwave-assisted peptide synthesizer (CEM Corporation, Mathews, NC, USA) in an Fmoc-based SPPS approach. All peptides were synthesized as C-terminal amides on a Rink Amide ProTide Resin (LL) resin (0.19-0.20 mmol/g resin substitution) in a 0.05 mmol scale. General conditions for Fmoc deprotection & amino acid coupling are listed in **table S1**. Fmoc deprotection was carried out with 10 wt% piperazine in EtOH/NMP (1/9, v/v). All amino acids were coupled with Oxyma/DIC as activators. The proteogenic amino acids glycine, tyrosine and lysine were coupled through a “single-coupling” approach. The non-canonical amino acids Abu, MfeGly, DfeGly and TfeGly were introduced with a “special coupling” cycle established by Leppkes *et al.*<sup>[3]</sup> It used elongated microwave heating time, reduced equivalents of the amino acid employed and additional washing steps between Fmoc deprotection and coupling step. For subsequent capping of N-terminal amino groups with acetic anhydride, a solution of Ac<sub>2</sub>O (10 % (v/v) and DIPEA (10 % (v/v) in DMF (6 mL) was added in three batches manually and the reaction was then shaken for 3 \* 10 min. For peptide cleavage, the dried resin was treated with 20 mL of TFA/water/TIPS (90/5/5, v/v) for 3 h at room temperature. Afterwards, the resin was washed thrice with TFA and CH<sub>2</sub>Cl<sub>2</sub>. Organic solvent was removed in vacuo and the peptides were precipitated in ice-cold Et<sub>2</sub>O and centrifuged. The precipitate was washed thrice more with Et<sub>2</sub>O and centrifuged. The supernatant was discarded, dissolved in water and lyophilized overnight before purification through preparative HPLC.

**Table S1:** Cycles for automated microwave-assisted SPPS with a 0.05 mmol scale on Liberty Blue peptide synthesizer. All reagents were dissolved in DMF, if not otherwise stated.

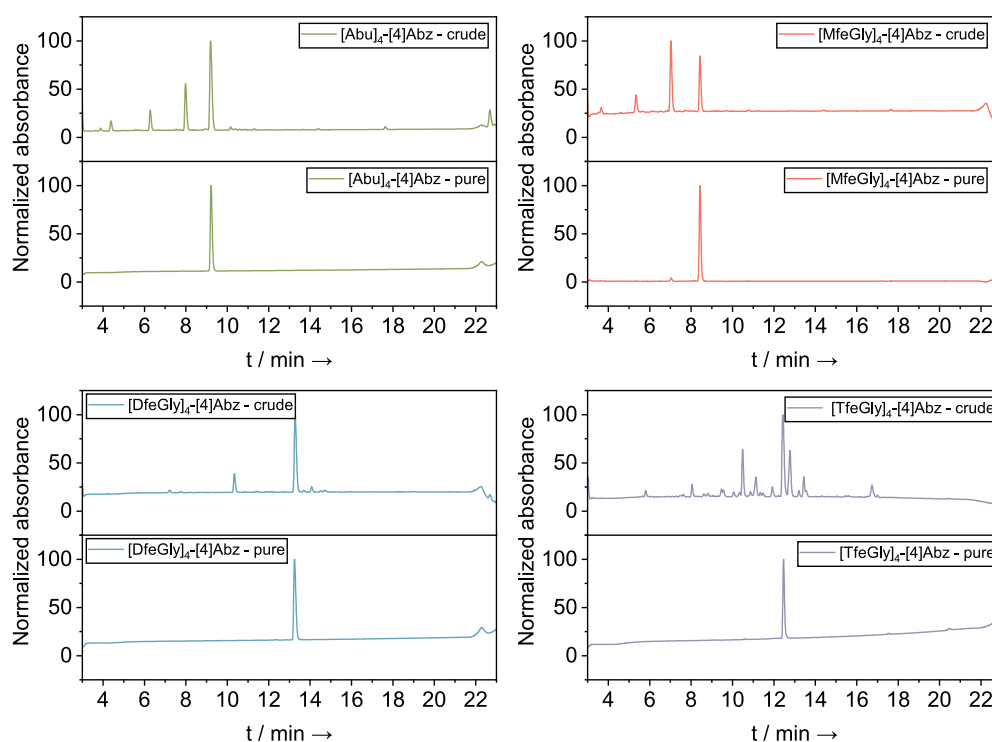
	<u>Process step</u>	<u>Reagents</u>			<u>Reaction conditions</u>		
		Name	Conc. [M]	Volume [mL]	Temp [°C]	Power [W]	Time [s]
Loading / Single coupling	[1] Deprotection	Piperazine	10 wt%	2 <sup>[1]</sup>	75	155	15
		HOBt	0.1		90	30	60
	[2] Washing (4*)	DMF	-	2	25	-	5
	[3] AA coupling	Fmoc-AA-OH	0.2	1.25	75	217	15
		DIC	1	0.5			
Oxyma		1	0.25	90	43	225	
DIPEA	0.1						
[4] Washing	DMF	-	2	25	-	5	
Special coupling	[1] Deprotection	Piperazine	10 wt%	2 <sup>[1]</sup>	75	155	15
		HOBt	0.1		90	30	60
	[2] Washing (4* - 9 cycles)	DMF	-	2	25	-	5
	[3] AA coupling	Fmoc-(F)AA- OH	0.05	1.25	75	217	15
		DIC	1	0.5			
Oxyma		1	0.25	90	43	585	
DIPEA	0.1						
[4] Washing (4*)	DMF	-	2	25	-	5	
<sup>[1]</sup> EtOH/NMP, 1/9, v/v							



## 2.2 Manual solid-phase peptide synthesis

The peptides Abu<sub>4</sub>[4]Abz **5a**, MfeGly<sub>4</sub>[4]Abz **5b**, DfeGly<sub>4</sub>[4]Abz **5c** and TfeGly<sub>4</sub>[4]Abz **5d** were synthesized using standard Fmoc-chemistry at room temperature in a 0.1 mmol scale. A NovaSyn®TGR resin (0.21 mmol / resin substitution) was chosen to obtain C-terminal peptide amides. Fmoc deprotection was carried out with a 20% piperidin in DMF. All amino acids were coupled with HATU/DIPEA as activators. Fmoc-[4]Abz-OH was loaded on the resin with 5 equivalents and double coupling. The non-canonical amino acids Abu, MfeGly, DfeGly and TfeGly were introduced through single coupling with only 1.5 equivalents of amino acid. Before each step (deprotection and coupling) the resin was washed with DMF and DCM. The N-terminal amine was kept free to provide solubility of these hydrophobic sequences. For peptide cleavage, the dried resin was treated with 10 mL of TFA/water/TIPS (95/2.5/2.5, v/v) for 3 h at room temperature. Afterwards, the resin was washed thrice with TFA and CH<sub>2</sub>Cl<sub>2</sub>. Afterwards, the crude product was dissolved in water and lyophilized overnight.

Standard conditions of manual SPPS are listed in **table S2**. HPLC chromatograms obtained from crude & pure peptide during synthesis are presented in **figure S2**.



**Figure S2:** HPLC chromatograms of crude and pure peptides. H<sub>2</sub>O + 0.1% TFA (A) and ACN + 0.1% TFA (B) served as eluents. The HPLC gradients were 10 → 40% (B) in 18 min for Abu<sub>4</sub>[4]Abz, MfeGly<sub>4</sub>[4]Abz and DfeGly<sub>4</sub>[4]Abz and 10 → 70% (B) in 18 min for TfeGly<sub>4</sub>[4]Abz.

**Table S2:** Process steps for manual SPPS. All reagents were dissolved in DMF.

Process step		Reagent	Reaction time
	<b>[1] Swelling</b>	5.0 mL DMF	2* 30 min
	<b>[2] Loading</b>	5 eq. Fmoc-[4]Abz-OH, 5 eq. HATU and 10 eq. DIPEA in 4.0 mL DMF	2 *60 min
	<b>[3] Washing</b>	5.0 mL DMF 5.0 mL DCM	3 * 1 min 3 * 1 min
<b>Coupling cycle</b>	<b>[4] Deprotection</b>	2.0 mL 20% piperidine in DMF	3* 10 min
	<b>[5] Washing</b>	5.0 mL DMF 5.0 mL DCM	3 * 1 min 3 * 1 min
	<b>[6] Coupling</b>	1.5 eq. Fmoc-(F)AA-OH, 1.5 eq. HATU and 3 eq. DIPEA in 2.0 mL DMF	1 * 60 min
	<b>[7] Washing</b>	5.0 mL DMF 5.0 mL DCM	3 * 1 min 3 * 1 min

## 2.3 Preparative & analytical HPLC

### **LaPrep $\Sigma$ HPLC system (preparative HPLC)**

Purification of the synthesized peptides was performed on a LaPrep  $\Sigma$  HPLC system (VWR International GmbH, Darmstadt, Germany), comprising a LaPrep  $\Sigma$  LP 1200 preparative solvent pump with 100 mL titanium pump head, a ternary low-pressure gradient, a dynamic mixing chamber, a 6-port-3-channel injection valve with an automated preparative 10 mL sample loop, a LaPrep  $\Sigma$  LP 3101 1-channel UV-detector, a LaPrep  $\Sigma$  semi-preparative flow cell with 0.5 mm path length and a LaPrep  $\Sigma$  LP2016 17-port/1-channel fractionation valve. A Kinetex<sup>®</sup> C18 RP-HPLC column with TMS endcapping (5  $\mu$ m, 100 Å, 250  $\times$  21.2 mm, Phenomenex<sup>®</sup>, Torrance, CA, USA) was used. A SecurityGuard<sup>™</sup> PREP Cartridge Holder Kit (21.20 mm ID, Ea, Phenomenex<sup>®</sup>, Torrance, CA, USA) holding a C18 cartridge (15  $\times$  21.2mm, Phenomenex<sup>®</sup>, Torrance, CA, USA) served as pre-column. As eluents deionized water and ACN, both containing 0.1% (v/v) TFA were applied. HPLC runs were performed according to the methods given in Table SX. Data analysis occurred with an EZChrom *Elite* software (Version 3.3.2 SP2, Agilent Technologies, Santa Clara, CA, USA).

### **Chromaster HPLC system (analytical HPLC)**

The VWR-Hitachi Chromaster HPLC 600 bar system (VWR International GmbH, Darmstadt, Germany) works with a low-pressure gradient, and comprises a 5160 pump with a 6-channel solvent degaser, an organizer, a 5260 autosampler with a 100  $\mu$ L sample loop, a 5310 column oven and a 5430 diode array detector with a standard flow cell (10 mm optical path length). A Kinetex<sup>®</sup> C18 column (5  $\mu$ m, 100 Å, 250  $\times$  4.6 mm, Phenomenex<sup>®</sup>, Torrance, CA, USA), was used. A SecurityGuard<sup>™</sup> Cartridge Kit (Ea, Phenomenex<sup>®</sup>, Torrance, CA, USA) with a C18 SecurityGuard<sup>™</sup> cartridge (4  $\times$  3.0 mm, Phenomenex<sup>®</sup>, Torrance, CA, USA) served as pre-column. Deionized water and ACN, both containing 0.1% (v/v) TFA, served as eluents. The flow rate was adjusted to 1 mL/min and the column was heated to 24°C. UV-detection of the peptides occurred at 220 nm or 280 nm while running a linear gradient of ACN + 0.1% (v/v) TFA. Data analysis was performed with EZChrom *Elite* software (version 3.3.2, Agilent Technologies, Santa Clara, CA, USA).

### **LaChrom ELITE® HPLC system (analytical HPLC)**

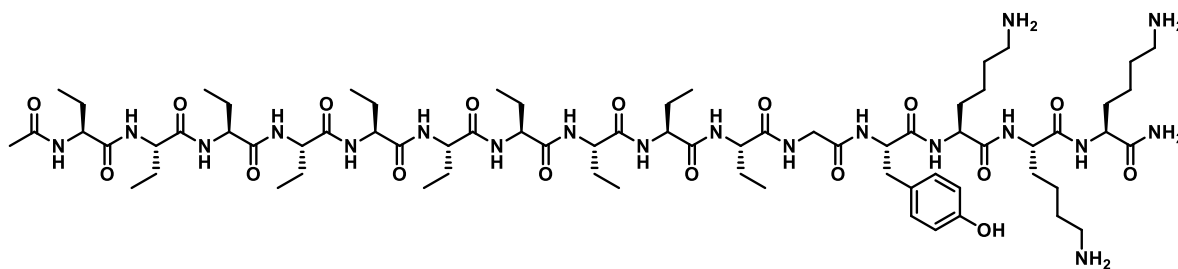
Analytical HPLC was carried out on a LaChrom ELITE®-HPLC-System from VWR-Hitachi (VWR International GmbH, Darmstadt, Germany). The system contains an organizer, two HPLC pumps (L-2130) with solvent degaser, an autosampler (L-2200) with a 100 µL sample loop, a diode array flow detector (L-2455), and a high-pressure gradient mixer. A Kinetex® C18 column (5 µm, 100 Å, 250 × 4.6 mm, Phenomenex®, Torrance, CA, USA) was used. A SecurityGuard™ Cartridge Kit (Ea, Phenomenex®, Torrance, CA, USA) holding a C8 or C18 SecurityGuard™ cartridge (4 × 3.0 mm, Phenomenex®, Torrance, CA, USA), respectively, served as pre-column. A flow rate of 1.0 mL/min was applied with deionized water and ACN, both containing 0.1% (v/v) TFA, as eluents. The used gradient methods are shown in Table 7.4, and the UV-detection occurred at 220 or 280 nm. Data analysis was performed with EZChrom *Elite* software (version 3.3.2, Agilent Technologies, Santa Clara, CA, USA).

## 2.4 Peptide synthesis: HPLC chromatograms and HRMS spectra

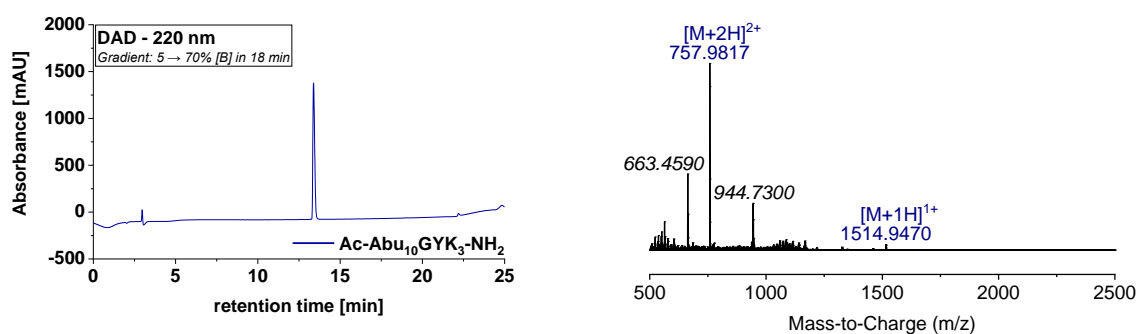
**Table S3:** Overview of fluoro-peptides studied in this work.

Peptide sequence	X	Compound number
<b>X<sub>10</sub></b> GY(K) <sub>3</sub>	Abu	<b>2a</b>
	MfeGly	<b>2b</b>
	DfeGly	<b>2c</b>
	TfeGly	<b>2d</b>
<b>X<sub>13</sub></b> GY(K) <sub>4</sub>	Abu	<b>3a</b>
	MfeGly	<b>3b</b>
	DfeGly	<b>3c</b>
	TfeGly	<b>3d</b>
<b>X<sub>15</sub></b> GY(K) <sub>4</sub>	Abu	<b>4a</b>
	MfeGly	<b>4b</b>
	DfeGly	<b>4c</b>
<b>X<sub>4</sub></b> [4]Abz	Abu	<b>5a</b>
	MfeGly	<b>5b</b>
	DfeGly	<b>5c</b>
	TfeGly	<b>5d</b>

### 2.4.1 Abu<sub>10</sub>GY(K)<sub>3</sub> 2a



**Figure S3:** Chemical structure of Abu<sub>10</sub>GY(K)<sub>3</sub>.

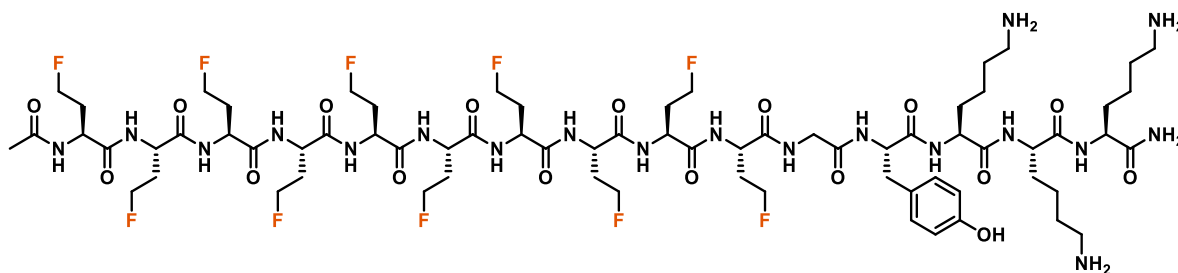


**Figure S4:** HPC chromatogram (left) and HRMS spectrum (right) of purified peptide Abu<sub>10</sub>GY(K)<sub>3</sub>.

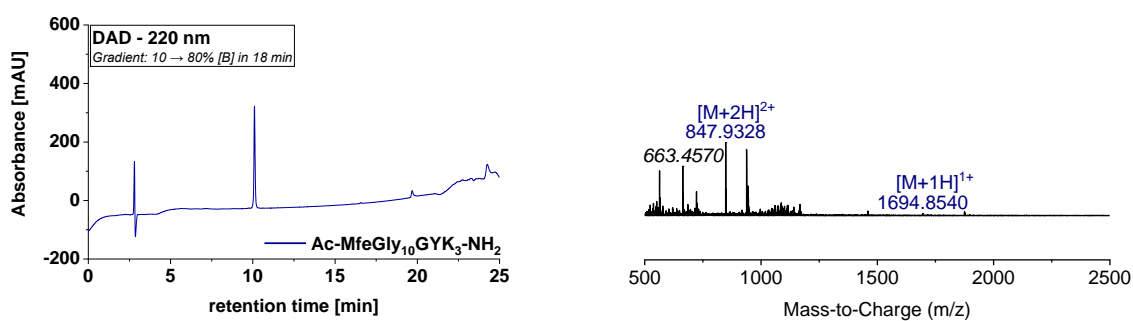
**Table S4:** Ion species (positive mode) calculated and observed for peptide Abu<sub>10</sub>GY(K)<sub>3</sub>.

Ion species	Mass (calc.)	Mass (obs.)
[M+H] <sup>+</sup>	1514.9422	1514.7700
[M+2H] <sup>2+</sup>	757.9750	757.9817

## 2.4.2 MfeGly<sub>10</sub>GY(K)<sub>3</sub> 2b



**Figure S5:** Chemical structure of MfeGly<sub>10</sub>GY(K)<sub>3</sub>.

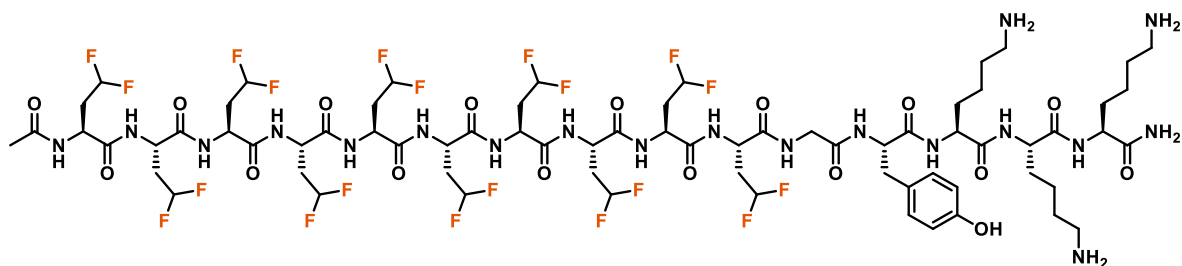


**Figure S6:** HPC chromatogram (left) and HRMS spectrum (right) of purified peptide MfeGly<sub>10</sub>GY(K)<sub>3</sub>.

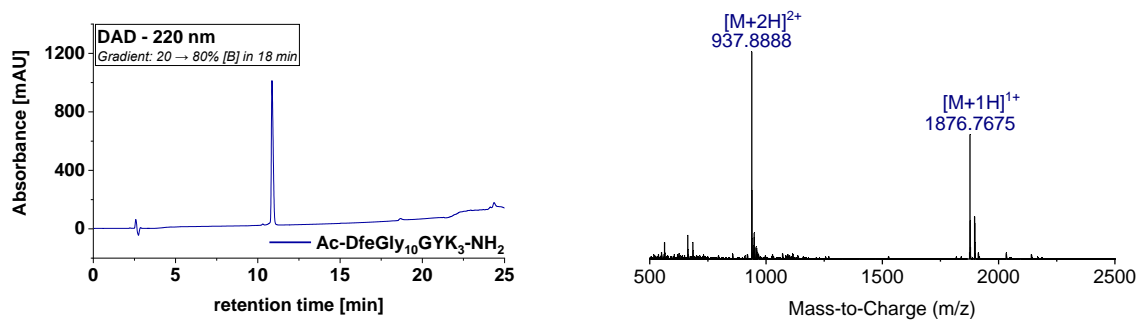
**Table S5:** Ion species (positive mode) calculated and observed for peptide MfeGly<sub>10</sub>GY(K)<sub>3</sub>.

Ion species	Mass (calc.)	Mass (obs.)
[M+H] <sup>+</sup>	1694.8480	1694.8540
[M+2H] <sup>2+</sup>	847.9279	847.9328

### 2.4.3 DfeGly<sub>10</sub>GY(K)<sub>3</sub> 2c



**Figure S7:** Chemical structure of DfeGly<sub>10</sub>GY(K)<sub>3</sub>.



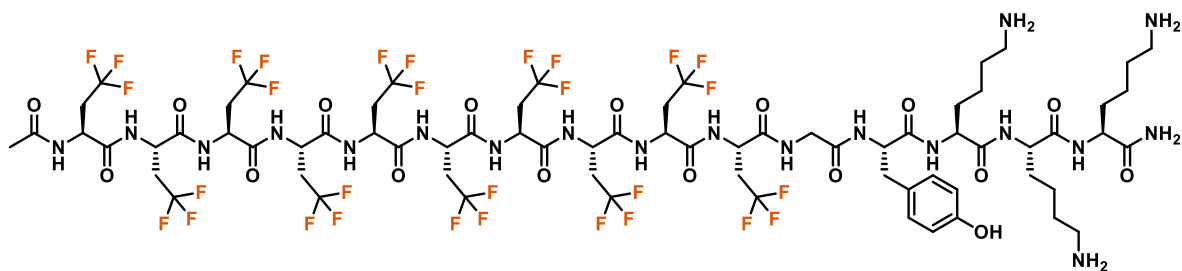
**Figure S8:** HPC chromatogram (left) and HRMS spectrum (right) of purified peptide DfeGly<sub>10</sub>GY(K)<sub>3</sub>.

**Table S6:** Ion species (positive mode) calculated and observed for peptide DfeGly<sub>10</sub>GY(K)<sub>3</sub>.

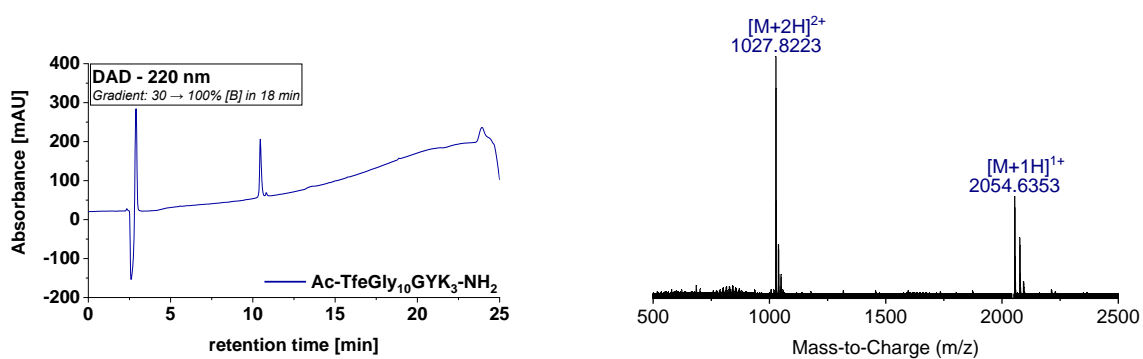
Ion species	Mass (calc.)	Mass (obs.)
[M+H] <sup>+</sup>	1874.7538	1874.7675
[M+2H] <sup>2+</sup>	937.8808	937.8888



## 2.4.4 TfeGly<sub>10</sub>GY(K)<sub>3</sub> 2d



**Figure S9:** Chemical structure of TfeGly<sub>10</sub>GY(K)<sub>3</sub>.

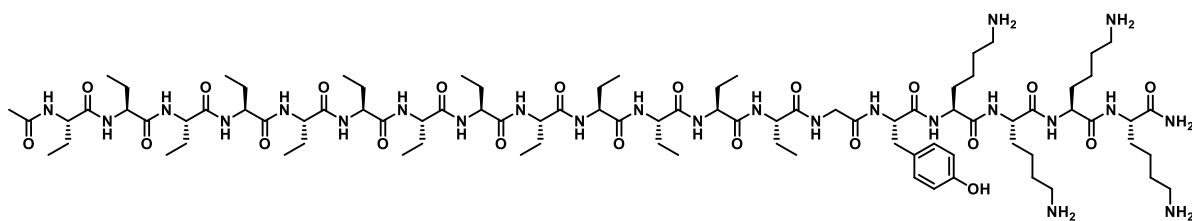


**Figure S10:** HPC chromatogram (left) and HRMS spectrum (right) of purified peptide TfeGly<sub>10</sub>GY(K)<sub>3</sub>.

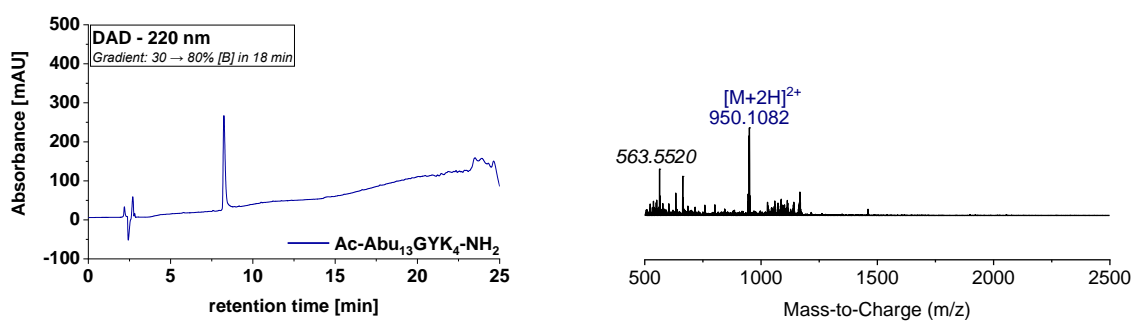
**Table S7:** Ion species (positive mode) calculated and observed for peptide TfeGly<sub>10</sub>GY(K)<sub>3</sub>.

Ion species	Mass (calc.)	Mass (obs.)
[M+H] <sup>+</sup>	2054.6596	2054.6353
[M+2H] <sup>2+</sup>	1027.8337	1027.8223

## 2.4.5 Abu<sub>13</sub>GY(K)<sub>4</sub> 3a



**Figure S11:** Chemical structure of Abu<sub>13</sub>GY(K)<sub>4</sub>.

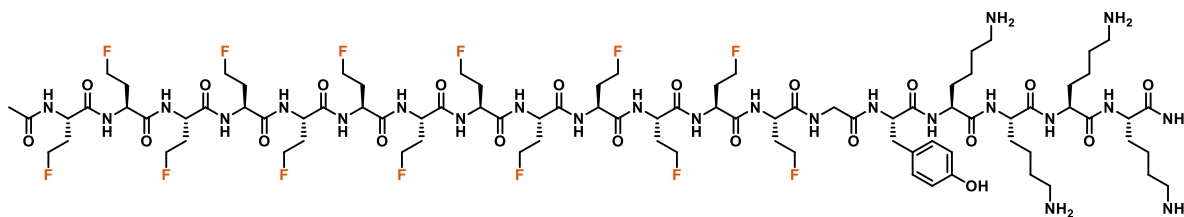


**Figure S12:** HPC chromatogram (left) and HRMS spectrum (right) of purified peptide Abu<sub>13</sub>GY(K)<sub>4</sub>.

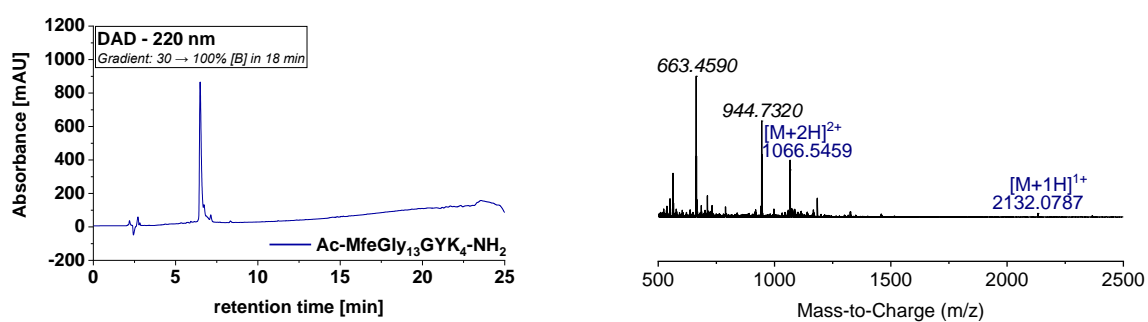
**Table S8:** Ion species (positive mode) calculated and observed for peptide Abu<sub>13</sub>GY(K)<sub>4</sub>.

Ion species	Mass (calc.)	Mass (obs.)
[M+H] <sup>+</sup>	1898.1876	-
[M+2H] <sup>2+</sup>	950.0977	950.1082

## 2.4.6 MfeGly<sub>13</sub>GY(K)<sub>4</sub> 3b



**Figure S13:** Chemical structure of MfeGly<sub>13</sub>GY(K)<sub>4</sub>.

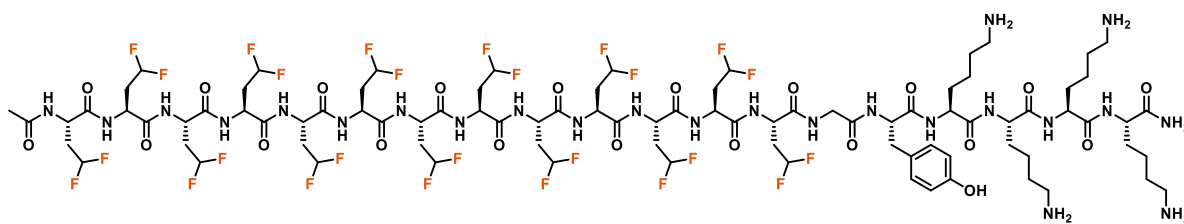


**Figure S14:** HPC chromatogram (left) and HRMS spectrum (right) of purified peptide MfeGly<sub>13</sub>GY(K)<sub>4</sub>.

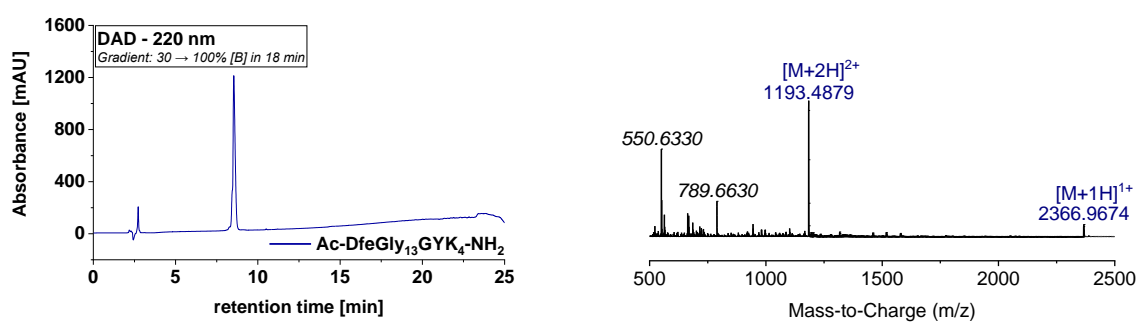
**Table S9:** Ion species (positive mode) calculated and observed for peptide MfeGly<sub>13</sub>GY(K)<sub>4</sub>.

Ion species	Mass (calc.)	Mass (obs.)
[M+H] <sup>+</sup>	2132.0652	2132.0787
[M+2H] <sup>2+</sup>	1067.5404	1067.5459

### 2.4.7. DfeGly<sub>13</sub>GY(K)<sub>4</sub> 3c



**Figure S15:** Chemical structure of DfeGly<sub>13</sub>GY(K)<sub>4</sub>.

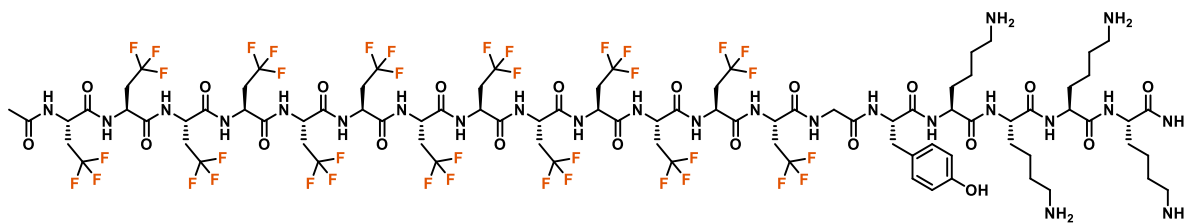


**Figure S16:** HPC chromatogram (left) and HRMS spectrum (right) of purified peptide DfeGly<sub>13</sub>GY(K)<sub>4</sub>.

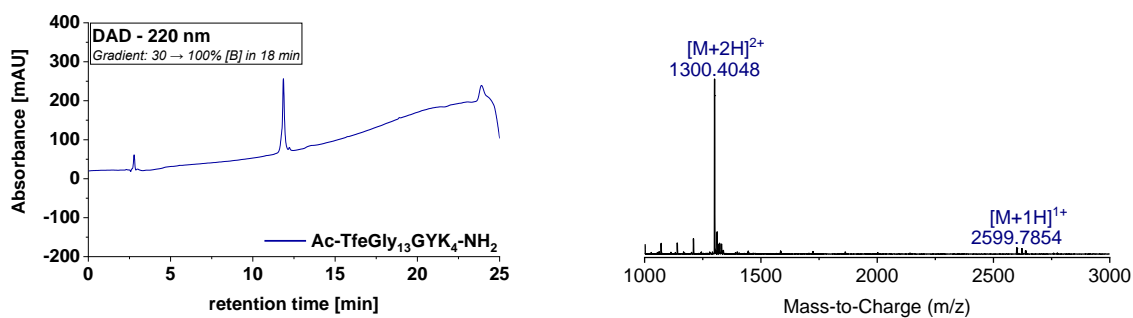
**Table S10:** Ion species (positive mode) calculated and observed for peptide DfeGly<sub>13</sub>GY(K)<sub>4</sub>.

Ion species	Mass (calc.)	Mass (obs.)
[M+H] <sup>+</sup>	2365.9505	2365.9674
[M+2H] <sup>2+</sup>	1183.4791	1183.4879

## 2.4.8 TfeGly<sub>13</sub>GY(K)<sub>4</sub> 3d



**Figure S17:** Chemical structure of TfeGly<sub>13</sub>GY(K)<sub>4</sub>.

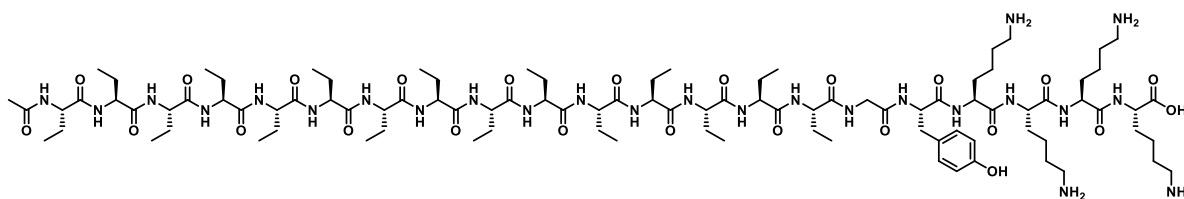


**Figure S18:** HPC chromatogram (left) and HRMS spectrum (right) of purified peptide TfeGly<sub>13</sub>GY(K)<sub>4</sub>.

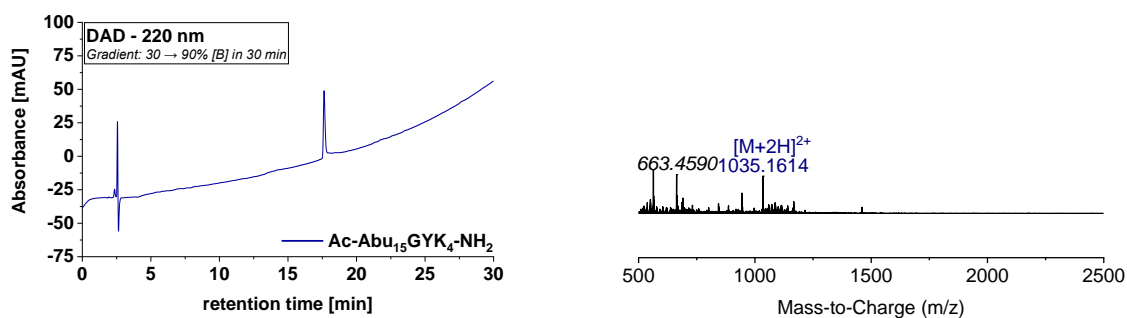
**Table S11:** Ion species (positive mode) calculated and observed for peptide TfeGly<sub>13</sub>GY(K)<sub>4</sub>.

Ion species	Mass (calc.)	Mass (obs.)
[M+H] <sup>+</sup>	2599.8280	2599.7854
[M+2H] <sup>2+</sup>	1300.4179	1300.4048

## 2.4.9 Abu<sub>15</sub>GY(K)<sub>4</sub> 4a



**Figure S19:** Chemical structure of Abu<sub>15</sub>GY(K)<sub>4</sub>.

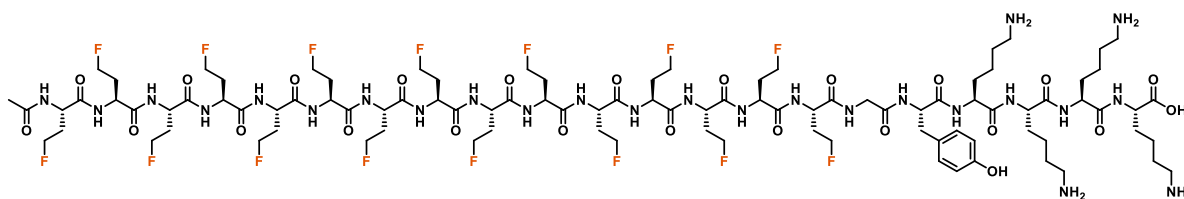


**Figure S20:** HPC chromatogram (left) and HRMS spectrum (right) of purified peptide Abu<sub>15</sub>GY(K)<sub>4</sub>.

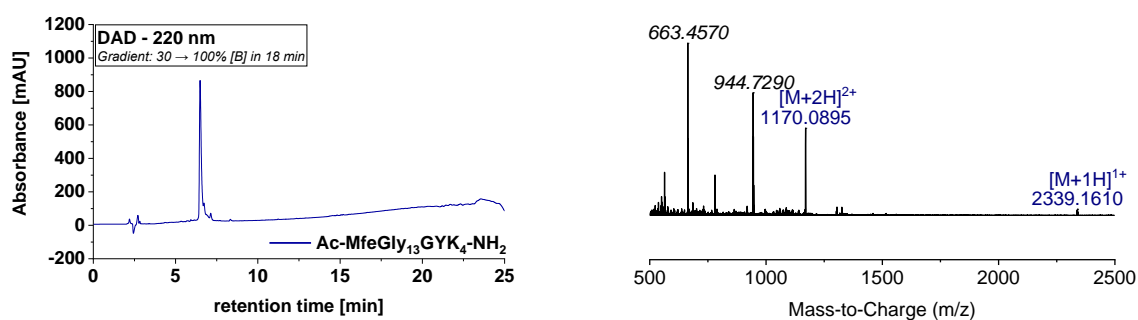
**Table S12:** Ion species (positive mode) calculated and observed for peptide Abu<sub>15</sub>GY(K)<sub>4</sub>.

Ion species	Mass (calc.)	Mass (obs.)
(M+H) <sup>+</sup>	2069.2850	-
(M+2H) <sup>2+</sup>	1.035.1464	1035.1614

## 2.4.10 MfeGly<sub>15</sub>GY(K)<sub>4</sub> 4b



**Figure S21:** Chemical structure of MfeGly<sub>15</sub>GY(K)<sub>4</sub>.

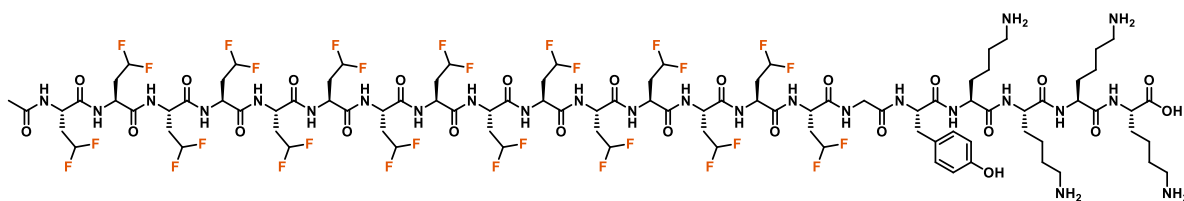


**Figure S22:** HPC chromatogram (left) and HRMS spectrum (right) of purified peptide MfeGly<sub>15</sub>GY(K)<sub>4</sub>.

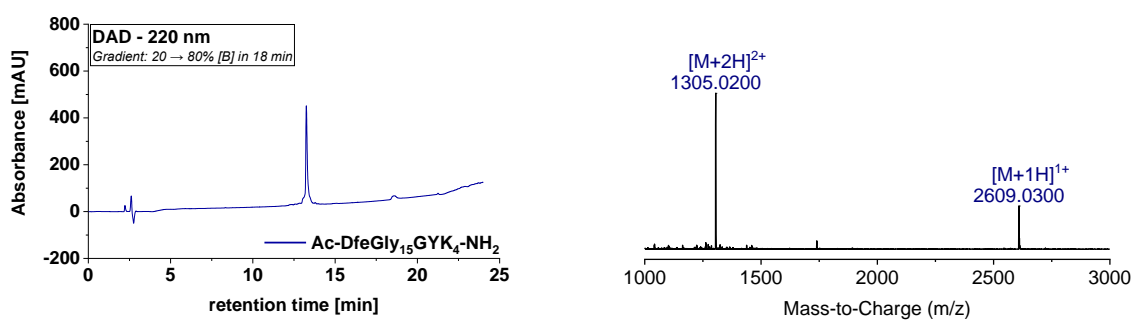
**Table S13:** Ion species (positive mode) calculated and observed for peptide MfeGly<sub>15</sub>GY(K)<sub>4</sub>.

Ion species	Mass (calc.)	Mass (obs.)
(M+H) <sup>+</sup>	2339.1437	2339.1610
(M+2H) <sup>2+</sup>	1170.0757	1170.0895

### 2.4.11 DfeGly<sub>15</sub>GY(K)<sub>4</sub> 4c



**Figure S23:** Chemical structure of DfeGly<sub>15</sub>GY(K)<sub>4</sub>.



**Figure S24:** HPC chromatogram (left) and HRMS spectrum (right) of purified peptide DfeGly<sub>15</sub>GY(K)<sub>4</sub>.

**Table S14:** Ion species (positive mode) calculated and observed for peptide MfeGly<sub>15</sub>GY(K)<sub>4</sub>.

Ion species	Mass (calc.)	Mass (obs.)
(M+H) <sup>+</sup>	2609.0024	2609.0300
(M+2H) <sup>2+</sup>	1305.0051	1205.0200



## 2.4.12 Abu<sub>4</sub>[4]Abz 5a

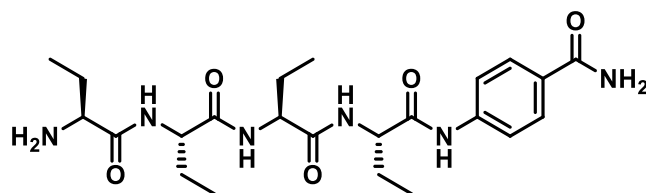


Figure S25: Chemical structure of [Abu]<sub>4</sub>-[4]Abz.

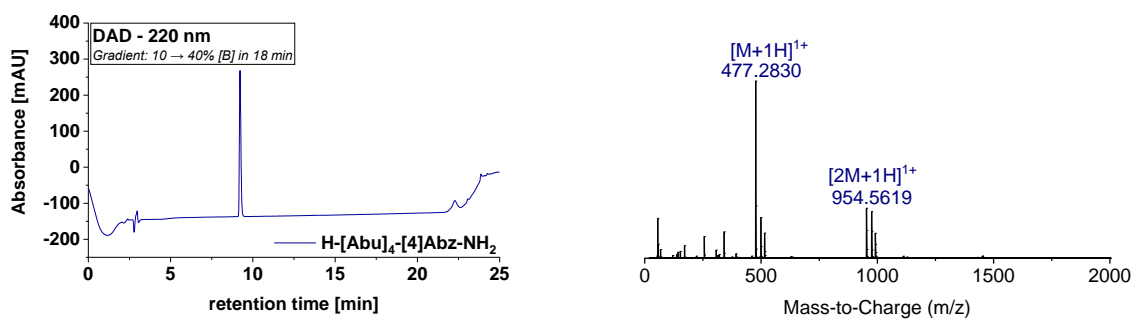
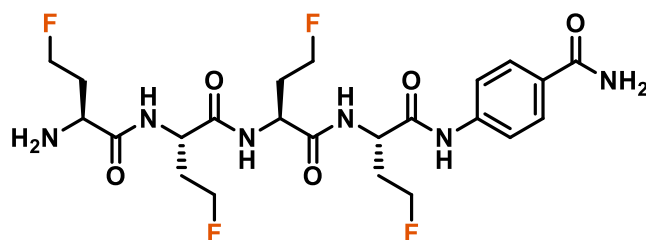


Figure S26: HPC chromatogram (left) and HRMS spectrum (right) of purified peptide [Abu]<sub>4</sub>-[4]Abz.

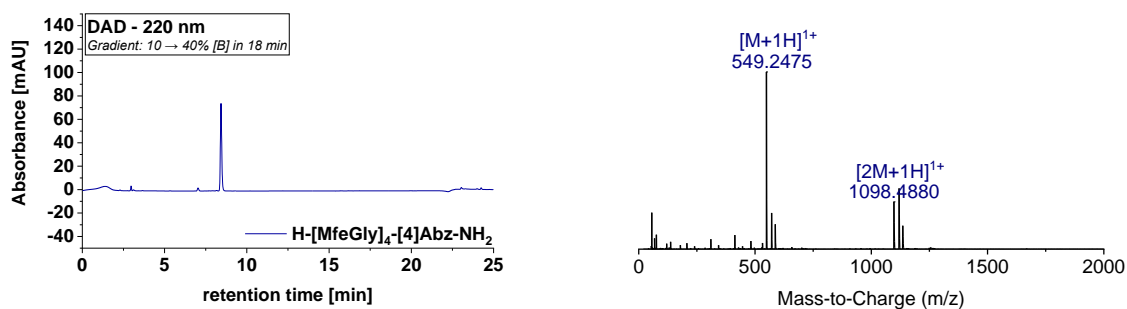
Table S15: Ion species (positive mode) calculated and observed for peptide [Abu]<sub>4</sub>-[4]Abz.

Ion species	Mass (calc.)	Mass (obs.)
(M+H) <sup>+</sup>	477.2825	477.2830
(2M+H) <sup>+</sup>	954.5650	954.5619

### 2.4.13 MfeGly<sub>4</sub>[4]Abz 5b



**Figure S27:** Chemical structure of [MfeGly]<sub>4</sub>-[4]Abz.

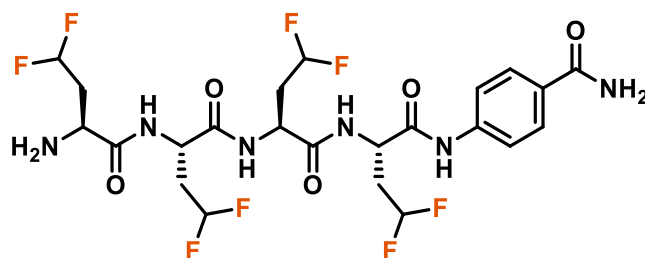


**Figure S28:** HPC chromatogram (left) and HRMS spectrum (right) of purified peptide [MfeGly]<sub>4</sub>-[4]Abz.

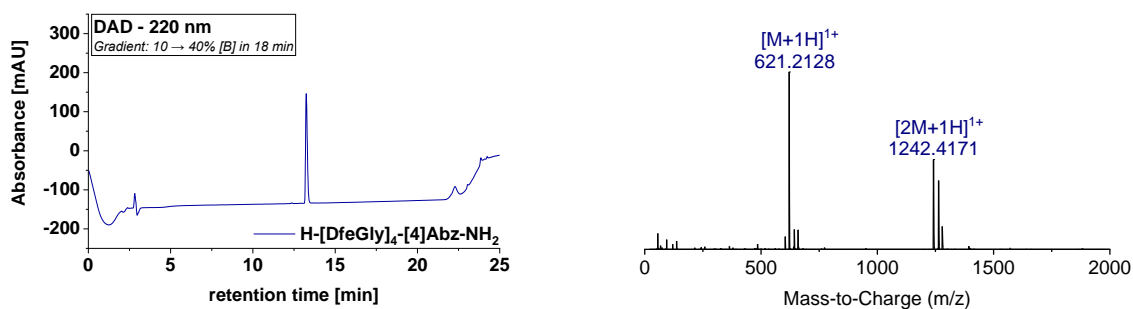
**Table S16:** Ion species (positive mode) calculated and observed for peptide [MfeGly]<sub>4</sub>-[4]Abz.

Ion species	Mass (calc.)	Mass (obs.)
(M+H) <sup>+</sup>	548.2448	549.2475
(M+2H) <sup>2+</sup>	1098.4896	1098.4880

### 2.4.14 DfeGly<sub>4</sub>[4]Abz 5c



**Figure S29:** Chemical structure of [DfeGly]<sub>4</sub>-[4]Abz.

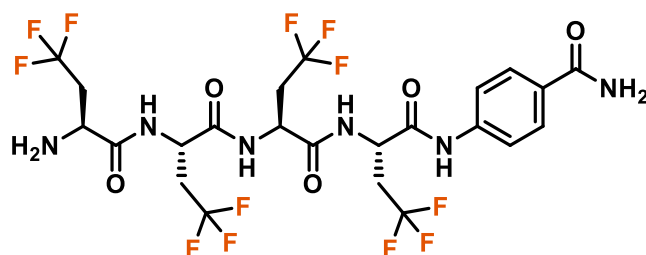


**Figure S30:** HPC chromatogram (left) and HRMS spectrum (right) of purified peptide [DfeGly]<sub>4</sub>-[4]Abz.

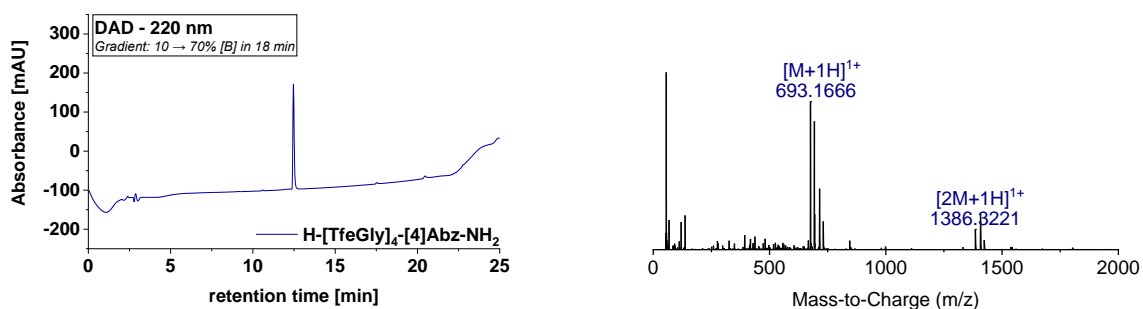
**Table S17:** Ion species (positive mode) calculated and observed for peptide [DfeGly]<sub>4</sub>-[4]Abz.

Ion species	Mass (calc.)	Mass (obs.)
(M+H) <sup>+</sup>	621.2071	621.2128
(M+2H) <sup>2+</sup>	1242.4142	1242.4171

## 2.4.15 TfeGly<sub>4</sub>[4]Abz 5d



**Figure S31:** Chemical structure of [TfeGly]<sub>4</sub>-[4]Abz.



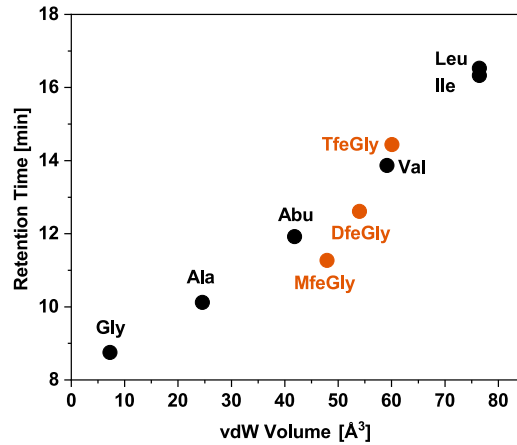
**Figure S32:** HPC chromatogram (left) and HRMS spectrum (right) of purified peptide [TfeGly]<sub>4</sub>-[4]Abz.

**Table S18:** Ion species (positive mode) calculated and observed for peptide [TfeGly]<sub>4</sub>-[4]Abz.

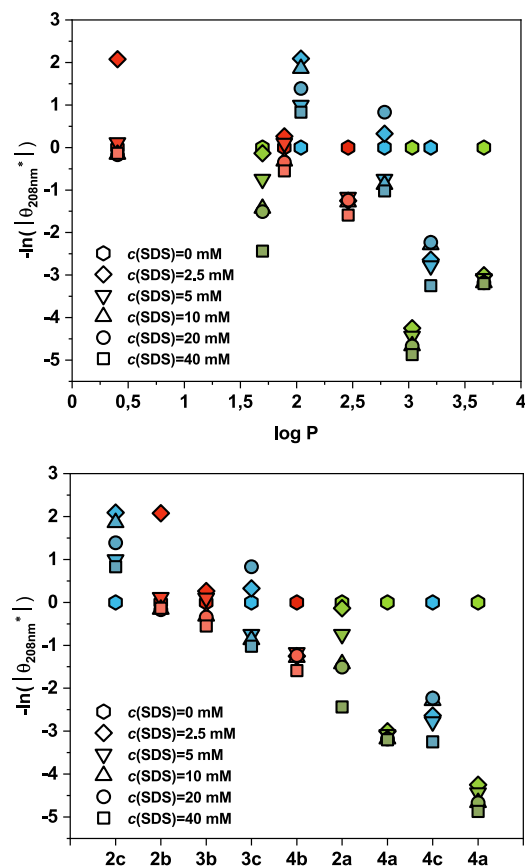
Ion species	Mass (calc.)	Mass (obs.)
(M+H) <sup>+</sup>	693.1694	693.1694
(M+2H) <sup>2+</sup>	1386.3388	1386.3221

### 3. Circular Dichroism and SEIRAS Infrared Spectroscopy – further data

#### 3.1 Fundamentals: Hydrophobicity Studies



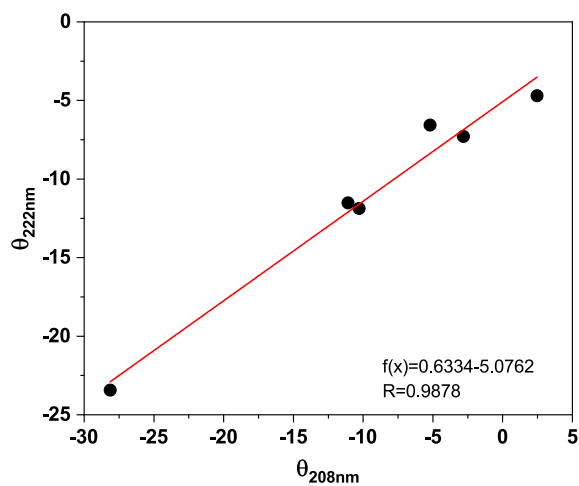
**Figure S33:** Retention times of amino acids plotted against the vdW volume of the side chains.



**Figure S34:** Normalized molar ellipticity ( $\theta_{208nm}^*$ ) plotted against the corresponding  $\log P$  values (**top**) or ordered by increasing intensity (**bottom**). ( $\theta_{208nm}^*$ ) =  $\theta_{208nm}$ (at specific SDS concentration) /  $\theta_{208nm}$ (at SDS concentration of 0 mM).

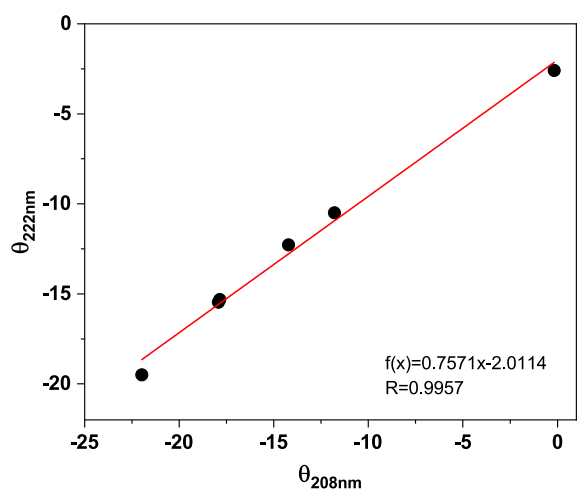
## 3.2 Parametric dual wavelength two-state test

### 3.1.1 Abu<sub>10</sub>GY(K)<sub>3</sub> 2a



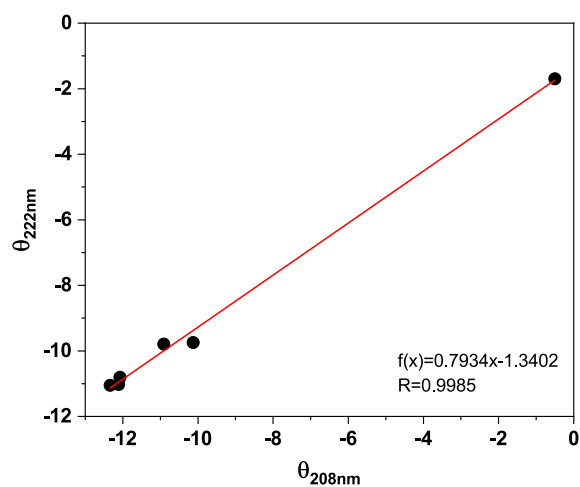
**Figure S35:** Dual wavelengths plot of  $\theta_{208}$  vs  $\theta_{222}$  for **2a** over the SDS concentrations of 0, 2.5, 5, 10, 20, 40 mM.

### 3.1.2 Abu<sub>13</sub>GY(K)<sub>4</sub> 3a



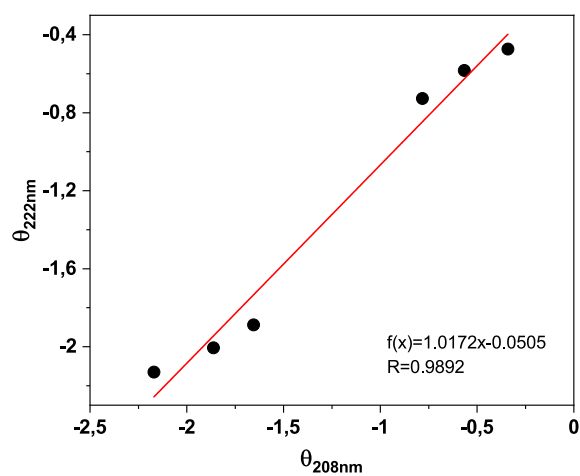
**Figure S36:** Dual wavelengths plot of  $\theta_{208}$  vs  $\theta_{222}$  for **3a** over the SDS concentrations of 0, 2.5, 5, 10, 20, 40 mM.

### 3.1.3 Abu<sub>15</sub>GY(K)<sub>4</sub> 4a



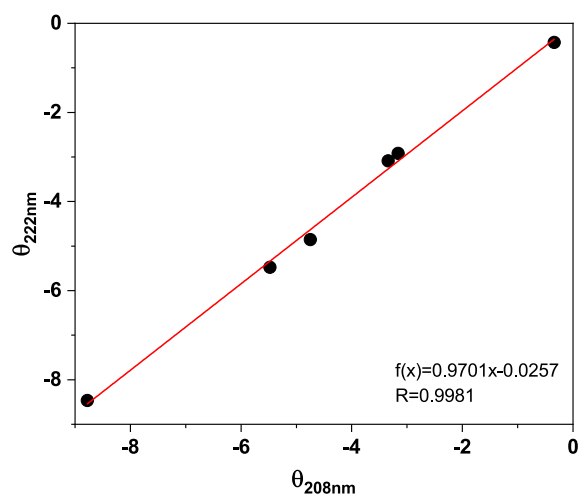
**Figure S37:** Dual wavelengths plot of  $\theta_{208}$  vs  $\theta_{222}$  for **4a** over the SDS concentrations of 0, 2.5, 5, 10, 20, 40 mM.

### 3.1.4 DfeGly<sub>13</sub>GY(K)<sub>4</sub> 3c



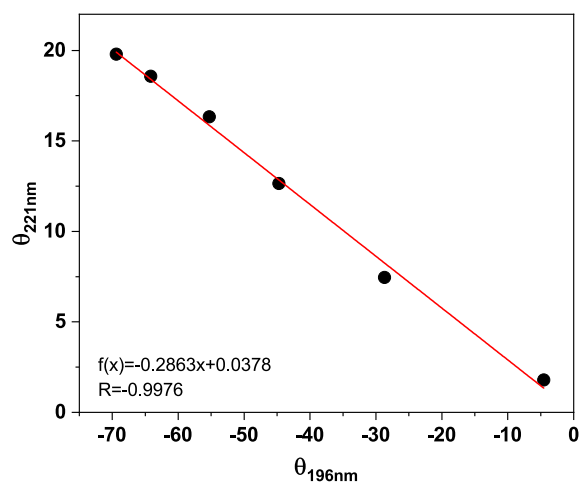
**Figure S38:** Dual wavelengths plot of  $\theta_{208}$  vs  $\theta_{222}$  for **3c** over the SDS concentrations of 0, 2.5, 5, 10, 20, 40 mM.

### 3.1.5 DfeGly<sub>15</sub>GY(K)<sub>4</sub> 4c



**Figure S39:** Dual wavelengths plot of  $\theta_{208}$  vs  $\theta_{222}$  for **4c** over the SDS concentrations of 0, 2.5, 5, 10, 20, 40 mM.

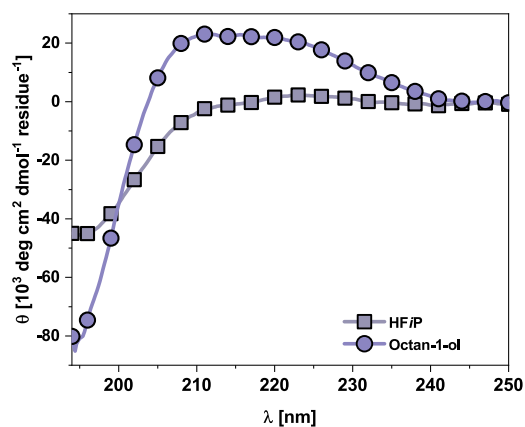
### 3.1.6 TfeGly<sub>13</sub>GY(K)<sub>4</sub> 3d



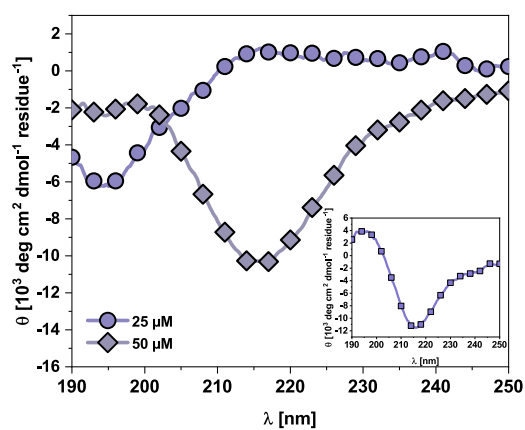
**Figure S40:** Dual wavelengths plot of  $\theta_{196}$  vs  $\theta_{221}$  for **3d** over the SDS concentrations of 0, 2.5, 5, 10, 20, 40 mM.



### 3.3 TfeGly<sub>10</sub>GY(K)<sub>3</sub> 2d

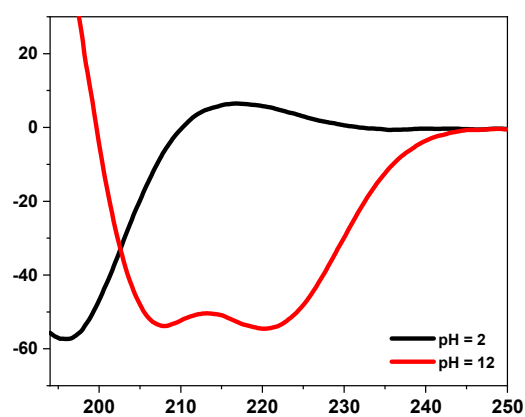


**Figure S41:** CD spectrum of **2d** (25 μM) in HFIP and octan-1-ol.



**Figure S42:** CD spectrum of **2d** at different concentrations (25 μM/50 μM) phosphate buffer (10 mM, pH = 7.4). Inlet shows the corresponding difference spectrum

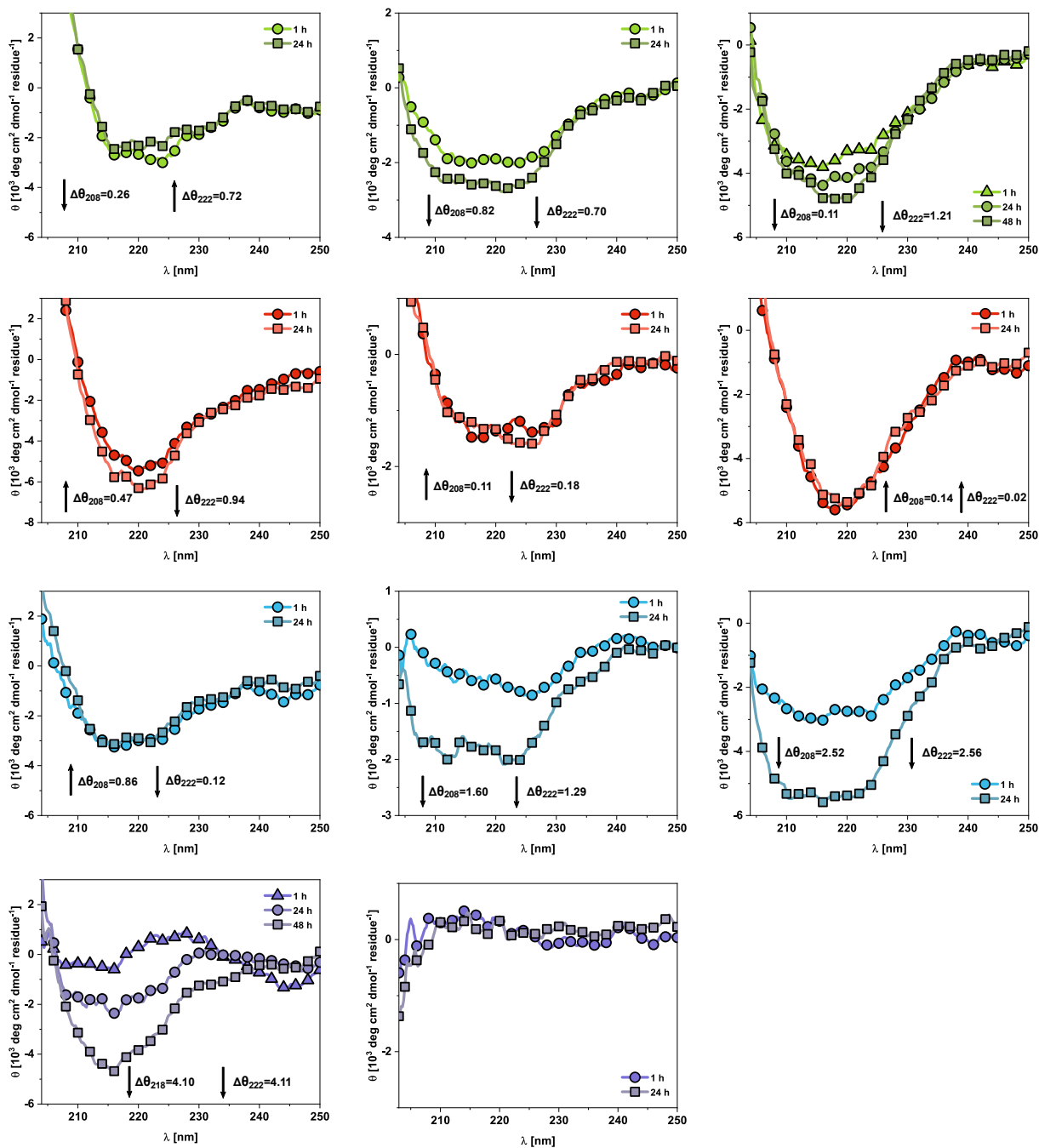
### 3.4 Poly(L-lysine)



**Figure S43:** CD spectrum of poly(L-lysine) at different pH values (pH = 2/12).

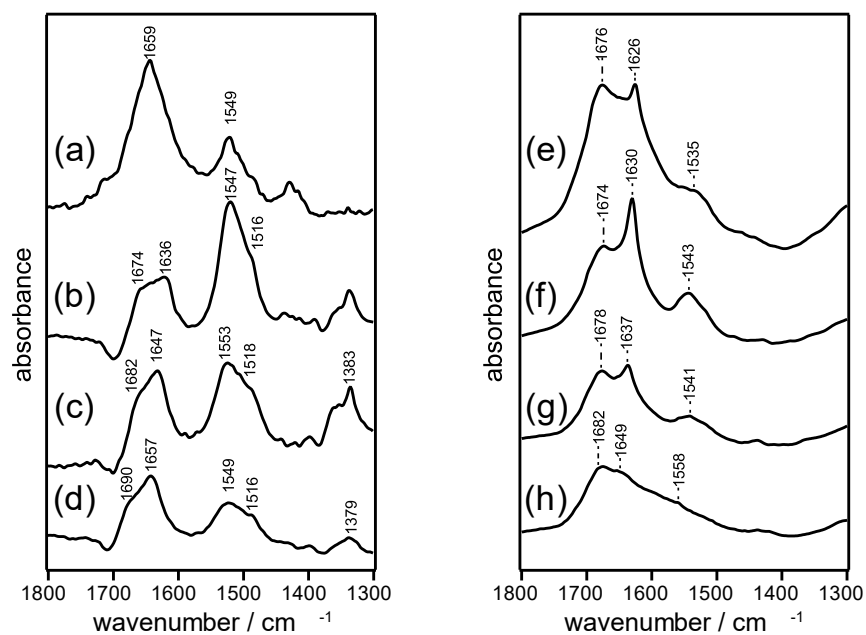
For a period of time, it was assumed that this structure could only be formed by this type of peptides. However, this changed when Tiffany and Krimm published a work showing that poly(L-lysine) and poly(L-glutamic acid) peptides can also adopt a PPII conformation (minimum at 198 nm; maximum at 218 nm).<sup>[4]</sup> The observed blue shift compared to the poly(L proline) peptides can be explained by the difference between secondary and tertiary amides.<sup>[5]</sup> This assumption was questioned by Mattice who showed that short dipeptides can also produce similar CD spectra.<sup>[6]</sup> Since at that time it was considered unlikely that such short peptides could adopt a distinct conformation, these results were used to refute the statement made by Tiffany and Krimm. As it was assumed that a minimum at 195 nm is characteristic of a random coil, a claim still made to this day, the structures of poly(L-lysine) and poly(L-glutamic acid) were described as unordered. Yet, there is now a substantial amount of work supporting Tiffany and Krimm's hypothesis. Thus, the working groups of Schweitzer-Stenner<sup>[7]</sup>, Kallenbach<sup>[8]</sup>, and others<sup>[9]</sup> showed that even short model peptides are capable to adopt a PPII conformation. Meanwhile, it can even be assumed that in the unfolded state proteins, certain stretches are not present as random coils, but in fact in an extended PPII conformation.<sup>[10]</sup> The CD spectrum of TfeGly<sub>13</sub>GY(K)<sub>4</sub> **3d** is in a great agreement with the literature spectra of poly(L-lysine), poly(L-glutamic acid), and other PPII helix forming peptides.

### 3.5 Time-dependent measurements in the presence of POPC/POPG



**Figure S44:** CD spectra of (from left to right) Abu<sub>10</sub>GY(K)<sub>3</sub> **2a**, Abu<sub>13</sub>GY(K)<sub>4</sub> **3a**, and Abu<sub>15</sub>GY(K)<sub>4</sub> **4a** (first row), MfeGly<sub>10</sub>GY(K)<sub>3</sub> **2b**, MfeGly<sub>13</sub>GY(K)<sub>4</sub> **3b**, and MfeGly<sub>15</sub>GY(K)<sub>4</sub> **4b** (Second row), DfeGly<sub>10</sub>GY(K)<sub>3</sub> **2c**, DfeGly<sub>13</sub>GY(K)<sub>4</sub> **3c**, and DfeGly<sub>15</sub>GY(K)<sub>4</sub> **4c** (third row), TfeGly<sub>10</sub>GY(K)<sub>3</sub> **2d** and TfeGly<sub>13</sub>GY(K)<sub>4</sub> **3d** (fourth row) in phosphate buffer (10 mM, pH = 7.4) in the presence of POPC/POPG = 1:1 after 1 h and 24 h (peptide concentration: 50  $\mu$ M).

### 3.6 Additional SEIRAS Spectra

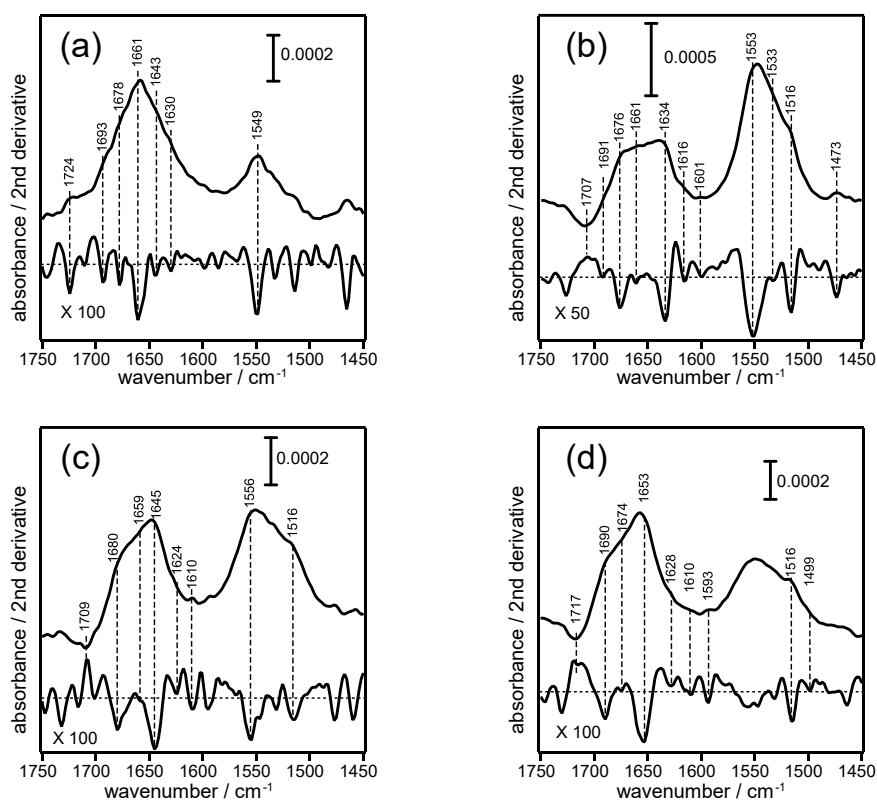


**Figure S45:** SEIRA spectra of the peptides adsorbed on the lipid (a) Abu<sub>13</sub>GY(K)<sub>4</sub> **3a**, (b) MfeGly<sub>13</sub>GY(K)<sub>4</sub> **3b**, (c) DfeGly<sub>13</sub>GY(K)<sub>4</sub> **3c**, (d) TfeGly<sub>13</sub>GY(K)<sub>4</sub> **3d** and ATR-IR spectra of the peptides without lipid (e) Abu<sub>13</sub>GY(K)<sub>4</sub> **3a**, (f) MfeGly<sub>13</sub>GY(K)<sub>4</sub> **3b**, (g) DfeGly<sub>13</sub>GY(K)<sub>4</sub> **3c**, (h) TfeGly<sub>13</sub>GY(K)<sub>4</sub> **3d**.

As a control for the spectra of the peptides adsorbed on the lipid bilayer, IR spectra of corresponding peptides in the absence of the lipid bilayer are shown in **Figure S45e-h**. Spectra of the samples were taken at standard ATR conditions by evaporating the water solvent. Amide I bands of each peptide show characteristic double peaks at 1672-1680 cm<sup>-1</sup> and at 1630-1649 cm<sup>-1</sup>. The lower band around 1620-1640 cm<sup>-1</sup> is particularly a marker band for the degree of intra- or intermolecular hydrogen bond interactions of the corresponding peptide backbones. A lower peak position of this band indicates stronger hydrogen bond interactions in the aggregate. With the increasing degree of fluorination, the corresponding band shifts to higher wavenumbers indicating weaker hydrogen bond interactions for high fluorinated peptides. Especially the spectra of DfeGly<sub>13</sub>GY(K)<sub>4</sub> **3c** and TfeGly<sub>13</sub>GY(K)<sub>4</sub> **3d** show an up-shifted band at 1637 and 1649 cm<sup>-1</sup>, respectively. These peak positions are no longer assigned to a typical aggregate but rather close to a plain random structure of the peptides. These results suggest that the fluorination of the Abu<sub>13</sub>GY(K)<sub>4</sub> **3a** side chain suppress the hydrogen bond interactions of the peptide backbones and prevent the formation of aggregated structures. Interestingly, these data draw a similar picture as already seen in the structural studies of trifluorinated oligomers. Similar to PPII formation, the CF<sub>3</sub> groups appear to be spaced farther apart, inhibiting aggregation processes.

The frequency range between 1700-1600  $\text{cm}^{-1}$  represents vibrational bands of the amide C=O stretching modes of the polypeptide. A broad feature of this band is a result of overlapping of different secondary structure components rise from different degree of hydrogen bonding strength among the amides.

To identify the contributions of individual secondary structure elements, a peak fitting had been carried out over the amide I band. Fitting was restricted to following five different secondary component in order to avoid overestimation of the fine structures, namely: **(1)  $\beta$ -turn/bend structures** appearing in the range between 1670 and 1685  $\text{cm}^{-1}$  indicative of weak hydrogen bonding due to disruption of intra/inter-hydrogen bond network among the peptide backbone (shown as blue), **(2) random structure** appearing between 1670-1660  $\text{cm}^{-1}$  indicative of weak hydrogen bonding among the peptide backbone (shown as yellow), **(3)  $\alpha$ -helical structures** appearing between 1645 and 1660  $\text{cm}^{-1}$  (shown as red), **(4) unordered and strongly hydrogen-bonded amide structures** appearing between 1635 and 1645  $\text{cm}^{-1}$  (shown as dark gray), **(5)  $\beta$ -aggregates/sheets** appearing 1610 and 1635  $\text{cm}^{-1}$  indicative of a formation of strong hydrogen bonds.<sup>[11]</sup>



**Figure S46.** SEIRA spectra (**top**) and the second derivative (**bottom**) spectra of **(a)** Abu<sub>13</sub>GY(K)<sub>4</sub> **3a**, **(b)** MfeGly<sub>13</sub>GY(K)<sub>4</sub> **3b**, **(c)** DfeGly<sub>13</sub>GY(K)<sub>4</sub> **3c**, and **(d)** TfeGly<sub>13</sub>GY(K)<sub>4</sub> **3d**.

It should be noted that distinction between  $\beta$ -aggregate and  $\beta$ -sheet is difficult to make by IR spectrum because they appear in same spectral range. Therefore, we included the contribution from  $\beta$ -sheet structures as part of the components under **(1)** and **(5)**.

As first step, we exploited the second derivative method to estimate initial peak position of each component. **Figure S46** shows the result of the second derivative of each polypeptide. In the second derivative spectra, inflexion points in the amide I band are observed as negative peaks. We employed these negative peaks as the starting peak positions for the estimation of each component.

After setting the initial peak position, we proceed to the peak fitting of the observed amide I band to elucidate contribution of each component. During this estimation process, we applied following constraints:

- 1)** The peak position of each component can change within the range of  $\pm 2 \text{ cm}^{-1}$  during the fitting. The range of the position shift was defined by the spectral resolution of obtained spectra ( $4 \text{ cm}^{-1}$ )
- 2)** The numbers of peaks are fixed to five components.
- 3)** The peak width of each component does not exceed more than  $20 \text{ cm}^{-1}$  to avoid overly broad peak shapes overlapping with the baseline.
- 4)** All peaks are Gaussian.

Results of the fittings are shown in **Figure 4d** in main text.

## 4. Estimation of log P values by HPLC

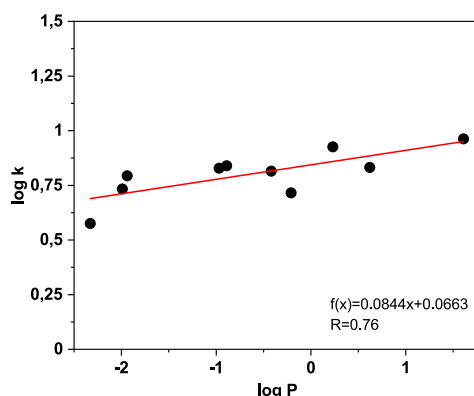
The log P values were estimated using a HPLC-based assay that was adapted from the O'Hagan group, which used this method to determine the lipophilicity of small fluorinated organic compounds.<sup>[12]</sup> We transferred this method to the field of peptide chemistry.

To estimate the hydrophobicity of fluorinated peptides **2-4**, a library of short peptides with known log P values was synthesized.<sup>[13]</sup> To ensure that the influence of both chain length and charges was considered, peptides of different lengths (tri-, tetra- and pentamers), with an amide or carboxylic acid functionalities at the C-terminus and blocked or unblocked N-terminal ends were synthesized. Subsequently, the retention times of these peptides were determined in triplicates using a reversed-phase C18 column. A gradient consisting of acetonitrile and water both with 0.1% TFA was used (MeCN:H<sub>2</sub>O (0.1% TFA) = 5:95 to 70:30, flow rate 1.0 mL/min). The peptides were injected at a concentration of 0.1 mM. The correlation between the retention time and the log P values was fitted using a linear function. The latter was then used to calculate the corresponding unknown log P values from the measured retention times. **Table S18** summarizes the peptide library and shows the determined retention times of the short peptides.

**Table S19:** Determined log k values for the reference peptides. Capacity factor  $k=(R_t - [\text{dead time of the column}]) / [\text{dead time of the column}]$ . Dead time of the column is the time period required for a solvent to pass through a column.

Entry	Peptides	log P <sup>4</sup>	R <sub>t1</sub> [min]	R <sub>t2</sub> [min]	R <sub>t3</sub> [min]	Average R <sub>t</sub> [min]	Capacity factor k	log k
1	Ac-FPIIV-NH2	1,61	29,52	29,48	29,49	29,50	9,171	0,962
2	Ac-WIG-NH2	0,62	22,58	22,6	22,62	22,60	6,793	0,832
3	H-WLLV-OH	0,23	27,36	27,35	27,35	27,35	8,432	0,926
4	Ac-IAV-NH2	-0,21	17,96	17,96	17,96	17,96	5,193	0,715
5	Ac-YPINV-NH2	-0,42	21,85	21,83	21,83	21,84	6,530	0,815
6	H-IVVVI-OH	-0,89	22,95	22,97	22,86	22,93	6,906	0,839
7	H-IIIIIG-OH	-0,97	22,42	22,42	22,43	22,42	6,732	0,828
8	H-SLAIV-OH	-1,94	20,91	20,92	20,93	20,92	6,214	0,793
9	H-SLI-OH	-1,99	18,62	18,61	18,6	18,61	5,417	0,734
10	H-FVG-OH	-2,33	13,83	13,82	13,82	13,82	3,767	0,576

To obtain the linear regression function, the determined log k values were plotted against the known log P values (**Figure S47**).



**Figure S47:** Log P values plotted against log k values and the corresponding linear fit function.

The obtained linear function was used to calculate the unknown log P values of fluorinated peptides **2-4** (**Table S19**). Same conditions as described above were used to determine the corresponding retention times.

**Table S20:** Log P values of fluorinated peptides **2-4** were estimated from determined log k values.

Peptides	R <sub>t1</sub> [min]	R <sub>t2</sub> [min]	R <sub>t3</sub> [min]	Average R <sub>t</sub> [min]	Capacity factor k	log k	log P
Abu <sub>10</sub> GY(K) <sub>3</sub> <b>2a</b>	29,14	29,13	29,09	29,12	9,041	0,956	1,70
MfeGly <sub>10</sub> GY(K) <sub>3</sub> <b>2b</b>	24,41	24,44	24,44	24,43	7,424	0,871	0,40
DfeGly <sub>10</sub> GY(K) <sub>3</sub> <b>2c</b>	30,54	30,54	30,52	30,53	9,529	0,979	2,04
TfeGly <sub>10</sub> GY(K) <sub>3</sub> <b>2d</b>	35,7	35,66	35,66	35,67	11,301	1,053	3,16
Abu <sub>13</sub> GY(K) <sub>4</sub> <b>3a</b>	35,06	35,06	35,03	35,05	11,086	1,045	3,03
MfeGly <sub>13</sub> GY(K) <sub>4</sub> <b>3b</b>	29,77	29,99	29,98	29,91	9,315	0,969	1,89
DfeGly <sub>13</sub> GY(K) <sub>4</sub> <b>3c</b>	33,83	33,89	33,87	33,86	10,677	1,028	2,79
TfeGly <sub>13</sub> GY(K) <sub>4</sub> <b>3d</b>	39,12	38,92	38,94	38,99	12,446	1,095	3,79
Abu <sub>15</sub> GY(K) <sub>4</sub> <b>4a</b>	38,37	38,34	38,33	38,35	12,223	1,087	3,67
MfeGly <sub>15</sub> GY(K) <sub>4</sub> <b>4b</b>	32,41	32,36	32,33	32,37	10,161	1,007	2,46
DfeGly <sub>15</sub> GY(K) <sub>4</sub> <b>4c</b>	35,91	35,88	35,82	35,87	11,369	1,056	3,20

To verify that the hydrophobicity of fluorinated peptides **2-4** was correctly estimated, classical octan-1-ol/water partitioning experiments were carried with the Abu<sub>10</sub>GY(K)<sub>3</sub> **2a** peptide. Other

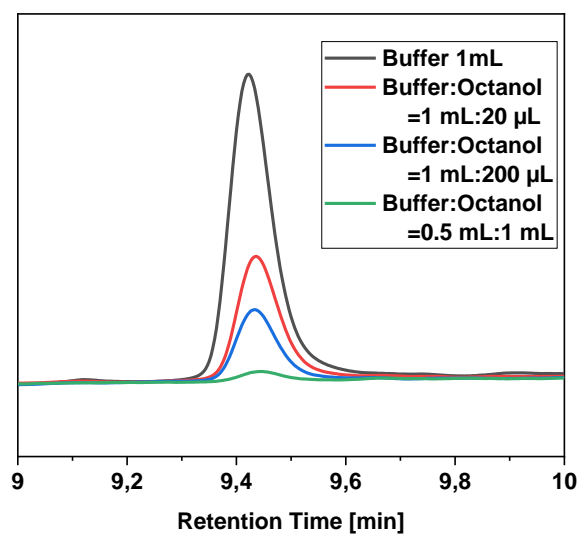


peptides precipitated during the experiments, making it impossible to determine the log P values using this method.

To determine the log P value of Abu<sub>10</sub>GY(K)<sub>3</sub> **2a** by partitioning experiments, according to Hill,<sup>5</sup> the peptide **2a** (0.5 mg) was dissolved in 10 mL octan-1-ol saturated phosphate buffer (10 mM, pH=7.4). Starting from this stock solution, four mixtures were prepared in HPLC sample vials:

- (1) stock solution 1 mL
- (2) octan-1-ol:stock=20 µL:1 mL
- (3) octan-1-ol:stock=200 µL:1 mL
- (4) octan-1-ol:stock=1 mL:500 µL

The vials were gently shaken for 90 min at 25 °C. Subsequently, the mixtures were analyzed by RP-HPLC. As stated by Hill, the aqueous phase can be analyzed directly from the HPLC vials as the injection needle can pass through the octan-1-ol phase without being contaminated by it.<sup>[14]</sup> The corresponding chromatograms are shown in **Figure S48**.



**Figure S48:** HPLC chromatograms of corresponding samples (1), (2), (3), and (4).

By integrating the peak area, the log P value can be calculated using the following equation:

$$\log P = \log \left( \frac{A_1 A_F V_W}{A_F V_O} \right) \quad (\text{eq. 1})$$

$A_1$ : peak area of the stock solution (sample (1))

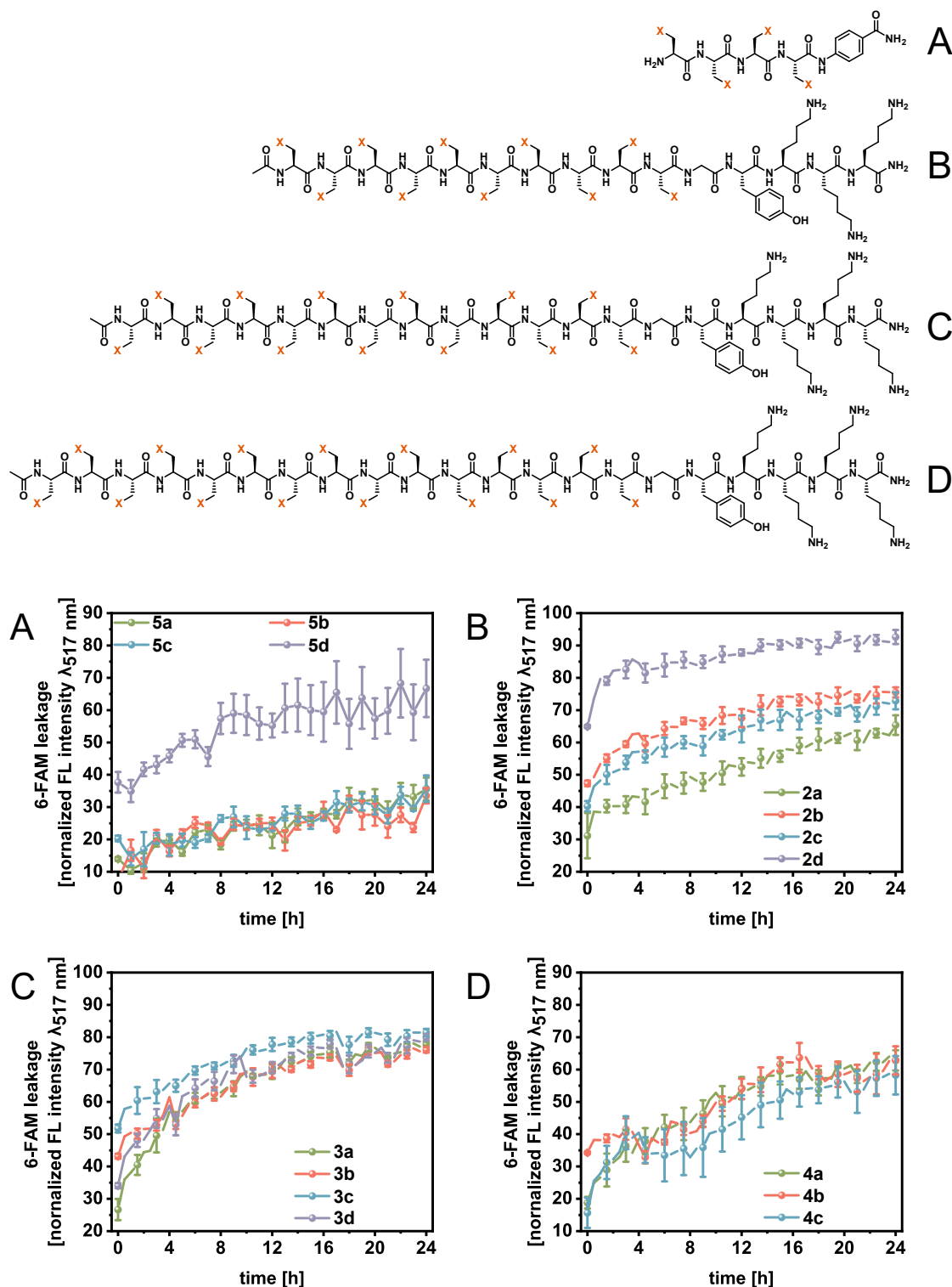
$A_F$ : peak area of the samples (2-4)

$V_O$ : volume of the octan-1-ol phase

$V_W$ : volume of the aqueous phase

For Abu<sub>10</sub>GY(K)<sub>3</sub> **2a** a log P value of 1.56±0.30 was determined, which is in an excellent agreement with the estimated log P value that was determined using the HPLC-based assay.

## 5. 6-FAM leaking assay – further data



**Figure S49:** Real-time monitoring of peptide-caused 6-FAM leaking: The dye was encapsulated in 5 mM liposome solution (POPC:POPC [1:1]) and its release upon incubation (37 °C, 24 h) with homooligopeptides  $[X]_4[4]Abz$  (A, 100  $\mu$ M),  $X_{10}GY(K)_3$  (B, 50  $\mu$ M),  $X_{13}GY(K)_4$  (C, 50  $\mu$ M) and  $X_{15}GY(K)_4$  (D, 50  $\mu$ M) was detected *via* fluorescence spectroscopy ( $\lambda_{ex}= 493$  nm/  $\lambda_{em}= 517$  nm). FL values were normalized to 100% dye release (5% (v/v) Triton X-100 in buffer).

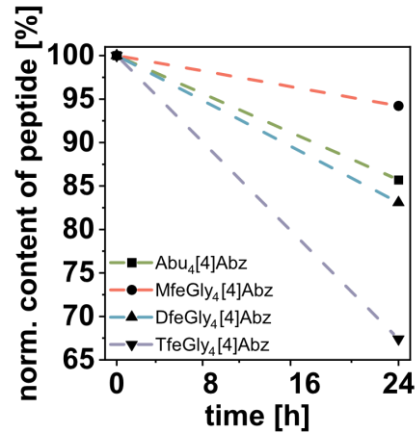
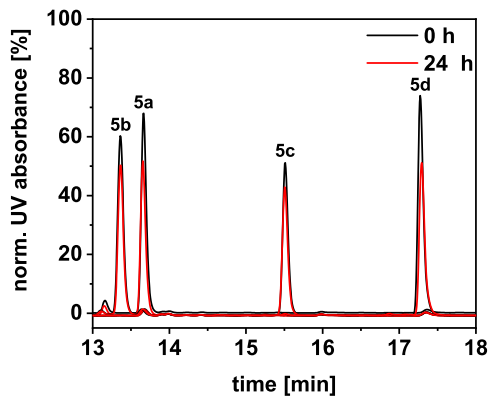
## 6. Peptide digestion assay

The proteolytic digestion studies of peptides were monitored through a Hitachi Primaide™ UV-HPLC system (VWR/Hitachi, Darmstadt, Germany). A Kinetex® RP-C18 (5 μM, 100 Å, 250 x 4.6 mm, Phenomenex®, USA) column and a SecurityGuard™ Cartridge Kit equipped with a C18 cartridge (4 x 3.0mm, Phenomenex®, USA)) as pre-column was used. As eluents water and ACN, both containing 0.1% (v/v) TFA were applied. A flow rate of 1 mL/min was used and UV-detection occurred at 280 nm for respective peptides. Data analysis was done with EZ Chrom ELITE software (version 3.3.2, Agilent). The calculation of remaining peptide amount was done with OriginPro 2020b (OriginLab Corporation, Northampton, MA, USA).

**Table S21:** Analytical HPLC conditions for peptide digestion assay (real-time monitoring).

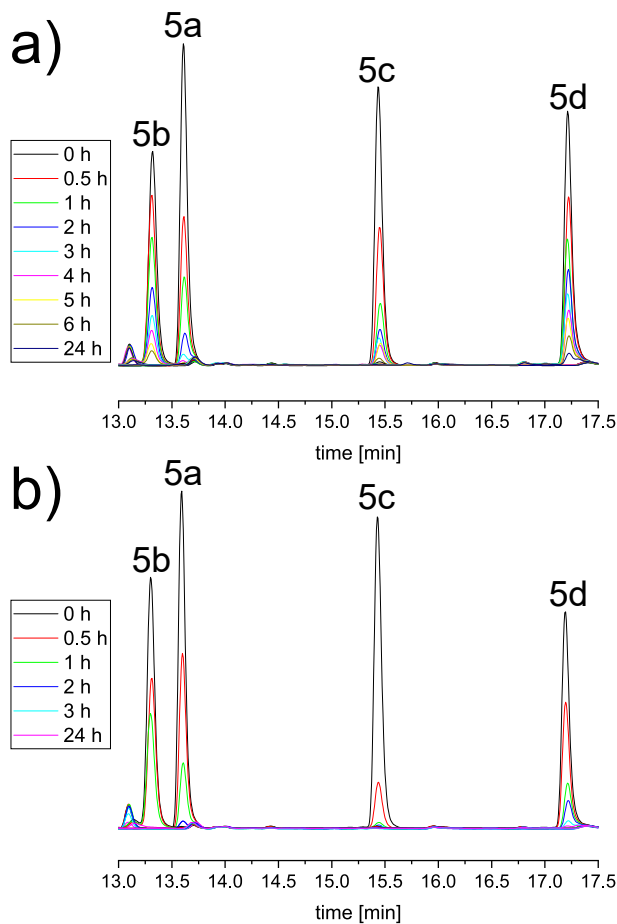
Time (min)	Eluent (A)	Eluent (B)	Flow (mL/min)
0.0	95.0	5.0	1.0
5.0	95.0	5.0	1.0
20.0	50.0	50.0	1.0
22.0	0.0	100.0	1.0
24.0	0.0	100.0	1.0
26.0	95.0	5.0	1.0
30.0	95.0	5.0	1.0

Due to the highly hydrophobic nature of the truncated homopeptides **5a-5d**, negative controls of these peptides were initially probed to determine the impact of peptide aggregation during the experiment. Here, the peptides (0.23 mM) were dissolved in 50 mM BTP + 20 mM CaCl<sub>2</sub>; pH 8 **without enzyme (!)** and incubated for 24 h at 30 °C as described in the main paper. Aliquots (15 μL) were diluted with 30% AcOH + 0.13 mM reference (90 μL) and the remaining content of soluble peptide was determined through HPLC analysis (all at DAD-280 nm) (see **Figure S50**). We detected partial aggregation these peptides while the amount of soluble peptide decreases with time. Obviously, the effect of aggregation enhances with increasing hydrophobicity of the fluorinated amino acids. (MfeGly < Abu < DfeGly < TfeGly). However, the loss in soluble peptide is rather neglectable with respect to the digestion profiles shown for elastase after 6 h and for proteinase k after 3 h in the main paper.



**Figure S50:** HPLC chromatograms (negative controls) of fluoropeptides Abu<sub>4</sub>[4]Abz **5a**, MfeGly<sub>4</sub>[4]Abz **5b**, DfeGly<sub>4</sub>[4]Abz **5c** and TfeGly<sub>4</sub>[4]Abz **5d** after incubation according to the standard digestion protocol after 0 h and 24 h (left). Schematic representation of normalized peptide content over a time period of 24 hours (right).

In **Figure S51**, HPLC chromatograms (all at DAD-280 nm) derived from the peptide digestion assays are illustrated. Peptide amounts decreased significantly faster than for the negative controls validating the degradation of substrates through both serine proteases elastase + proteinase k.



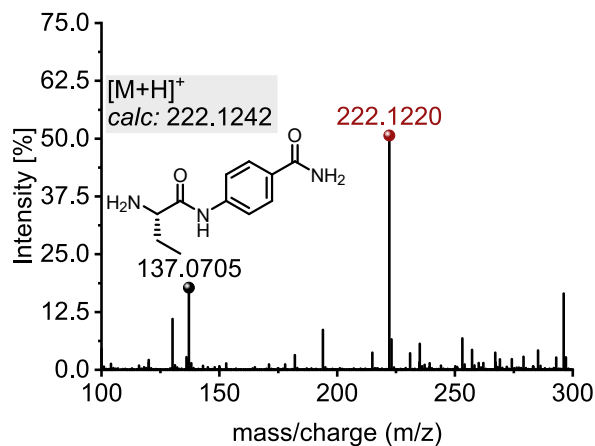
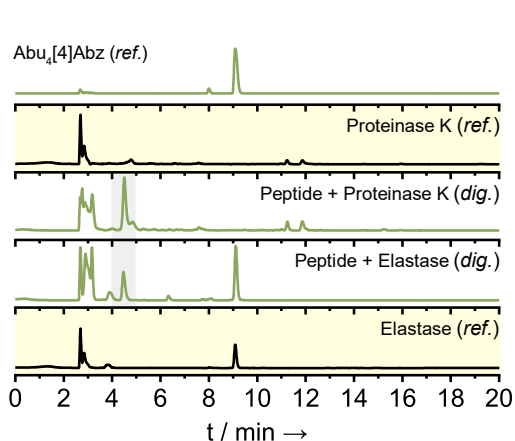
**Figure S51:** Real-time monitoring on the proteolytic digestion profile of fluoropeptides Abu<sub>4</sub>[4]Abz **5a**, MfeGly<sub>4</sub>[4]Abz **5b**, DfeGly<sub>4</sub>[4]Abz **5c** and TfeGly<sub>4</sub>[4]Abz **5d** (each 230 μM) in **a)** elastase (0.91 μM) or **b)** proteinase K (0.0091 μM) dissolved in 50 mM Bis-tris propane + 20 mM CaCl<sub>2</sub> (pH 8) [75%] + DMSO [25%] and incubation at 30 °C.

For identification of digestion products derived from Abu<sub>4</sub>[4]Abz **5a**, MfeGly<sub>4</sub>[4]Abz **5b**, DfeGly<sub>4</sub>[4]Abz **5c** and TfeGly<sub>4</sub>[4]Abz **5d**, non-quenched aliquots were taken from the reaction mixture and screened through HPLC analysis (all at DAD-280 nm) after 24 h incubation to ensure complete proteolysis of the substrate. For each peptide, **one particular digestion fragment** cleaved from the full-length peptide was identified *via* HPLC (highlighted in grey color in the chromatograms) and, subsequently, analyzed by ESI–ToF mass analysis on an Agilent 6220 ESI–ToF–MS spectrometer (Agilent Technologies, Santa Clara, CA, USA). The HPLC conditions are listed in **table 22** and the HPLC & MS spectra in **Figure 51-54**. Comparison of given analytical data on enzymatic digestion to the full-length peptides reference HPLC chromatograms [“**Peptide (ref.)**”, each top chromatogram in **Figure 51-54**] before addition of the enzymatic solution confirmed complete consumption of the substrate. Further reference HPLC chromatograms [“**Proteinase K (ref.)**” and “**Elastase (ref.)**”, highlighted in yellow] of the buffered enzyme stock solutions were recorded to differ between the HPLC signals of formed digestion products [“**Peptide + Proteinase K (dig.)**” and “**Peptide + Elastase (dig.)**”] and enzyme-related autolysis.

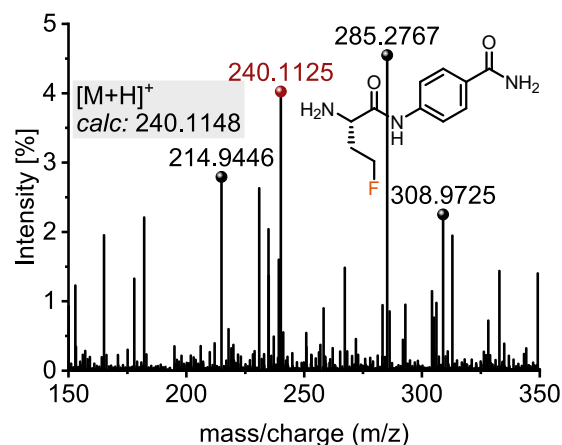
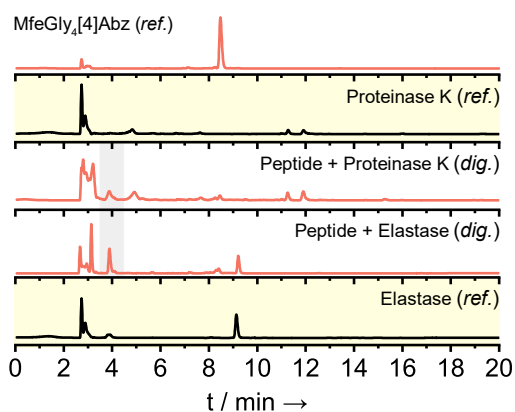
**Table S22:** Analytical HPLC conditions for peptide digestion assay (fragment-identification).

Time (min)	Eluent (A)	Eluent (B)	Flow (mL/min)
0.0	90.0	10.0	1.0
18.0	60.0	40.0	1.0
20.0	0	100.0	1.0
22.0	0	100.0	1.0
23.0	90.0	10.0	1.0
25.0	90.0	10.0	1.0

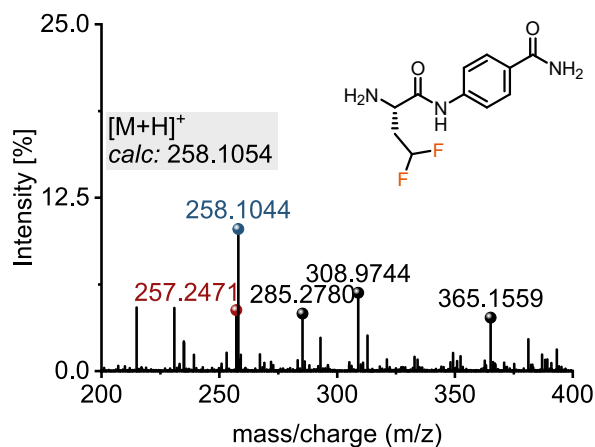
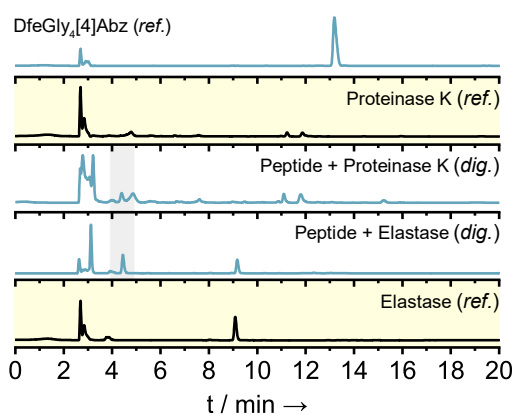
It becomes apparent that detection and identification of the Abz-labeled fragments Abu[4]Abz, MfeGly[4]Abz, DfeGly[4]Abz and TfeGly[4]Abz validates the existence of a predominant cleaving site for the fluoropeptides. For both digestive enzymes, two consecutive amino acids “Abu-Abu”, “MfeGly-MfeGly”, “DfeGly-DfeGly” and “TfeGly-TfeGly” serve as P1-P1’ residues (according to *Schechter & Berger* nomenclature) bearing the hydrolyzed amide bond.<sup>[15]</sup> A proposed model on enzyme-substrate recognition is illustrated in **Figure 55**.



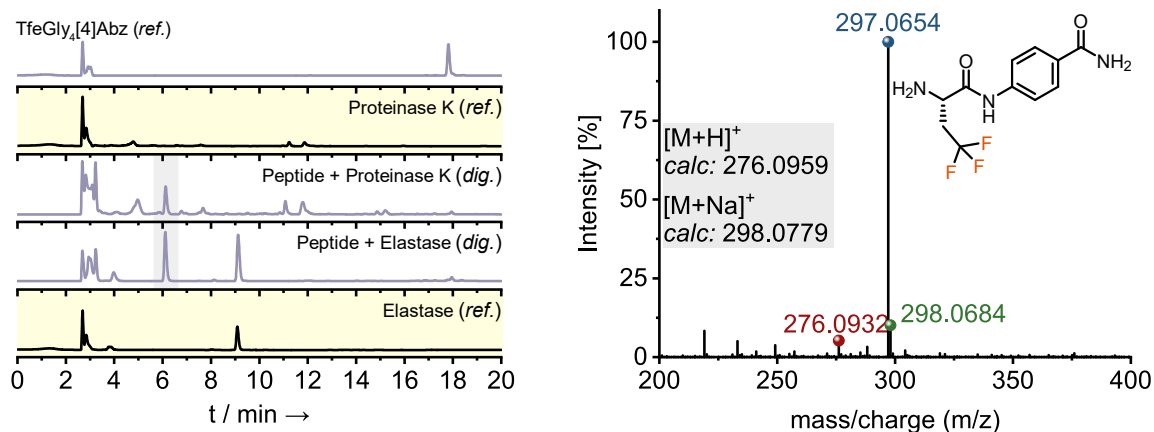
**Figure S51:** Digestion-fragment analysis on the proteolytic digestion profile of Abu<sub>4</sub>[4]Abz **5a** (230 μM) in elastase (0.91 μM) and proteinase K (0.0091 μM) dissolved in 50 mM Bis-tris propane + 20 mM CaCl<sub>2</sub> (pH 8) [75%] + DMSO [25%] after 24 h incubation at 30 °C. The Abz-labeled compound Abu[4]Abz (HPLC signal is highlighted in grey) was determined as main digestion product *via* HRMS.



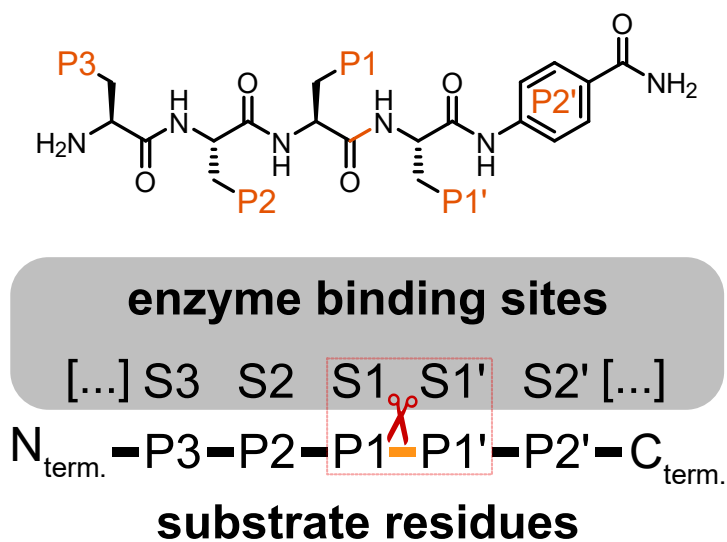
**Figure S52:** Digestion-fragment analysis on the proteolytic digestion profile of MfeGly<sub>4</sub>[4]Abz **5b** (230 μM) in elastase (0.91 μM) and proteinase K (0.0091 μM) dissolved in 50 mM Bis-tris propane + 20 mM CaCl<sub>2</sub> (pH 8) [75%] + DMSO [25%] after 24 h incubation at 30 °C. The Abz-labeled compound MfeGly[4]Abz (HPLC signal is highlighted in grey) was determined as main digestion product *via* HRMS.



**Figure S53:** Digestion-fragment analysis on the proteolytic digestion profile of DfeGly<sub>4</sub>[4]Abz **5c** (230 μM) in elastase (0.91 μM) and proteinase K (0.0091 μM) dissolved in 50 mM Bis-tris propane + 20 mM CaCl<sub>2</sub> (pH 8) [75%] + DMSO [25%] after 24 h incubation at 30 °C. The Abz-labeled compound DfeGly[4]Abz (HPLC signal is highlighted in grey) was determined as main digestion product *via* HRMS.



**Figure S54:** Digestion-fragment analysis on the proteolytic digestion profile of TfeGly<sub>4</sub>[4]Abz **5d** (230 μM) in elastase (0.91 μM) and proteinase K (0.0091 μM) dissolved in 50 mM Bis-tris propane + 20 mM CaCl<sub>2</sub> (pH 8) [75%] + DMSO [25%] after 24 h incubation at 30 °C. The Abz-labeled compound TfeGly<sub>4</sub>[4]Abz (HPLC signal is highlighted in grey) was determined as main digestion product *via* HRMS.



**Figure S55:** Simplified model of enzyme-substrate interaction despite the side chains' fluorine-content according to Schechter & Berger nomenclature.<sup>[15]</sup>



## 7. References

- [1] T. Hohmann, M. Dyrks, S. Chowdhary, M. Weber, D. Nguyen, J. Moschner, B. Kokschi, *The Journal of Organic Chemistry* **2022**, *87*, 10592-10604.
- [2] J. Han, R. Takeda, X. Liu, H. Konno, H. Abe, T. Hiramatsu, H. Moriwaki, V. A. Soloshonok, *Molecules (Basel, Switzerland)* **2019**, *24*, 4521.
- [3] J. Leppkes, N. Dimos, B. Loll, T. Hohmann, M. Dyrks, A. R. Wieseke, B. G. Keller, B. Kokschi, *RSC Chemical Biology* **2022**.
- [4] M. L. Tiffany, S. Krimm, *Biopolymers* **1968**, *6*, 1379-1382.
- [5] R. W. Woody, *Journal of the American Chemical Society* **2009**, *131*, 8234-8245.
- [6] W. L. Mattice, *Biopolymers* **1974**, *13*, 169-183.
- [7] aF. Eker, X. Cao, L. Nafie, R. Schweitzer-Stenner, *Journal of the American Chemical Society* **2002**, *124*, 14330-14341; bF. Eker, K. Griebenow, R. Schweitzer-Stenner, *Journal of the American Chemical Society* **2003**, *125*, 8178-8185; cR. Schweitzer-Stenner, F. Eker, K. Griebenow, X. Cao, L. A. Nafie, *Journal of the American Chemical Society* **2004**, *126*, 2768-2776; dR. Schweitzer-Stenner, T. Measey, L. Kakalis, F. Jordan, S. Pizzanelli, C. Forte, K. Griebenow, *Biochemistry* **2007**, *46*, 1587-1596.
- [8] aZ. Shi, C. A. Olson, D. Rose George, L. Baldwin Robert, R. Kallenbach Neville, *Proceedings of the National Academy of Sciences* **2002**, *99*, 9190-9195; bZ. Liu, K. Chen, A. Ng, Z. Shi, R. W. Woody, N. R. Kallenbach, *Journal of the American Chemical Society* **2004**, *126*, 15141-15150.
- [9] aM. A. Kelly, B. W. Chellgren, A. L. Rucker, J. M. Troutman, M. G. Fried, A.-F. Miller, T. P. Creamer, *Biochemistry* **2001**, *40*, 14376-14383; bA. L. Rucker, T. P. Creamer, *Protein science : a publication of the Protein Society* **2002**, *11*, 980-985; cA. L. Rucker, C. T. Pager, M. N. Campbell, J. E. Qualls, T. P. Creamer, *Proteins: Structure, Function, and Bioinformatics* **2003**, *53*, 68-75; dE. A. Bienkiewicz, A. Y. Moon Woody, R. W. Woody, *Journal of Molecular Biology* **2000**, *297*, 119-133; eA. K. Pandey, K. M. Thomas, C. R. Forbes, N. J. Zondlo, *Biochemistry* **2014**, *53*, 5307-5314.
- [10] Z. Shi, R. W. Woody, N. R. Kallenbach, in *Advances in Protein Chemistry, Vol. 62*, Academic Press, **2002**, pp. 163-240.
- [11] A. Barth, *Biochim Biophys Acta* **2007**, *1767*, 1073-1101.
- [12] A. Rodil, S. Bosisio, M. S. Ayoub, L. Quinn, D. B. Cordes, A. M. Z. Slawin, C. D. Murphy, J. Michel, D. O'Hagan, *Chemical Science* **2018**, *9*, 3023-3028.
- [13] aM. Akamatsu, Y. Yoshida, H. Nakamura, M. Asao, H. Iwamura, T. Fujita, *Quantitative Structure-Activity Relationships* **1989**, *8*, 195-203; bM. Akamatsu, S.-I. Okutani, K. Nakao, N. J. Hong, T. Fujita, *Quantitative Structure-Activity Relationships* **1990**, *9*, 189-194; cM. Akamatsu, T. Fujita, *Journal of Pharmaceutical Sciences* **1992**, *81*, 164-174.
- [14] K. Valkó, in *Handbook of Analytical Separations, Vol. 1* (Ed.: K. Valkó), Elsevier Science B.V., **2000**, pp. 535-583.
- [15] I. Schechter, A. Berger, *Biochemical and Biophysical Research Communications* **1967**, *27*, 157-162.

---

### 6.3 Establishing fluorine containing amino acids as an orthogonal tool in coiled coil assembly

T. Hohmann, P. Dubatouka, K. Pfeifer, B. Kokschi, *Biomacromolecules* **2023**, *24*, 3357–3369.

*Submitted*: 26 April 2023; *Publication date*: 28 June 2023

Published by American Chemical Society

The published work is available online: <https://doi.org/10.1021/acs.biomac.3c00427>

#### Individual contributions of the authors

I (Freie Universität Berlin) developed the overall project, synthesized and purified all peptides, carried out the CD, SEC-MALS, and FRET measurements, performed the disulfide exchange assays, and wrote the manuscript. Beate Kokschi (Freie Universität Berlin) guided on project planning, data interpretation, and manuscript writing. Palina Dubatouka (Freie Universität Berlin) and Katharina Pfeifer (Freie Universität Berlin) assisted me in synthesis, purification, and analysis.

#### Rationale and summary of the project

Over the last 20 years, fluorine has proven to be an outstanding tool for modifying properties, particularly thermal stability, of coiled coil motifs. Various working groups demonstrated that incorporating aliphatic fluorinated amino acids into the hydrophobic core of CC structures can drastically improve the stability towards thermal and chemical denaturation. In this work, a combinatorial approach was envisioned to study the influence of fluorination at position *a* on the properties of a parallel heterodimeric CC motif. Using a combinatorial library provided an opportunity to screen fluorinated amino acids with different fluorinated binding partners, something that has not been investigated in this way before. Subsequently, the observed trends were exploited to design a platform for fluorine-directed CC self-assembly.

The well-established VPK/VPE system was used to design the respective combinatorial library. Different fluorinated and non-fluorinated  $\beta$ -branched residues were introduced at all positions *a* of this motif. In the scope of this work, the following amino acids were utilized: Val, (2*S*,3*S*)-TfVal **22**, (2*S*,3*R*)-TfVal **23**, Ile, *allo*-isoleucine (*alle*), 5<sup>3</sup>-(2*S*,3*R*)-TfIle **25**, and 5<sup>3</sup>-(2*S*,3*S*)-TfIle **26**. Consequently, a combinatorial library consisting of seven VPK and seven VPE peptides (28 combinations) was studied *via* CD, SEC-MALS, and FRET measurements (*Figure 6.3, a*).

SEC-MALS measurements revealed the oligomerization state of each combination. Interestingly, only VPK(Val)-VPE(Val), VPK(Ile)-VPE(Ile), and VPK(Ile)-VPE(Val) combinations retained the dimeric structure. The remaining combinations exhibited the formation of trimeric, and in the case of the VPK((3S)-TfIle)-VPE((3S)-TfIle) pairing, even of a tetrameric structure. This observation was highly unexpected since the VPK(Ile)-VPE(Ile) combination is sterically much more demanding than, for example, VPK(Val)-VPE(TfVal) pairings. The introduction of a CF<sub>3</sub>-group is sufficient to disrupt the dimeric oligomerization state while utilizing two additional methyl functionalities was tolerated.

CC orientation was investigated *via* fluorescence-based FRET measurements (*Figure 6.3, b.*). At the N-terminus of all VPK peptides, a fluorescence donor residue, *ortho*-aminobenzoic acid (*o*Abz), was introduced. Respectively, 3-nitrotyrosine (3-NO<sub>2</sub>-Tyr) was incorporated at the N-terminus of all VPE peptides to serve as a fluorescence quencher. In the case of a parallel arrangement, both functionalities would be placed in close spatial proximity, resulting in the fluorescence quenching. An antiparallel orientation, in turn, would not contribute to any alteration of the corresponding fluorescence. For all 28 combinations, a decrease in fluorescence was observed, strongly indicating that at least two peptides (VPK and VPE) are placed in a parallel arrangement. However, the orientation of the third peptide (in the case of trimeric structures) is ambiguous. A disulfide exchange assay (DSA) was performed to obtain a more detailed picture. In this context, the VPK/VPE model was modified, introducing S<sup>t</sup>Bu-protected cysteine at the N-terminus and a tryptophane residue at one position *f* to allow peptide concentration determination. VPK<sub>C</sub>(Val)-VPE<sub>C</sub>((3S)-TfVal) and VPK<sub>C</sub>((3S)-TfVal)-VPE<sub>C</sub>((3S)-TfIle) combinations were studied since both displayed the formation of distinct trimers. The peptides were equilibrated at 2:1 or 1:2 ratios in a redox buffer to ensure the formation of a single trimeric species and subsequently analyzed by HPLC and high-resolution mass spectrometry (HRMS). In the case of a fully parallel orientation, two different disulfide bridged dimers can be formed. On the contrary, the presence of an up-up-down trimer would result in the formation of a single disulfide bridged structure. VPK<sub>C</sub>((3S)-TfVal)-VPE<sub>C</sub>((3S)-TfIle) = 2:1 DSA experiment displayed the presence of two dimers in an approximate ratio of 2:1, strongly hinting the predisposition for up-up-up trimer formation (*Figure 6.3, b.*). DSA studies of VPK<sub>C</sub>((3S)-TfVal)-VPE<sub>C</sub>((3S)-TfIle) = 1:2 and VPK<sub>C</sub>(Val)-VPE<sub>C</sub>((3S)-TfVal) = 2:1 revealed a similar picture. The formation of two dimeric structures was observed. However, the experimental ratio deviated to a greater extent from the ideal 2:1 ratio and hence could reflect the presence of the corresponding up-up-down species. Finally, the VPK<sub>C</sub>(Val)-VPE<sub>C</sub>((3S)-TfVal) = 1:2 combination showed the presence of a single disulfide bridged dimer, indicating the strong preference to form the up-up-down trimer.



These results demonstrate that the orientation of the CC trimers varies depending on the particular combination and the ratios utilized in this context.

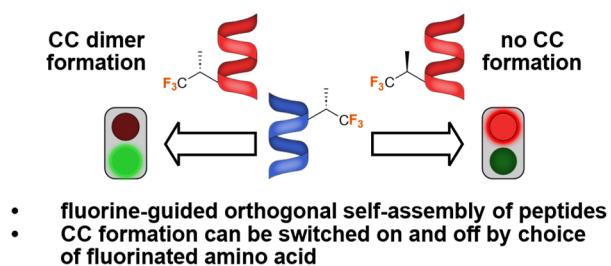
Thermal denaturation measurements were performed to investigate the stabilities of each combination, revealing various trends in the influence of fluorination and stereochemistry (*Figure 6.3, c.*). (3*S*)-TfIle-peptide formed highly stable CC structures with all available binding partners. This fluorinated building block showed greater potential to stabilize the CC motif than the combinations with the respective non-fluorinated analog, Ile, indicating the positive influence of fluorination on CC stabilities. In contrast, (3*S*)-TfVal-peptides displayed low melting points with a series of different peptides. For example, the VPK((3*S*)-TfVal)-VPE((3*S*)-TfVal) combination represented the least stable combination and was already denatured at room temperature. Furthermore, the crucial significance of the stereochemistry within the amino acid side chains was revealed. Compared to the (3*S*)-residue, (3*R*)-TfVal-peptides demonstrated improved stabilizing properties. Additionally, peptides containing alle and (3*R*)-TfIle residues formed less stable CC structures than the corresponding (3*S*)-isomers. Overall, this thorough investigation of thermal CC stabilities demonstrated that the widespread influence of fluorination on the stability of CC structures can be overestimated. At the same time, the precise location of the perfluorinated groups within the hydrophobic core can exert a strong influence on the thermal stability of the CC motif.

In the second part, fluorine-guided CC assembly properties of the VPK/VPE motif were studied (*Figure 6.3, d.*). The design of VPK/VPE peptides was modified to enable the respective investigations *via* DEA. Comparable to the studies regarding the orientation of CC structures, Cys(S<sup>t</sup>Bu) was introduced at the N-terminus and a Trp residue at one position *f*. Furthermore, asparagine was incorporated at position *a*23 to specify the dimeric oligomerization state of this altered VPK<sub>N</sub>/VPE<sub>N</sub> system. The corresponding library was reduced to focus on the fluorinated CC peptides, utilizing Val, (3*S*)-TfVal **22**, (3*R*)-TfVal **23**, (3*R*)-TfIle **25**, and (3*S*)-TfIle **26** residues. First, the respective assembly properties were studied in a combinatorial fashion. Different peptide pairs were equilibrated in a redox buffer, and after 48 hours, the mixtures were analyzed *via* HPLC and HRMS. Val- and (3*S*)-TfIle-containing peptides formed disulfide bridged dimers with all available binding partners. However, selective CC formation was observed in the case of (3*S*)-TfVal and (3*R*)-TfIle peptides, demonstrating the potential of fluorinated amino acids to direct orthogonal CC assembly processes (*Figure 6.3, d.*). Therefore, utilizing (3*S*)-TfVal- and (3*R*)-TfIle-peptides allows the CC formation to be turned on and off. Finally, competition experiments were conducted. First, eight VPK<sub>N</sub>/VPE<sub>N</sub> peptides, excluding the strongly binding VPK<sub>N</sub>((3*S*)-TfIle) and VPE<sub>N</sub>((3*S*)-TfIle), were mixed and equilibrated. As expected, the respective peptides displayed orthogonal CC pair formation. Only CC dimers containing Val and (3*R*)-TfVal residues were detected in this context. The formation of

(3*S*)-TfVal- and (3*R*)-TfIle-containing dimers was not observed. A similar experiment, however, involving all ten peptides, presented a contrary picture. Nine combinations were identified, seven of which involved (3*S*)-TfIle-peptides.

This work demonstrates the ability of aliphatic fluorinated amino acids to direct intermolecular interactions between peptides. Introducing different fluorinated amino acids at the hydrophobic positions creates diversity, which can be exploited to disrupt or improve CC formation. This strategy represents another tool to fine-tune and guide peptide-peptide interactions.

## Publication and supporting information



Establishing Fluorine-Containing Amino Acids as an Orthogonal Tool in Coiled Coil Assembly  
T. Hohmann, P. Dubatouka, K. Pfeifer, B. Kokschi, *Biomacromolecules* **2023**, *24*, 3357–3369.  
DOI: 10.1021/acs.biomac.3c00427

For copyright reasons, the article is not included in the online version of this thesis.  
An electronic version of the article is available.  
<https://doi.org/10.1021/acs.biomac.3c00427>

## 7 Unpublished Results – *All-Cis* Pentafluorinated Cyclohexylalanine

In *Section 2* of this thesis, the multifaceted ways in which fluorine can define intermolecular interactions were discussed in detail. The dipole-dipole interactions caused by the strong polarization of the C-F bond can play an essential role in these processes. To date, probably the most extreme example of strongly polarized interactions between fluorinated species has been presented by the O'Hagan group. The on-site fluorination of cyclohexane leads to the introduction of a strong dipole moment, which consequently dictates the corresponding intermolecular interactions. In this context, O'Hagan working group developed the pentafluorinated version **131** of the unnatural amino acid cyclohexylalanine **130** (Cha). Like the fluorinated Janos-faced cyclohexyl species that were previously discussed, the introduction of five fluorine atoms occurred on one side of the cyclohexyl moiety. For the studies described in this thesis's scope, the pentafluorinated cyclohexylalanine **131** (F<sup>5</sup>-Cha) was provided by the O'Hagan working group. The fluorinated amino acid was Fmoc-protected and thus could be used under standard SPPS conditions. Two different model systems were selected to study the properties of this novel fluorinated building block in the context of peptide chemistry. The first system was published by Aravinda *et al.* in 2003 and was designed to study aromatic-aromatic interactions between phenylalanine (Phe) residues.<sup>[276]</sup> The aminoisobutyric acid- (Aib) and Phe-rich system was crystallized, and the respective intermolecular interactions could be studied in this context. The second system was published by Tatko and Waters and focused on the potential of Phe, in comparison to other residues such as Cha, to stabilize the  $\beta$ -hairpin structure.<sup>[277]</sup> Interestingly, even though the nature of the intermolecular interactions between Phe-Phe and Cha-Cha is entirely different, the stabilization potential of both pairs was almost identical. It is quite apparent that both systems highlighted the role of intermolecular interaction between Phe or Cha residues in the context of peptide chemistry. Since the steric properties of F<sup>5</sup>-Cha **131** are comparable to those of Phe and Cha and the influence of the intermolecular interactions between the respective F<sup>5</sup>-Cha **131** residues on peptide properties was the key focus of this work, the F<sup>5</sup>-Cha **131** was introduced into the discussed sequences instead of Phe or Cha residues and the respective effects on structural properties were compared to the non-fluorinated analogs.

### Hydrophobicity of F<sup>5</sup>-Cha

Before the influence of F<sup>5</sup>-Cha **131** on the structural properties of peptide models was studied, attention fell upon the properties of the amino acid itself. It was interesting to examine how the respective polarity of the fluorinated amino acid would change compared to the



non-fluorinated derivative. A well-established HPLC-based assay was used to tackle this question (Figure 7.1).

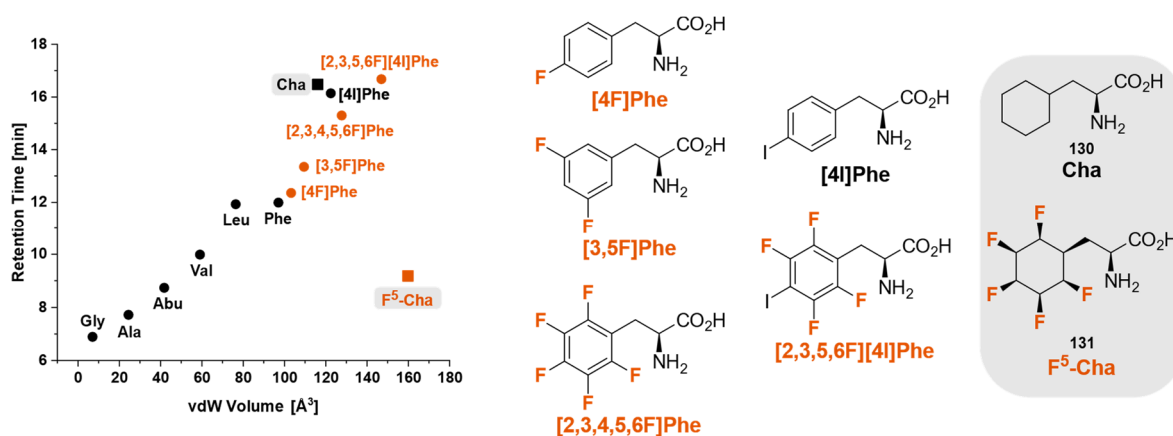
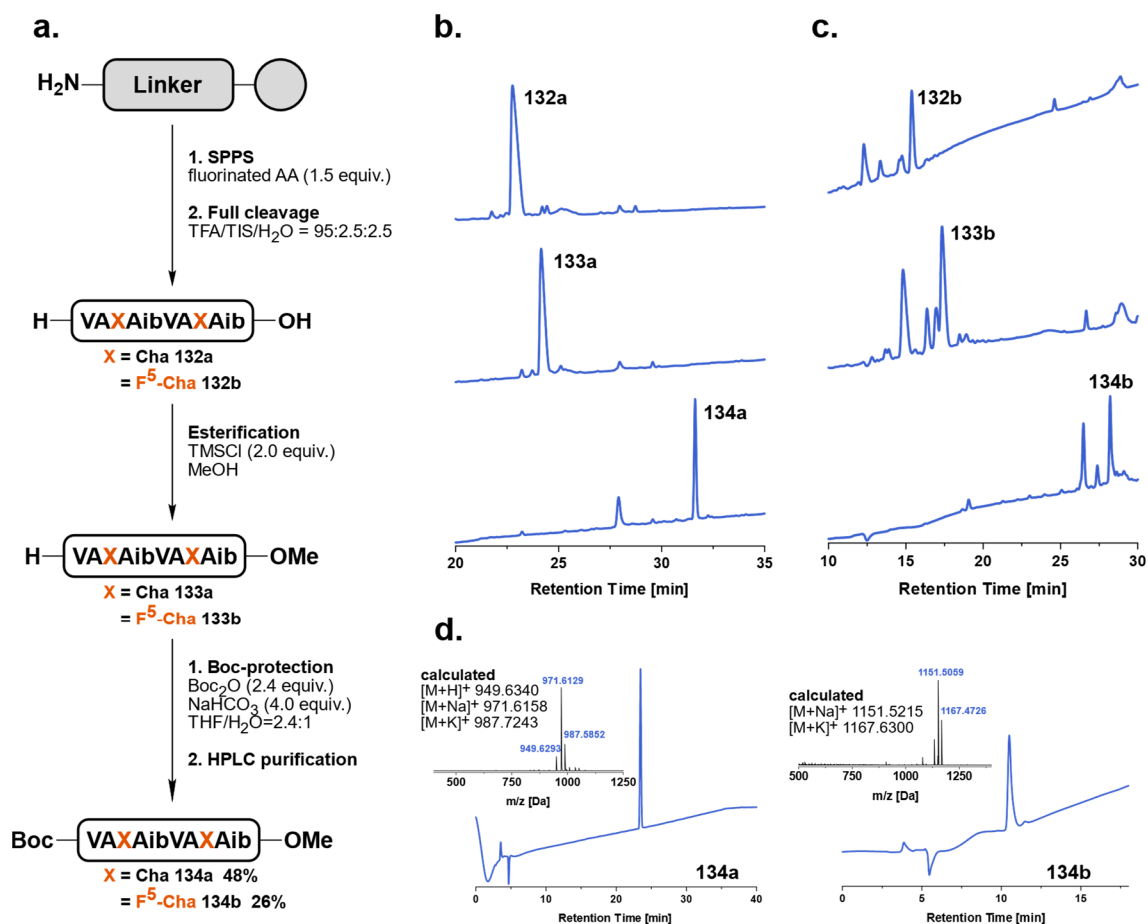


Figure 7.1: Hydrophobicity plot containing the novel F<sup>5</sup>-Cha amino acid. The vdW volumes of respective side chains were calculated using an approach described by Zhao *et al.*<sup>[278]</sup> The structures of selected fluorinated amino acids are shown.

The retention time of a series of Fmoc-protected amino acids was plotted against the van der Waals volumes of the corresponding side chains. The van der Waals volumes of the amino acid side chains were calculated using the protocol described by Zhao *et al.*<sup>[278]</sup> This approach provides insight into the relationship between the structure and the respective polarity. This is particularly evident from the impact of partial fluorination on the respective hydrophobicity. As already discussed, MfeGly **17** is less hydrophobic than the non-fluorinated analog (Abu) despite the increased size of the side chain. DfeGly **18** has nearly the same polarity as Abu, and TfeGly **19** is more hydrophobic than the non-fluorinated variant. These observations highlight the potential of partial fluorination to increase the polarity of the respective compounds relatively. At the same time, the introduction of fully fluorinated CF<sub>3</sub>-groups can lead to a significant increase in hydrophobicity. These considerations are also supported by the trends observed for the fluorinated derivatives of norvaline. A detailed discussion regarding the hydrophobicity of fluorinated amino acids can be found in Section 6. Based on these results, the hydrophobicity of F<sup>5</sup>-Cha **131** was expected to decrease compared to Cha **130**. Still, the drop in the respective hydrophobicity was imposing. The pentafluorinated variant **131** eluted six minutes before the non-fluorinated analog **130**. Additionally, this trend contrasts with the fluorination of Phe, where hydrophobicity is significantly enhanced with an increasing number of fluorine atoms (Figure 7.1). These results indicate a strong dipole moment within the structure of F<sup>5</sup>-Cha **131** and subsequently hint at the potential of this building block in modifying inter- and intramolecular interactions in the context of peptide and protein environments.

## Aib-rich model

The original sequence published by Aravinda *et al.* was synthesized *via* a solution-phase approach. Since the available quantity of F<sup>5</sup>-Cha **131** was limited, the respective synthetic strategy was redesigned. The synthesis was first established with the non-fluorinated Cha-containing peptide **134a**. On the one hand, the synthesis should be optimized without using the valuable F<sup>5</sup>-Cha **131**; on the other hand, **134a** would allow a critical comparison with the fluorinated version **134b**.



**Figure 7.2:** a. Synthetic strategy to obtain Aib-rich peptides **134a** and **134b**. b. and c. HPLC chromatograms of crude Aib-rich peptides **132**, **133**, and **134**. d. HPLC chromatograms and HRMS spectra of purified peptides **134a** and **134b**.

The main sequence was synthesized using standard microwave-assisted SPPS conditions (Figure 7.2, a.). Cha residues **130** could be incorporated at elevated temperature (90 °C) using only 1.5 equiv. This was somewhat surprising since the coupling between sterically hindered Aib residue and Cha **130** was considered potentially troublesome before synthesis. Still, the uncapped peptide **132a** was obtained with an excellent yield of 55% and was used without further purification. The esterification of the C-terminus was carried out by forming a carbon acid chloride species using TMSCl and its *in situ* conversion to the desired methyl ester group.

The obtained peptide **133a** was used without additional purification steps (*Figure 7.2, b.*). Finally, the N-terminal capping with the *tert*-butyloxycarbonyl (Boc) group was performed using Boc<sub>2</sub>O and NaHCO<sub>3</sub>, and the desired product **134a** was obtained after HPLC purification and additional desalting step with an excellent overall yield of 48%. The established synthetic pathway could be applied to the synthesis of the F<sup>5</sup>-Cha peptide **134b** (AbP(F<sup>5</sup>-Cha)) (*Figure 7.2, a., c.*). The final product **134b** was isolated with a slightly lower yield of 26%.

With both peptides in hand, a broad range of different crystallization conditions was screened for both (*Table 7.1*).

*Table 7.1:* Overview over the screened crystallization conditions (prec. = precipitate).

Solvent	Concentration [mg/mL]		
	2	5	10
MeOH	prec.	prec.	prec.
MeOH:H <sub>2</sub> O=8:2	prec.	prec.	prec.
MeOH:H <sub>2</sub> O=6:4	prec.	prec.	prec.
MeOH:H <sub>2</sub> O=1:1	prec.	prec.	prec.
CHCl <sub>3</sub>	prec.	prec.	prec.
CHCl <sub>3</sub> :H <sub>2</sub> O=8:2	prec.	prec.	prec.
CHCl <sub>3</sub> :H <sub>2</sub> O=6:4	prec.	prec.	prec.
Ether	prec.	prec.	prec.
Ether:H <sub>2</sub> O=6:4	prec.	prec.	prec.

Unfortunately, no crystal formation was observed despite a thorough screen that included different solvents, solvent mixtures, and concentrations. As described by Aravinda *et al.* with the original system, a slow evaporation technique was used. In all cases, the respective peptide precipitated from the solution.

### β-hairpin system

To study the ability of F<sup>5</sup>-Cha **131** to stabilize the β-hairpin motif, the respective amino acid was introduced at two selected positions next to the C- and N-termini of the peptide sequence **135b**. A non-fluorinated version of the peptide containing Cha **135a**, which Tatko and Waters studied in the original work, was also targeted. After synthesizing and isolating both peptides, the samples were analyzed *via* HRMS. Surprisingly, the experimental data did not agree with the calculated values for both peptides. In both cases, a peptide with a (+1) mass was isolated (*Figure 7.3, a.*). The literature review revealed that hydrolysis of the Gln residue (Q→E) is probably responsible for this observation.<sup>[279]</sup> The respective mechanism occurs *via* a cyclic intermediate, illustrated in *Figure 7.2, b.* with Asn as an example.<sup>[280]</sup> Since F<sup>5</sup>-Cha **131**

was available in limited quantities, it was nevertheless decided to work with the Q→E versions of the peptides. Both peptides were obtained with yields of 28% (Cha-peptide **139a**) and 20% (F<sup>5</sup>-Cha-peptide **139b**) (Figure 7.3, c.).

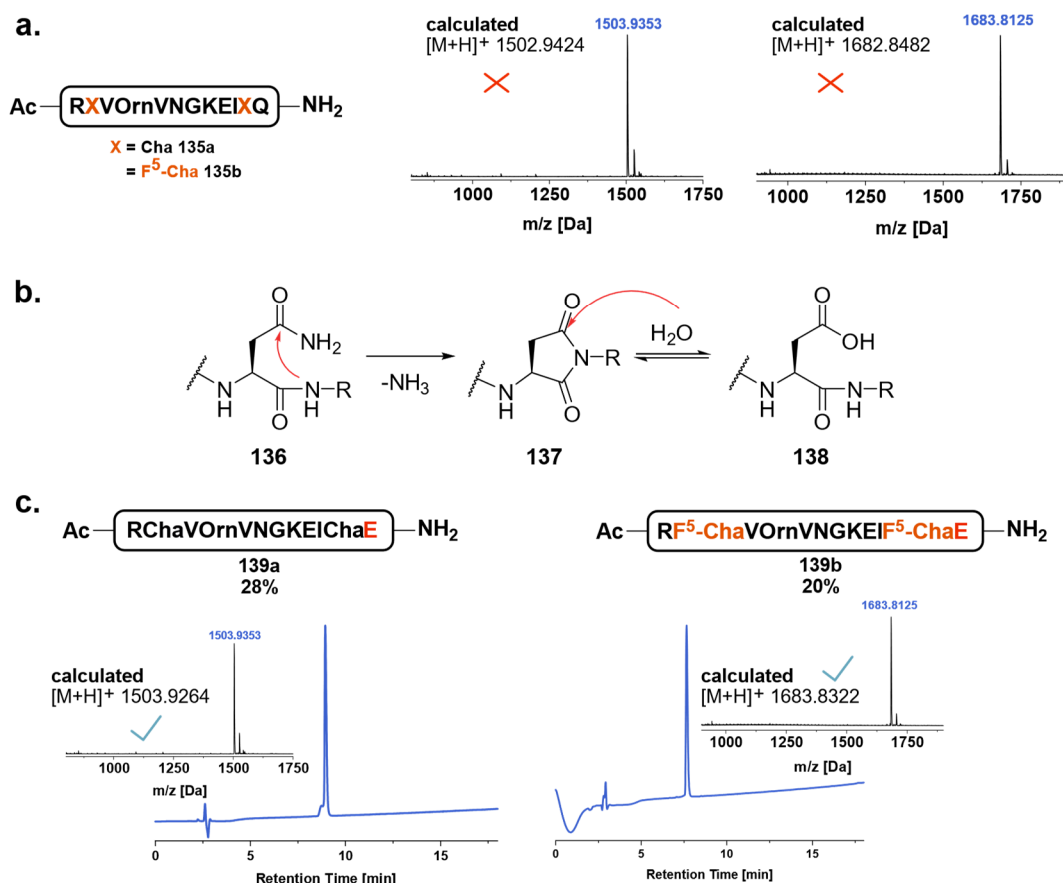


Figure 7.3: a. Sequences of the envisioned  $\beta$ -hairpin peptides **135a** and **135b**. The obtained exact masses of isolated peptides did not agree with the calculated values. b. Mechanism of the hydrolysis of an asparagine residue. c. HPLC chromatograms and HRMS spectra of the isolated peptides **139a** and **139b**.

The structural properties of both peptides were studied *via* CD measurements. First, concentration and pH-dependent measurements were carried out. Both peptides seemed only to form a  $\beta$ -hairpin structure at higher concentrations (Figure 7.4). At lower concentrations, the formation of a random coil structure was observed. No distinctive differences could be observed between different pH values (Figure 7.4, b.). Nevertheless, the measurements at different concentrations showed distinct differences between the two peptides. Cha-peptide **139a** displayed the formation of a  $\beta$ -hairpin structure at a concentration of 3 mM. In the case of the fluorinated analog **139b**, a  $\beta$ -hairpin spectrum, without an additional band below 210 nm indicating a random coil fraction, was obtained only at a concentration of 6 mM (Figure 7.4, c.). This convincingly demonstrates that Cha exhibits a more vital ability to stabilize the  $\beta$ -hairpin motif. Additionally, the influence of metal ions on the structural properties of the F<sup>5</sup>-Cha-peptide **139b** was studied (Figure 7.4, d.). From previous studies of the O'Hagan working group and

others, it is known that fluorinated Janus face cyclohexane compounds can interact with ions in the gas phase.

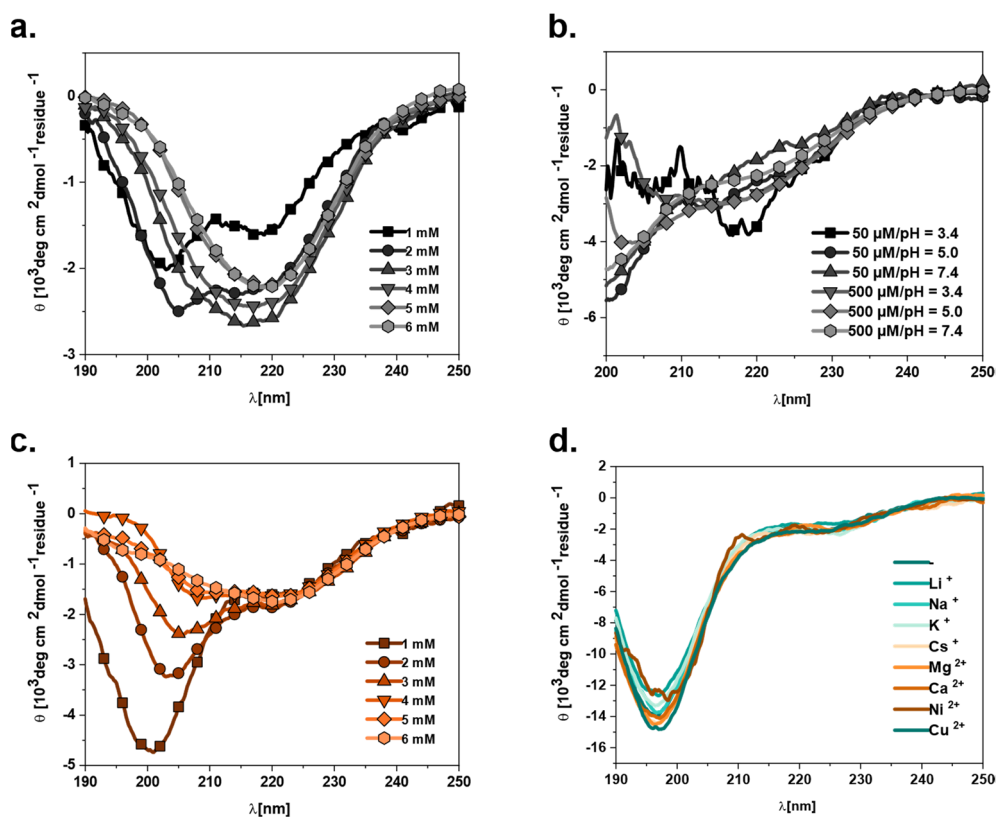


Figure 7.4: a. CD spectra of **139a** at different peptide concentrations. b. CD spectra of **139a** at different pH values. c. CD spectra of **139b** at different peptide concentrations. d. CD spectra of **139b** in the presence of selected cations.

Therefore, it was envisioned that metal ions might interact with corresponding F<sup>5</sup>-Cha residues **131**, destabilizing or stabilizing the respective peptide motif. A series of alkali-, alkaline earth-, and transition metals was screened at pH=7.4 (Figure 7.4, d.). However, no structural changes could be observed.

## Conclusion

Before proposing future studies and peptide models that could be used to investigate the great potential of F<sup>5</sup>-Cha **131** to engineer inter- and intramolecular interactions of peptides or proteins, the model systems described in this thesis should be discussed more closely. The original Aib-rich peptide is a highly hydrophobic species consisting of solely hydrophobic amino acids: valine, aminoisobutyric acid, alanine, and phenylalanine. Furthermore, both ends of the respective peptide are capped, eliminating charges from the peptide sequence. This peptide can only be dissolved in solvent mixtures with a high organic fraction. Therefore, it is unsurprising that during slow evaporation of an aqueous MeOH solution, the peptides interact as the

water content constantly increases and finally crystallizes from the respective solution. The second model system was a  $\beta$ -hairpin-forming peptide. Previous studies showed that this motif could be stabilized either by hydrophobic interactions between two Cha residues at two specific positions in the sequence or by aromatic-aromatic interactions between two phenylalanine residues at the same peptide positions. Furthermore, since the  $\beta$ -hairpin formation was only observed at high concentrations, some intermolecular interactions between monomeric peptide species should be significant in this process. It cannot be overlooked that in both systems, the novel F<sup>5</sup>-Cha building block **131** was introduced into an environment dominated by strictly hydrophobic interactions. At first glance, this also seems conclusive since the structural properties of this amino acid offer a comparison with the canonical Phe or the non-canonical Cha. Nevertheless, the hydrophobicity study carried out first already illustrated that F<sup>5</sup>-Cha **131** features high polarity within its side chain. Therefore, applying this building block in such hydrophobic sequences or regions of peptides may be out of place. F<sup>5</sup>-Cha **131** should instead be viewed as a sterically demanding variant of polar amino acids, such as lysine and glutamic acid, and used accordingly.

## 8 Experimental Section

This part will describe the experiments performed in the scope of the unpublished section. The experimental protocols used in the context of the published results can be found in the experimental sections of the respective publications (*Section 6*).

### 8.1 General information

High-resolution mass spectra (HRMS) of the synthesized peptides were measured on an Agilent 6220 ESI-TOF MS instrument (Agilent Technologies, Santa Clara, CA, U.S.A.) using a spray voltage of 4 kV and adjusting the desolvation gas to 15 psi. The peptides, dissolved in MeCN/H<sub>2</sub>O, were injected into the spray chamber using a syringe pump with flow rates of 45  $\mu$ L/min. Other parameters were adjusted for maximal abundance of [M+H]<sup>+</sup>, [M+Na]<sup>+</sup>, or [M+K]<sup>+</sup>. Milli-Q Advantage A10 Ultrapure Water Purification System (Millipore, Billerica, MA, U.S.A.) was used to obtain deionized water. Other chemicals were purchased from commercial sources and used without additional purification.

#### Peptide synthesis

Peptides were prepared using the Liberty Blue automated microwave-assisted peptide synthesizer (CEM Corporation, Mathews, NC, USA). Aib-rich peptides were synthesized on a Cl-MPA ProTide (LL) resin (0.22 mmol/g resin substitution), and  $\beta$ -hairpin peptides were prepared on a Rink amide (LL) resin (0.30 mmol/g resin substitution). All peptides were synthesized on a 0.05 mmol scale. Detailed microwave-assisted SPPS conditions are summarized in *Table 8.1*. For Fmoc-deprotection, piperazine (10 wt%) dissolved in EtOH/NMP=1/9 (v/v) was used. Ethyl cyanohydroxyiminoacetate (Oxyma) and *N,N'*-diisopropylcarbodiimide (DIC) were used as coupling reagents. All amino acids were incorporated *via* single coupling. Cha **130** and F<sup>5</sup>-Cha **131** were introduced using only 1.5 equiv of the respective building blocks. This modified coupling cycle was established in our working group and uses prolonged microwave heating time (10 min) and additional washing steps.  $\beta$ -Hairpin peptides were capped with Ac<sub>2</sub>O/DIPEA/DMF=1:1:8 (5 mL) (3x 10 min). Full cleavage was performed using TFA/H<sub>2</sub>O/TIPS=95:2.5:2.5 (5 mL). The reaction mixture was shaken for 3 h at room temperature. Subsequently, the resin was washed with TFA (3x 5 mL) and CH<sub>2</sub>Cl<sub>2</sub> (3x 5 mL). Organic solvents were removed under reduced pressure, and the peptides were precipitated in ice-cold Et<sub>2</sub>O and centrifuged. The precipitate was washed with ice-cold Et<sub>2</sub>O (3x 5 mL) and centrifuged. The supernatant was removed, and the peptides were dissolved in water, lyophilized overnight, and purified *via* preparative HPLC.

Table 8.1: Conditions for microwave-assisted SPPS on a Liberty Blue peptide synthesizer (0.05 mmol scale).

		Reagents			Reaction Conditions		
		Name	Conc. [M]	Volume [mL]	Temp [°C]	Power [W]	Time [s]
Single Coupling	<b>Deprotection</b> (in EtOH/NMP= 1/9 (v/v))	Piperazine	10 wt%	2	75	155	15
		HOBt	0.1		90	30	60
	<b>Washing (4x)</b>	DMF	-	2	25	-	5
	<b>AA coupling</b> (in DMF)	Fmoc-AA-OH	0.2	1.25	75	217	15
		DIC	1				
		Oxyrna	1	0.25	90	43	225
		DIPEA	0.1				
<b>Washing (4x)</b>	DMF	-	2	25	-	5	
Coupling Cha/F <sup>5</sup> -Cha	<b>Deprotection (in EtOH/NMP= 1/9 (v/v))</b>	Piperazine	10 wt%	2	75	155	15
		HOBt	0.1		90	30	60
	<b>Washing (4-9 cycles)</b>	DMF	-	2	25	-	5
	<b>AA coupling</b> (in DMF)	Fmoc-(F)AA-OH	0.05	1.25	75	217	15
		DIC	1				
		Oxyrna	1	0.25	90	43	585
		DIPEA	0.1				
<b>Washing (4x)</b>	DMF	-	2	25	-	5	

### Analytical HPLC

A Chromaster 600 bar DAD-System with CSM software (VWR/Hitachi, Darmstadt, Germany) was used for analytical HPLC measurements. The system works with a low-pressure gradient containing an HPLC-pump (5160) with a 6-channel solvent degasser, an organizer, an autosampler (5260) with a 100  $\mu\text{L}$  sample loop, a column oven (5310) and a diode array flow detector (5430). A Kinetex C18 column (5  $\mu\text{m}$ , 250  $\text{\AA}$   $\sim$  4.6 mm, Phenomenex®, Torrance, CA, USA) was used. Water and MeCN, both containing 0.1% (v/v) TFA, were used as eluents with a flow rate of 1  $\text{mL min}^{-1}$ . Sample detection occurred at 220 nm. The data analysis was performed using an EZ Chrom ELITE software (version 3.3.2, Agilent).

The hydrophobicity of fluorinated amino acids was estimated *via* an HPLC-based assay established by our group. The Fmoc-protected amino acids were dissolved in MeCN:H<sub>2</sub>O(0.1% TFA)=4:6 (0.1 mM), and the respective solution was subsequently filtered (0.2 mm pore size). A linear gradient MeCN:H<sub>2</sub>O=4:6 $\rightarrow$ 70:30, 30 min was used at room temperature, and each measurement was performed in triplicate. The obtained retention times were plotted against



the corresponding side chain van der Waals volumes. The van der Waals volumes were calculated according to Zhao *et al.*<sup>[278]</sup>

### Preparative HPLC

The obtained peptides were purified on a low pressure HPLC system (Knauer GmbH, Berlin, Germany) sold by VWR (Darmstadt, Germany). The system works with a LaPrep Sigma preparative pump (LP1200), a ternary low-pressure gradient, a dynamic mixing chamber, a 6-port-3-channel injection valve with an automated preparative 10 mL sample loop, a LaPrep Sigma standard 1-channel-UV-detector (LP3101), a flow cell with 0.5 mm thickness and a 16-port LaPrep Sigma fractionation valve (LP2016). A Kinetex RP C18 end-capped (5  $\mu$ M, 100 Å, 250  $\times$  21.2 mm, Phenomenex, U.S.A.) HPLC-column was used. An additional precolumn (Security Guard<sup>TM</sup> PREP Cartridge Holder Kit (21.20 mm, ID, Phenomenex, U.S.A.)) was used to protect the main column. Water and MeCN, both containing 0.1% (v/v) TFA, were used as eluents. During the runs, a flow rate of 15 mL min<sup>-1</sup> was applied, and the compound detection occurred at 220 nm.

### Circular dichroism

Circular dichroism measurements were carried out on a Jasco J-810 spectropolarimeter using a quartz cuvette of 0.1/1 mm path length at 20 °C. A JACSO PFD-350S Peltier element was used for temperature control. Each shown CD value displays the mean of at least three independent measurements. The data were collected at 0.2 nm intervals, 2 nm bandwidth, and 2 s response time using a nitrogen flow rate of 3.5 L min<sup>-1</sup>. The spectra were recorded in the far-UV range (250–190 nm), and the signals of the blank solvent were subtracted. To normalize ellipticity  $\theta_{\text{Obs}}$  into molar ellipticity per residue, the following formula was used:  $[\theta] = \theta_{\text{Obs}}/10000 \text{ l N c}$  with  $l$  = path length [cm],  $N$  = number of residues,  $c$  = concentration [mol L<sup>-1</sup>].

## 8.2 Peptide synthesis and characterization

### H-Aib-Cha-peptide-OH **132a**



H-Aib-Cha-peptide-OH **132a** was prepared according to the general procedure described in *Section 8*. The desired product was obtained in sufficient purity and used without further purification (23 mg, 55%).

### Boc-Aib-Cha-peptide-OMe **134a**



Crude H-Aib-Cha-peptide-OH **132a** (23 mg, 0.028 mmol, 1.0 equiv.) was dissolved in MeOH (200  $\mu\text{L}$ ), and TMSCl (7.11  $\mu\text{L}$ , 0.056 mmol, 2.0 equiv.) was added. The reaction mixture was stirred at 23 °C for 2 h. The progress of the reaction was monitored by analytical HPLC. After the finished reaction, the solvent was removed under reduced pressure, and the crude product was used without additional purification steps. The peptide ester **133a** was dissolved in THF/H<sub>2</sub>O=2.4:1 (1 mL). Subsequently, Boc<sub>2</sub>O (14.7 mg, 0.067 mmol, 2.4 equiv.) and NaHCO<sub>3</sub> (9.4 mg, 0.11 mmol, 4.0 equiv.) were added to the solution. The reaction solution was stirred for 16 h at 23 °C. Afterwards, the solvent was removed under reduced pressure, and the respective crude product was purified by preparative HPLC (MeOH:H<sub>2</sub>O(0.1% TFA)=60:40→100:0, 18 min). The desired product **134a** was obtained as colorless powder (23 mg, 48%).

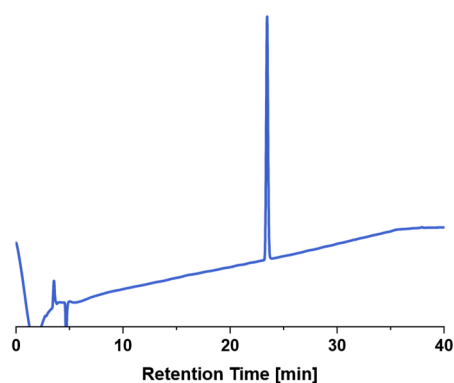


Figure 8.1: HPLC chromatogram of purified **134a** (MeOH:H<sub>2</sub>O (0.1% TFA (v/v))=60:40→100:0, 40 min).

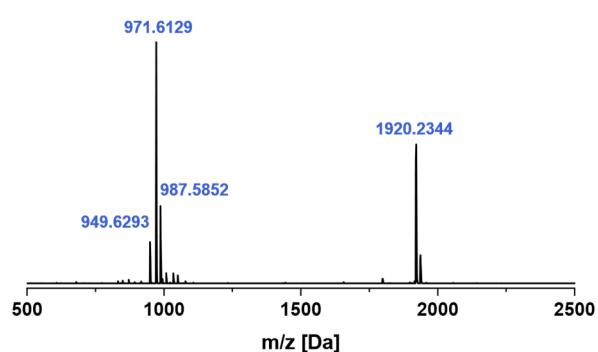
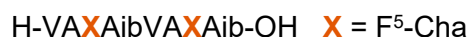


Figure 8.2: Mass spectrum of **134a**.

Table 8.2: Calculated and obtained masses for **134a**.

	Theoretical Mass [Da]	Experimental Mass [Da]
[M+H] <sup>+</sup>	949.6340	949.6293
[M+Na] <sup>+</sup>	971.6159	971.6129
[M+K] <sup>+</sup>	987.7243	987.5852
[2M+Na] <sup>+</sup>	1920.2418	1920.2344

### H-Aib-F<sup>5</sup>-Cha-peptide-OH **132b**



H-Aib-F<sup>5</sup>-Cha-peptide-OH **132b** was prepared according to the general procedure described in *Section 8*. The desired product was obtained in sufficient purity and used without further purification (21 mg, 42%).

### Boc-Aib-F<sup>5</sup>-Cha-peptide-OMe **134b**



Crude H-Aib-F<sup>5</sup>-Cha-peptide-OH **132b** (21 mg, 0.021 mmol, 1.0 equiv.) was dissolved in MeOH (180  $\mu\text{L}$ ), and TMSCl (5.33  $\mu\text{L}$ , 0.042 mmol, 2.0 equiv.) was added. The reaction mixture was stirred at 23 °C for 2 h. The progress of the reaction was monitored by analytical HPLC. After finished reaction, the solvent was removed under reduced pressure, and the crude product was used without additional purification steps. The peptide ester **133b** was dissolved in THF/H<sub>2</sub>O=2.4:1 (1 mL). Subsequently, Boc<sub>2</sub>O (11.0 mg, 0.05 mmol, 2.4 equiv.) and NaHCO<sub>3</sub> (7.1 mg, 0.084 mmol, 4.0 equiv.) were added to the solution. The reaction solution was stirred for 16 h at 23 °C. Afterwards, the solvent was removed under reduced pressure, and the respective crude product was purified by preparative HPLC (MeOH:H<sub>2</sub>O(0.1% TFA)=60:40→100:0, 18 min). The desired product **134b** was obtained as colorless powder (14.7 mg, 26%).

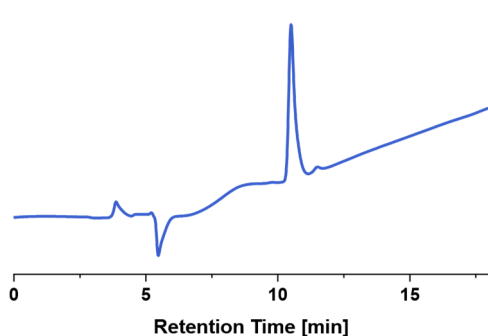


Figure 8.3: HPLC chromatogram of **134b** (MeOH:H<sub>2</sub>O (0.1% TFA (v/v))=70:30→100:0, 18 min).

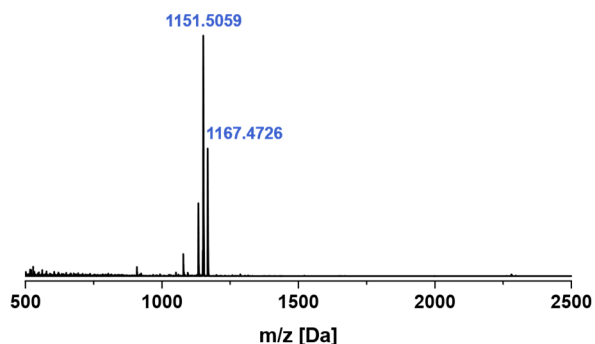


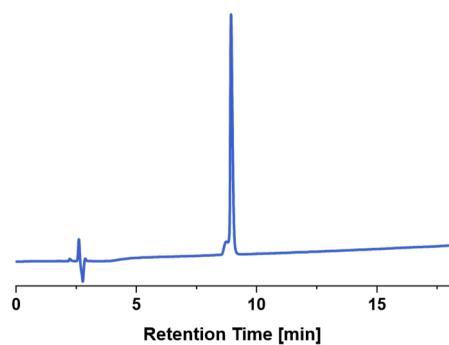
Figure 8.4: Mass spectrum of **134b**.

Table 8.3: Calculated and obtained masses for **134b**.

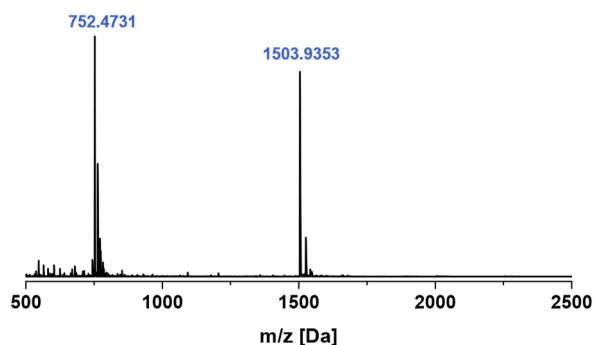
	Theoretical Mass [Da]	Experimental Mass [Da]
[M+Na] <sup>+</sup>	1151.5215	1151.5059
[M+K] <sup>+</sup>	1167.6300	1167.4726

**Ac- $\beta$ -hairpin-Cha-peptide-NH<sub>2</sub> 139a**

Ac- $\beta$ -hairpin-Cha-peptide-NH<sub>2</sub> **139a** was prepared according to the general procedure described in *Section 8*. The desired peptide was purified *via* preparative HPLC (MeCN:H<sub>2</sub>O (0.1% TFA)=20:90 $\rightarrow$ 70:30, 18 min). The product was lyophilized and was subsequently obtained as a colorless powder (23 mg, 28%).



*Figure 8.5:* HPLC chromatogram of purified **139a** (MeCN:H<sub>2</sub>O (0.1% TFA (v/v))=20:80 $\rightarrow$ 70:30, 18 min).



*Figure 8.6:* Mass spectrum of **139a**.

*Table 8.3:* Calculated and obtained masses for **139a**.

	<i>Theoretical Mass [Da]</i>	<i>Experimental Mass [Da]</i>
<b>+1</b>	1503.9264	1503.9353
<b>+2</b>	752.4592	752.4731

**Ac-β-hairpin-F<sup>5</sup>-Cha-peptide-NH<sub>2</sub> 139b**



Ac-β-hairpin-F<sup>5</sup>Cha-peptide-NH<sub>2</sub> **139b** was prepared according to the general procedure described in Section 8. The desired peptide was purified *via* preparative HPLC (MeCN:H<sub>2</sub>O (0.1% TFA)=20:90→70:30, 18 min). The product was lyophilized and was subsequently obtained as a colorless powder (17 mg, 20%).

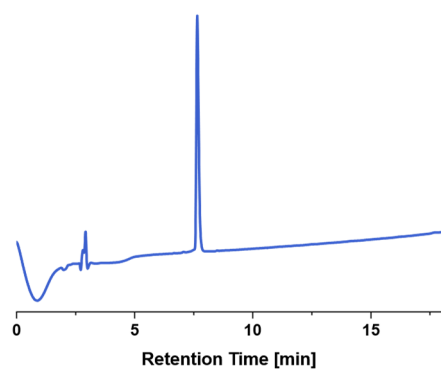


Figure 8.7: HPLC chromatogram of purified **139b** (MeCN:H<sub>2</sub>O (0.1% TFA (v/v))=20:80→70:30, 18 min).

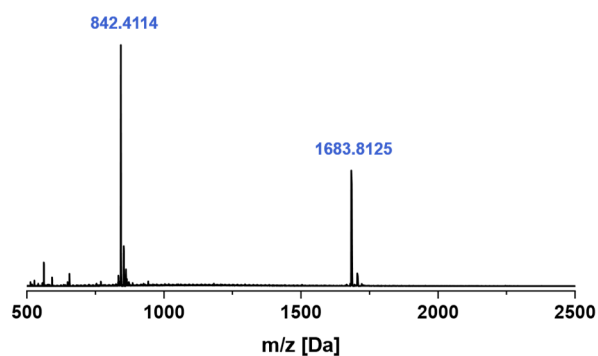


Figure 8.8: Mass spectrum of **139b**.

Table 8.4: Calculated and obtained masses for **139b**.

	<i>Theoretical Mass [Da]</i>	<i>Experimental Mass [Da]</i>
<b>+1</b>	1683.8322	1683.8125
<b>+2</b>	842.4121	842.4114

## 9 Summary and Outlook

Per- and polyfluorinated systems can provide a set of unique properties highly relevant to the fields of bioorganic chemistry, medicinal chemistry, and material sciences. Despite this, peptides containing large amounts of fluorinated building blocks are vastly uncharted. In this doctoral thesis, the first approaches have been made to close this gap (*Figure 9.1*). To enable the studies of highly fluorinated peptides, a synthetic strategy for preparing a variety of aliphatic fluorinated amino acids on a gram-scale was first developed. Unrestricted access to these building blocks allowed the synthesis and characterization of peptides composed almost exclusively of fluorinated amino acids (“fluoropeptides”). The main emphasis was placed on the structural properties within hydrophobic environments and the proteolytic stability of this new class of peptides. In addition, the novel synthesis of fluorinated valine and isoleucine derivatives permitted the investigation of the highly fluorinated coiled coil peptides in a combinatorial manner, which has not been conducted previously. The trends revealed in this study can be employed to predict and control assembly processes between coiled coil peptides utilizing selected fluorinated amino acids. Additionally, the structural properties of the novel Janus-faced fluorinated cyclohexylalanine amino acid were investigated in the context of helix- and  $\beta$ -hairpin-forming peptide models.

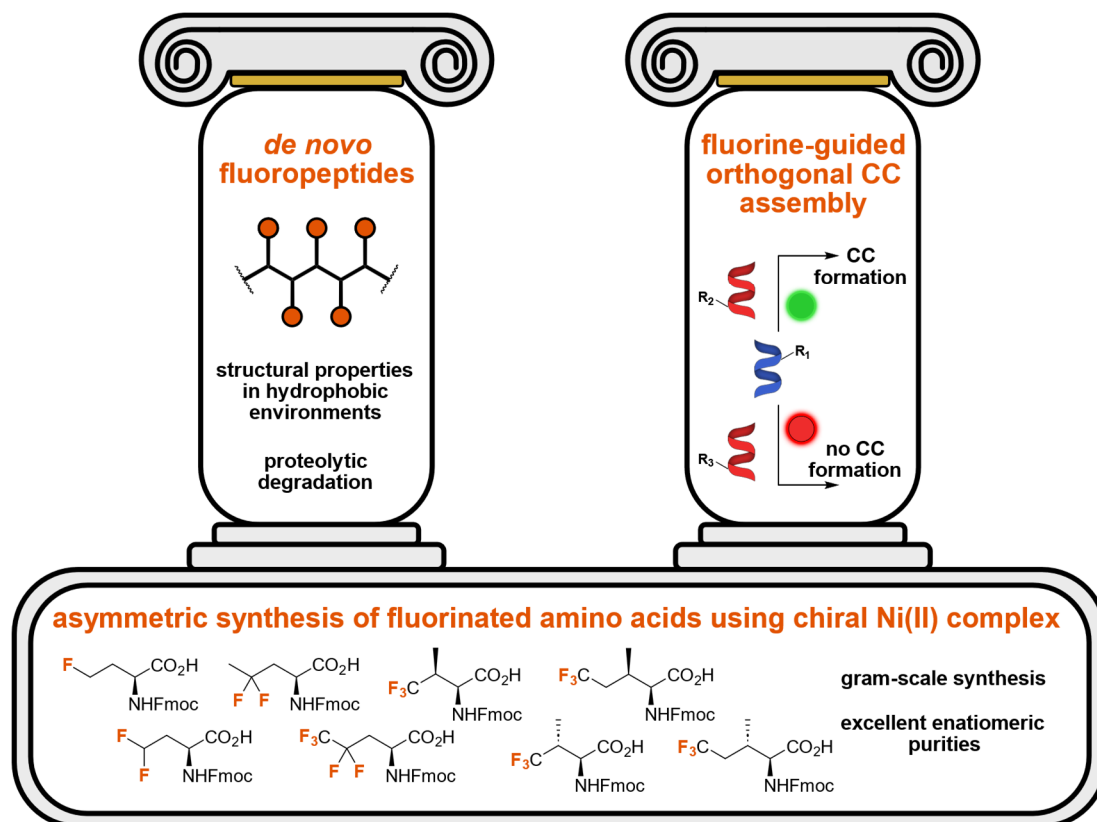


Figure 9.1: Overview of the three projects studied in this Ph. D. work.

In the following, the corresponding projects will be summarized, and possible future developments will be outlined.

### **Gram-scale asymmetric synthesis of fluorinated amino acids using a chiral nickel(II) complex**

*Summary:* Fluorinated amino acids are potent tools in the context of peptide and protein engineering. Various intrinsic properties of fluorinated amino acids, such as  $\alpha$ -helix propensity and hydrophobicity, play a vital role in this process. Still, the synthesis of these precious building blocks can be challenging. The described strategies are mostly multi-step syntheses that require several chromatographic purification steps and yield the desired products on a milligram scale.

This work presents a two-step synthesis to access a broad range of aliphatic Fmoc-protected fluorinated amino acids. The described approach is based on the chiral Ni(II) Schiff base complex **112**. In the first step of the synthetic protocol, the Ni(II) complex **112** was alkylated with high diastereoselectivities. The stereochemistry of several alkylated Ni(II) complexes was characterized by X-ray crystallography and 1D NOESY measurements. After hydrolysis and subsequent Fmoc-protection, the fluorinated amino acids were obtained. Mono-, di-, pentafluorinated, and fluorinated  $\beta$ -branched amino acids were synthesized on a gram-scale with high enantiomeric purities, illustrating the variety of fluorinated amino acids that can be generated by this method. In this context, the first synthesis of the Fmoc-protected version of pentafluorinated norvaline derivative and its application in SPPS was described. Furthermore, a strategy to obtain fluorinated alkyl iodides, key substrates in the synthesis described above, was presented. Finally, synthesized fluorinated amino acids were characterized by their hydrophobicity and  $\alpha$ -helix propensity.

*Outlook:* First, this method can be further expanded to synthesize various fluorinated amino acids. For example,  $\gamma$ -branched aliphatic fluorinated amino acids, such as (2*S*,4*S*)-trifluoroleucine **28** and (2*S*,4*R*)-trifluoroleucine **29**, different fluorinated versions of phenylalanine with a particular focus on CF<sub>3</sub>-containing analogs (**140** and **141**), and fluorinated methionine derivatives might be exciting targets (*Figure 9.2, a.*). Furthermore, fluorinated amino acids with additional functionalities would pose a particular challenge. The respective synthetic strategies would require an introduction of side-chain protecting groups to produce building blocks suitable for SPPS. In this context, difluoroaspartic acid (DfAsp) is an intriguing candidate. Introducing the respective protecting group, such as the allyl group, could occur either at the complex **142**, after hydrolysis **143**, or after Fmoc-protection of the amine functionality **144** (*Figure 9.2, b.*).

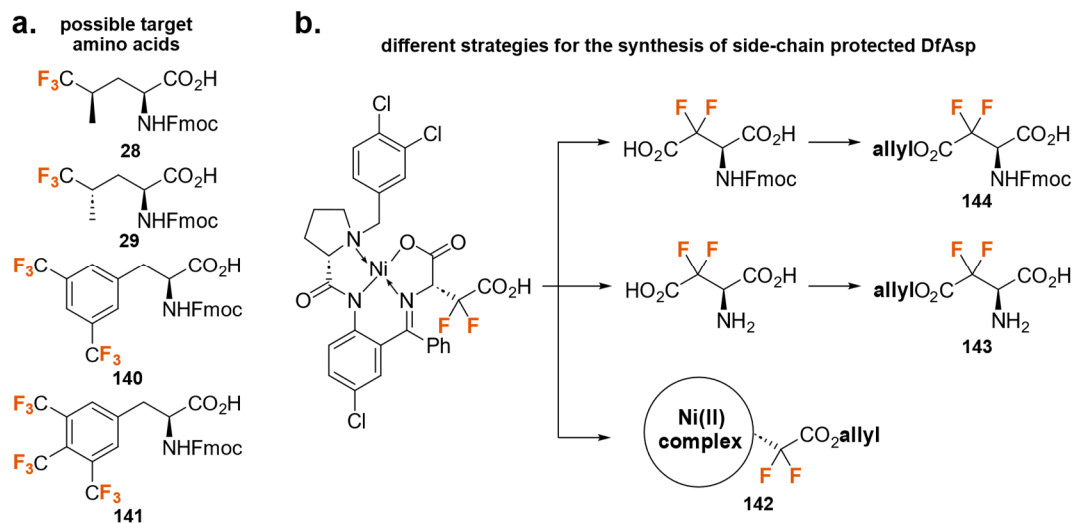


Figure 9.2: a. New fluorinated amino acids of interest. b. Different proposed strategies for the synthesis of DfAsp.

Finally, studies focusing on the Ni(II) complex could be performed. The Soloshonok complex **112** displayed excellent diastereoselectivities in the corresponding alkylation reactions, but the yields could be further improved. Other ligands, such as the Hamari ligand, might be explored as potential modifications to enhance the reactivities in synthesizing fluorinated amino acids.



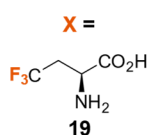
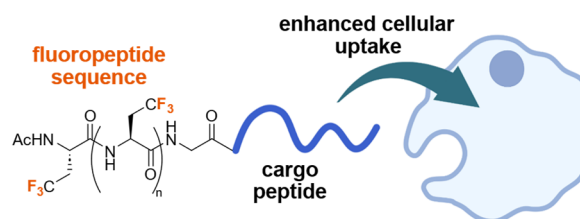
### **Introducing aliphatic fluoro-peptides: perspectives on folding properties, membrane partition and proteolytic stability**

*Summary:* Depending on the nature of the fluorinated amino acids, introducing these building blocks can direct hydrophobicity, secondary structure formation, proteolytic stability, or modify the bioactivity. Nevertheless, despite a tremendous amount of research in the last two decades, peptides consisting exclusively of fluorinated amino acids have yet to be described.

In this work, a new class of fluoro-peptides built by fluorinated aliphatic amino acids is presented. The structural properties of these peptide foldamers were studied regarding the degree of fluorination and the peptide length. Structural investigations revealed a fluorine-induced  $\beta$ -strand to  $\alpha$ -helix transition in the presence of micelles or liposomes. In the instance of TfeGly-derived fluoro-peptides, an unusual formation of PPII helix was observed. The insertion of fluoro-peptides into POPC:POPG unilamellar vesicles was further studied using a combination of CD, SEIRAS, and fluorescence-based leakage assays. Furthermore, this work presented the first study on the proteolytic stability of peptide sequences consisting exclusively of fluorinated amino acids. Unexpectedly, all sequences were enzymatically degraded regardless of the degree of fluorination. Hence, the fluoro-peptides presented in this work could play an intriguing role in developing fluorinated peptide-based biomaterials.

*Outlook:* One of the pivotal aspects of the revealed structural properties of fluoro-peptides is the intrinsic tendency of the trifluorinated systems to form a PPII helix. However, data is based solely on CD measurements, and these new structures must be analyzed further. Different strategies can be employed to study the respective structural preferences in more detail. First, the length of TfeGly-containing peptides could be reduced to significantly improve the compound's solubility. This would allow structural investigations at higher concentrations *via* NMR spectroscopy. Determination of  $^3J_{\alpha\text{HN}}$  coupling constants and additional NOESY measurements should provide enough information to determine the conformational composition of TfeGly oligomers. Furthermore, the spatial proximity of  $\text{CF}_3$ -groups in an  $\alpha$ -helical structure was suggested as the main driving force for destabilizing the corresponding conformation. Two TfeGly **19** residues could be introduced at different distances from each other into an  $\alpha$ -helical model peptide to investigate this hypothesis (*Figure 9.3, a.*). Molar ellipticity values at 222 nm, obtained *via* CD studies, would reflect the helical fraction of the respective peptides. The peptide with both TfeGly residues in  $i, i+4$  distance should display the lowest helical fraction value since both  $\text{CF}_3$ -groups would be placed in the shortest distance possible.

**a. proposed peptide sequences**Ac YGGKAAA **XX**AAAAKAAAAK NH<sub>2</sub>Ac YGGKAAA **XX**XAAAKAAAAK NH<sub>2</sub>Ac YGGKAAA **XAA**XAAKAAAAK NH<sub>2</sub>Ac YGGKAAA **XAAA**XAKAAAAK NH<sub>2</sub>

**CD measurements**  
(ellipticity at 222 nm )
**b. fluoropeptides for cytosolic delivery**

*Figure 9.3:* a. Proposed sequences to study TfeGly-containing  $\alpha$ -helical peptides. b. Fluoropeptide sequence attached to a cargo peptide to improve cytosolic delivery. Created with BioRender®.

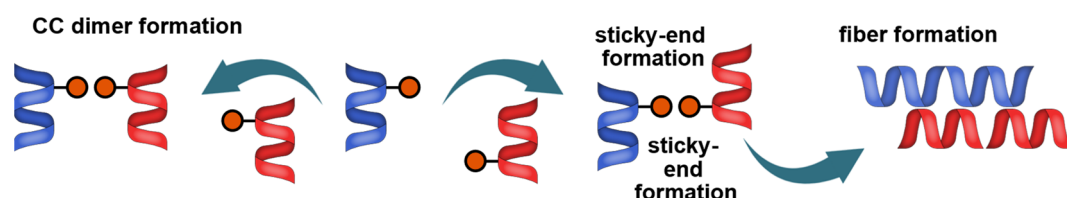
Additionally, the potential of fluoropeptide sequences should be studied in the context of cytosolic delivery (*Figure 9.3, b.*). For example, polyfluorinated alkyl chains of cargo peptides could be exchanged by fluoropeptide sequences focusing on the respective cell permeability. Otherwise, co-block peptides consisting of a fluoropeptide and a polar sequence could be investigated in this context. Alternatively, a polymer backbone, such as PEG, could replace the hydrophilic sequence. Subsequently, the ability of these models to serve as cargo systems for cytosolic delivery should be studied.

## Establishing fluorine containing amino acids as an orthogonal tool in coiled coil assembly

**Summary:** The  $\alpha$ -helical CC is an exceptionally well-studied and widely applied protein motif with potential applications including regulation of protein-protein interactions, intracellular transport, and formation of supramolecular structures. Specifically for the last topic, the rational control over assembly processes between individual coiled coil peptides is crucial.

This work demonstrated that peptide self-assembly can be directed using different fluorinated amino acids at the hydrophobic core positions of the CC primary structure. In the first part of this study, the interactions between CC peptides containing different fluorinated building blocks were investigated, applying a combinatorial approach. By examining each combination *via* CD, SEC, and FRET measurements, important information was obtained on each pair's thermal stability, oligomerization state, and orientation. These data were used to design fluorine-guided orthogonal coiled coil assembly rationally. The formation of coiled-coil dimers can be induced and prevented by choosing a specific fluorinated amino acid. In addition, the selective formation of specific pairs could be observed when up to eight different CC peptides were combined. This work introduces fluorinated amino acids as an additional tool to direct peptide self-assembly, expanding the possibilities for the design and control of supramolecular structure formation.

**Outlook:** An obvious continuation of this project would be using the identified fluorine-based assembly behavior in forming supramolecular structures (*Figure 9.4*). For this purpose, a CC, which assembles into higher-ordered structures by fluorine-directed interactions, could be designed. Again, a parallel heterodimeric system might be used, introducing fluorinated amino acids at specific heptads of the respective hydrophobic core. By choosing the suitable combination, fluorinated heptads could preferably interact with each other, producing sticky ends and subsequently driving the formation of a fibrillar structure. This study would be the first example of a rationality-designed CC-based fiber-forming peptide, which assembles into higher-ordered structures exclusively by fluorine-guided interactions.



*Figure 9.4:* The proposed mechanism for the formation of CC-based fibres. Created with BioRender®.

Furthermore, a comparable study could be performed, investigating fluorinated derivatives of leucine at positions *d* of a heterodimeric CC motif in a combinatorial manner. Residues at positions *d* point directly into the hydrophobic interior and should display stronger direct interactions with each other.

### **Properties of all-cis pentafluorinated cyclohexylalanine in different peptide environments**

*Summary:* Janus-faced fluorinated cyclohexane molecules are fascinating compounds with unique properties. In this project, the properties of F<sup>5</sup>-Cha **131** were investigated in the context of two peptide models. First, a helical Aib-rich sequence was utilized, which was previously used to study aromatic-aromatic interactions *via* X-ray diffraction. In this case, phenylalanine residues were substituted by F<sup>5</sup>-Cha **131**, and the isolated peptide was submitted to different crystallization conditions. Additionally, F<sup>5</sup>-Cha **131** residues were incorporated into a  $\beta$ -hairpin motif and compared with the non-fluorinated Cha-containing analog. Both residues displayed the potential to stabilize the  $\beta$ -hairpin structure. Furthermore, the conformational properties were studied in the presence of various cations. Finally, an HPLC-based hydrophobicity study revealed that F<sup>5</sup>-Cha **131** is significantly less hydrophobic than the non-fluorinated derivative. Remarkably, the last observation strongly suggests that despite the steric demand of this building block, F<sup>5</sup>-Cha **131** should be viewed as a polar residue and, therefore, utilized in less hydrophobic environments.

*Outlook:* As already thoroughly discussed in the scope of this thesis, coiled coil peptides provide a powerful model for studying intermolecular interactions. In a CC motif, the polar amino acids play a crucial role in the positions *e* and *g*, stabilizing the structure and ensuring the selectivity of the respective interactions. F<sup>5</sup>-Cha **131** residue could be an exciting building block to engineer the polar interactions between the positions *e* and *g* of the corresponding CC motif. First, the large size of F<sup>5</sup>-Cha **131** could significantly affect the oligomerization state of the CC motif. Furthermore, since F<sup>5</sup>-Cha **131** should only interact with itself, this building block could be a powerful tool to fine-tune the selectivity between CC-forming peptides. Depending on the position of the F<sup>5</sup>-Cha **131** residue, CC formation could be switched on and off. Due to its unique structural and electrostatic properties, F<sup>5</sup>-Cha **131** could be a precise tool to direct peptide-peptide interactions in the cosmos of highly diverse but often unspecific intermolecular interactions.

## 10 Bibliography

- [1] J. Dumas, E. Peligot, *Ann. Pharm.* **1835**, *15*, 1–60.
- [2] A. Tressaud, *Angew. Chem. Int. Ed.* **2006**, *45*, 6792–6796.
- [3] R. Britton, V. Gouverneur, J.-H. Lin, M. Meanwell, C. Ni, G. Pupo, J.-C. Xiao, J. Hu, *Nat. Rev. Methods Primers* **2021**, *1*, 47.
- [4] P. Kirsch, in *Modern Fluoroorganic Chemistry* (Eds.: P. Kirsch), Wiley-VCH Verlag GmbH & Co. KGaA, Weinheim, Germany, **2013**, pp. 1–24.
- [5] R. D. Chambers, in *Fluorine in Organic Chemistry* (Eds.: R. D. Chambers), Blackwell Publishing Ltd, Oxford, UK, **2004**, pp. 1–22.
- [6] M. Inoue, Y. Sumii, N. Shibata, *ACS Omega* **2020**, *5*, 10633–10640.
- [7] J. Han, L. Kiss, H. Mei, A. M. Remete, M. Ponikvar-Svet, D. M. Sedgwick, R. Roman, S. Fustero, H. Moriwaki, V. A. Soloshonok, *Chem. Rev.* **2021**, *121*, 4678–4742.
- [8] D. B. Harper, D. O'Hagan, *Nat. Prod. Rep.* **1994**, *11*, 123–133.
- [9] C. Dong, F. Huang, H. Deng, C. Schaffrath, J. B. Spencer, D. O'Hagan, J. H. Naismith, *Nature* **2004**, *427*, 561–565.
- [10] Y. Pan, *ACS Med. Chem. Lett.* **2019**, *10*, 1016–1019.
- [11] A. A. Berger, J. S. Völler, N. Budisa, B. Koksich, *Acc. Chem. Res.* **2017**, *50*, 2093–2103.
- [12] M. Salwiczek, E. K. Nyakatura, U. I. M. Gerling, S. Ye, B. Koksich, *Chem. Soc. Rev.* **2012**, *41*, 2135–2171.
- [13] J. M. Monkovic, H. Gibson, J. W. Sun, J. K. Montclare, *Pharmaceuticals* **2022**, *15*, 1201.
- [14] N. Wiberg, in *Lehrbuch Der Anorganischen Chemie* (Ed.: A.F. Holleman), De Gruyter, Berlin, Germany, **2008**, pp. 112–185.
- [15] N. Wiberg, in *Lehrbuch Der Anorganischen Chemie* (Ed.: A.F. Holleman), De Gruyter, Berlin, Germany, **2008**, pp. 2143–2153.
- [16] N. Wiberg, in *Lehrbuch Der Anorganischen Chemie* (Ed.: A.F. Holleman), De Gruyter, Berlin, Germany, **2008**, pp. 312–416.
- [17] N. Wiberg, in *Lehrbuch Der Anorganischen Chemie* (Ed.: A.F. Holleman), De Gruyter, Berlin, Germany, **2008**, pp. 430–496.
- [18] C. Housecroft, A. Sharpe, in *Inorganic Chemistry* (Ed.: C. Housecroft, A. Sharpe), Pearson International, London, UK, **2018**, pp. 75–105.
- [19] D. O'Hagan, *Chem. Soc. Rev.* **2008**, *37*, 308–319.
- [20] H. V Phan, J. R. Durig, *J. Mol. Struct.: THEOCHEM* **1990**, *209*, 333–347.
- [21] R. J. Abraham, A. D. Jones, M. A. Warne, R. Rittner, C. F. Tormena, *J. Chem. Soc., Perkin Trans. 2* **1996**, 533–539.

- 
- [22] B. J. van der Veken, S. Truyen, W. A. Herrebout, G. Watkins, *J. Mol. Struct.* **1993**, *293*, 55–58.
- [23] J. W. Banks, A. S. Batsanov, J. A. K. Howard, D. O'Hagan, H. S. Rzepa, S. Martin-Santamaria, *J. Chem. Soc., Perkin Trans. 2* **1999**, 2409–2411.
- [24] C. Thiehoff, Y. P. Rey, R. Gilmour, *Isr. J. Chem.* **2017**, *57*, 92–100.
- [25] J. J. Irwin, T.-K. Ha, J. D. Dunitz, *Helv. Chim. Acta* **1990**, *73*, 1805–1817.
- [26] D. Christen, H.-G. Mack, S. Rüdiger, H. Oberhammer, *J. Am. Chem. Soc.* **1996**, *118*, 3720–3723.
- [27] D. O'Hagan, C. Bilton, J. A. K. Howard, L. Knight, D. J. Tozer, *J. Chem. Soc., Perkin Trans. 2* **2000**, 605–607.
- [28] C. R. S. Briggs, D. O'Hagan, H. S. Rzepa, A. M. Z. Slawin, *J. Fluor. Chem.* **2004**, *125*, 19–25.
- [29] C. Thiehoff, M. C. Holland, C. Daniliuc, K. N. Houk, R. Gilmour, *Chem. Sci.* **2015**, *6*, 3565–3571.
- [30] D. C. Lankin, N. S. Chandrakumar, S. N. Rao, D. P. Spangler, J. P. Snyder, *J. Am. Chem. Soc.* **1993**, *115*, 3356–3357.
- [31] A. Sun, D. C. Lankin, K. Hardcastle, J. P. Snyder, *Chem. - Eur. J.* **2005**, *11*, 1579–1591.
- [32] N. E. J. Gooseman, D. O'Hagan, A. M. Z. Slawin, A. M. Teale, D. J. Tozer, R. J. Young, *Chem. Commun.* **2006**, 3190–3192.
- [33] D. C. Lankin, G. L. Grunewald, F. A. Romero, I. Y. Oren, J. P. Snyder, *Org. Lett.* **2002**, *4*, 3557–3560.
- [34] C. R. S. Briggs, M. J. Allen, D. O'Hagan, D. J. Tozer, A. M. Z. Slawin, A. E. Goeta, J. A. K. Howard, *Org. Biomol. Chem.* **2004**, *2*, 732–740.
- [35] N. E. J. Gooseman, D. O'Hagan, M. J. G. Peach, A. M. Z. Slawin, D. J. Tozer, R. J. Young, *Angew. Chem. Int. Ed.* **2007**, *46*, 5904–5908.
- [36] J. P. Lere-Porte, J. Petrissans, S. Gromb, *J. Mol. Struct.* **1977**, *40*, 159–166.
- [37] J. P. Lere-Porte, J. Petrissans, *J. Mol. Struct.* **1978**, *48*, 289–292.
- [38] A. Y. Meyer, *J. Mol. Struct.* **1978**, *49*, 383–394.
- [39] P. Klæboe, D. Powell, R. Stølevik, Ø. Vorren, O. Bastiansen, G. Braathen, L. Fernholt, G. Gundersen, C. Nielsen, B. Cyvin, S. Cyvin, *Acta Chem. Scand.* **1982**, *36a*, 471–484.
- [40] L.-G. Hammarström, T. Liljefors, J. Gasteiger, *J. Comput. Chem.* **1988**, *9*, 424–440.
- [41] D. Wu, A. Tian, H. Sun, *J. Phys. Chem. A* **1998**, *102*, 9901–9905.
- [42] M. Nicoletti, D. O'Hagan, A. M. Z. Slawin, *J. Am. Chem. Soc.* **2005**, *127*, 482–483.
- [43] L. Hunter, D. O'Hagan, A. M. Z. Slawin, *J. Am. Chem. Soc.* **2006**, *128*, 16422–16423.
- [44] L. Hunter, A. M. Z. Slawin, P. Kirsch, D. O'Hagan, *Angew. Chem. Int. Ed.* **2007**, *46*, 7887–7890.

- [45] L. Hunter, P. Kirsch, J. T. G. Hamilton, D. O'Hagan, *Org. Biomol. Chem.* **2008**, *6*, 3105–3108.
- [46] L. Hunter, D. O'Hagan, *Org. Biomol. Chem.* **2008**, *6*, 2843–2848.
- [47] L. Hunter, P. Kirsch, A. M. Z. Slawin, D. O'Hagan, *Angew. Chem. Int. Ed.* **2009**, *48*, 5457–5460.
- [48] D. O'Hagan, *J. Org. Chem.* **2012**, *77*, 3689–3699.
- [49] N. Santschi, R. Gilmour, *Nat. Chem.* **2015**, *7*, 467–468.
- [50] A. J. Durie, A. M. Z. Slawin, T. Lebl, P. Kirsch, D. O'Hagan, *Chem. Commun.* **2011**, *47*, 8265–8267.
- [51] A. J. Durie, A. M. Z. Slawin, T. Lebl, P. Kirsch, D. O'Hagan, *Chem. Commun.* **2012**, *48*, 9643–9645.
- [52] A. J. Durie, A. M. Z. Slawin, T. Lebl, D. O'Hagan, *Angew. Chem. Int. Ed.* **2012**, *51*, 10086–10088.
- [53] N. S. Keddie, A. M. Z. Slawin, T. Lebl, D. Philp, D. O'Hagan, *Nat. Chem.* **2015**, *7*, 483–488.
- [54] Z. Fang, N. Al-Maharik, A. M. Z. Slawin, M. Bühl, D. O'Hagan, *Chem. Commun.* **2016**, *52*, 5116–5119.
- [55] C. J. Thomson, Q. Zhang, N. Al-Maharik, M. Bühl, D. B. Cordes, A. M. Z. Slawin, D. O'Hagan, *Chem. Commun.* **2018**, *54*, 8415–8418.
- [56] Z. Fang, D. B. Cordes, A. M. Z. Slawin, D. O'Hagan, *Chem. Commun.* **2019**, *55*, 10539–10542.
- [57] A. J. Durie, T. Fujiwara, R. Cormanich, M. Bühl, A. M. Z. Slawin, D. O'Hagan, *Chem. - Eur. J.* **2014**, *20*, 6259–6263.
- [58] M. S. Ayoub, D. B. Cordes, A. M. Z. Slawin, D. O'Hagan, *Org. Biomol. Chem.* **2015**, *13*, 5621–5624.
- [59] M. S. Ayoub, D. B. Cordes, A. M. Z. Slawin, D. O'Hagan, *Beilstein J. Org. Chem.* **2015**, *11*, 2671–2676.
- [60] T. Bykova, N. Al-Maharik, A. M. Z. Slawin, D. O'Hagan, *Org. Biomol. Chem.* **2016**, *14*, 1117–1123.
- [61] J. L. Clark, R. M. Neyyappadath, C. Yu, A. M. Z. Slawin, D. B. Cordes, D. O'Hagan, *Chem. - Eur. J.* **2021**, *27*, 16000–16005.
- [62] M. P. Wiesenfeldt, Z. Nairoukh, W. Li, F. Glorius, *Science* **2017**, *357*, 908–912.
- [63] M. P. Wiesenfeldt, T. Knecht, C. Schleppehorst, F. Glorius, *Angew. Chem. Int. Ed.* **2018**, *57*, 8297–8300.

- 
- [64] D. Moock, M. P. Wiesenfeldt, M. Freitag, S. Muratsugu, S. Ikemoto, R. Knitsch, J. Schneidewind, W. Baumann, A. H. Schäfer, A. Timmer, M. Tada, M. R. Hansen, F. Glorius, *ACS Catal.* **2020**, *10*, 6309–6317.
- [65] C. Yu, A. Kütt, G.-V. Rösenthaller, T. Lebl, D. B. Cordes, A. M. Z. Slawin, M. Bühl, D. O'Hagan, *Angew. Chem. Int. Ed.* **2020**, *59*, 19905–19909.
- [66] J. H. Simons, L. P. Block, *J. Am. Chem. Soc.* **1937**, *59*, 1407.
- [67] B. E. Smart, in *Organofluorine Chemistry: Principles and Commercial Applications* (Eds.: R.E. Banks, B.E. Smart, J.C. Tatlow), Springer US, Boston, MA, **1994**, pp. 57–88.
- [68] R. A. Cormanich, D. O'Hagan, M. Bühl, *Angew. Chem. Int. Ed.* **2017**, *56*, 7867–7870.
- [69] C. Bunn, E. R. Howells, *Nature* **1954**, *174*, 549–551.
- [70] E. K. Watkins, W. L. Jorgensen, *J. Phys. Chem. A* **2001**, *105*, 4118–4125.
- [71] D. A. Dixon, *J. Phys. Chem.* **1992**, *96*, 3698–3701.
- [72] G. D. Smith, R. L. Jaffe, D. Y. Yoon, *Macromolecules* **1994**, *27*, 3166–3173.
- [73] U. Röthlisberger, K. Laasonen, M. L. Klein, M. Sprik, *J. Chem. Phys.* **1996**, *104*, 3692–3700.
- [74] S. S. Jang, M. Blanco, W. A. Goddard, G. Caldwell, R. B. Ross, *Macromolecules* **2003**, *36*, 5331–5341.
- [75] J. A. Fournier, R. K. Bohn, Jr. Montgomery John A., M. Onda, *J. Phys. Chem. A* **2010**, *114*, 1118–1122.
- [76] B. E. Smart, *J. Fluor. Chem.* **2001**, *109*, 3–11.
- [77] Q. A. Huchet, B. Kuhn, B. Wagner, H. Fischer, M. Kansy, D. Zimmerli, E. M. Carreira, K. Müller, *J. Fluor. Chem.* **2013**, *152*, 119–128.
- [78] B. Linclau, Z. Wang, G. Compain, V. Paumelle, C. Q. Fontenelle, N. Wells, A. Weymouth-Wilson, *Angew. Chem. Int. Ed.* **2016**, *55*, 674–678.
- [79] A. Rodil, S. Bosisio, M. S. Ayoup, L. Quinn, D. B. Cordes, A. M. Z. Slawin, C. D. Murphy, J. Michel, D. O'Hagan, *Chem. Sci.* **2018**, *9*, 3023–3028.
- [80] A. L. Henne, C. J. Fox, *J. Am. Chem. Soc.* **1951**, *73*, 2323–2325.
- [81] K.-U. Goss, *Environ. Sci. Technol.* **2008**, *42*, 456–458.
- [82] M. Morgenthaler, E. Schweizer, A. Hoffmann-Röder, F. Benini, R. E. Martin, G. Jaeschke, B. Wagner, H. Fischer, S. Bendels, D. Zimmerli, J. Schneider, F. Diederich, M. Kansy, K. Müller, *ChemMedChem* **2007**, *2*, 1100–1115.
- [83] J. D. Dunitz, R. Taylor, *Chem. - Eur. J.* **1997**, *3*, 89–98.
- [84] D. D. DesMarteau, Z. Q. Xu, M. Witz, *J. Org. Chem.* **1992**, *57*, 629–635.
- [85] K.-T. Wei, D. L. Ward, *Acta Crystallogr., Sect. B: Struct. Sci., Cryst. Eng. Mater.* **1976**, *32*, 2768–2773.



- [86] J. D. Dunitz, *ChemBioChem* **2004**, *5*, 614–621.
- [87] W. Caminati, S. Melandri, P. Moreschini, P. G. Favero, *Angew. Chem. Int. Ed.* **1999**, *38*, 2924–2925.
- [88] T. J. Barbarich, C. D. Rithner, S. M. Miller, O. P. Anderson, S. H. Strauss, *J. Am. Chem. Soc.* **1999**, *121*, 4280–4281.
- [89] H.-J. Schneider, *Chem. Sci.* **2012**, *3*, 1381–1394.
- [90] P. A. Champagne, J. Desroches, J.-F. Paquin, *Synthesis* **2015**, *47*, 306–322.
- [91] R. E. Rosenberg, *J. Phys. Chem. A* **2016**, *120*, 7519–7528.
- [92] R. E. Rosenberg, *J. Phys. Chem. A* **2018**, *122*, 4521–4529.
- [93] R. E. Rosenberg, B. K. Chapman, R. N. Ferrill, E. S. Jung, C. A. Samaan, *J. Phys. Chem. A* **2020**, *124*, 3851–3858.
- [94] V. Mzozoyana, F. R. van Heerden, C. Grimmer, *Beilstein J. Org. Chem.* **2020**, *16*, 190–199.
- [95] C. R. Pitts, M. A. Siegler, T. Lectka, *J. Org. Chem.* **2017**, *82*, 3996–4000.
- [96] A. J. Peloquin, D. A. Kure, A. R. Jennings, C. D. McMillen, S. T. Iacono, W. T. Pennington, *Cryst. Growth. Des.* **2020**, *20*, 5484–5492.
- [97] M. G. Holl, C. R. Pitts, T. Lectka, *Angew. Chem. Int. Ed.* **2018**, *57*, 2758–2766.
- [98] M. T. Scerba, C. M. Leavitt, M. E. Diener, A. F. DeBlase, T. L. Guasco, M. A. Siegler, N. Bair, M. A. Johnson, T. Lectka, *J. Org. Chem.* **2011**, *76*, 7975–7984.
- [99] C. D. Sessler, M. Rahm, S. Becker, J. M. Goldberg, F. Wang, S. J. Lippard, *J. Am. Chem. Soc.* **2017**, *139*, 9325–9332.
- [100] J. A. Erickson, J. I. Mcloughlin, *J. Org. Chem.* **1995**, *60*, 1626–1631.
- [101] Y. Zafrani, D. Yeffet, G. Sod-Moriah, A. Berliner, D. Amir, D. Marciano, E. Gershonov, S. Saphier, *J. Med. Chem.* **2017**, *60*, 797–804.
- [102] Y. Zafrani, G. Sod-Moriah, D. Yeffet, A. Berliner, D. Amir, D. Marciano, S. Elias, S. Katalan, N. Ashkenazi, M. Madmon, E. Gershonov, S. Saphier, *J. Med. Chem.* **2019**, *62*, 5628–5637.
- [103] J. P. Shanahan, D. M. Mullis, M. Zeller, N. K. Szymczak, *J. Am. Chem. Soc.* **2020**, *142*, 8809–8817.
- [104] J. H. Hildebrand, D. R. F. Cochran, *J. Am. Chem. Soc.* **1949**, *71*, 22–25.
- [105] R. D. Dunlap, R. G. Bedford, J. C. Woodbrey, S. D. Furrow, *J. Am. Chem. Soc.* **1959**, *81*, 2927–2930.
- [106] R. L. Scott, *J. Phys. Chem.* **1958**, *62*, 136–145.
- [107] A. Grosse, G. Cady, *Ind. Eng. Chem.* **1947**, *39*, 367–374.
- [108] I. T. Horváth, in *Handbook of Fluorous Chemistry* (Ed.: J. A. Gladysz, D. P. Curran, I. T. Horváth), Wiley-VCH Verlag GmbH & Co. KGaA, Weinheim, Germany, **2004**, pp. 5–10.

- 
- [109] M. Cametti, B. Crousse, P. Metrangolo, R. Milani, G. Resnati, *Chem. Soc. Rev.* **2012**, *41*, 31–42.
- [110] M. P. Krafft, J. G. Riess, *Chem. Rev.* **2009**, *109*, 1714–1792.
- [111] I. T. Horváth, J. Rábai, *Science* **1994**, *266*, 72–75.
- [112] A. Studer, S. Hadida, R. Ferritto, S.-Y. Kim, P. Jeger, P. Wipf, D. P. Curran, *Science* **1997**, *275*, 823–826.
- [113] Z. Luo, Q. Zhang, Y. Oderaotoshi, D. P. Curran, *Science* **2001**, *291*, 1766–1769.
- [114] B. P. Binks, P. D. I. Fletcher, S. N. Kotsev, R. L. Thompson, *Langmuir* **1997**, *13*, 6669–6682.
- [115] N. Ramasubbu, R. Parthasarathy, Peter. Murray-Rust, *J. Am. Chem. Soc.* **1986**, *108*, 4308–4314.
- [116] T. V Rybalova, I. Yu. Bagryanskaya, *J. Struct. Chem.* **2009**, *50*, 741–753.
- [117] K. Reichenbächer, H. I. Süß, J. Hulliger, *Chem. Soc. Rev.* **2005**, *34*, 22–30.
- [118] R. M. Osuna, V. Hernández, J. T. L. Navarrete, E. D’Oria, J. J. Novoa, *Theor. Chem. Acc.* **2011**, *128*, 541–553.
- [119] R. A. Cormanich, R. Rittner, D. O’Hagan, M. Bühl, *J. Phys. Chem. A* **2014**, *118*, 7901–7910.
- [120] H. Omorodion, B. Twamley, J. A. Platts, R. J. Baker, *Cryst. Growth. Des.* **2015**, *15*, 2835–2841.
- [121] I. Tirota, A. Mastropietro, C. Cordiglieri, L. Gazzera, F. Baggi, G. Baselli, M. G. Bruzzone, I. Zucca, G. Cavallo, G. Terraneo, F. Baldelli Bombelli, P. Metrangolo, G. Resnati, *J. Am. Chem. Soc.* **2014**, *136*, 8524–8527.
- [122] N. A. Meanwell, *J. Agric. Food. Chem.* **2023**, DOI 10.1021/acs.jafc.3c00765.
- [123] E. P. Gillis, K. J. Eastman, M. D. Hill, D. J. Donnelly, N. A. Meanwell, *J. Med. Chem.* **2015**, *58*, 8315–8359.
- [124] S. Purser, P. R. Moore, S. Swallow, V. Gouverneur, *Chem. Soc. Rev.* **2008**, *37*, 320–330.
- [125] K. Müller, C. Faeh, F. Diederich, *Science* **2007**, *317*, 1881–1886.
- [126] H.-J. Böhm, D. Banner, S. Bendels, M. Kansy, B. Kuhn, K. Müller, U. Obst-Sander, M. Stahl, *ChemBioChem* **2004**, *5*, 637–643.
- [127] D. O’Hagan, *J. Fluor. Chem.* **2010**, *131*, 1071–1081.
- [128] N. A. Meanwell, *J. Med. Chem.* **2018**, *61*, 5822–5880.
- [129] S. Huhmann, B. Koksich, *Eur. J. Org. Chem.* **2018**, *2018*, 3667–3679.
- [130] L. M. Gottler, H.-Y. Lee, C. E. Shelburne, A. Ramamoorthy, E. N. G. Marsh, *ChemBioChem* **2008**, *9*, 370–373.
- [131] A. A. Berger, J.-S. Völler, N. Budisa, B. Koksich, *Acc. Chem. Res.* **2017**, *50*, 2093–2103.

- [132] M. Schüler, D. O'Hagan, A. M. Z. Slawin, *Chem. Commun.* **2005**, 4324–4326.
- [133] M. P. Martin, J.-Y. Zhu, H. R. Lawrence, R. Pireddu, Y. Luo, R. Alam, S. Ozcan, S. M. Sebti, N. J. Lawrence, E. Schönbrunn, *ACS Chem. Biol.* **2012**, *7*, 698–706.
- [134] G. Deniau, A. M. Z. Slawin, T. Lebl, F. Chorki, J. P. Issberner, T. van Mourik, J. M. Heygate, J. J. Lambert, L.-A. Etherington, K. T. Sillar, D. O'Hagan, *ChemBioChem* **2007**, *8*, 2265–2274.
- [135] X.-G. Hu, D. S. Thomas, R. Griffith, L. Hunter, *Angew. Chem. Int. Ed.* **2014**, *53*, 6176–6179.
- [136] P. Bentler, N. Erdeljac, K. Bussmann, M. Ahlqvist, L. Knerr, K. Bergander, C. G. Daniliuc, R. Gilmour, *Org. Lett.* **2019**, *21*, 7741–7745.
- [137] J. B. I. Sap, C. F. Meyer, J. Ford, N. J. W. Straathof, A. B. Dürr, M. J. Lelos, S. J. Paisey, T. A. Mollner, S. M. Hell, A. A. Trabanco, C. Genicot, C. W. am Ende, R. S. Paton, M. Tredwell, V. Gouverneur, *Nature* **2022**, *606*, 102–108.
- [138] S. Ye, B. Loll, A. A. Berger, U. Mülöw, C. Alings, M. C. Wahl, B. Kokschi, *Chem. Sci.* **2015**, *6*, 5246–5254.
- [139] J. Leppkes, N. Dimos, B. Loll, T. Hohmann, M. Dyrks, A. Wieseke, B. G. Keller, B. Kokschi, *RSC Chem. Biol.* **2022**, *3*, 773–782.
- [140] L. Wehrhan, J. Leppkes, N. Dimos, B. Loll, B. Kokschi, B. G. Keller, *J. Phys. Chem. B* **2022**, *126*, 9985–9999.
- [141] F. Narjes, K. F. Koehler, U. Koch, B. Gerlach, S. Colarusso, C. Steinkühler, M. Brunetti, S. Altamura, R. De Francesco, V. G. Matassa, *Bioorg. Med. Chem. Lett.* **2002**, *12*, 701–704.
- [142] N. Malquin, K. Rahgoshay, N. Lensen, G. Chaume, E. Miclet, T. Brigaud, *Chem. Commun.* **2019**, *55*, 12487–12490.
- [143] J. A. Olsen, D. W. Banner, P. Seiler, U. Obst Sander, A. D'Arcy, M. Stihle, K. Müller, F. Diederich, *Angew. Chem. Int. Ed.* **2003**, *42*, 2507–2511.
- [144] N. Rozatian, D. R. W. Hodgson, *Chem. Commun.* **2021**, *57*, 683–712.
- [145] C. N. Neumann, T. Ritter, *Angew. Chem. Int. Ed.* **2015**, *54*, 3216–3221.
- [146] T. Liang, C. N. Neumann, T. Ritter, *Angew. Chem. Int. Ed.* **2013**, *52*, 8214–8264.
- [147] S. Dix, M. Jakob, M. N. Hopkinson, *Chem. - Eur. J.* **2019**, *25*, 7635–7639.
- [148] J. Moschner, V. Stulberg, R. Fernandes, S. Huhmann, J. Leppkes, B. Kokschi, *Chem. Rev.* **2019**, *119*, 10718–10801.
- [149] K. W. Laue, S. Kröger, E. Wegelius, G. Haufe, *Eur. J. Org. Chem.* **2000**, *2000*, 3737–3743.
- [150] L. Wang, Z. Zha, W. Qu, H. Qiao, B. P. Lieberman, K. Plössl, H. F. Kung, *Nucl. Med. Biol.* **2012**, *39*, 933–943.

- 
- [151] J. Leppkes, T. Hohmann, B. Kokschi, *J. Fluor. Chem.* **2020**, *232*, 109453.
- [152] D. Winkler, K. Burger, *Synthesis* **1996**, *1996*, 1419–1421.
- [153] S. N. Osipov, T. Lange, P. Tsouker, J. Spengler, L. Hennig, B. Kokschi, S. Berger, S. M. El-Kousy, K. Burger, *Synthesis* **2004**, *2004*, 1821–1829.
- [154] W. M. Clark, C. Bender, *J. Org. Chem.* **1998**, *63*, 6732–6734.
- [155] T. Yajima, H. Nagano, *Org. Lett.* **2007**, *9*, 2513–2515.
- [156] U. Larsson, R. Carlson, J. Leroy, *Acta Chem. Scand.* **1993**, *47*, 380–390.
- [157] Q. Chen, X.-L. Qiu, F.-L. Qing, *J. Org. Chem.* **2006**, *71*, 3762–3767.
- [158] J. A. Pigza, T. Quach, T. F. Molinski, *J. Org. Chem.* **2009**, *74*, 5510–5515.
- [159] C. Benhaim, L. Bouchard, G. Pelletier, J. Sellstedt, L. Kristofova, S. Daigneault, *Org. Lett.* **2010**, *12*, 2008–2011.
- [160] H. Erdbrink, I. Peuser, U. I. M. Gerling, D. Lentz, B. Kokschi, C. Czekelius, *Org. Biomol. Chem.* **2012**, *10*, 8583–8586.
- [161] X. Xing, A. Fichera, K. Kumar, *J. Org. Chem.* **2002**, *67*, 1722–1725.
- [162] Z. Wang, L. Resnick, *Tetrahedron* **2008**, *64*, 6440–6443.
- [163] F. A. Davis, P. S. Portonovo, R. E. Reddy, Y. Chiu, *J. Org. Chem.* **1996**, *61*, 440–441.
- [164] H. Erdbrink, E. K. Nyakatura, S. Huhmann, U. I. M. Gerling, D. Lentz, B. Kokschi, C. Czekelius, *Bellstein J. Org. Chem.* **2013**, *9*, 2009–2014.
- [165] H. Biava, N. Budisa, *J. Fluor. Chem.* **2013**, *156*, 372–377.
- [166] J. L. Aceña, A. E. Sorochinsky, H. Moriwaki, T. Sato, V. A. Soloshonok, *J. Fluor. Chem.* **2013**, *155*, 21–38.
- [167] A. E. Sorochinsky, J. L. Aceña, H. Moriwaki, T. Sato, V. Soloshonok, *Amino Acids* **2013**, *45*, 1017–1033.
- [168] J. L. Aceña, A. E. Sorochinsky, V. Soloshonok, *Amino Acids* **2014**, *46*, 2047–2073.
- [169] Yu. N. Belokon, I. E. Zel'tser, V. I. Bakhmutov, M. B. Saporovskaya, M. G. Ryzhov, A. I. Yanovskii, Yu. T. Struchkov, V. M. Belikov, *J. Am. Chem. Soc.* **1983**, *105*, 2010–2017.
- [170] Yu. N. Belokon, A. G. Bulychev, S. V. Vitt, Yu. T. Struchkov, A. S. Batsanov, T. V. Timofeeva, V. A. Tsyryapkin, M. G. Ryzhov, L. A. Lysova, *J. Am. Chem. Soc.* **1985**, *107*, 4252–4259.
- [171] Y. N. Belokon', V. I. Tararov, V. I. Maleev, T. F. Savel'eva, M. G. Ryzhov, *Tetrahedron: Asymmetry* **1998**, *9*, 4249–4252.
- [172] Y. Zou, J. Han, A. S. Saghyan, A. F. Mkrtchyan, H. Konno, H. Moriwaki, K. Izawa, V. A. Soloshonok, *Molecules* **2020**, *25*, 2739.
- [173] A. E. Sorochinsky, J. L. Aceña, H. Moriwaki, T. Sato, V. A. Soloshonok, *Amino Acids* **2013**, *45*, 691–718.

- [174] J. Wang, D. Lin, S. Zhou, X. Ding, V. A. Soloshonok, H. Liu, *J. Org. Chem.* **2011**, *76*, 684–687.
- [175] Y. N. Belokon, V. I. Maleev, T. F. Savel'eva, M. A. Moskalenko, D. A. Pripadchev, V. N. Khrustalev, A. S. Saghiyan, *Amino Acids* **2010**, *39*, 1171–1176.
- [176] V. A. Soloshonok, V. P. Kukhar, S. V Galushko, N. Yu. Svistunova, D. V Avilov, N. A. Kuz'mina, N. I. Raevski, Y. T. Struchkov, A. P. Pysarevsky, Y. N. Belokon, *J. Chem. Soc., Perkin Trans. 1* **1993**, 3143–3155.
- [177] F. Drouet, A. F. M. Noisier, C. S. Harris, D. P. Furkert, M. A. Brimble, *Eur. J. Org. Chem.* **2014**, *2014*, 1195–1201.
- [178] V. A. Soloshonok, D. V Avilov, V. P. Kukhar, L. Van Meervelt, N. Mischenko, *Tetrahedron Lett.* **1997**, *38*, 4671–4674.
- [179] J. Han, T. T. Romoff, H. Moriwaki, H. Konno, V. A. Soloshonok, *ACS Omega* **2019**, *4*, 18942–18947.
- [180] Y. N. Belokon', K. A. Kochetkov, T. D. Churkina, N. S. Ikonnikov, S. A. Orlova, V. V. Smirnov, A. A. Chesnokov, *Mendeleev Commun.* **1997**, *7*, 137–138.
- [181] V. A. Soloshonok, H. Ueki, T. K. Ellis, T. Yamada, Y. Ohfune, *Tetrahedron Lett.* **2005**, *46*, 1107–1110.
- [182] A. S. Saghiyan, A. S. Dadayan, S. A. Dadayan, A. F. Mkrtychyan, A. V Geolchanyan, L. L. Manasyan, H. R. Ajvazyan, V. N. Khrustalev, H. H. Hambardzumyan, V. I. Maleev, *Tetrahedron Asymmetry* **2010**, *21*, 2956–2965.
- [183] M. Jörres, X. Chen, J. L. Aceña, C. Merkens, C. Bolm, H. Liu, V. A. Soloshonok, *Adv. Synth. Catal.* **2014**, *356*, 2203–2208.
- [184] J. Li, S. Zhou, J. Wang, A. Kawashima, H. Moriwaki, V. A. Soloshonok, H. Liu, *Eur. J. Org. Chem.* **2016**, *2016*, 999–1006.
- [185] R. Takeda, A. Kawamura, A. Kawashima, T. Sato, H. Moriwaki, K. Izawa, H. Abe, V. A. Soloshonok, *Org. Biomol. Chem.* **2018**, *16*, 4968–4972.
- [186] T. K. Ellis, H. Ueki, T. Yamada, Y. Ohfune, V. A. Soloshonok, *J. Org. Chem.* **2006**, *71*, 8572–8578.
- [187] Y. Nian, J. Wang, H. Moriwaki, V. A. Soloshonok, H. Liu, *Dalton Trans.* **2017**, *46*, 4191–4198.
- [188] O. A. Levitskiy, O. I. Aglamazova, V. A. Soloshonok, H. Moriwaki, T. V Magdesieva, *Chem. - Eur. J.* **2020**, *26*, 7074–7082.
- [189] T. T. Romoff, A. B. Palmer, N. Mansour, C. J. Creighton, T. Miwa, Y. Ejima, H. Moriwaki, V. A. Soloshonok, *Org. Process Res. Dev.* **2017**, *21*, 732–739.

- 
- [190] T. T. Romoff, B. G. Ignacio, N. Mansour, A. B. Palmer, C. J. Creighton, H. Abe, H. Moriwaki, J. Han, H. Konno, V. A. Soloshonok, *Org. Process Res. Dev.* **2020**, *24*, 294–300.
- [191] J. Han, R. Takeda, X. Liu, H. Konno, H. Abe, T. Hiramatsu, H. Moriwaki, V. A. Soloshonok, *Molecules* **2019**, *24*, 4521.
- [192] Z. Yin, H. Moriwaki, H. Abe, T. Miwa, J. Han, V. A. Soloshonok, *ChemistryOpen* **2019**, *8*, 701–704.
- [193] H. Mei, Z. Yin, T. Miwa, H. Moriwaki, H. Abe, J. Han, V. A. Soloshonok, *Symmetry* **2019**, *11*, 578.
- [194] H. Mei, J. Han, R. Takeda, T. Sakamoto, T. Miwa, Y. Minamitsuji, H. Moriwaki, H. Abe, V. A. Soloshonok, *ACS Omega* **2019**, *4*, 11844–11851.
- [195] Y. Tokairin, Y. Shigeno, J. Han, G.-V. Röschenthaler, H. Konno, H. Moriwaki, V. A. Soloshonok, *ChemistryOpen* **2020**, *9*, 93–96.
- [196] C. Li, G.-F. Wang, Y. Wang, R. Creager-Allen, E. A. Lutz, H. Scronce, K. M. Slade, R. A. S. Ruf, R. A. Mehl, G. J. Pielak, *J. Am. Chem. Soc.* **2010**, *132*, 321–327.
- [197] M. A. Miller, E. M. Sletten, *ChemBioChem* **2020**, *21*, 3451–3462.
- [198] A. T. Preslar, F. Tantakitti, K. Park, S. Zhang, S. I. Stupp, T. J. Meade, *ACS Nano* **2016**, *10*, 7376–7384.
- [199] A. T. Preslar, L. M. Lilley, K. Sato, S. Zhang, Z. K. Chia, S. I. Stupp, T. J. Meade, *ACS Appl. Mater. Interfaces* **2017**, *9*, 39890–39894.
- [200] Y. Yuan, S. Ge, H. Sun, X. Dong, H. Zhao, L. An, J. Zhang, J. Wang, B. Hu, G. Liang, *ACS Nano* **2015**, *9*, 5117–5124.
- [201] Y. Yuan, H. Sun, S. Ge, M. Wang, H. Zhao, L. Wang, L. An, J. Zhang, H. Zhang, B. Hu, J. Wang, G. Liang, *ACS Nano* **2015**, *9*, 761–768.
- [202] C. Ge, J. Yang, S. Duan, Y. Liu, F. Meng, L. Yin, *Nano Lett.* **2020**, *20*, 1738–1746.
- [203] L. Zhang, S. Lin, Y. Li, B. Li, Y. Yang, *New J. Chem.* **2021**, *45*, 3193–3201.
- [204] L. Zhang, S. Lin, Q. Tong, Y. Li, Y. Wang, Y. Li, B. Li, Y. Yang, *Chirality* **2019**, *31*, 992–1000.
- [205] G. Rong, C. Wang, L. Chen, Y. Yan, Y. Cheng, *Sci. Adv.* **2020**, *6*, eaaz1774.
- [206] N. Chuard, K. Fujisawa, P. Morelli, J. Saabach, N. Winssinger, P. Metrangolo, G. Resnati, N. Sakai, S. Matile, *J. Am. Chem. Soc.* **2016**, *138*, 11264–11271.
- [207] J. Václavík, R. Zschoche, I. Klimánková, V. Matoušek, P. Beier, D. Hilvert, A. Togni, *Chem. - Eur. J.* **2017**, *23*, 6490–6494.
- [208] K. Rahimidashghoul, I. Klimánková, M. Hubálek, M. Korecký, M. Chvojka, D. Pokorný, V. Matoušek, L. Fojtík, D. Kavan, Z. Kukačka, P. Novák, P. Beier, *Chem. - Eur. J.* **2019**, *25*, 15779–15785.

- [209] S. M. Brittain, S. B. Ficarro, A. Brock, E. C. Peters, *Nat. Biotechnol.* **2005**, *23*, 463–468.
- [210] C. M. Tressler, N. J. Zondlo, *J. Org. Chem.* **2014**, *79*, 5880–5886.
- [211] C. M. Tressler, N. J. Zondlo, *ACS Chem. Biol.* **2020**, *15*, 1096–1103.
- [212] C. M. Tressler, N. J. Zondlo, *Org. Lett.* **2016**, *18*, 6240–6243.
- [213] B. C. Buer, B. J. Levin, E. N. G. Marsh, *J. Pept. Sci.* **2013**, *19*, 308–314.
- [214] C. M. Tressler, N. J. Zondlo, *Biochemistry* **2017**, *56*, 1062–1074.
- [215] S. Ellipilli, K. N. Ganesh, *J. Org. Chem.* **2015**, *80*, 9185–9191.
- [216] S. Ellipilli, S. Palvai, K. N. Ganesh, *J. Org. Chem.* **2016**, *81*, 6364–6373.
- [217] S. Ellipilli, R. vasudeva Murthy, K. N. Ganesh, *Chem. Commun.* **2016**, *52*, 521–524.
- [218] X. Cai, H. Zhu, Y. Zhang, Z. Gu, *ACS Appl. Mater. Interfaces* **2017**, *9*, 9402–9415.
- [219] X. Cai, R. Jin, J. Wang, D. Yue, Q. Jiang, Y. Wu, Z. Gu, *ACS Appl. Mater. Interfaces* **2016**, *8*, 5821–5832.
- [220] T. Wu, L. Wang, S. Ding, Y. You, *Macromol. Biosci.* **2017**, *17*, 1700114.
- [221] A. P. Piccionello, G. Pitarresi, A. Pace, D. Triolo, P. Picone, S. Buscemi, G. Giammona, *J. Drug. Target* **2012**, *20*, 433–444.
- [222] J. Zhu, Y. Xiao, H. Zhang, Y. Li, Y. Yuan, Z. Yang, S. Chen, X. Zheng, X. Zhou, Z.-X. Jiang, *Biomacromolecules* **2019**, *20*, 1281–1287.
- [223] S. Ma, J. Zhou, Y. Zhang, Y. He, Q. Jiang, D. Yue, X. Xu, Z. Gu, *ACS Appl. Mater. Interfaces* **2016**, *8*, 28468–28479.
- [224] S. Ma, J. Zhou, Y. Zhang, B. Yang, Y. He, C. Tian, X. Xu, Z. Gu, *ACS Appl. Mater. Interfaces* **2019**, *11*, 7731–7742.
- [225] S. Ma, J. Zhou, A. R. M. Wali, Y. He, X. Xu, J. Z. Tang, Z. Gu, *J. Mater. Sci. Mater. Med.* **2015**, *26*, 219.
- [226] R. Godbout, S. Légaré, M. Auger, C. Carpentier, F. Otis, M. Auger, P. Lagüe, N. Voyer, *PLoS One* **2016**, *11*, e0166587-.
- [227] M. Auger, T. Lefèvre, F. Otis, N. Voyer, M. Auger, *Pept. Sci.* **2019**, *111*, e24051.
- [228] H. Meng, K. Kumar, *J. Am. Chem. Soc.* **2007**, *129*, 15615–15622.
- [229] S. H. Medina, M. S. Michie, S. E. Miller, M. J. Schnermann, J. P. Schneider, *Angew. Chem. Int. Ed.* **2017**, *56*, 11404–11408.
- [230] S. E. Kirberger, S. D. Maltseva, J. C. Manulik, S. A. Einstein, B. P. Weegman, M. Garwood, W. C. K. Pomerantz, *Angew. Chem. Int. Ed.* **2017**, *56*, 6440–6444.
- [231] S. K. Holmgren, K. M. Taylor, L. E. Bretscher, R. T. Raines, *Nature* **1998**, *392*, 666–667.
- [232] S. K. Holmgren, L. E. Bretscher, K. M. Taylor, R. T. Raines, *Chem. Biol.* **1999**, *6*, 63–70.
- [233] J. A. Hodges, R. T. Raines, *J. Am. Chem. Soc.* **2003**, *125*, 9262–9263.

- 
- [234] L. E. Bretscher, C. L. Jenkins, K. M. Taylor, M. L. DeRider, R. T. Raines, *J. Am. Chem. Soc.* **2001**, *123*, 777–778.
- [235] J. M. Dones, I. C. Tanrikulu, J. V Chacko, A. B. Schroeder, T. T. Hoang, A. L. F. Gibson, K. W. Eliceiri, R. T. Raines, *Org. Biomol. Chem.* **2019**, *17*, 9906–9912.
- [236] A. Niemz, D. A. Tirrell, *J. Am. Chem. Soc.* **2001**, *123*, 7407–7413.
- [237] S. Chowdhary, R. F. Schmidt, A. K. Sahoo, T. tom Dieck, T. Hohmann, B. Schade, K. Brademann-Jock, A. F. Thünemann, R. R. Netz, M. Gradzielski, B. Kokschi, *Nanoscale* **2022**, *14*, 10176–10189.
- [238] A. N. Lupas, J. Bassler, *Trends Biochem. Sci.* **2017**, *42*, 130–140.
- [239] D. N. Woolfson, G. J. Bartlett, M. Bruning, A. R. Thomson, *Curr. Opin. Struct. Biol.* **2012**, *22*, 432–441.
- [240] D. N. Woolfson, *Adv. Protein Chem.* **2005**, *70*, 79–112.
- [241] D. N. Woolfson, in *Fibrous Proteins: Structures and Mechanisms* (Eds.: D.A.D. Parry, J.M. Squire), Springer International Publishing, Cham, **2017**, pp. 35–61.
- [242] W. M. Dawson, F. J. O. Martin, G. G. Rhys, K. L. Shelley, R. L. Brady, D. N. Woolfson, *Chem. Sci.* **2021**, *12*, 6923–6928.
- [243] A. R. Thomson, C. W. Wood, A. J. Burton, G. J. Bartlett, R. B. Sessions, R. L. Brady, D. N. Woolfson, *Science* **2014**, *346*, 485–488.
- [244] M. J. Pandya, G. M. Spooner, M. Sunde, J. R. Thorpe, A. Rodger, D. N. Woolfson, *Biochemistry* **2000**, *39*, 8728–8734.
- [245] M. G. Ryadnov, D. N. Woolfson, *Angew. Chem. Int. Ed.* **2003**, *42*, 3021–3023.
- [246] E. F. Banwell, E. S. Abelardo, D. J. Adams, M. A. Birchall, A. Corrigan, A. M. Donald, M. Kirkland, L. C. Serpell, M. F. Butler, D. N. Woolfson, *Nat. Mater.* **2009**, *8*, 596–600.
- [247] J. M. Fletcher, R. L. Harniman, F. R. H. Barnes, A. L. Boyle, A. Collins, J. Mantell, T. H. Sharp, M. Antognozzi, P. J. Booth, N. Linden, M. J. Miles, R. B. Sessions, P. Verkade, D. N. Woolfson, *Science* **2013**, *340*, 595–599.
- [248] M. L. Diss, A. J. Kennan, *J. Am. Chem. Soc.* **2008**, *130*, 1321–1327.
- [249] E. H. C. Bromley, R. B. Sessions, A. R. Thomson, D. N. Woolfson, *J. Am. Chem. Soc.* **2009**, *131*, 928–930.
- [250] C. Aronsson, S. Danmark, F. Zhou, P. Öberg, K. Enander, H. Su, D. Aili, *Sci. Rep.* **2015**, *5*, 14063.
- [251] C. Jäckel, W. Seufert, S. Thust, B. Kokschi, *ChemBioChem* **2004**, *5*, 717–720.
- [252] C. Jäckel, M. Salwiczek, B. Kokschi, *Angew. Chem. Int. Ed.* **2006**, *45*, 4198–4203.
- [253] M. Salwiczek, B. Kokschi, *ChemBioChem* **2009**, *10*, 2867–2870.
- [254] E. K. Nyakatura, O. Reimann, T. Vagt, M. Salwiczek, B. Kokschi, *RSC Adv.* **2013**, *3*, 6319–6322.



- [255] T. Vagt, E. Nyakatura, M. Salwiczek, C. Jäckel, B. Kokschi, *Org. Biomol. Chem.* **2010**, *8*, 1382–1386.
- [256] M. Salwiczek, S. Samsonov, T. Vagt, E. Nyakatura, E. Fleige, J. Numata, H. Cölfen, M. T. Pisabarro, B. Kokschi, *Chem. - Eur. J.* **2009**, *15*, 7628–7636.
- [257] Y. Tang, G. Ghirlanda, N. Vaidehi, J. Kua, D. T. Mainz, W. A. Goddard, W. F. DeGrado, D. A. Tirrell, *Biochemistry* **2001**, *40*, 2790–2796.
- [258] Y. Tang, G. Ghirlanda, W. A. Petka, T. Nakajima, W. F. DeGrado, D. A. Tirrell, *Angew. Chem. Int. Ed.* **2001**, *40*, 1494–1496.
- [259] Y. Tang, D. A. Tirrell, *J. Am. Chem. Soc.* **2001**, *123*, 11089–11090.
- [260] S. Son, I. C. Tanrikulu, D. A. Tirrell, *ChemBioChem* **2006**, *7*, 1251–1257.
- [261] B. Bilgiçer, A. Fichera, K. Kumar, *J. Am. Chem. Soc.* **2001**, *123*, 4393–4399.
- [262] B. Bilgiçer, K. Kumar, *Proc. Natl. Acad. Sci. U. S. A.* **2004**, *101*, 15324–15329.
- [263] N. Naarmann, B. Bilgiçer, H. Meng, K. Kumar, C. Steinem, *Angew. Chem. Int. Ed.* **2006**, *45*, 2588–2591.
- [264] J. K. Montclare, S. Son, G. A. Clark, K. Kumar, D. A. Tirrell, *ChemBioChem* **2009**, *10*, 84–86.
- [265] K.-H. Lee, H.-Y. Lee, M. M. Slutsky, J. T. Anderson, E. N. G. Marsh, *Biochemistry* **2004**, *43*, 16277–16284.
- [266] H.-Y. Lee, K.-H. Lee, H. M. Al-Hashimi, E. N. G. Marsh, *J. Am. Chem. Soc.* **2006**, *128*, 337–343.
- [267] L. M. Gottler, R. de la Salud-Bea, E. N. G. Marsh, *Biochemistry* **2008**, *47*, 4484–4490.
- [268] B. C. Buer, R. de la Salud-Bea, H. M. Al Hashimi, E. N. G. Marsh, *Biochemistry* **2009**, *48*, 10810–10817.
- [269] B. C. Buer, J. L. Meagher, J. A. Stuckey, E. N. G. Marsh, *Proc. Natl. Acad. Sci. U. S. A.* **2012**, *109*, 4810–4815.
- [270] B. C. Buer, B. J. Levin, E. N. G. Marsh, *J. Am. Chem. Soc.* **2012**, *134*, 13027–13034.
- [271] B. Bilgiçer, X. Xing, K. Kumar, *J. Am. Chem. Soc.* **2001**, *123*, 11815–11816.
- [272] B. Bilgiçer, K. Kumar, *Tetrahedron* **2002**, *58*, 4105–4112.
- [273] T. Hohmann, P. Dubatouka, K. Pfeifer, B. Kokschi, *Biomacromolecules* **2023**, *24*, 3357–3369.
- [274] T. Hohmann, M. Dyrks, S. Chowdhary, M. Weber, D. Nguyen, J. Moschner, B. Kokschi, *J Org Chem* **2022**, *87*, 10592–10604.
- [275] T. Hohmann, S. Chowdhary, K. Ataka, J. Er, G. H. Dreyhsig, J. Heberle, B. Kokschi, *Chem. - Eur. J.* **2023**, *29*, e202203860.
- [276] S. Aravinda, N. Shamala, C. Das, A. Sriranjini, I. L. Karle, P. Balaram, *J. Am. Chem. Soc.* **2003**, *125*, 5308–5315.

- [277] C. D. Tatko, M. L. Waters, *J. Am. Chem. Soc.* **2002**, *124*, 9372–9373.
- [278] Y. H. Zhao, M. H. Abraham, A. M. Zissimos, *J. Org. Chem.* **2003**, *68*, 7368–7373.
- [279] Y. Yang, in *Side Reactions in Peptide Synthesis* (Ed.: Y. Yang), Academic Press, Oxford, UK, **2016**, pp. 323–346.
- [280] S. Capasso, L. Mazzearella, F. Sica, A. Zagari, S. Salvadori, *J. Chem. Soc., Perkin Trans. 2* **1993**, 679–682.